

<https://doi.org/10.15388/vu.thesis.809>

<https://orcid.org/0000-0002-6869-6169>

VILNIUS UNIVERSITY

CENTER FOR PHYSICAL SCIENCES AND TECHNOLOGY

Sukomol Barua

Anode and cathode materials for energy conversion systems

DOCTORAL DISSERTATION

Natural Sciences,
Chemistry (N 003)

VILNIUS 2025

The dissertation was prepared between 2021 and 2025 at the State Research Institute Center for Physical Science and Technology (FTMC).

The research was supported by the Research Council of Lithuania (Mobility funding – P-DAK-23-78, P-DAK-24-37, P-DAK-25-28 and financial grant based on study result – P-DAP-23-201, P-DAP-25-146).

Academic supervisor – Dr. Aldona Balčiūnaitė (Center for Physical Sciences and Technology, Natural Sciences, Chemistry – N 003).

This doctoral dissertation will be defended in a public/closed meeting of the Dissertation Defence Panel:

Chairman: Prof. Habil. Dr. Aivaras Kareiva (Vilnius University, Natural Sciences, Chemistry – N 003).

Members:

Prof. Dr. Ingrida Ancutienė (Kaunas University of Technology, Natural sciences, Chemistry – N003),

Dr. Milda Petrulėvičienė (State Research Institute Center for Physical Sciences and Technology, Natural sciences, Chemistry – N003),

Prof. Dr. Biljana Šljukić Paunković (University of Belgrade, Faculty of Physical Chemistry, Natural Sciences, Chemistry – N 003),

Prof. Dr. Vida Vičkačkaitė (Vilnius University, Natural Sciences, Chemistry – N 003).

The dissertation shall be defended in English at a public meeting of the Dissertation Defence Panel at 1 pm on the 19th of September, 2025, in meeting room E302 of the Center for Physical Sciences and Technology.

Address: Saulėtekio ave. 3, Meeting Room No. E302, Vilnius, Lithuania
Tel. +37052649211; e-mail: office@ftmc.lt

The text of this dissertation can be accessed at the libraries Vilnius University, as well as on the website of Vilnius University: www.vu.lt/lt/naujienos/ivykiu-kalendorius

<https://doi.org/10.15388/vu.thesis.809>

<https://orcid.org/0000-0002-6869-6169>

VILNIAUS UNIVERSITETAS
FIZINIŲ IR TECHNOLOGIJOS MOKSLŲ CENTRAS

Sukomol Barua

Anodo ir katodo medžiagos energijos konversijos sistemoms

DAKTARO DISERTACIJA

Gamtos mokslai,
Chemija (N 003)

VILNIUS 2025

Disertacija rengta 2021–2025 metais Valstybinis mokslinių tyrimų institutas Fizinių ir technologijos mokslų centras.

Mokslinius tyrimus rėmė Lietuvos mokslų taryba (Parama išvykoms – P-DAK-23-78, P-DAK-24-37, P-DAK-25-28 ir Parama doktorantams už studijų rezultatus – P-DAP-23-201, P-DAP-25-146).

Mokslinė vadovė – dr. Aldona Balčiūnaitė (VMTI Fizinių ir technologijos mokslų centras, gamtos mokslai, chemija – N 003)

Gynimo taryba:

Pirmininkas:

prof. habil. dr. Aivaras Kareiva (Vilniaus universitetas, gamtos mokslai, chemija – N 003).

Nariai:

prof. dr. Ingrida Ancutienė (Kauno technologijos universitetas, gamtos mokslai, chemija – N 003),

dr. Milda Petrulevičienė (VMTI Fizinių ir technologijos mokslų centras, gamtos mokslai, chemija – N 003),

prof. dr. Biljana Šljukić Paunković (Belgrado universitetas, Fizikinės chemijos fakultetas, gamtos mokslai, chemija – N 003)

prof. dr. Vida Vičkačkaitė (Vilniaus universitetas, gamtos mokslai, chemija – N 003).

Disertacija ginama viešame Gynimo tarybos posėdyje 2025 m. rugsėjo mėn. 19 d. 13 val. VMTI Fizinių ir technologijos mokslų centro posėdžių salėje E302 anglų kalba.

Adresas: Saulėtekio al. 3, Vilnius, Lietuva, tel. +37052649211, el. paštas office@ftmc.lt

Disertaciją galima peržiūrėti Vilniaus universiteto biblioteko ir VU interneto svetainėje adresu: <https://www.vu.lt/naujienos/ivykiu-kalendorius>

PADĖKA/ACKNOWLEDGMENTS

First and foremost, I extend my heartfelt gratitude to The ALMIGHTY for blessing me with perseverance and driving me in the right direction during my entire journey of doctoral studies.

I am extending my sincere and respectful appreciation to my supervisor, Dr. Aldona Balčiūnaitė, whose guidance, encouragement, and invaluable insights have been instrumental in shaping this research. I would also like to mention our HOD, Dr. Loreta. Tamašauskaitė-Tamašiūnaitė and Prof. habil. Dr. Eugenijus Norkus for their patience, faith and unwavering support that inspired me to push boundaries and strive for excellence. I am truly fortunate to have had the opportunity to learn under their mentorship.

I am also profoundly thankful to my parents, whose unconditional love, sacrifices, and true belief in me have been the foundation of my academic pursuits. Their consistent encouragement and support, both emotionally and intellectually, have given me the strength to overcome tons of challenges and keep moving forward. This achievement is as much theirs as it is mine. I would also remember my late Grandparents, especially my Grandmother, who gave her blessings to my Mom when I was actually in her womb.

I would like to thank the Chair and all examining committee members for their feedback, support and assistance throughout the preparation of this thesis. I would like to thank the Center for Physical Science and Technology and the Lietuvos Mokslo Taryba (LMT) for their assistance and support throughout my studies and research.

Finally, I do express my appreciation to all of my colleagues, all of my teachers from school-level up to universities, friends, and everyone who has contributed to this journey, whether through academic discussions, words of motivation, or moments of laughter. Your support has made this endeavor not only possible but also enriching.

Last but certainly not least, I want to thank my beloved wife and our baby boy for their years-long inspiration, patience and understanding throughout this journey.

I am deeply grateful to all of those unsung heroes of my life and remembering them who have shaped my entire life, built and supported me along the way.

Love and respect to ALL.

TABLE OF CONTENTS

INTRODUCTION.....	9
MAIN GOAL	10
TASKS	11
SCIENTIFIC NOVELTY.....	11
STATEMENTS OF DEFENCE.....	12
CONTRIBUTIONS OF THE AUTHOR	12
1. LITERATURE REVIEW	13
1.1. Hydrogen Energy – The Renewable Power Source	13
1.2. Fundamentals of electrochemical water electrolysis.....	16
1.3. Seawater electrolysis – The most sustainable approach.....	18
1.4. Electrocatalysts – The ultimate armour.....	20
2. MATERIALS AND METHODS	24
2.1. Materials and chemicals	24
2.2. Substrate preparation.....	24
2.3. Fabrication of 3D binary NiMo/Ti electrocatalysts	25
2.4. Fabrication of 3D binary NiMn/Ti electrocatalysts	25
2.5. Fabrication of 3D ternary NiMnCo/Ti electrocatalysts.....	27
2.6. Electrochemical measurements	28
2.7. Characterization of synthesized binary and ternary electrocatalysts	29
3. RESULTS AND DISCUSSION	30
3.1. Synthesis and characterization of 3D NiMo/Ti electrocatalysts	30
3.1.1. Morphology of 3D NiMo/Ti electrocatalysts.....	30
3.1.2. Electrocatalytic investigations of 3D NiMo/Ti catalysts for HER and OER performance.....	31
3.2. Synthesis and characterization of 3D NiMn/Ti electrocatalysts	32
3.2.1. Microstructure and morphology of 3D NiMn/Ti electrocatalysts	32
3.2.2. Electrocatalytic activity of 3D NiMn/Ti electrocatalysts for HER.....	34

3.2.3. Electrocatalytic activity of 3D NiMn/Ti electrocatalysts for OER.....	38
3.2.4. Overall seawater splitting performance of optimized 3D NiMn/Ti electrocatalysts.....	41
3.3. Synthesis and characterization of 3D NiMnCo/Ti electrocatalysts..	43
3.3.1. Microstructure and Morphology of 3D NiMnCo/Ti electrocatalysts	43
3.3.2. Electrocatalytic activity of 3D NiMnCo/Ti electrocatalysts for HER in alkaline, simulated seawater and alkaline seawater media ...	46
CONCLUSION	50
SANTRAUKA LIETUVIŲ KALBA	52
ĮVADAS.....	52
DARBO TIKSLAS	53
DARBO UŽDAVINIAI	54
MOKSLINIS NAUJUMAS	54
GINAMIEJI TEIGINIAI	55
AUTORIAUS INDĖLIS	55
EKSPERIMENTO METODIKA	56
REZULTATŲ APTARIMAS	58
IŠVADOS.....	63
REFERENCES.....	65
LISTS OF PUBLICATIONS	77
PUBLICATION IN PRESS	77
OTHER PUBLICATION.....	179
LIST OF CONFERENCE PRESENTATIONS	179
LIST OF OTHER CONFERENCE PRESENTATIONS.....	181
LIST OF AWARDS	182
CURRICULUM VITAE	183

LIST OF ABBREVIATIONS

3D	Three-dimensional
ASW	Alkaline Seawater (1.0 M KOH + natural seawater)
BP	British Petroleum
CA	Chronoamperometry
CCUS	Carbon capture utilization and storage
CIER	Chlorine Evolution Reaction
CP	Chronopotentiometry
CV	Cyclic Voltammetry
DSE	Direct Seawater Electrolysis
DHBT	Dynamic Hydrogen Bubble Template
DI	Deionized water
DOE	The U.S. Department of Energy
ECSA	Electrochemically active surface area
EJ	Exajoule (10^{18} Joules)
GHG	Greenhouse Gas
GW	Gigawatts (10^9 Watts)
HER	Hydrogen Evolution Reaction
ICP-OES	Inductively Coupled Plasma Optical Emission Spectroscopy
IEA	International Energy Agency
IRENA	International Renewable Energy Agency
LDHs	Layered Double Hydroxides
LSV	Linear Sweep Voltammetry
LSVs	Linear Sweep Voltammograms
NZE	Net Zero Emissions
OCP	Open Circuit Potential
OER	Oxygen Evolution Reaction
OWS	Overall Water Splitting
PGM	Platinum Group Metal
RHE	Reversible Hydrogen Electrode
SCE	Saturated Calomel Electrode
SEM	Scanning Electron Microscopy
SMR	Steam Methane Reforming
SSW	Simulated Seawater (1.0 M KOH + 0.5 M NaCl)
C_{dl}	Double layer capacitance (μF)
C_s	Specific capacitance ($\mu\text{F cm}^{-2}$)
j	Current density (mA cm^{-2})
η	Overpotential (mV)

INTRODUCTION

Energy security and uninterrupted energy supply have emerged as significant global concerns as the ever-increasing population growth and industrialization have resulted in the rapid depletion of natural resources. Limited fossil fuel-driven energy sources have always been the backbone of early human civilization till today and after the industrial renaissance, the global energy demand is increasing exponentially [1]. Combustion of fossil fuels, e.g., coal, petroleum and natural gas emits millions of tons of carbon dioxide (CO_2), carbon monoxide (CO), sulfur dioxide (SO_2), nitrogen oxide gases (NO_x) and methane (CH_4) which are commonly known as greenhouse gases. The vast consumption of fossil fuels not only depletes the natural resources but also results in significant challenges for the existence of mankind as global warming, climate change, environmental pollution, the rise of sea level and other environmental complications are the consequential threats of the overconsumption of long-chained hydrocarbons. Moreover, the fossil fuel reserves are also very inadequate and geospecific, therefore, their drastic depletion could lead to energy shortfalls and geopolitical conflicts. Therefore, a surge in interest in alternative, environmentally friendly, and sustainable renewable energy sources has gained considerable attention over the last decades [2, 3].

In order to address both energy security and environmental sustainability by mitigating the emission of greenhouse gases, hydrogen (H_2) can be considered as a key emerging substitute for fossil fuels which definitely can serve as the most promising energy source by means of highest gravimetric energy density ($\sim 142 \text{ MJ kg}^{-1}$) leaving zero carbon footprint, rich elemental abundance on earth and scalability [4, 5]. The sources of hydrogen are diverse, and hydrogen can be classified into three categories: green hydrogen, blue hydrogen, and gray hydrogen, according to the production technologies [6]. Grey hydrogen is the most common type of hydrogen produced mainly by steam methane reforming (SMR), whereas blue hydrogen is obtained via decarbonization of grey hydrogen by CCUS (carbon capture utilization and storage) technology. Zero to low-carbon green hydrogen production relies on water electrolysis powered by renewable sources, such as wind, solar, geothermal, and bioenergy, which can be considered as the most promising alternative to traditional fossil fuels for industrial-scale production of high-purity hydrogen with zero carbon emissions [7]. The electrosynthesis of hydrogen through water splitting comprises two key half-reactions: the cathodic hydrogen evolution reaction (HER) and the anodic oxygen evolution

reaction (OER), whereas it requires ca. 9 L of pure water stoichiometrically to produce 1 kg of hydrogen [8, 9].

The electrocatalytic water splitting under standard conditions is thermodynamically unfavorable due to the four-electron transfer sluggish kinetics of OER, which contribute to relatively higher overpotentials and can be considered as the main bottleneck for the overall electrochemical water splitting [10]. The process of water electrolysis requires a minimum energy of 39.4 kWh kg⁻¹ to produce H₂ at 100% efficiency, while a typical electrolyzer consumes up to 50 kWh to produce 1 kg of H₂, although higher efficiencies can be achieved under extreme pressure and temperature conditions [11]. However, the oceanic seawater constitutes approximately 97.5% of the world's total water reserve, and the availability of usable freshwater resources remains a significant challenge for the advancement of electrolyzer technology due to increasing global population growth associated with the demands of modern living standards. Practical, realistic water splitting can only be possible by overcoming these barriers.

The state-of-the-art platinum group metal (PGM) catalysts exhibit outstanding electrocatalytic activity for water electrolyzers, where Pt and Pt-based catalysts are the benchmark electrocatalysts for HER and Ir/Ru-based (IrO₂/RuO₂) materials are considered as the high-performance commercially available catalysts for OER [12-15]. However, the low natural reserves and high cost of precious PGM catalysts are the primary hurdles hindering the industrial-scale production and commercialization of hydrogen by electrocatalytic water splitting. Therefore, the designing and development of a cost-effective, stable and high-efficient bifunctional electrocatalyst is the key factor to breaking the technical bottleneck of renewable green hydrogen production from overall freshwater/seawater splitting.

MAIN GOAL

To fabricate non-noble transition metal-based (Ni, Mo, Mn and Co) electrocatalysts by electrodeposition method via dynamic hydrogen bubble template (DHBT) technique, characterize their microstructures, compositions, surface morphologies and evaluation of electrocatalytic activity and stability of synthesized electrodes for hydrogen evolution reaction (HER), oxygen evolution reaction (OER) and overall water splitting in alkaline freshwater/seawater electrolytes.

TASKS

- Fabrication of non-noble transition metal-based (Ni and Mo) electrocatalysts, and investigation of their electrocatalytic HER and OER activity and stability in alkaline media (herein 1.0 M NaOH).
- Fabrication of binary Ni and Mn-based electrocatalysts with variable concentration of manganese salts using additives and evaluation of their HER and OER electrocatalytic activity and stability in alkaline media (herein 1.0 M KOH), simulated seawater and alkaline seawater.
- Characterization of the synthesized NiMn/Ti electrocatalysts and explanation of their enhanced catalytic activity.
- Investigation of overall seawater splitting performance in lab-scale using synthesized bifunctional optimized NiMn/Ti electrocatalysts in an assembled two-electrode seawater electrolyzer.
- Synthesis of Ni, Mn and Co incorporated ternary electrodes with variable cobalt salt concentrations using additives and investigation of the electrocatalytic HER performance and stability in alkaline freshwater, simulated seawater and alkaline seawater.
- Characterization of synthesized NiMnCo/Ti electrocatalysts and explanation of their enhanced catalytic activity.

SCIENTIFIC NOVELTY

- A simple, low-cost electrochemical deposition method via the dynamic hydrogen bubble template (DHBT) technique was applied to synthesize binary and ternary 3D non-noble metal-based electrocatalysts. The catalytic performance and stability of the fabricated electrocatalysts were investigated for water splitting applications in alkaline freshwater, simulated seawater, and alkaline natural seawater.
- It was established for the first time that the electrochemically synthesized NiMn/Ti-5 electrocatalyst, prepared using the DHBT technique, exhibits superior electrocatalytic HER activity and stability due to the formation of a highly porous architecture.
- It was demonstrated for the first time that the NiMn/Ti-1 and NiMn/Ti-5 electrode pair (electrodeposited from bath solutions with $\text{Ni}^{2+}:\text{Mn}^{2+}$ molar ratios of 1:1 and 1:5, respectively) can be effectively assembled in a two-electrode seawater electrolyzer as the anode and cathode, respectively, to achieve a lower cell voltage than platinum-based systems.
- The outstanding performance and long-term stability (up to 50 hours) of the developed ternary 3D NiMnCo/Ti electrocatalysts revealed HER activity for

the first time with an ultra-low overpotential (29 mV at 10 mA cm⁻²), comparable to that of commercially available noble-metal-based electrodes.

STATEMENTS OF DEFENCE

- The electrochemical deposition method using the Dynamic Hydrogen Bubble Template (DHBT) technique enables the deposition of binary and ternary electrocatalysts with various compositions onto Ti substrates.
- Electrochemically deposited 3D electrocatalysts exhibit a high electrochemically active surface area (ECSA), which exceeds their geometric area by more than 100 times, resulting in significantly enhanced catalytic activity, particularly for the Hydrogen Evolution Reaction (HER).
- The optimized binary HER and OER electrocatalysts synthesized via the DHBT method were employed as the cathode and anode, respectively and demonstrate efficient overall alkaline seawater splitting performance superior to the noble metal-based electrolyzer system.
- All optimized electrocatalysts maintained long-term stability during electrolysis under harsh seawater conditions, without significant potential fluctuations and with negligible current density decay, confirming their structural integrity and practical applicability in sustainable hydrogen production.

CONTRIBUTIONS OF THE AUTHOR

The author of this dissertation formulated all of the electroplating bath solutions and investigated electrolytes, fabricated binder-free self-supported coatings (herein 3D electrocatalysts and catalyst-samples) by electrochemical deposition on Ti (titanium) substrate. The author was responsible for preparing samples for characterization by SEM and ICP-OES. The author of this dissertation performed all of the electrochemical analysis reported in this work to evaluate the HER, OER and overall water splitting performance by LSV measurements as well as the investigations of stability by chronoamperometry and chronopotentiometry. In addition, the author conducted the data analysis, the interpretation of the results of experiments, designed their graphic illustrations and prepared all publications listed below. The author wrote this dissertation himself, with proper referencing employed for all information obtained from sources other than the original works of the author. Furthermore, the author presented the obtained results at many national and international conferences (both oral and poster presentations).

1. LITERATURE REVIEW

1.1. Hydrogen Energy – The Renewable Power Source

Harnessing clean and renewable energy to combat climate change and reduce reliance on fossil fuels, hydrogen energy has emerged as the most promising and powerful alternative. The concept of hydrogen energy as the ‘fuel of the future’ stands out for its abundance, versatility, and potential to replace traditional fossil fuels, providing a clean, sustainable, and flexible energy carrier. Approximately 80% of the world's energy is currently derived from traditional hydrocarbon-based fossil fuels, including coal, oil, and natural gas, which are the primary contributors to greenhouse gas (GHG) emissions [16]. The overconsumption of conventional fossil fuels not only aggravates environmental pollution and global warming but also hinders global energy security due to their rapid depletion and limited reserves. As a result, to address these challenges, extensive research thrusts have been placed and a surge in interest in sustainable, environmentally friendly, and alternative energy sources has been observed over the last few decades [17, 18].

Hydrogen (H_2) can be considered as one of the key emerging substitutes for fossil fuels, which can potentially serve as the most promising energy carrier due to its numerous advantages, including high gravimetric energy density, rich elemental abundance on Earth for scalability, non-toxic and clean combustion products with zero carbon footprint. Therefore, aiming for net-zero carbon emissions, hydrogen energy is increasingly viewed as a cornerstone of a renewable energy future.

More than 100 current and planned hydrogen production technologies have been reported to date, where the vast majority are focused on the steam conversion of fossil fuels, especially the natural gas steam reforming. Notably, the Steam Methane Reforming (SMR) technology is the most common and widely used method for producing hydrogen on an industrial scale but is responsible for releasing a significant amount of CO_2 and other toxic emissions and contributing to climate change. In a decarbonized world, the share of renewable energy supply must increase to mitigate the GHG footprint [19]. According to the International Energy Agency (IEA), to achieve Net-Zero Emissions (NZE) by 2050, the proportion of low-carbon hydrogen rises from 10% in 2020 to 70% in 2030 and the global hydrogen use stood at 90 Mt (million tons) in 2020 is predicted to reach above 200 Mt by 2030 [20].

According to the production route, the hydrogen cleanness level can be classified with color coding: mainly grey, brown, blue, green, and others, such as turquoise hydrogen [21-24]. Grey hydrogen is produced from fossil fuels,

and according to the World Energy Council, currently 96% of hydrogen is produced from fossil fuels via carbon-intensive processes, either through SMR of natural gas or coal gasification [25]. The production of one ton of hydrogen in this process produces about 10 tons of CO_2 . Blue hydrogen is produced from fossil fuels like grey hydrogen, but the CO_2 emitted during the production is sequestered via CCUS to mitigate emissions. Green hydrogen is the cleanest and most sustainable form of hydrogen, which is produced by electrolysis of water, while electrolysis uses only electricity from renewable energy sources such as wind, solar, or hydropower. However, brown hydrogen is produced from the gasification of black coal or lignite and releases carbon dioxide and carbon monoxide into the atmosphere, while the turquoise hydrogen is derived from the thermal decomposition of natural gas, i.e., methane pyrolysis or cracking into hydrogen and carbon at a temperature range from 600 to 1200 °C. Instead of CO_2 , this process produces black carbon (soot) as a by-product in the form of solid carbon.

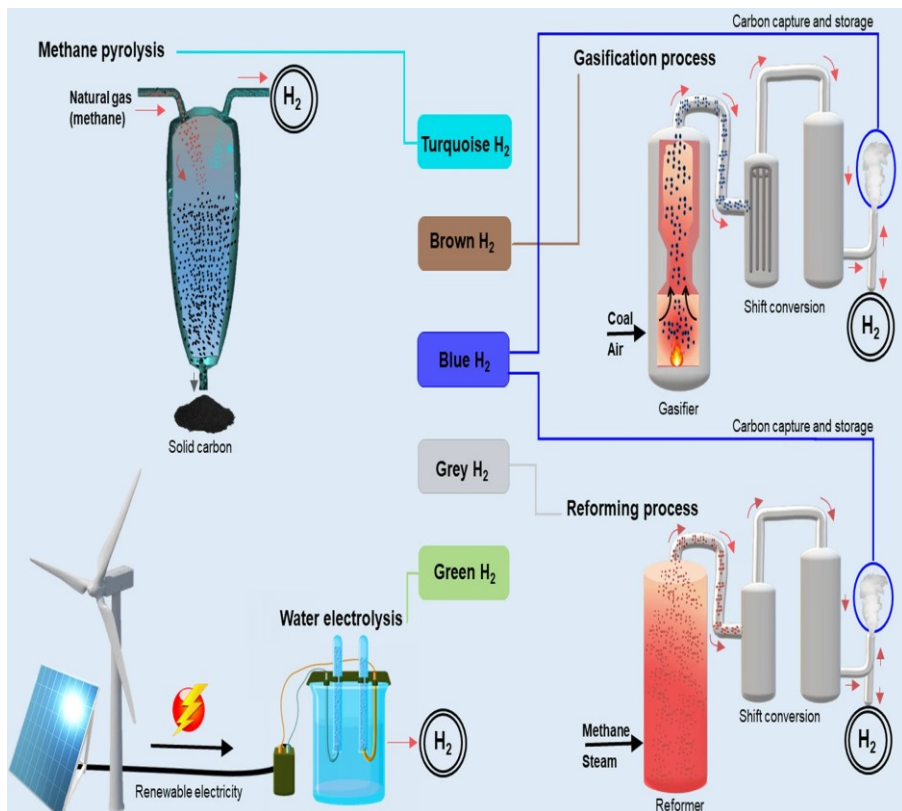


Figure 1. Schematic illustration of different hydrogen production pathways. Reprinted under the Creative Commons CC BY license from Ref. [24]

In the literature, extensive research on hydrogen production, utilization, transportation and storage has drawn tremendous attention over the last few years. The statistics on the volume of yearly published works and their associated countries/regions in the Web of Science (Clarivate Analytics) database are plotted in Fig. 2. These data are generated using “hydrogen production and storage” and “water splitting” as keywords in the website (<https://www.webofscience.com/wos/woscc/basic-search>).

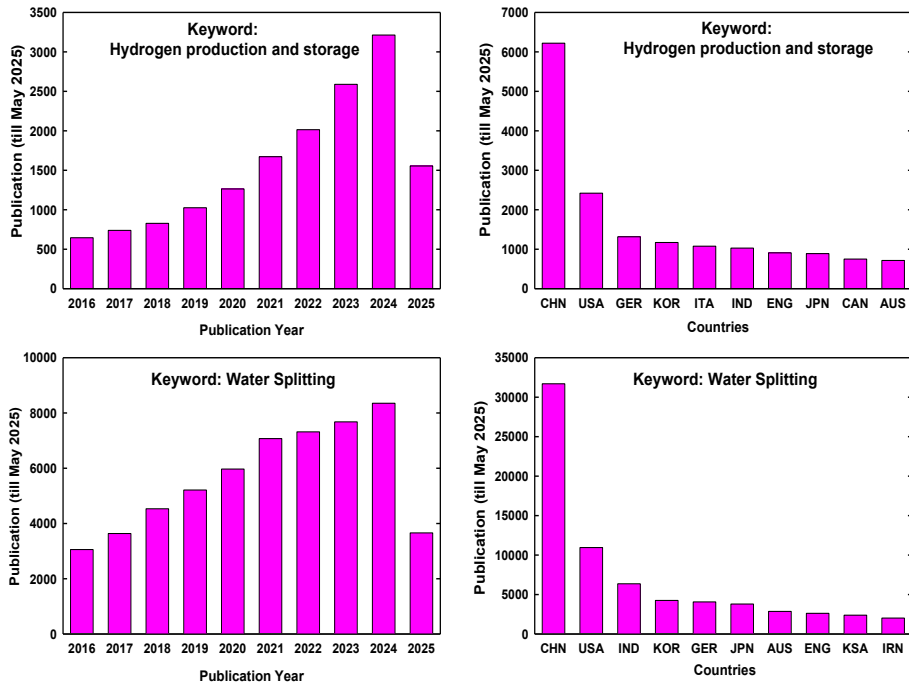
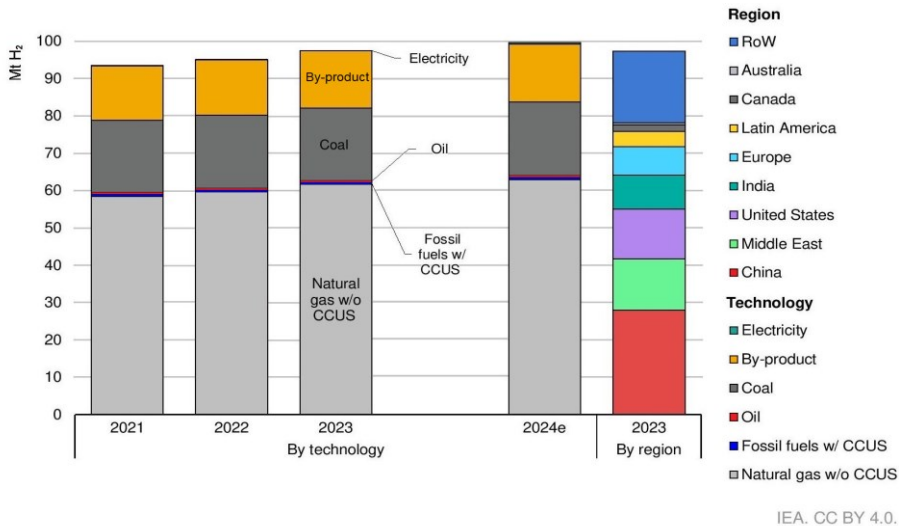


Figure 2. Number of publications per year and their associated countries as reported by Web of Science (Clarivate Analytics) via using the keywords “Hydrogen production and storage” and “Water splitting” in the search bar.

According to the IEA’s Global Hydrogen Report 2024, the annual hydrogen production reached 97 Mt (million tonnes) in 2023, practically all derived from unabated fossil fuels and the estimated global production could approach ca.100 Mt by the end of 2024. China is the largest producer of hydrogen worldwide, with almost 30% share of the total production, followed by the United States and the Middle East with 14% each [26]. Moreover, the IEA’s recent coal report states that the global coal demand is set to reach a new all-time high in 2024, particularly in Asia, where coal-fired power generation has been slow to decline [27].



Notes: By-product hydrogen from the chlor-alkali industry is not included. CCUS = carbon capture utilisation and storage; RoW = rest of world; 2024e= estimate for 2024. The estimated value for 2024 is a projection based on trends observed until June 2024.

Figure 3. Global hydrogen production by technology and by region in 2021-2024. Reprinted under the Creative Commons CC BY license from Ref. [26].

1.2. Fundamentals of electrochemical water electrolysis

Electrosynthesis of water or the electrochemical decomposition of water, i.e., water splitting, incorporates two half-reactions: i) the cathodic hydrogen evolution reaction (HER) and ii) the anodic oxygen evolution reaction OER. HER is the reaction where hydrogen (H₂) is produced via the reduction of either proton (H⁺) or H₂O at the cathode depending on the pH of the electrolyte, and the OER is the reaction where oxygen (O₂) is evolved via the oxidation of either the hydroxyl ion (OH⁻) or H₂O at the anode depending on the pH of the electrolyte. The electrocatalytic water splitting is a promising, environment-friendly and straightforward approach for industrial-scale production of hydrogen with high purity. However, the water splitting reaction is an endergonic process, i.e., the electrochemical overall water splitting under standard conditions (298 K and 1 bar pressure) is a thermodynamically unfavorable uphill reaction that requires a thermodynamic Gibbs free energy of 237 kJ mol⁻¹, corresponding to the theoretical limit of 1.23 V. However, in a real system, a standard enthalpy of 285.8 kJ, corresponding to a voltage of 1.48 V, is referred to as the thermo-neutral voltage to split liquid water into its gaseous elements [28]. Hence, to exceed this energy barrier, additional energy in the form of “overpotential” is required for the decomposition of pure water into its constituents. Moreover, the electrical conductivity of pure water is practically insignificant; thus, an electrolyte (an acid or alkali, or a salt) is

added to it, and different electrocatalysts are used to increase the efficiency of water electrolysis by minimizing the overpotential [29]. The overall water electrolysis process on the electrocatalysts' surface can be illustrated with the following schematic representation, half-cell and overall reactions occur under acidic and alkaline medium [30, 31].

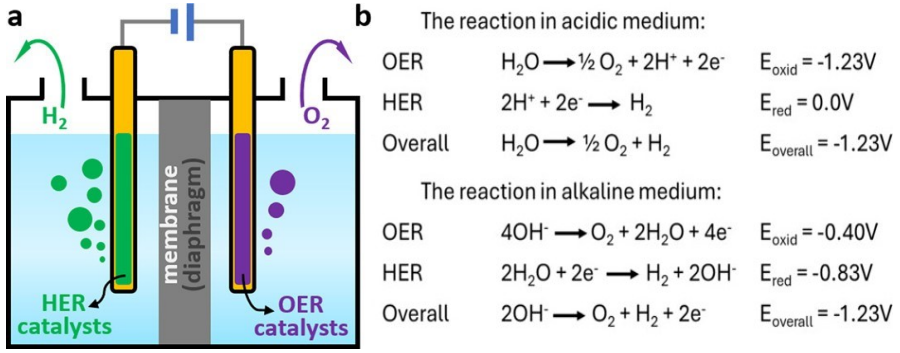


Figure 4. (a) Schematic illustration of a conventional water electrolyzer and (b) half-cell reactions of water splitting under acidic and alkaline conditions.

In brief, the cathodic HER is a key half-cell reaction that occurs via a two-electron transfer, and regardless of the pH of the solution, the electrocatalytic HER consists of two primary steps, namely hydrogen adsorption and hydrogen desorption. The adsorption step is known as the Volmer reaction, while the desorption (or evolution) takes place either by the Heyrovsky reaction (electrochemical route) or the Tafel reaction (chemical route) [32, 33]. On the contrary, the OER is a sluggish reaction involving a multistep four-electron transfer process at the anode. The four-electron transfer process involves relatively slower kinetics than HER, which is considered the rate-limiting step that constrains the efficiency of the overall water splitting process [34-36]. In an acidic environment, liquid water is oxidized into hydrogen and oxygen, while in an alkaline or neutral medium, the hydroxyl ions are oxidized as oxygen and water. The OER kinetics and reaction pathways depend entirely on the material by which the reaction is catalysed. The reaction mechanisms and efficiency of reactions are subject to electrolytes and electrocatalysts used [33, 37]. For instance, Ir and Ru-based electrocatalysts perform efficiently in acidic than in alkaline medium, whereas non-noble metals like iron (Fe), nickel (Ni) and cobalt (Co) based catalysts show superior OER activity in alkaline medium [38-41]. Despite several reported multi-step OER mechanisms [33], common reaction intermediates such as *oxo* (*O), *peroxo* (*OOH), and *hydroxo* (*OH) species are produced and adsorbed on the catalyst surface. Therefore, overcoming the sluggish OER

kinetics is the main technical bottleneck for sustainable electrochemical water electrolysis and the production and commercialization of green hydrogen from electrocatalytic water splitting.

1.3. Seawater electrolysis – The most sustainable approach

Seawater electrolysis has emerged as a promising, more viable and sustainable alternative compared to freshwater electrolysis since 1975, when it was first realized that seawater can be directly used to produce hydrogen.

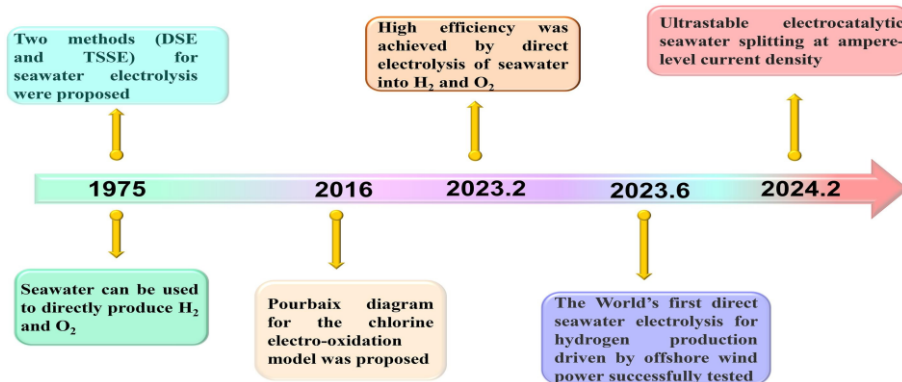
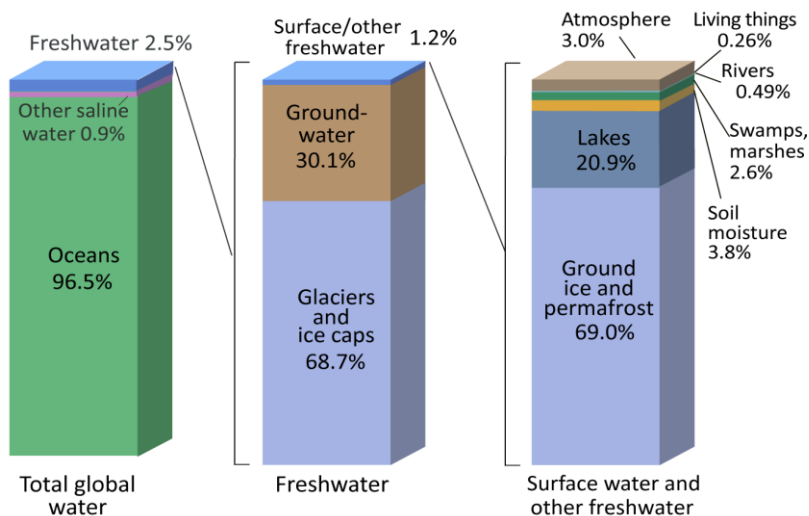


Figure 5. A brief timeline of the development of seawater electrolysis. DSE – direct seawater electrolysis; TSSE – two-step seawater electrolysis. Reprinted with permission from Ref. [42].

In the current energy landscape, water splitting plays a significant role and provides a solid foundation for the transformation into a green and sustainable world to complete the low-carbon transition and realize the goal of NZE. However, hydrogen production consumes about 1.5 billion cubic metres (m^3) of freshwater to date, representing less than 5% of the energy sector's total water consumption. The electrolysis process requires about 10 litres of water to produce 1 kilogram of hydrogen ($1/kg H_2$) as feedstock and a total of 30-70 $l/kg H_2$ as feedstock and cooling together, depending on the electrolyser technology and the local climate conditions [26]. But freshwater resources are scarce and unevenly distributed worldwide; thus, the limited availability and shortage crisis of surface water creates a barrier to freshwater electrolysis. Many countries across the world, including Jordan, Yemen, Kuwait, Libya, Israel, Palestine, Tunisia, Algeria, and sub-Saharan countries in the Middle East are facing a terrible shortfall of freshwater for their livelihood, making the real-life scenario nearly impossible to electrolyze vital freshwater for hydrogen production [43-45].

Water covers 70% of the total surface on Earth, while the oceanic seawater constitutes approximately 97.5% of the total water reserves, and only about 2.5% is freshwater. According to the U.S. Geological Survey and other reports, nearly two-thirds of these freshwater resources are either frozen in glaciers or otherwise unavailable for humans to utilize [46-48].



Credit: U.S. Geological Survey, Water Science School. <https://www.usgs.gov/special-topic/water-science-school>
 Data source: Igor Shiklomanov's chapter "World fresh water resources" in Peter H. Gleick (editor), 1993, *Water in Crisis: A Guide to the World's Fresh Water Resources*. (Numbers are rounded).

Figure 6. The distribution of water on, in, and above the Earth from Ref [49].

Direct seawater electrolysis (DSE) technology can mitigate the critical burden on vital freshwater resources by using abundant saline water as an electrolyte. Despite its potential benefits, the DSE poses significant challenges for the large-scale production of hydrogen and limits the efficiency of the electrolyzer system. At first, the presence of corrosive chloride ions (Cl^-), as well as other various unwanted ionic species, including Ca^{2+} , Mg^{2+} , Na^+ , Br^- , and SO_4^{2-} , adversely affects the performance of electrolyzers and catalytic activity of the electrocatalyst [50-57]. The natural presence of aggressive Cl^- ions degenerate low current efficiency by the chlorine evolution reaction (CIER) in the anode, competing with OER. Besides, the CIER could turn into the most critical encounter in the seawater splitting process, as aggressive hypochlorite (ClO^-) species form during the reaction can become a detrimental threat to contaminate the electrolyte environment. Moreover, the formation of insoluble precipitates, e.g., $\text{Ca}(\text{OH})_2$ and $\text{Mg}(\text{OH})_2$, on the electrode surface blocks the active sites and hinders the long-term durability of electrocatalysts, thereby shortening the lifespan of the electrolyzer.

Furthermore, microorganisms and small particles present in seawater lead to the poisoning of catalytic active sites, corrosion, surface deactivation or passivation of the electrodes, and thus, significantly affect the catalytic performance and durability of electrocatalysts, subsequently affecting the ultimate commercialization prospect of seawater splitting [58-63].

Hence, considering the scarcity of freshwater and its widespread daily use, abundant seawater is the most promising substitute as feedstock for the industrial-scale production of high-purity hydrogen.

1.4. Electrocatalysts – The ultimate armour

Despite the availability of plentiful natural seawater resources, the high costs of green hydrogen energy still remain a substantial hindrance to its far-reaching adoption due to the inherent costs associated with the hydrogen production. According to the International Renewable Energy Agency (IRENA), at present, the production of green hydrogen costs two to three times more than blue hydrogen, on average [64]. Referring to the European Commission's July 2020 hydrogen strategy, the estimated costs for the conventional fossil-based hydrogen are around 1.5 €/kg for the EU, whereas the estimated costs for fossil-based hydrogen using CCUS are approx. 2 €/kg, and renewable hydrogen are between 2.5-5.5 €/kg [65]. Under the 1.5 °C Scenario by IRENA (2021), hydrogen and its derivatives will account for 12% of final energy use by 2050 and to reach the milestone, some 5000 GW (gigawatts, 10^9 Watts) of electrolyzer capacity will be required by 2050, up from just 0.3 GW today [66]. According to BP's statistical review (2021) [67], the total global renewable energy (solar, wind, hydro energy etc.) consumption increased from 28.82 EJ (Exajoule, 10^{18} Joules) in 2019 to 31.71 EJ in 2020 and to achieve the 1.5 °C Scenario in 2050, the total demand for hydrogen-based fuels would need to grow to 15 exajoules (EJ) and 63 EJ by 2030 and 2050, respectively [68]. To meet these statistical data from several Energy Outlooks, policy support and global investments are the most crucial factors for the rapid expansion of both renewable power and electrolyzer capacity. In the recent past, the U.S. Department of Energy (DOE) not only unveiled the *Updated Hydrogen Program Plan* and *National Hydrogen Strategy and Roadmap* but also launched the *Hydrogen Shot* program to restrain the cost of clean hydrogen to \$1 per kilogram within a decade [69-71].

Green hydrogen production through water splitting is still in its infancy, and the integrated production cost is considered as the main barrier to the energy transition. However, the elevated cost of electrocatalytic freshwater/seawater splitting is attributed to the electrodes used in the water electrolyzers. The state-of-the-art platinum group metal (PGM) catalysts demonstrate outstanding electrocatalytic activity for water splitting, while Pt-based catalysts are the commercially used electrocatalysts for HER [12, 13, 72, 73], and Ru or Ir-oxide based electrocatalysts exhibit the most efficient performance for OER [74-76]. Unfortunately, despite their effectiveness, the limited availability and high costs of precious PGM electrocatalysts restrict the widespread application in industrial-scale electrolysis technologies. Therefore, extensive efforts have been dedicated towards earth-abundant, inexpensive, non-noble transition metals to design, develop and synthesize low-cost, highly efficient and durable electrocatalysts with potential to reduce the energy barriers in HER/OER and overall water splitting processes.

To find potential substitutes, the use of non-noble transition metal-based catalysts has received tremendous attention in recent years and various transition metal-based materials, including transition-metal-based oxides [77-79], sulfides [80, 81], nitrides [82, 83], phosphides [84, 85], hydroxides and LDHs [86-88], alloys [89, 90], MOFs [91, 92], MXenes [93] etc. have emerged as alternative potential candidates to replace precious PGM catalysts for HER, OER and overall water splitting applications. The key criteria of non-noble transition metals for designing and screening as electrocatalytic materials over PGMs are:

- i) Moderate binding energy for adsorption of intermediates (according to the Sabatier Principle).
- ii) Good electrical conductivity for efficient charge transfer during electrolysis.
- iii) Superior stability under acidic or alkaline operating conditions.
- iv) Electronic structure tuneability via alloying or doping.
- v) Abundant and low-cost for practical and scalable applications.

Different state-of-the-art procedures, methods, and sophisticated engineering techniques are followed and applied to enhance electrocatalytic performance via inducing electronic and structural modification strategies during the fabrication of efficient, purpose-oriented HER, OER and(or) bifunctional electrocatalysts.

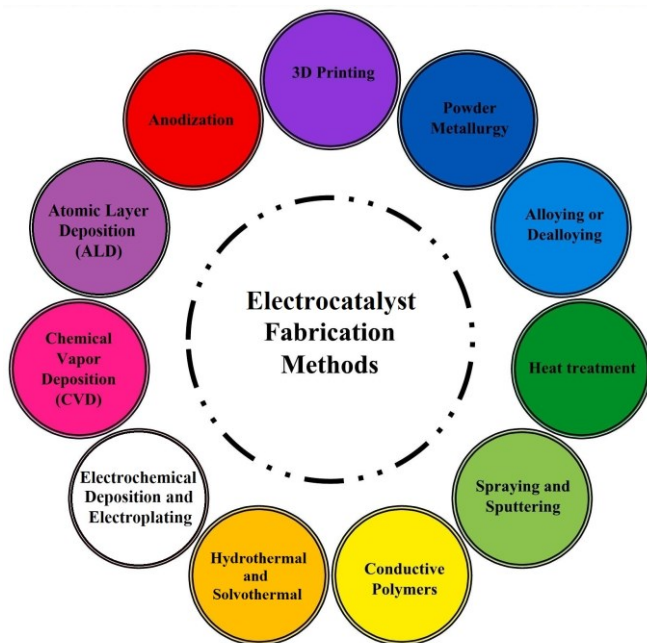


Figure 7. The fabrication methods of electrocatalysts for water splitting. Reprinted with permission from Ref. [94].

Among the abovementioned fabrication methods, the electrodeposition method (or electroplating) is a widely used technique for synthesizing electrodes. Fabricated catalysts by this procedure demonstrate several superior and exceptional advantages over others as follows [95-100]:

- i) Simple, low-cost and scalable method with large-scale and batch processing, ideal for industrial applications.
- ii) Precise control ability over the thickness and microstructure (e.g., roughness, porosity) of the deposited layer by adjusting deposition parameters (e.g., current density, deposition potential, deposition time, precursor concentration and electrolyte composition).
- iii) Energy-efficient and compatible with heat-sensitive materials, as performed at or near room temperature.
- iv) Large electrochemically active surface area (ECSA) with uniform coverage on 3D surfaces and porous structures.
- v) Versatile and a wide variety of substrates, e.g., metals, metal oxides, alloys, and conducting polymers can be used for electroplating.

Over and above, the electrodeposition method using dynamic hydrogen bubble template (DHBT) technique is one of the well-known, widely used promising approaches due to its facile, cost-effective, time-saving, controllable and binder-free technology [101,102]. Fabricated electrocatalyst with high surface area is pivotal for enhancing the exposure of active sites and facilitating efficient mass transport. This is where the DHBT technique plays a significant role. The noble DHBT technique is a powerful strategy for improving the performance of synthesized electrocatalysts via creating porous structures with high surface areas through surface defects, doping, morphology regulation, catalyst anchoring, and interface heterostructure engineering [103-107]. This unique technique operates through a dynamic interplay of hydrogen evolution during electrochemical deposition, generating a porous morphology on the substrate surface. The key principle is the use of hydrogen bubbles formed during electrolysis as a template to introduce controlled porosity. This technique utilizes in situ generated H_2 bubbles as dynamic templates and as soon as the catalytic components are deposited, hydrogen bubbles evolve at the electrode surface due to the electrochemical reduction of protons or water as shown in the following equations [108]. The electrochemical deposition method using the dynamic hydrogen bubble template (DHBT) technique is illustrated with a graphical representation below.

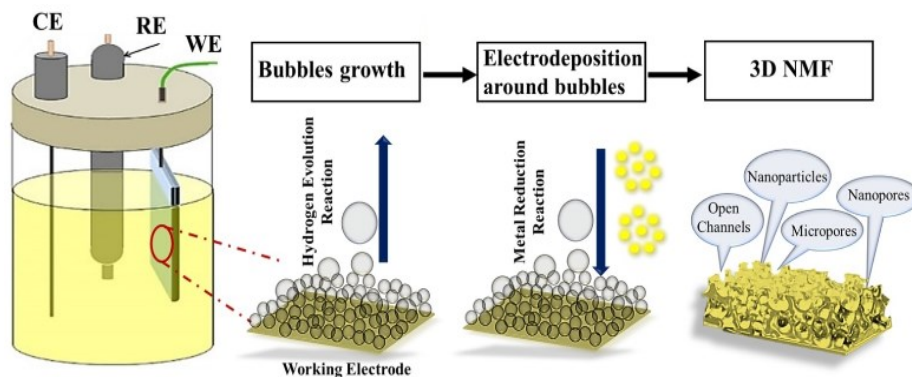
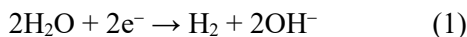


Figure 8. Graphical representation of electrocatalyst synthesis using the DHBT technique. NMF – Nanoporous Metal Foam. Reprinted with permission from Ref. [109].

2. MATERIALS AND METHODS

2.1. Materials and chemicals

All chemicals used were of analytical grade and used as-received unless stated otherwise. The natural seawater was collected from the Baltic Sea coastline (Klaipėda seashore region, Lithuania, 55°42'45" N, 21°08'06" E). The main chemicals and materials used in this research are provided in Table 1.

Table 1. Materials and reagents used for the experiments in this work.

Material	Formula	Purity	Source
Stainless steel foil (0.2 mm)	-	-	Alfa Aesar (Germany)
Titanium foil (0.127 mm)	Ti	99.7%	Sigma-Aldrich (USA)
Nickel sulfate hexahydrate	NiSO ₄ ·6H ₂ O	>98%	Chempur Company (Germany)
Sodium molybdate dihydrate	Na ₂ MoO ₄ ·2H ₂ O	>99.5%	
Manganese chloride tetrahydrate	MnCl ₂ ·4H ₂ O	>99%	
Cobalt nitrate hexahydrate	Co(NO ₃) ₂ ·6H ₂ O	>98%	
Sulfuric acid	H ₂ SO ₄	96%	
Hydrochloric acid	HCl	35-38%	
Sodium hydroxide	NaOH	98.8%	
Potassium hydroxide	KOH	85%	
Ammonium sulfate	(NH ₄) ₂ SO ₄	99%	
Boric acid	H ₃ BO ₃	99.5%	

2.2. Substrate preparation

Before fabrication of each electrode, the Ti substrates were cut from Ti foil with a size being 1×1 cm (electrochemical measurements and structural characterization). After cutting, the surface of the substrates was sanded to 1000 grit and degreased with ethanol to remove the native surface oxide layer. Afterwards, the Ti plates were thoroughly rinsed with deionized water (DI), followed by their activation via pretreatment in diluted H₂SO₄ (1:1 vol.) for 10 s at 70 °C and repeating the rinsing with deionized water.

2.3. Fabrication of 3D binary NiMo/Ti electrocatalysts

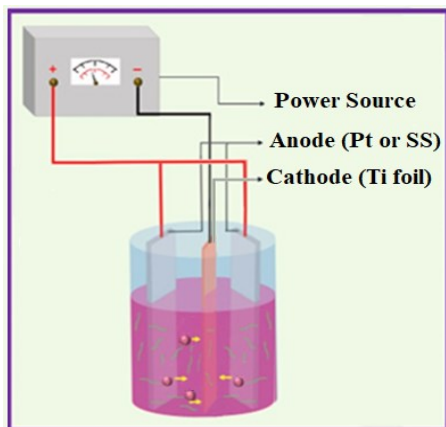


Figure 9. Schematic representation of the one-step electrodeposition process for the fabrication of binary and ternary electrodes investigated in this research.

To synthesize 3D binary NiMo/Ti electrocatalysts by electrochemical deposition through a dynamic hydrogen bubble template (DHBT) technique, electroplating solution baths were formulated as detailed in Table 2.

Table 2. The composition of the electrochemical baths and electroplating condition parameters.

Catalysts	Concentration (M)			Plating conditions		
	Ni ²⁺ _(aq)	Mo ⁶⁺ _(aq)	pH*	T, (°C)	<i>j</i> , (mA cm ⁻²)	<i>t</i> , (min)
NiMo/Ti-1	0.1	0.03	~1	25	50**	3
					500***	3
NiMo/Ti-2	0.2	0.03	~1	25	50**	3
					500***	3
NiMo/Ti-3	1.0	0.03	~1	25	50**	3
					500***	3

* 1.5 M H₂SO₄ and 1 M HCl

Current densities applied during 1st step** and 2nd step*** of electrodeposition

2.4. Fabrication of 3D binary NiMn/Ti electrocatalysts

The fabrication of 3D NiMn/Ti electrocatalysts was also carried out under the same plating conditions described above. Key differences were:

i) The concentration of Ni²⁺ ion was constant (0.2 M) with variable ionic concentrations (from 0.2 M up to 1.0 M) of Mn²⁺.

ii) 0.5 M of $(\text{NH}_4)_2\text{SO}_4$ was added as a modifier of the coating morphology and 0.3 M boric acid (H_3BO_3) was used as a pH stabilizer additionally during the preparation of each solution bath. The formulation of chemical bath solutions and plating conditions are given in Table 3.

Table 3. The composition of the electrochemical baths and electroplating condition parameters.

Catalysts	Concentration (M)				Plating conditions			
	$\text{Ni}^{2+}_{(\text{aq})}$	$\text{Mn}^{2+}_{(\text{aq})}$	$(\text{NH}_4)_2\text{SO}_4$	H_3BO_3	pH*	T, (°C)	j, (mA cm^{-2})	t, (min)
Ni/Ti	0.2	-	0.5	0.3	~1	25	50** 500***	3 3
Mn/Ti	-	1.0	0.5	0.3	~1	25	50** 500***	3 3
NiMn/Ti-1	0.2	0.2	0.5	0.3	~1	25	50** 500***	3 3
NiMn/Ti-2	0.2	0.4	0.5	0.3	~1	25	50** 500***	3 3
NiMn/Ti-3	0.2	0.6	0.5	0.3	~1	25	50** 500***	3 3
NiMn/Ti-4	0.2	0.8	0.5	0.3	~1	25	50** 500***	3 3
NiMn/Ti-5	0.2	1.0	0.5	0.3	~1	25	50** 500***	3 3

* 1.5 M H_2SO_4 and 1 M HCl

Current densities applied during 1st step** and 2nd step*** of electrodeposition

2.5. Fabrication of 3D ternary NiMnCo/Ti electrocatalysts

Fabrication and investigative analysis were carried out for efficient non-noble transition metal-based electrodes for green hydrogen production, where a noble 3D ternary NiMnCo/Ti electrocatalysts were synthesized with variable concentrations of cobalt (Co). Two key differences were:

i) an increase in concentration of pH stabilizer (H_3BO_3) in the solution baths

ii) changes in applied current densities and deposition timing. Detailed compositions and plating conditions are summarized in Table 4 below.

Table 4. The composition of the electrochemical baths and electroplating condition parameters.

Catalysts	Concentration (M)				Plating conditions				
	Ni ²⁺ (aq)	Mn ²⁺ (aq)	Co ²⁺ (aq)	(NH ₄) ₂ SO ₄	H ₃ BO ₃	pH*	T, (°C)	j, (mA cm ⁻²)	t, (min)
NiMn/Ti	0.2	1.0	-	0.5	0.5	~1	25	50** 100***	10 5
NiCo/Ti	0.2	-	0.2	0.5	0.5	~1	25	50** 100***	10 5
NiMnCo/Ti-1	0.2	1.0	0.1	0.5	0.5	~1	25	50** 100***	10 5
NiMnCo/Ti-2	0.2	1.0	0.2	0.5	0.5	~1	25	50** 100***	10 5

* 1.5 M H_2SO_4 and 1 M HCl

Current densities applied during 1st step** and 2nd step*** of electrodeposition

Moreover, a few monometallic and bimetallic catalyst-samples were also fabricated alongside for the comparison of activity using the same additives and unaltered plating conditions. After electroplating, all synthesized electrocatalysts and catalyst-samples were removed, thoroughly rinsed with deionized water, air-dried at room temperature, marked and carefully stored for subsequent investigations.

2.6. Electrochemical measurements

The electrochemical investigations have been performed to determine the electrocatalytic HER, OER and overall water splitting (OWS) performance via linear sweep voltammetry (LSV) using a computer-controlled potentiostat PGSTAT302 equipped with the Electrochemical Software (Nova 2.1.4, Metrohm Autolab B.V., Utrecht, The Netherlands). A standard three-electrode cell was used for all electrochemical measurements, with the fabricated electrode of a geometric area of 2 cm² as a working electrode, a saturated calomel electrode (SCE) used as a reference electrode, and a graphite rod used as a counter electrode. All applied potentials in the three-electrode system corresponding to SCE were calibrated to the reversible hydrogen electrode (RHE) unless stated otherwise by using the following equation:

$$E_{\text{RHE}} = E_{\text{SCE}} + 0.242 \text{ V} + 0.059 \text{ V} \times \text{pH}_{\text{solution}} \quad (3)$$

The electrolyte used in electrochemical measurements described in this work was initially a 1.0 M NaOH solution as an alkaline medium. Afterwards, 1.0 M KOH solution was used as the alkaline environment in all performed electrochemical investigations. Moreover, this research work has been extended and diversified using artificial (simulated) seawater and alkaline natural seawater for HER, OER and OWS investigations. Prior to every measurement, the working electrolyte was deaerated with argon (Ar) in a set-up cell for 20 min.

The electrocatalytic activity of the synthesized electrodes was investigated by Linear Sweep Voltammetry. The catalytic performance for HER and OER of all fabricated electrodes was evaluated by recording LSV polarization curves at a temperature range from 25 °C to 75 °C. The LSVs were recorded from the open circuit potential (OCP) to -0.43 V (vs. RHE) for HER at a potential scan rate of 10 mV s⁻¹. For OER activity measurements, the selected potential region was OCP to 2.06 V (vs. RHE) at the same scan rate. The OWS performance was evaluated in a two-electrode cell using alkaline seawater where two optimal 3D binary NiMn/Ti electrocatalysts were employed as anode and cathode and the LSVs were recorded in a selected

voltage region from 1.0 V up to 2.6 V at a potential scan rate of 10 mV s⁻¹. The electrochemically active surface area (ECSA) of the optimized 3D NiMnCo/Ti-2 electrocatalyst was determined from the measurements of double layer capacitance (C_{dl}) by recording CV curves in the 1.0 M KOH solution at several scan rates (5-50 mV s⁻¹) in the non-faradaic region [110].

Moreover, the long-term stability of the fabricated optimized electrocatalysts was evaluated by recording the chronoamperometry (CA) curves at a constant potential of -0.23 V (vs. RHE) and 1.81 V (vs. RHE) for HER and OER, respectively along with chronopotentiometric (CP) measurements at a constant current density of 10 mA cm⁻² for both reactions. A multi-step chronopotentiometric analysis was also conducted with variable current densities ranging from 20 mA cm⁻² to 100 mA cm⁻² to assess the robustness and exceptional stability of the optimized 3D NiMnCo/Ti-2 electrode as an outstanding HER electrocatalyst, in a gradual ascending-descending order.

2.7. Characterization of synthesized binary and ternary electrocatalysts

Scanning electron microscopy. The microstructure and surface morphology of synthesized binary and ternary electrocatalysts were investigated using a Helios TM4000Plus scanning electron microscope (Hitachi, Tokyo, Japan) equipped with an energy dispersive X-ray spectrometer (AZtecOne detector, Oxford Instruments, United Kingdom). The microspherical surface morphology of the optimized ternary electrocatalyst was examined and the size (diameter) of the deposited particles was measured using the ImageJ desktop application.

Inductively Coupled Plasma Optical Emission Spectroscopy. The metal loadings of fabricated binary and ternary electrocatalysts were identified using an Optima 7000DV inductively coupled plasma optical emission spectrometer (Perkin Elmer, Waltham, MA, USA). ICP-OES spectra were collected at these reported wavelengths:

$$\lambda_{Ni} \text{ 231.604 nm, } \lambda_{Mn} \text{ 202.031 nm, } \lambda_{Co} \text{ 257.610 nm and } \lambda_{Co} \text{ 228.616 nm.}$$

3. RESULTS AND DISCUSSION

3.1. Synthesis and characterization of 3D NiMo/Ti electrocatalysts

3.1.1. Morphology of 3D NiMo/Ti electrocatalysts

The topside scanning electron microscopy (SEM) images of the electrochemically deposited 3D binary NiMo/Ti electrocatalysts are demonstrated in Figure 10. The surface morphologies of synthesized 3D NiMo/Ti-1 and NiMo/Ti-2 (Fig. 10a, b) electrocatalysts were not significant enough, although the substrate surface was uniformly covered with crack-free, smooth and evenly dispersed Ni and Mo particles.

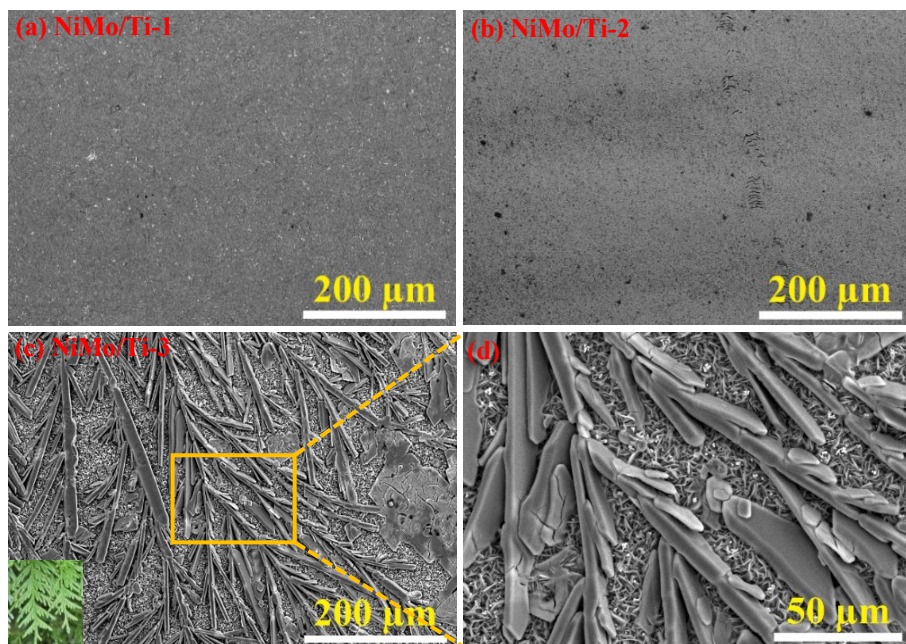


Figure 10. SEM images of fabricated 3D NiMo/Ti-1 (a), NiMo/Ti-2 (b) and NiMo/Ti-3 (c) electrocatalysts and the optimal 3D NiMo/Ti-3 electrode with higher magnification (d). The inset shows an image of cedar leaves.

The NiMo/Ti-3 electrocatalyst with comparably higher Ni^{2+} ion (1.0 M) concentration forms a unique cedar leaf-like structure, which covers the entire Ti substrate surface (Fig. 10c). Those leaf-like Ni-Mo architectures with higher magnification (Fig. 10d) portray an irregular stack of well-defined, randomly distributed microstructures of discrete sizes and shapes.

The mass of the elements (metal loadings) on the Ti substrate was determined by ICP-OES analysis.

The Ni metal loadings in NiMo/Ti-1 and NiMo/Ti-2 electrodes were proximate to one another as a function of the adjacent $\text{Ni}^{2+}:\text{Mo}^{6+}$ ratio of bath solutions (Table 2), whereas the NiMo/Ti-3 electrocatalyst has a higher Ni-loading. The synthesized 3D binary NiMo/Ti electrocatalysts contained ca. 82.8-93.7 wt.% of Ni and 17.2-6.3 wt.% of Mo. The Mo-loadings in all three fabricated electrodes were analogous due to the constant ionic concentration (0.03 M) of Mo^{6+} in the bath solutions.

3.1.2. Electrocatalytic investigations of 3D NiMo/Ti catalysts for HER and OER performance

The electrocatalytic activity of synthesized NiMo/Ti electrodes was investigated by Linear Sweep Voltammetry in an Ar-saturated 1.0 M NaOH as alkaline electrolyte at 25 °C. The optimized NiMo/Ti-3 electrocatalyst fabricated from the bath solution with higher Ni-content (1.0 M), exhibits enhanced HER activity with a minimum overpotential of 288 mV to gain the benchmark current density of 10 mA cm^{-2} in alkaline electrolyte. For OER, the NiMo/Ti-3 electrocatalyst demonstrates a modest overpotential of 580 mV. The recorded anodic and cathodic LSVs of fabricated 3D NiMo/Ti electrocatalysts were used to extract the corresponding Tafel plots simultaneously for HER and OER. The Tafel slope values for NiMo/Ti-1, NiMo/Ti-2, and NiMo/Ti-3 electrocatalysts were 100, 101, and 130 mV dec^{-1} for HER and for OER polarization curves, the obtained Tafel slope values were 167, 93 and 169 mV dec^{-1} , respectively. The stability of the optimized NiMo/Ti-3 electrocatalyst was evaluated via chronoamperometric (CA) measurement at -0.23 V (vs. RHE) for HER for 2 hours. Moreover, the CA investigation was carried out with the same time span at a constant potential of 1.81 V (vs. RHE) to evaluate the durability for OER analysis. The recorded voltammograms along with other results are demonstrated and listed in Fig. 11 and Table 5.

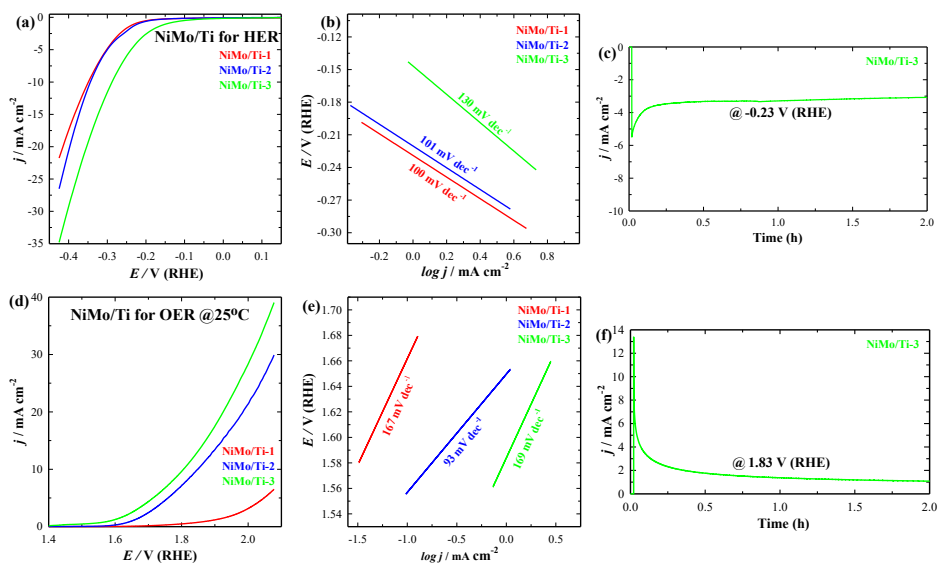


Figure 11. HER (a) and OER (d) polarization curves of 3D NiMo/Ti catalysts in 1.0 M NaOH at 25 °C and a potential scan rate of 10 mV s⁻¹ with corresponding extracted Tafel plots (b, e) and the chronoamperometric curves (c, f) of the optimized NiMo/Ti-3 electrocatalyst at constant potentials.

Table 5. Summarized electrochemical data of the investigated 3D NiMo/Ti electrocatalysts toward HER and OER in 1.0 M NaOH.

	Catalysts	Current density (mA cm ⁻²) at 25 °C		η_{10} (mV) at 25 °C	Tafel slope (mV dec ⁻¹)
		-0.43 V (RHE)	2.06 V (RHE)		
HER	NiMo/Ti-1	21.75	-	349	99.6
	NiMo/Ti-2	26.5	-	344	100.5
	NiMo/Ti-3	34.81	-	288	130.4
OER	NiMo/Ti-1	-	6.52	-	167
	NiMo/Ti-2	-	29.91	620	93
	NiMo/Ti-3	-	39.05	580	169

3.2. Synthesis and characterization of 3D NiMn/Ti electrocatalysts

3.2.1. Microstructure and morphology of 3D NiMn/Ti electrocatalysts

3D nickel-manganese (NiMn) binary coatings were fabricated via the electrodeposition method using the DHBT technique and to synthesize an enhanced and efficient bifunctional electrocatalyst with favorable surface morphology, two additives namely (NH₄)₂SO₄ and boric acid (H₃BO₃), were

used as modifier of the coating morphology and pH stabilizer, respectively. The synthesized 3D NiMn/Ti electrocatalysts are demonstrated in Fig. 12.

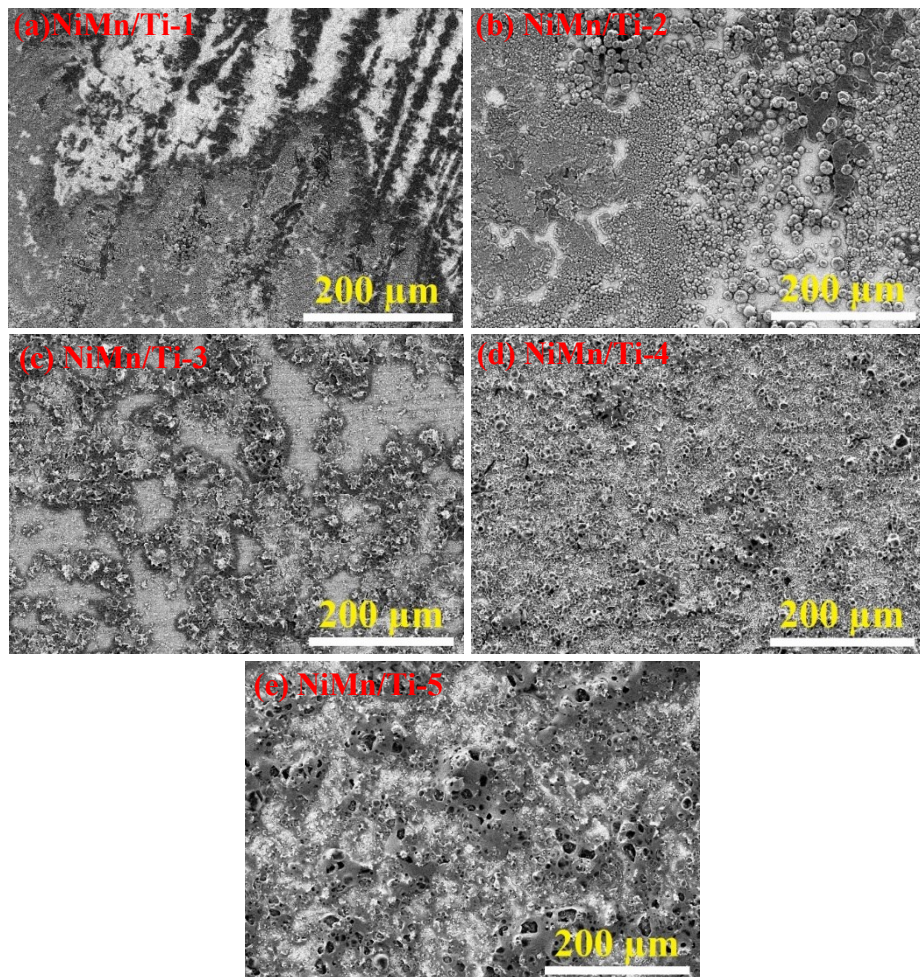


Figure 12. SEM images of fabricated binary 3D NiMn/Ti (a-e), electrocatalysts via the electrochemical deposition method using the DHBT technique.

From the SEM images, it can be seen that the five NiMn/Ti electrocatalysts fabricated with variable manganese concentrations (0.2 M to 1.0 M) exhibit different unique surface morphology. The synthesized electrocatalysts were denominated as NiMn/Ti- n ($n = 1, 2, 3, 4$ and 5), according to the composition of $\text{Ni}^{2+}:\text{Mn}^{2+}$ molar ratios in the solution baths (e.g., NiMn/Ti-1 and NiMn/Ti-5 electrodes were electrodeposited from the bath solutions with $\text{Ni}^{2+}:\text{Mn}^{2+}$ molar ratios of 1:1 and 1:5, respectively). As-

synthesized NiMn/Ti-1 catalyst demonstrates a typical globular morphology with smaller nodules, covering the substrate surface, as demonstrated in Fig. 12a. The tiny nodules enlarged to micro-sized in the case of NiMn/Ti-2 electrode with an increase of Mn-content ($\text{Ni}^{2+}:\text{Mn}^{2+} = 1:2$) in the plating solution. The top side view of NiMn/Ti-3 catalyst exhibits an uneven, coarse, flake-like heterostructured surface morphology, as shown in Fig. 12c. It is noteworthy that the higher cell voltages were recorded during the electrodeposition using bath solutions with higher $\text{Ni}^{2+}:\text{Mn}^{2+}$ molar ratios. Moreover, as the NiMn coatings were deposited under acidic conditions to ensure the generation of vigorous hydrogen bubbles, the formation of bubbles during electroplating was also successively escalating. As a consequence of those above factors, this can be anticipated that the number of deposited Ni and Mn particles started to agglomerate on the Titanium substrate by forming smaller mounds or humps-like structures while the electroplating of binary NiMn/Ti-4 catalyst was conducted. Finally, the surface morphology of NiMn/Ti-5 electrocatalyst has turned into a unique micro-sized porous architecture with an abundance of pores with distinctly different sizes via applying the dynamic hydrogen bubble template technique. As exhibited in Fig. 12e, the presence of infinite pores of different sizes on the synthesized NiMn/Ti-5 electrocatalyst will facilitate the creation of more channels for electrolyte diffusion, accelerate the efficiency of electron transport and enhance the number of active sites.

The mass of the elements (metal loadings) on the Ti substrate was determined by ICP-OES analysis.

Fabricated 3D binary NiMn/Ti electrocatalysts possessed Ni content of ca. 44-86.6 wt.% and Mn-loading of ca. 13.4-56 wt.%. The total metal loadings ($\mu\text{g}_{\text{metal}}\text{cm}^{-2}$) on the synthesized electrocatalysts have gradually increased with the increase of Mn-concentration in the bath solutions and varied from ca. 100 up to 1223.5 $\mu\text{g}_{\text{metal}}\text{cm}^{-2}$.

3.2.2. Electrocatalytic activity of 3D NiMn/Ti electrocatalysts for HER

The electrocatalytic activity of synthesized 3D NiMn/Ti electrocatalysts was investigated for HER by recording LSVs in 1.0 M KOH solution, simulated seawater (1.0 M KOH + 0.5 M NaCl, $\text{pH} \approx 14$) and alkaline seawater (1.0 M KOH + natural seawater, $\text{pH} \approx 13.9$) at 25 °C. To check the repeatability, each electrode was prepared three times and the LSVs were recorded for each electrode. Fabricated 3D NiMn/Ti-5 electrocatalyst with the highest Mn-content (i.e., metal-loading) exhibits the outstanding HER activity among all

electrodes in these investigating electrolytes. The optimized NiMn/Ti-5 electrocatalyst exhibits enhanced HER activity with a minimum overpotential of 127 mV to gain the benchmark current density of 10 mA cm⁻² in alkaline electrolyte, which was superior to those of 145 mV and 150 mV for the NiMn/Ti-4 and NiMn/Ti-3 electrodes, respectively. In addition, the natural seawater collected from the Baltic Sea near the Klaipėda seashore region has been used to formulate the alkaline seawater and the LSV analysis was conducted using the electrochemically deposited optimized NiMn/Ti-5 electrocatalyst. An exceptional HER performance was demonstrated by the 3D NiMn/Ti-5 electrocatalyst in chlorine and other impurity-rich alkaline seawater, outperforming the activity in alkaline media, where a least overpotential of 79 mV was required to achieve a current density of 10 mA cm⁻². Impressively, to attain this benchmark current density, an ultra-low overpotential of 64 mV was required for this optimized NiMn/Ti-5 electrocatalyst in simulated seawater, where the natural seawater was substituted with deionized water, maintaining the approximate salinity.

According to the investigations carried out on synthesized 3D NiMn/Ti electrocatalysts for HER, the binary 3D NiMn/Ti-5 delivers the superior electrocatalytic activity under all three investigating electrolytes. Notably, the catalytic activity was declining gradually with a subsequent decrease of Mn-content on electrodes and the prepared NiMn/Ti-1 electrocatalyst exhibits the lowest HER performance. The required lower overpotentials (η_{10}) of the best-performing three NiMn/Ti HER electrocatalysts to reach the current density of 10 mA cm⁻² are as follows:

In alkaline media:

$$\text{NiMn/Ti-5 (127 mV)} > \text{NiMn/Ti-4 (145 mV)} > \text{NiMn/Ti-3 (150 mV)}$$

In ASW media:

$$\text{NiMn/Ti-5 (79 mV)} > \text{NiMn/Ti-4 (89 mV)} > \text{NiMn/Ti-3 (140 mV)}$$

In SSW media:

$$\text{NiMn/Ti-5 (64 mV)} > \text{NiMn/Ti-4 (79 mV)} > \text{NiMn/Ti-3 (140 mV)}$$

The recorded HER polarization curves of fabricated 3D NiMn/Ti electrocatalysts were used to extract the corresponding Tafel plots investigated under all three electrolytes and the elevation of the column bars denotes the required overpotentials to achieve the benchmark current densities of 10, 20, and 50 mA cm⁻² as depicted in in Fig. 13 and listed in Table 6.

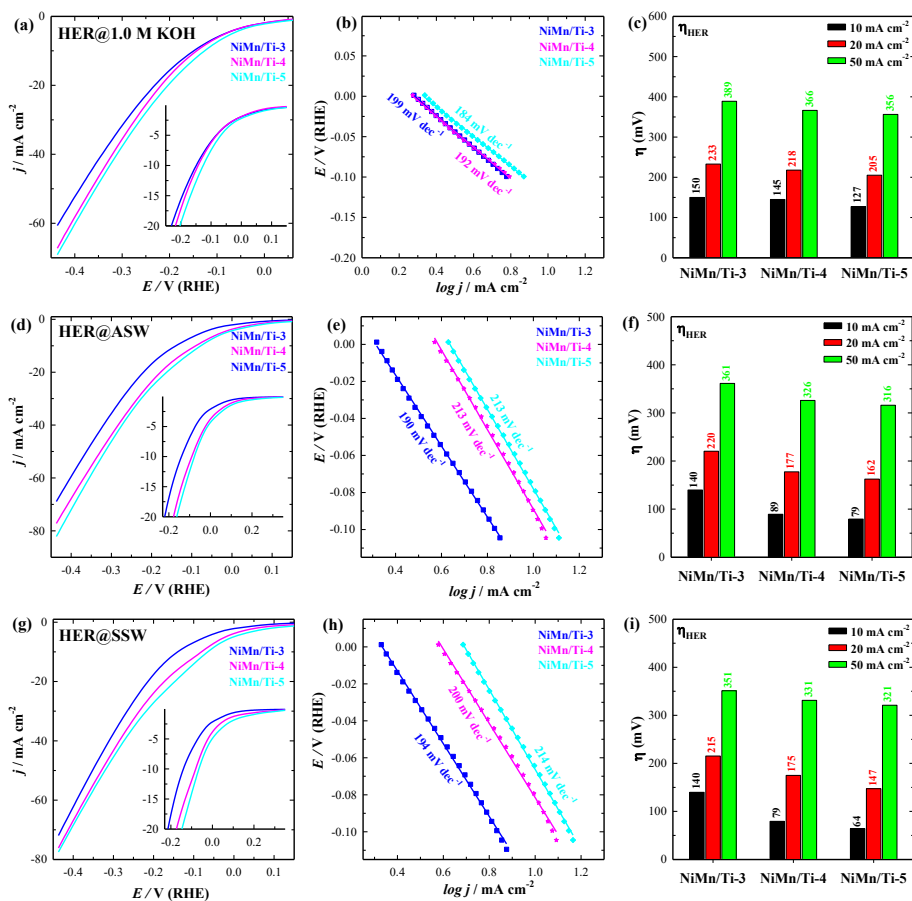


Figure 13. The HER polarization curves of the three best-performing 3D NiMn/Ti catalysts in 1.0 M KOH, ASW and SSW at 25 °C and 10 mV s⁻¹ potential scan rate (a, d, g) with corresponding extracted Tafel plots (b, e, h) and required overpotentials to reaching the current densities of 10, 20 and 50 mA cm⁻² (c, f, i), respectively.

The Tafel slopes for NiMn/Ti-3, NiMn/Ti-4, and NiMn/Ti-5 electrocatalysts in alkaline media (1.0 M KOH) are 199, 192, and 184 mV dec⁻¹, respectively. A lower Tafel slope generally indicates more efficient electrocatalytic performance because it signifies faster reaction kinetics and lower overpotential required for the same current density. Moreover, the evaluation of stability and maintaining structural integrity during the investigation is a pivotal criterion to determine the long-term economic viability and cost-effectiveness of any electrode prior to practical applications. Thus, the durability of the optimized NiMn/Ti-5 electrocatalyst was investigated under all three formulated electrolytes via the chronopotentiometry (CP) method at a fixed current density of 10 mA cm⁻²

and the chronoamperometric (CA) analysis at a constant potential of -0.23 V (vs. RHE) for 10 hours at 25 °C. The optimized 3D NiMn/Ti-5 electrocatalyst exhibited a marginal fluctuation of potentials (ca. 15-57 mV) under all three investigating electrolytes, whereas the CA investigations demonstrated superior current retentions of around 85% upon calculation after the completion of analysis. All obtained results and their graphic illustrations are demonstrated in Fig. 14.

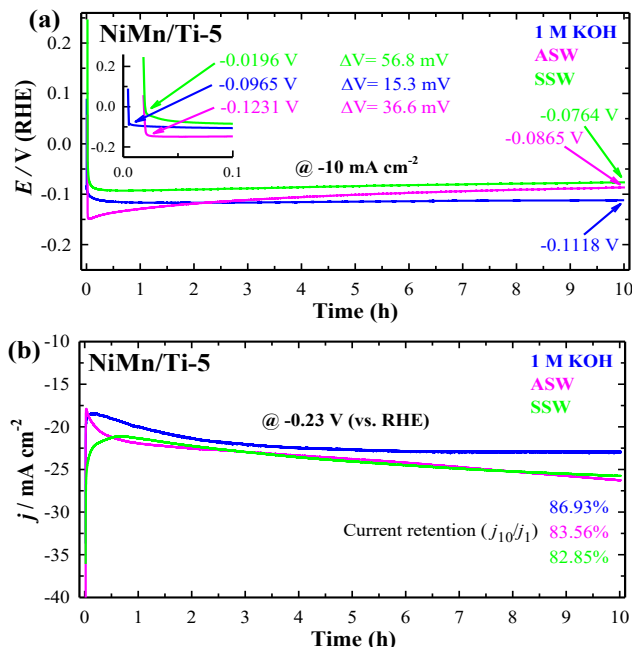


Figure 14. CP (a) and CA (b) plots of optimized NiMn/Ti-5 electrocatalyst at a constant current density of 10 mA cm^{-2} and at a constant potential of -0.23 V (vs. RHE) for 10 hours under all three electrolytes, respectively.

Table 6. Summarized electrochemical data of the investigated 3D NiMn/Ti electrocatalysts toward HER under investigating electrolytes at 25 °C.

Electrolytes	Catalysts	Current density (mA cm^{-2}) at $-0.43 \text{ V (vs. RHE)}$ and $25 \text{ }^{\circ}\text{C}$	η_{10} (mV) at $25 \text{ }^{\circ}\text{C}$	Tafel slope (mV dec^{-1})
1.0 M KOH	NiMn/Ti-3	60.65	150	199
	NiMn/Ti-4	67.25	145	192
	NiMn/Ti-5	69.12	127	184
ASW	NiMn/Ti-3	68.92	140	190
	NiMn/Ti-4	77.21	89	213
	NiMn/Ti-5	82.17	79	213
SSW	NiMn/Ti-3	71.95	140	194
	NiMn/Ti-4	76.12	79	200
	NiMn/Ti-5	77.49	64	214

3.2.3. Electrocatalytic activity of 3D NiMn/Ti electrocatalysts for OER

The synthesized binary 3D NiMn/Ti electrocatalysts were also investigated for the electrocatalytic OER activity via recording the LSVs in 1.0 M KOH solution, simulated seawater (1.0 M KOH + 0.5 M NaCl) and alkaline seawater (1.0 M KOH + natural seawater) at 25 °C. The repeatability of electrocatalytic OER performance was cross-checked for each investigated electrode.

The 3D binary NiMn/Ti-1 electrocatalyst, which was fabricated from the bath solution with $\text{Ni}^{2+}:\text{Mn}^{2+}$ molar proportion of 1:1, demonstrates an exceptional OER activity in alkaline media with a minimum overpotential of 356 mV to achieve the current density of 10 mA cm^{-2} . This OER activity outperforms the corresponding NiMn/Ti-2 (361 mV) and NiMn/Ti-3 (371 mV) electrocatalysts. Notably, the OER performance of 3D NiMn/Ti electrocatalysts has gradually declined with the increase of Mn-loadings on the synthesized electrodes; thus, the best-performing three NiMn/Ti OER electrocatalysts (namely NiMn/Ti-1, NiMn/Ti-2 and NiMn/Ti-3) were investigated thoroughly by conducting the LSV analysis. The optimized NiMn/Ti-1 electrocatalyst also demonstrated a relatively reasonable OER performance in alkaline seawater and simulated seawater, where the required overpotentials to gain the benchmark current density of 10 mA cm^{-2} were 388 mV and 386 mV, respectively. The OER activity exhibited a modest deterioration in ASW and SSW for the following reasons:

i) The chlorine evolution reaction (CIER) is a competing reaction that simultaneously takes place on the electrode during OER, which detrimentally affects the working electrolyte via the formation of hypochlorite and other chloride by-products at higher pH and causes low current efficiency.

ii) The presence of Ca^{2+} , Mg^{2+} , Br^- , SO_4^{2-} ions, along with a broad spectrum of bacteria, suspended solid microparticles and other impurities present in natural seawater ultimately leads to the formation of precipitates, poisoning, leaching and deactivation of the surface-active sites of OER electrocatalysts.

According to the OER investigations conducted using these synthesized 3D NiMn/Ti electrocatalysts under all three investigating electrolytes, the optimized 3D NiMn/Ti-1 electrocatalyst with the lowest Mn-loading of $13.43 \mu\text{g cm}^{-2}$ demonstrates the efficient OER performance. To achieve the benchmark current density of 10 mA cm^{-2} , the best-performing three NiMn/Ti OER electrocatalysts based on their required overpotentials under investigative electrolytes are listed as follows:

In alkaline media:

NiMn/Ti-1 (356 mV) > NiMn/Ti-2 (361 mV) > NiMn/Ti-3 (371 mV)

In ASW media:

NiMn/Ti-1 (388 mV) > NiMn/Ti-2 (406 mV) > NiMn/Ti-3 (446 mV)

In SSW media:

NiMn/Ti-1 (386 mV) > NiMn/Ti-2 (413 mV) > NiMn/Ti-3 (454 mV)

The recorded polarization curves of the investigated 3D NiMn/Ti OER electrocatalysts under all three electrolytes were used to extract their corresponding Tafel plots and the altitude of the column bars denotes the required overpotentials to achieve the benchmark current densities of 10, 20, and 50 mA cm⁻² as demonstrated in Fig. 15 and listed in Table 7.

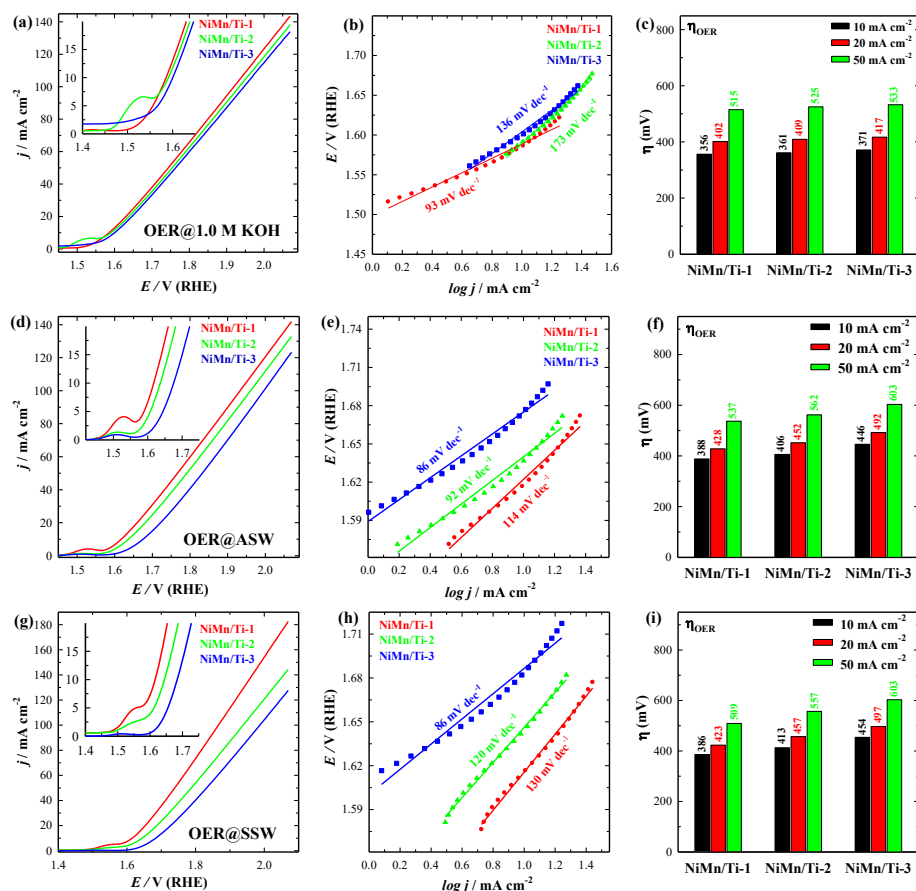


Figure 15. The OER polarization curves of three best-performing 3D NiMn/Ti catalysts in 1.0 M KOH, ASW and SSW at 25 °C and 10 mV s⁻¹ potential scan rate (a, d, g) with their corresponding extracted Tafel plots (b, e, h) and required overpotentials to reaching the current densities of 10, 20 and 50 mA cm⁻² (c, f, i), respectively.

A comparatively lower Tafel slope value for the optimized NiMn/Ti-1 (93 mV dec^{-1}) electrocatalyst was obtained in alkaline media (1.0 M KOH) than the corresponding binary NiMn/Ti-2 (173 mV dec^{-1}), and NiMn/Ti-3 (136 mV dec^{-1}) electrocatalysts.

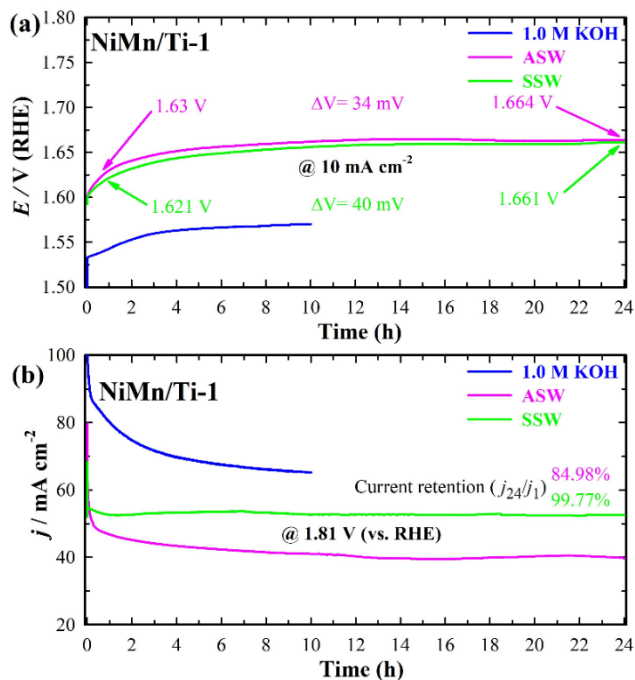


Figure 16. Chronopotentiometry at 10 mA cm^{-2} (a) and chronoamperometry at 1.81 V (vs. RHE) (b) plots of optimized NiMn/Ti-1 electrocatalyst for 10 hours in 1.0 M KOH and 24 hours in alkaline seawater and simulated seawater, respectively.

Moreover, as exhibited in Fig. 16, the chronopotentiometry and chronoamperometric plots of optimized NiMn/Ti-1 electrocatalyst at a constant potential of 1.81 V (vs. RHE) and a constant current density of 10 mA cm^{-2} demonstrate superior long-term stability in 1.0 M KOH, alkaline seawater and simulated seawater, respectively. The optimized NiMn/Ti-1 electrocatalyst exhibited a nominal fluctuation of potentials (ca. 34-40 mV) in SSW and ASW, whereas the CA investigations resulted in exceptional current retentions of ca. 85-99% upon calculation after 24 hours of analysis.

Table 7. Summarized electrochemical data of the investigated 3D NiMn/Ti electrocatalysts toward OER in 1.0 M KOH, ASW and SSW at 25 °C.

Electrolytes	Catalysts	Current density (mA cm ⁻²) at 2.06 V (vs. RHE) and 25 °C	η_{10} (mV) at 25 °C	Tafel slope (mV dec ⁻¹)
1.0 M KOH	NiMn/Ti-1	143.54	356	93
	NiMn/Ti-2	138.28	361	173
	NiMn/Ti-3	133.94	371	136
ASW	NiMn/Ti-1	141.97	388	114
	NiMn/Ti-2	132.92	406	92
	NiMn/Ti-3	123.3	446	86
SSW	NiMn/Ti-1	182.57	386	130
	NiMn/Ti-2	144.36	413	120
	NiMn/Ti-3	127.68	454	86

3.2.4. Overall seawater splitting performance of optimized 3D NiMn/Ti electrocatalysts

It was determined from the thorough investigations that the synthesized binary 3D NiMn/Ti electrocatalysts possess superior bifunctional characteristics for overall water splitting (OWS) application. Fabricated 3D NiMn/Ti-5 electrocatalyst demonstrated outstanding HER activity, whereas the 3D NiMn/Ti-1 electrocatalyst exhibited reasonable OER efficiency with long-term durability in both ASW and SSW. As one of the prime objectives of this research was to synthesize efficient electrocatalysts for renewable hydrogen production from water splitting and the oceanic seawater is the most abundant resource, therefore, the optimized 3D NiMn/Ti electrocatalyst for HER (NiMn/Ti-5) and OER (NiMn/Ti-1) were assembled as cathode and anode for investigating the overall alkaline seawater splitting performance, respectively. A two-electrode seawater electrolyzer was installed using ASW as the working electrolyte and equipped with both optimized electrocatalysts. For comparing the electrolytic cell efficiency, another two-electrode seawater (ASW) electrolyzer was equipped with fabricated NiMn/Ti-1 electrocatalysts as anode and a platinum (ca. 2 cm² geometric area) sheet as cathode. The [NiMn/Ti-5₍₋₎||NiMn/Ti-1₍₊₎] electrolyzer assembly requires only 1.619 V cell voltage to achieve the current density of 10 mA cm⁻² while the noble metal-based electrolyzer [Pt₍₋₎||NiMn/Ti-1₍₊₎] assembly necessitates a 0.075 V higher cell voltage at 25 °C. The recorded lower cell voltage of this binary 3D bifunctional seawater electrolyzer proves its competitiveness with other recently reported non-noble metal-based materials for OWS performance in SSW/ASW. Moreover, a 10 hours long continuous durability investigation of the equipped [NiMn/Ti-5₍₋₎||NiMn/Ti-1₍₊₎] electrolyzer shows no significant

potential degradation throughout the analysis period. The assembled electrolyzer and the obtained results for overall seawater splitting performance are illustrated and depicted in Fig. 17.

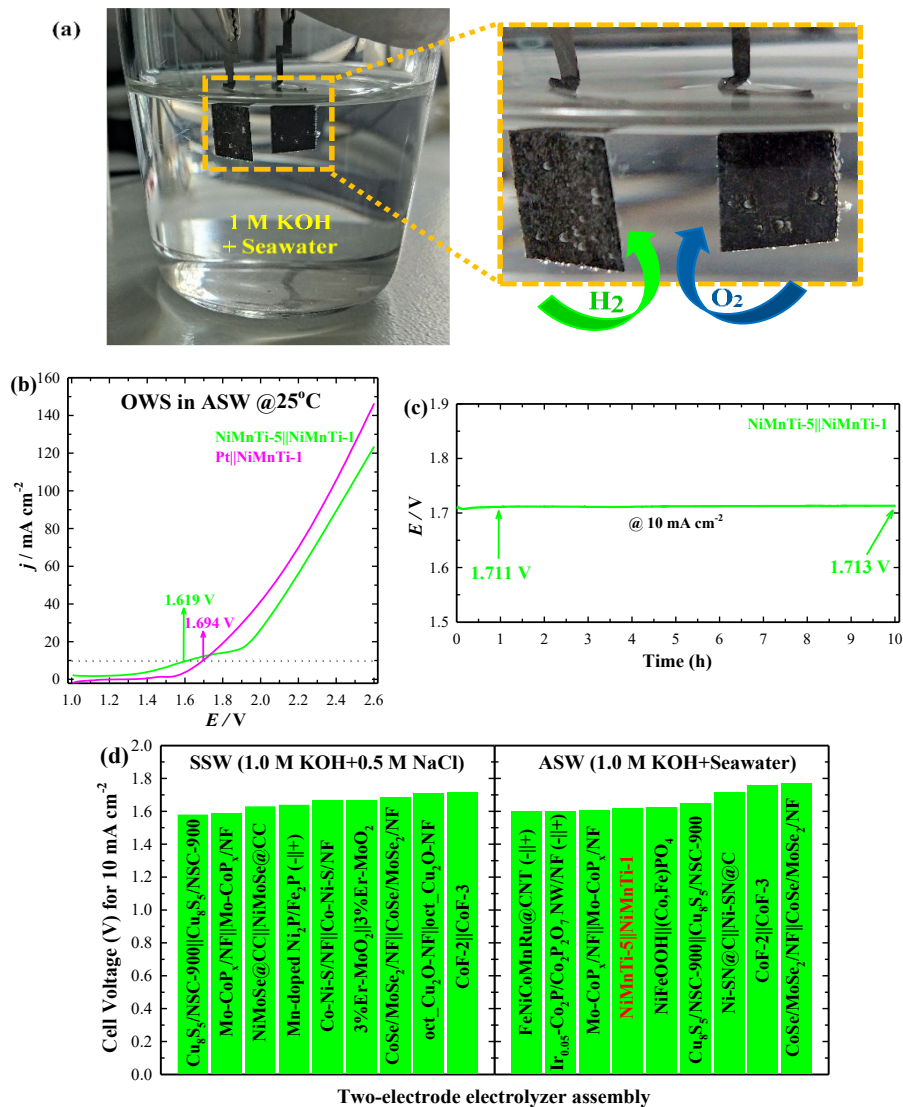


Figure 17. A digital photograph of our assembled two-electrode alkaline seawater electrolyzer $[\text{NiMn}/\text{Ti}-5_{(-)}||\text{NiMn}/\text{Ti}-1_{(+)}]$ with generation of H_2 and O_2 bubbles (a). The LSV polarization plots of overall alkaline seawater splitting at 25 °C (b) and a durability investigation of our equipped binary 3D bifunctional seawater electrolyzer for 10 h (c). A comparison of OWS performance (d) in ASW and SSW to achieve 10 mA cm^{-2} current density by recently reported non-noble metal-based electrolyzer assembly [111-123].

3.3. Synthesis and characterization of 3D NiMnCo/Ti electrocatalysts

3.3.1. Microstructure and Morphology of 3D NiMnCo/Ti electrocatalysts

The ternary 3D nickel-manganese-cobalt (NiMnCo) electrocatalysts were also fabricated via the electrochemical deposition method using the DHBT technique. To design and develop an enhanced and efficient HER electrocatalyst for freshwater/seawater splitting application with favorable surface morphology, two additives were introduced, namely ammonium sulfate, $(\text{NH}_4)_2\text{SO}_4$ and boric acid (H_3BO_3). Ammonium sulfate plays the role as a modifier of the coating morphology of the electrodes, while boric acid is a well-known pH stabilizer of solutions. The surface morphology of synthesized 3D ternary NiMnCo/Ti electrocatalysts and 3D binary catalyst-samples is demonstrated in Fig. 18. The synthesized electrocatalysts were denominated as NiMnCo/Ti- n ($n = 1, 2$), according to the molar concentration of Co^{2+} ions in the solution baths (herein, we simplified the catalysts' acronyms with integer numbers. The 3D NiMnCo/Ti-1 and NiMnCo/Ti-2 electrodes were electrochemically synthesized from the bath solutions with Co^{2+} ion concentrations of 0.1 M and 0.2 M, respectively).

From the SEM image exhibited in Fig. 18a, the surface morphology of NiMnCo/Ti-2 electrocatalyst demonstrates cauliflower curd-shaped microspherical architecture directly deposited on conducting Ti substrate by a facile one-step electrodeposition method. Those compactly grown microspheres covered the entire surface of the substrate. The SEM image with higher magnification (Fig. 18a'), vividly demonstrates different dimensions of cauliflower curd-like microspheres piled up with ca. 7-14 μm in diameter that are uniformly dispersed on the substrate surface. The NiMnCo/Ti-1 electrocatalyst also exhibits look-alike microspherical morphologies where the grains are not well separated rather integrated within clusters as depicted in Fig. 18b. The binary NiCo/Ti catalyst-sample demonstrates a rough and porous, clustered surface texture with finer granularity within each cluster in Fig. 18c, whereas the NiMn/Ti sample-electrode exhibits uneven surface texture with variation in roughness as exhibited in Fig. 18d.

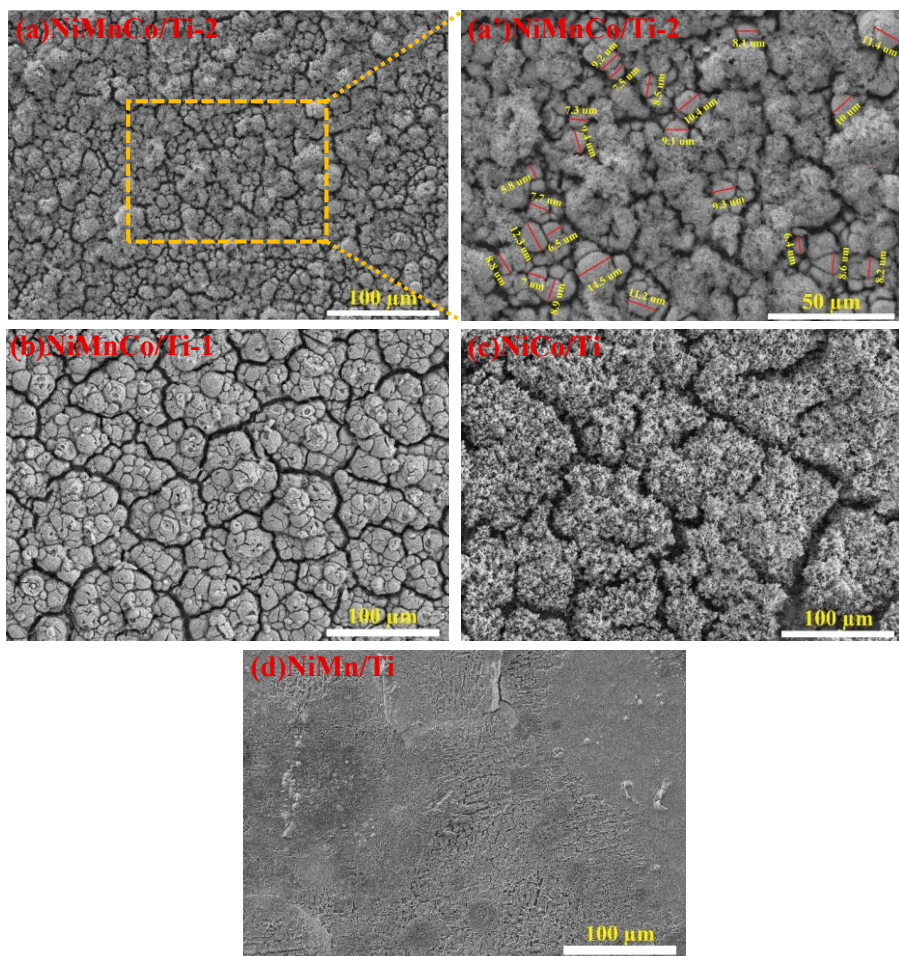


Figure 18. SEM views of synthesized ternary 3D NiMnCo/Ti-2 (a, a'), NiMnCo/Ti-1 (b) electrocatalysts and binary NiCo/Ti (c) and NiMn/Ti (d) catalyst-samples.

The metal loadings of synthesized 3D ternary electrocatalysts and binary catalyst-samples on the Ti substrate were determined by ICP-OES analysis.

The fabricated 3D ternary NiMnCo/Ti electrocatalysts contained ca. 15.7-19.6 wt.% of Ni content, ca. 20.4-27.8 wt.% of Mn content and approx. 52.6-63.8 wt.% of Co content. The total metal loadings on the synthesized 3D ternary electrocatalysts and binary catalyst-samples were as follows:

NiMnCo/Ti-1 ($312 \mu\text{g cm}^{-2}$), NiMnCo/Ti-2 ($351 \mu\text{g cm}^{-2}$), NiMn/Ti ($235 \mu\text{g cm}^{-2}$) and NiCo/Ti ($728 \mu\text{g cm}^{-2}$).

Additionally, the electrochemically active surface area (ECSA) of the synthesized 3D NiMnCo/Ti-2 electrocatalyst was determined from the measurements of double layer capacitance (C_{dl}) by recording CV curves in the 1.0 M KOH solution at various scan rates (5-50 mV s^{-1}) in the non-faradaic region (Fig. 19).

The charging current, I_c , of the electrodes at each scan rate was determined from the CVs via Equation (4):

$$I_c [\text{A}] = (I_{\text{anodic}} - I_{\text{cathodic}})_{\text{OCP}} \quad (4)$$

C_{dl} values were evaluated by plotting a graph of charging current vs. scan rate and calculating the slope, as shown by Eq. (5):

$$\text{Slope} = C_{dl} [\text{F}] = \Delta I_c [\text{A}] / \Delta v [\text{V s}^{-1}] \quad (5)$$

Subsequently, the ECSA value for the optimized NiMnCo/Ti-2 electrocatalyst was calculated using the specific capacitance (C_s) value of $40 \mu\text{F cm}^{-2}$ [110] and Eq. (6):

$$\text{ECSA} [\text{cm}^2] = C_{dl} [\mu\text{F}] / C_s [\mu\text{F cm}^{-2}] \quad (6)$$

C_{dl} was found to be 11.88 mF and the calculated ECSA value for NiMnCo/Ti-2 was 297 cm^2 , which is significantly larger than the geometric area of the catalyst. The NiMnCo/Ti-2 catalyst exhibited a high surface area, indicative of a high number of active sites and, consequently, significant electrocatalytic activity for HER.

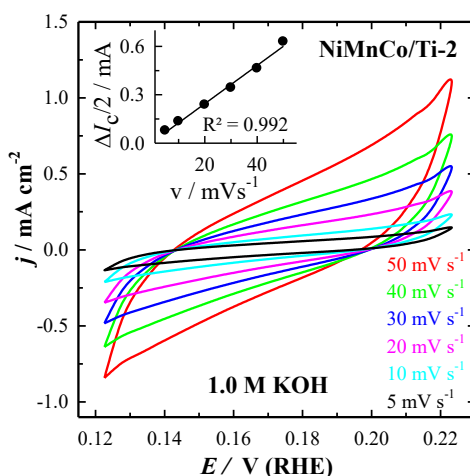


Figure 19. CVs of NiMnCo/Ti-2 in N_2 -saturated 1.0 M KOH in the non-faradaic potential region at different scan rates. The inset represents capacitive current as a function of scan rate.

3.3.2. Electrocatalytic activity of 3D NiMnCo/Ti electrocatalysts for HER in alkaline, simulated seawater and alkaline seawater media

The electrocatalytic HER performance of fabricated 3D NiMnCo/Ti electrocatalysts was investigated by recording LSVs in 1.0 M KOH solution, SSW (1.0 M KOH + 0.5 M NaCl) and ASW (1.0 M KOH + natural seawater) at 25 °C. Multiple electrodes were synthesized to monitor and verify the replicability of recorded LSVs for each electrocatalyst and catalyst-sample.

At first, the polarization curves of fabricated 3D ternary NiMnCo/Ti-1, NiMnCo/Ti-2 electrocatalysts and two binary catalyst-samples, namely, NiMn/Ti and NiCo/Ti were recorded in alkaline media (1.0 M KOH solution) to investigate the electrocatalytic HER activity. An enhanced HER activity was demonstrated by the synthesized 3D NiMnCo/Ti-2 electrocatalyst as a nominal overpotential of 66 mV was recorded to achieve the benchmark 10 mA cm⁻² current density, outnumbering the respective NiMnCo/Ti-1 (99 mV), NiMn/Ti (245 mV) and NiCo/Ti (283 mV) electrodes, respectively.

After establishing NiMnCo/Ti-2 electrode as an excellent electrocatalyst in alkaline fresh water (1.0 M KOH), the LSV investigations were then carried out in formulated alkaline seawater and simulated seawater media for H₂ production, where all synthesized electrodes underwent chlorine and contaminant-rich adverse conditions. The self-supported ternary 3D NiMnCo/Ti-2 electrocatalyst exhibited the highest HER activity in alkaline seawater and simulated seawater compared to other materials. As-synthesized 3D NiMnCo/Ti-2 electrocatalyst demonstrated ultra-low overpotentials of 59, 111, and 210 mV to achieve current densities of 10, 20 and 50 mA cm⁻² in alkaline seawater, while the lowest required overpotentials of 29 mV (η_{10}), 84 mV (η_{20}), and 195 mV (η_{50}) were registered in simulated seawater. Moreover, the synthesized ternary 3D NiMnCo/Ti-1 electrocatalyst also exhibited promising HER performance under all three investigating electrolytes with reasonably minimum overpotentials of 99 mV (1.0 M KOH), 99 mV (ASW) and 89 mV (SSW) to achieve the benchmark 10 mA cm⁻² current density. The required overpotentials (η_{10}) of fabricated electrocatalysts and catalyst-samples are as follows:

In alkaline media:

NiMnCo/Ti-2 (66 mV) > NiMnCo/Ti-1 (99 mV) > NiMn/Ti (245 mV)
> NiCo/Ti (283 mV)

In ASW media:

NiMnCo/Ti-2 (59 mV) > NiMnCo/Ti-1 (99 mV) > NiMn/Ti (205 mV)
> NiCo/Ti (270 mV)

In SSW media:

$$\text{NiMnCo/Ti-2 (29 mV)} > \text{NiMnCo/Ti-1 (89 mV)} > \text{NiMn/Ti (195 mV)} \\ > \text{NiCo/Ti (267 mV)}$$

The recorded LSV polarization curves of fabricated electrodes were used to extract the corresponding Tafel plots investigated under all three electrolytes and the required overpotentials to achieve the benchmark current densities of 10, 20, and 50 mA cm⁻² were illustrated with the elevation of the column bars as depicted in in Fig. 20 and listed in Table 8.

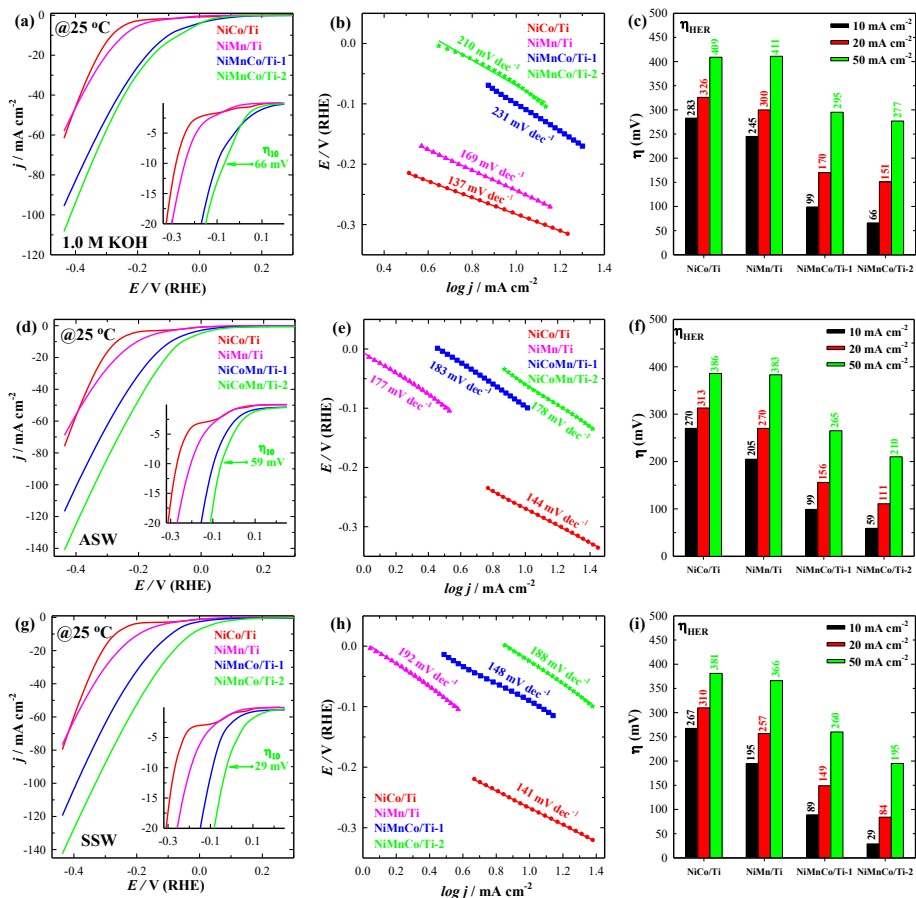


Figure 20. The HER polarization curves of synthesized 3D ternary NiMnCo/Ti electrocatalysts and binary catalyst-samples in 1.0 M KOH, ASW and SSW at 25 °C and 10 mV s⁻¹ potential scan rate (a, d, g) with their corresponding extracted Tafel plots (b, e, h) and required overpotentials to reaching the current densities of 10, 20 and 50 mA cm⁻² (c, f, i), respectively.

The Tafel slope values for the optimized ternary 3D NiMnCo/Ti-2 electrocatalyst were 210, 178, and 188 mV dec⁻¹ for HER in alkaline media (1.0 M KOH), alkaline seawater and simulated seawater, respectively.

Table 8. Summarized electrochemical data of the investigated 3D ternary electrocatalysts and binary catalyst-samples toward HER in 1.0 M KOH, alkaline seawater and simulated seawater at 25 °C.

Electrolytes	Catalysts	Current density (mA cm ⁻²) at -0.43 V (vs. RHE) and 25 °C	η_{10} (mV) at 25 °C	Tafel slope (mV dec ⁻¹)
1.0 M KOH	NiCo/Ti	61.5	283	137
	NiMn/Ti	58	245	169
	NiMnCo/Ti-1	95.5	99	231
	NiMnCo/Ti-2	108.3	66	210
ASW	NiCo/Ti	75.8	270	144
	NiMn/Ti	68.8	205	177
	NiMnCo/Ti-1	116.7	99	183
	NiMnCo/Ti-2	141.1	59	178
SSW	NiCo/Ti	79.7	267	141
	NiMn/Ti	76.7	195	192
	NiMnCo/Ti-1	119.5	89	148
	NiMnCo/Ti-2	142.5	29	188

Moreover, to evaluate the applicability for practical use, the optimized NiMnCo/Ti-2 electrocatalyst was investigated by 50 hours long continuous operation under all three electrolyte conditions. The durability of the optimized NiMnCo/Ti-2 electrocatalyst was evaluated by conducting long-term chronopotentiometry (CP) at a fixed current density of 10 mA cm⁻² and chronoamperometry (CA) at a constant potential of -0.23 V (vs. RHE).

The synthesized 3D NiMnCo/Ti-2 electrocatalyst demonstrated an outstanding electrocatalytic stability by the CP investigations, as the optimized electrocatalyst exhibited insignificant fluctuation of potentials (ca. 4-21 mV) after 50 hours of analysis. The CA investigations were also conducted using the optimized NiMnCo/Ti-2 electrocatalyst, resulting in exceptional current retentions of ca. 90-95% upon calculation after 50 hours. Nevertheless, a multi-step CP analysis with variable current densities ranging from 20 mA cm⁻² to 100 mA cm⁻² was also carried out in 1.0 M KOH and simulated seawater for 18 hours to prove the robust nature and enhanced durability of the synthesized electrocatalyst. The findings are illustrated and demonstrated in Fig. 21.

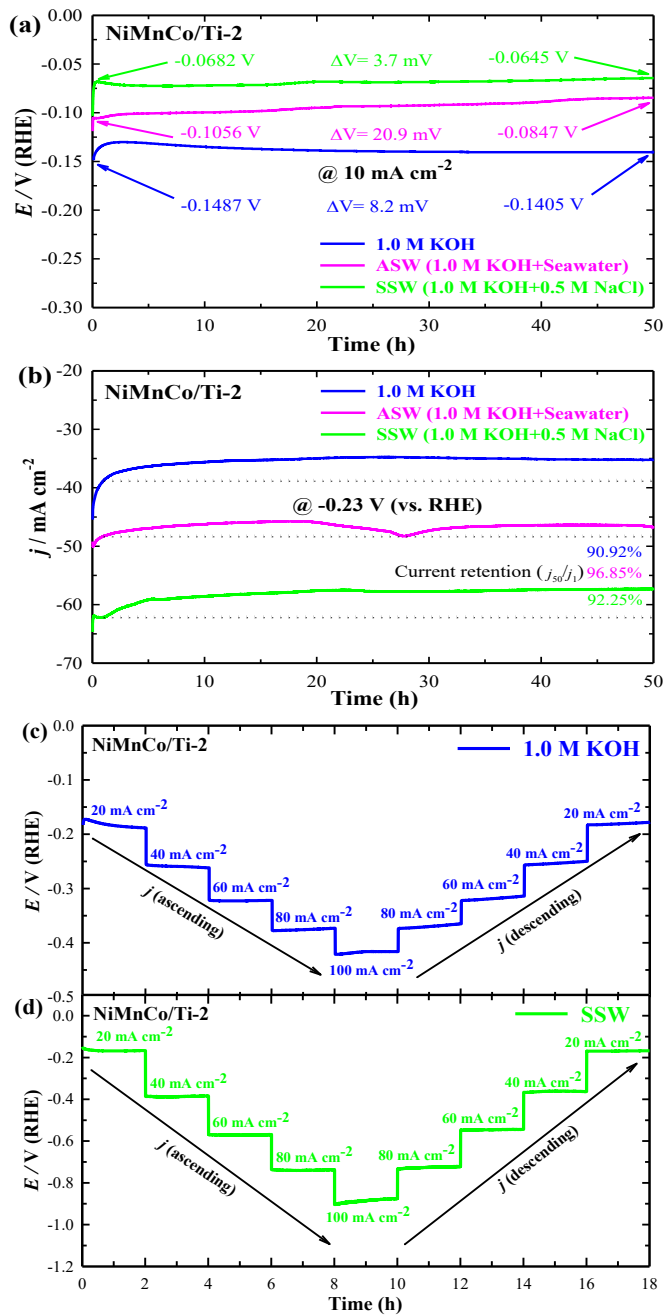


Figure 21. Chronopotentiometry at 10 mA cm^{-2} (a) and chronoamperometry at -0.23 V (vs. RHE) (b) plots of optimized NiMnCo/Ti-2 electrocatalyst for 50 hours under 1.0 M KOH, alkaline seawater and simulated seawater, respectively. A multi-step chronopotentiometry analysis with variable current densities ranging from 20 mA cm^{-2} to 100 mA cm^{-2} for 18 hours under 1.0 M KOH (c) and simulated seawater (d).

CONCLUSION

- Non-noble transition metal-based 3D NiMo/Ti electrocatalysts were successfully synthesized via the electrochemical deposition method through a dynamic hydrogen bubble template (DHBT) technique and their electrocatalytic HER and OER activity was investigated in alkaline media (1.0 M NaOH). The fabricated 3D NiMo/Ti electrocatalysts have exhibited modest HER and OER performance in alkaline media.
- The synthesized 3D NiMn/Ti electrocatalysts exhibit enhanced HER performance in alkaline media, simulated seawater (SSW) and alkaline seawater (ASW), where the performance of the optimized NiMn/Ti-5 electrocatalyst was exceptional. To achieve the benchmark current density of 10 mA cm^{-2} by the efficient 3D NiMn/Ti-5 HER electrocatalyst, the minimum required overpotentials were 127 mV (1.0 M KOH), 79 mV (ASW) and 64 mV (SSW), whereas the best-performing 3D NiMn/Ti-1 OER electrocatalyst requires reasonably lower overpotentials of 356 mV (1.0 M KOH), 388 mV (ASW) and 386 mV (SSW). The optimized NiMn/Ti-5 HER electrocatalyst and NiMn/Ti-1 OER electrocatalyst underwent long-term stability tests for 10 hours and 24 hours, respectively, where no significant deterioration of potentials was found.
- The optimized NiMn/Ti-5 electrocatalyst demonstrated enhanced HER performance in all three investigated electrolytes due to its unique porous surface morphology, featuring a high density of pores with distinctly different sizes. These interconnected pores increase the number of active sites, promote the formation of multiple channels for electrolyte diffusion, and accelerate electron transport efficiency.
- The best-performing 3D NiMn/Ti-5 and NiMn/Ti-1 electrocatalysts were assembled as the cathode and anode, respectively, in a two-electrode alkaline seawater (ASW) electrolyzer to evaluate overall water splitting (OWS) performance. The $[\text{NiMn/Ti-5}_{(-)}||\text{NiMn/Ti-1}_{(+)}]$ configuration exhibited superior OWS activity, achieving a current density of 10 mA cm^{-2} at 25°C with a cell voltage of 1.619 V, outperforming the precious noble metal-based $[\text{Pt}_{(-)}||\text{NiMn/Ti-1}_{(+)}]$ electrolyzer (1.694 V).
- Finally, noble 3D ternary NiMnCo/Ti electrocatalysts were fabricated via electrodeposition using the DHBT technique. The optimized NiMnCo/Ti-2 electrocatalyst, featuring a cauliflower curd-like microspherical surface morphology, demonstrated outstanding and highly efficient HER activity in all three investigated electrolytes. The ultra-low overpotentials required to reach the benchmark current density of 10 mA cm^{-2} were 66 mV (1.0 M

KOH), 59 mV (ASW), and 29 mV (SSW). The optimized 3D NiMnCo/Ti-2 electrocatalyst showed remarkable stability across all electrolytes, with current retention around 90-95% and insignificant potential fluctuations after 50 hours of testing. Additionally, the NiMnCo/Ti-2 electrocatalyst underwent a multi-step chronopotentiometric test with varying current densities from 20 to 100 mA cm⁻² in 1.0 M KOH and SSW media, maintaining exceptional stability throughout.

- The electrochemically active surface area (ECSA) of the optimized 3D NiMnCo/Ti-2 electrocatalyst was 297 cm², approximately 150 times larger than its geometric surface area. This high ECSA value indicates the possibility of a high number of active sites, significantly enhancing its electrocatalytic activity for the HER. Consequently, the enhanced and outstanding electrocatalytic performance for HER, combined with superior long-term stability in alkaline freshwater and seawater, demonstrates the robustness and structural integrity of the synthesized electrocatalyst, confirming its viability for practical large-scale hydrogen production from realistic seawater.

IVADAS

Energetinis saugumas ir nenutrūkstamas energijos tiekimas tapo svarbiais pasaulinio masto iššūkiais, nes sparčiai augantis gyventojų skaičius ir pramonės plėtra lemia greitą gamtinių išteklių sekimą. Riboti, iškastiniu kuru pagrįsti energijos šaltiniai nuo seniausių civilizacijos laikų buvo pagrindinis energijos šaltinis, o po pramonės revoliucijos pasaulinis energijos poreikis ėmė augti eksponentiškai [1]. Iškastinio kuro – anglies, naftos ir gamtinių dujų – deginimas išskiria milijonus tonų anglies dioksido (CO_2), anglies monoksido (CO), sieros dioksido (SO_2), azoto oksidų (NO_x) ir metano (CH_4), bendrai vadinamų šiltnamio efektą sukeliančiomis dujomis. Didelis iškastinio kuro vartojimas ne tik eikvoja gamtinius išteklius, bet ir kelia rimtą grėsmę žmonijai: globalinis atšilimas, klimato kaita, aplinkos tarša, jūros lygio kilimas ir kitos ekologinės pasekmės yra tiesioginis perteklinio angliavandenilių deginimo rezultatas. Be to, iškastinio kuro atsargos yra ribotos ir geografiškai netolygiai pasiskirsčiusios, todėl spartus jų išeikvojimas gali lemti energijos stygių ir skatinti geopolitinius konfliktus. Dėl šių priežasčių per pastaruosius dešimtmečius itin išaugo susidomėjimas alternatyviais, aplinkai draugiškais ir tvariais atsinaujinančiais energijos šaltiniais [2, 3].

Siekiant spręsti tiek energetinio saugumo, tiek aplinkos tvarumo klausimus mažinant šiltnamio efektą sukeliančių dujų emisiją, vandenilis (H_2) laikomas viena perspektyviausių alternatyvų iškastiniam kurui. Jis pasižymi didžiausiu energijos tankiu masės vienetui (apie 142 MJ/kg), neišskiria anglies dioksido, yra gausiai paplitęs Žemėje ir lengvai pritaikomas įvairioms reikmėms [4, 5]. Vandenilio šaltiniai yra įvairūs, o pagal gamybos technologijas jis skirstomas į tris pagrindines kategorijas: žaliąjį, mėlynąjį ir pilkąjį vandenilį [6]. Pilkasis vandenilis – tai dažniausiai pasitaikanti vandenilio rūšis, gaminama taikant garinio metano reformavimo technologiją. Mėlynasis vandenilis gaunamas iš pilkojo, taikant anglies dioksido surinkimo, saugojimo arba panaudojimo technologijas. Žaliojo vandenilio gamyba, pasižyminti nulinėmis arba labai mažomis anglies emisijomis, grindžiama vandens elektrolize, vykdoma naudojant atsinaujinančius energijos šaltinius, tokius kaip vėjas, saulė, geoterminė ar bioenergija. Šis metodas laikomas perspektyviausia alternatyva tradiciniam iškastiniam kurui, siekiant pramoniniu mastu gaminti aukšto grynumo vandenilį be anglies emisijų [7]. Vandenilio sintezė elektrolizės būdu apima dvi pagrindines pusreakcijas: katodinę vandenilio išsiskyrimo reakciją (HER) ir anodinę deguonies

išsiskyrimo reakciją (OER). Norint pagaminti 1 kg vandenilio, stochiometriškai reikia apie 9 litrų gryno vandens [8, 9].

Elektrokatalitinis vandens skaidymas standartinėmis sąlygomis yra termodinamiškai nepalankus procesas dėl lėtos keturių elektronų pernašos kinetikos, būdingos deguonies išsiskyrimo reakcijai OER. Ši kinetinė inercija lemia santykinai didelius viršįtampius ir laikoma pagrindiniu kliuviniu visam elektrocheminiam vandens skaidymo procesui [10]. Norint pasiekti 100 % efektyvumą, vandens elektrolizės procesui reikia mažiausiai 39,4 kWh energijos vienam kilogramui vandenilio pagaminti, tačiau įprastas elektrolizeris tam sunaudoja iki 50 kWh, nors esant aukštam slėgiui ir temperatūrai galima pasiekti didesnę efektyvumą [11]. Vis dėlto apie 97 % visų pasaulio vandens išteklių sudaro vandenynų ir jūrų vanduo, o tinkamo naudoti gėlo vandens prieinamumas išlieka reikšmingu iššūkiu elektrolizerių technologijų plėtrai, ypač atsižvelgiant į spartų pasaulio gyventojų skaičiaus augimą ir su tuo susijusius šiuolaikinio gyvenimo standartų poreikius. Praktinis ir realus vandens skaidymas gali būti įgyvendintas tik įveikus šias kliūtis.

Pažangiausi platinos grupės metalų (PGM) katalizatoriai pasižymi išskirtiniu elektrokatalitiniu aktyvumu vandens elektrolizeriuose: Pt ir Pt pagrindu sukurti katalizatoriai laikomi etaloniniais HER (vandenilio išsiskyrimo reakcijos) elektrokatalizatoriais, o Ir ir Ru pagrindu sukurti junginiai ($\text{IrO}_2/\text{RuO}_2$) – aukštos kokybės, komerciškai prieinami OER (deguonies išsiskyrimo reakcijos) katalizatoriai [12-15]. Vis dėlto ribotos šių tauriųjų metalų atsargos gamtoje ir jų didelė kaina yra pagrindiniai veiksniai, trukdantys pramoniniu mastu plėtoti ir komercializuoti vandenilio gamybą elektrokatalitinio vandens skaidymo būdu. Todėl ekonomiškai efektyvus, stabilus ir didelio našumo bifunkcinio elektrokatalizatoriaus kūrimas bei tobulinimas yra esminis žingsnis siekiant įveikti technologinius barjerus atsinaujinančio žaliojo vandenilio gamyboje iš gėlo ir jūros vandens.

DARBO TIKSLAS

Taikant dinaminio vandenilio burbulų šablono (DHBT) metodą, sukurti netauriųjų pereinamųjų metalų (Ni, Mo, Mn ir Co) pagrindu veikiančius elektrokatalizatorius, ištirti jų mikrostruktūrą, cheminę sudėtį, paviršiaus morfologiją bei įvertinti sukurtų elektrodų elektrokatalitinį aktyvumą ir stabilumą vandenilio išsiskyrimo reakcijoje (HER), deguonies išsiskyrimo reakcijoje (OER) ir bendrame vandens skaidyme šarminiuose gėlojo ir jūros vandens elektrolituose.

DARBO UŽDAVINIAI

- Sukurti netauriųjų pereinamųjų metalų (Ni ir Mo) pagrindu veikiančius elektrokatalizatorius ir ištirti jų elektrokatalitinį aktyvumą bei stabilumą HER ir OER reakcijose šarminėje terpėje.
- Sukurti binarius Ni ir Mn pagrindu veikiančius elektrokatalizatorius, naudojant skirtingas mangano druskų koncentracijas bei priedus, ir įvertinti jų HER ir OER aktyvumą bei stabilumą šarminėje terpėje, dirbtiniame jūros vandenyje ir šarminiame natūraliame jūros vandenyje.
- Susintetintų NiMn/Ti elektrokatalizatorių apibūdinimas ir jų padidėjusio katalitinio aktyvumo priežasčių paaiškinimas.
- Ištirti bendro jūros vandens skaidymo efektyvumą laboratorinio lygmens dviejų elektrodų elektrolizeryje, naudojant optimizuotus bifunkcinius NiMn/Ti elektrokatalizatorius.
- Susintetinti trinarus elektrodus, kurių sudėtyje yra Ni, Mn ir Co, keičiant kobalto druskų koncentraciją, ir ištirti Co įtaką HER reakcijos aktyvumui ir stabilumui šarminiuose gėlo ir jūros vandens elektrolituose.
- Apibūdinti NiMn/Ti ir NiMnCo/Ti elektrokatalizatorius bei pateikti galimą jų padidėjusio HER aktyvumo priežasčių paaiškinimą.

MOKSLINIS NAUJUMAS

- Paprastas, mažų sąnaudų elektrocheminio nusodinimo metodas, taikant dinaminio vandenilio burbulo šablono (DHBT) techniką, buvo pritaikytas binarių ir ternarių 3D netauriųjų metalų pagrindu sukurtų elektrokatalizatorių sintezei. Sukurtų elektrokatalizatorių katalitinis aktyvumas ir stabilumas buvo ištirti vandens skaidymui šarminiame gėlame vandenyje, imituotame jūros vandenyje ir šarminiame natūraliame jūros vandenyje.
- Pirmą kartą nustatyta, kad elektrochemiškai susintetintas NiMn/Ti-5 elektrokatalizatorius, panaudojant DHBT techniką, pasižymi puikiu HER elektrokatalitiniu aktyvumu ir stabilumu dėl susiformavusios itin porėtos struktūros.
- Pirmą kartą parodyta, kad NiMn/Ti-1 ir NiMn/Ti-5 elektrodų pora (nusodinta iš tirpalų, kurių $\text{Ni}^{2+}:\text{Mn}^{2+}$ moliniai santykiai atitinkamai 1:1 ir 1:5) gali būti efektyviai panaudota dviejų elektrodų jūros vandens elektrolizeryje kaip anodas ir katodas, pasiekiant mažesnę elemento įtampą nei platinos pagrindu sukurtiems elektrodams.

- Išskirtinis sukurtų ternarinių 3D NiMnCo/Ti elektrokatalizatorių veikimas ir ilgalaikis stabilumas (iki 50 val.) parodė HER aktyvumą su itin mažu viršįtampiu (29 mV esant 10 mA cm^{-2}), kuris prilygsta komerciškai prieinamiems tauriųjų metalų pagrindu sukurtiems elektrodams.

GINAMIEJI TEIGINIAI

- Elektrocheminio nusodinimo metodas, taikant dinaminio vandenilio burbulo šablono (DHBT) techniką, leidžia formuoti įvairios binarinės ir ternarinės sudėties elektrokatalizatorius ant titano (Ti) paviršių.
- Elektrochemiškai nusodinti 3D elektrokatalizatoriai pasižymi dideliu elektrochemiškai aktyvaus paviršiaus plotu (ECSA), kuris daugiau nei 100 kartų viršija jų geometrinį plotą, o tai lemia žymiai padidėjusį katalitinį aktyvumą, ypač vandenilio išsiskyrimo reakcijoje (HER).
- Naudojant DHBT metodą susintetinti optimizuoti binariniai HER ir OER elektrokatalizatoriai buvo panaudoti atitinkamai kaip katodas ir anodas, ir parodė efektyvų bendrą šarminio jūros vandens skaidymą, pranokstantį tauriųjų metalų pagrindu veikiančių elektrolizerių sistemas.
- Visi optimizuoti elektrokatalizatoriai išlaikė ilgalaikį stabilumą elektrolizės metu esant agresyvioms jūros vandens sąlygoms – be reikšmingų potencialo svyravimų ir su nereikšmingu srovės tankio sumažėjimu, patvirtindami savo struktūrinį vientisumą ir praktinį pritaikomumą tvariai vandenilio gamybai.

AUTORIAUS INDĖLIS

Disertacijos autorius suformulavo visas galvaninio nusodinimo vones ir tiriamąsias elektrolitų sudėtis, taip pat elektrocheminio nusodinimo būdu ant titano (Ti) pagrindo sukūrė rišiklio nenaudojančias, savaime palaikančias 3D elektrokatalizatorių dangas. Autorius buvo atsakingas už mėginių paruošimą charakterizavimui taikant SEM ir ICP-OES metodus. Visi šiame darbe pateikti elektrocheminiai tyrimai, skirti HER, OER ir bendro vandens skaidymo (OWS) efektyvumui įvertinti, buvo atlikti autoriaus, taikant LSV matavimus bei atliekant stabilumo tyrimus naudojant chronoamperometriją ir chronopotenciometriją. Be to, autorius atliko duomenų analizę, eksperimentinių rezultatų interpretavimą, parengė grafinę medžiagą ir visus žemiau išvardintus mokslinius straipsnius. Disertaciją autorius parašė savarankiškai, tinkamai nurodydamas šaltinius visai informacijai, kuri nėra jo originalus darbas. Gauti rezultatai buvo pristatyti nacionalinėse ir tarptautinėse konferencijose – tiek žodiniuose, tiek stendiniuose pranešimuose.

EKSPERIMENTO METODIKA

Pagrindo paruošimas.

Prieš kiekvieno elektrodo gamybą titano (Ti) pagrindai buvo išpjaušyti iš folijos į 1×1 cm dydžio kvadratus skirtus tiek elektrocheminiams matavimams, tiek struktūrinei charakterizacijai. Po pjovimo paviršius buvo šlifuojamas naudojant iki 1000 gritų abrazyvą ir nuriebalinamas etanolio, siekiant pašalinti natūralų oksido sluoksnį. Vėliau plokštelės buvo kruopščiai nuplaunamos dejonizuotu vandeniu ir aktyvuojamos trumpai (10 s), panardinant į praskiestą sieros rūgštį (H₂SO₄, 1:1 tūrio santykiu) 70 °C temperatūroje. Po to jos dar kartą nuplaunamos dejonizuotu vandeniu.

3D binarių ir trinarių elektrokatalizatorių sintezė.

Rišiklio nenaudojantys, atramos nereikalaujantys 3D binariai (NiMo/Ti, NiMn/Ti) ir trinariai (NiMnCo/Ti) elektrokatalizatoriai buvo susintetinti taikant paprastą, mažų sąnaudų elektrocheminio nusodinimo metodą, pasitelkiant dinaminio vandenilio burbulų šablono (DHBT) techniką. Buvo suformuluotos galvaninio nusodinimo vonelės, o nusodinimo procesai atlikti pagal 2, 3 ir 4 lentelėse (25, 26 ir 27 psl.) pateiktus parametrus. Taip pat buvo pagaminti keli vieno elemento pagrindu sudaryti elektrokatalizatorių pavyzdžiai (pvz., Ni/Ti, Mn/Ti) bei binarių (pvz., NiMn/Ti, NiCo/Ti) katalizatorių variantai, siekiant palyginti jų aktyvumą, naudojant tuos pačius priedus ir nekeičiant nusodinimo sąlygų. Po nusodinimo visi elektrokatalizatoriai buvo nuplauti dejonizuotu vandeniu ir išdžiovinti kambario temperatūroje.

Elektrocheminiai matavimai ir charakterizavimas.

Elektrocheminiai tyrimai buvo atlikti siekiant įvertinti HER, OER ir bendro vandens skaidymo (OWS) reakcijų efektyvumą, taikant linijinę voltamperometriją (LSV). Matavimai atlikti naudojant PGSTAT302 potenciostatą su programine įranga Nova 2.1.4 (Metrohm Autolab B.V., Utrechtas, Nyderlandai). Visi eksperimentai buvo vykdomi standartinėje trijų elektrodų celėje, kurioje darbinis elektrodas turėjo 2 cm² plotą, palyginamasis elektrodas buvo prisotintas kalomelio elektrodas (SCE), o pagalbinis – grafito strypas. Visi išmatuoti potencialai buvo konvertuoti į reversinio vandenilio elektrodo (RHE) skalę pagal šią formulę:

$$E_{\text{RHE}} = E_{\text{SCE}} + 0.242 \text{ V} + 0.059 \text{ V} \times \text{pH}_{\text{tirpalo}} \quad (3)$$

Pradiniuose tyrimuose kaip šarminė terpė buvo naudojamas 1,0 M NaOH tirpalas kaip šarminė terpė, vėliau – 1,0 M KOH. Tyrimai taip pat išplėsti, įtraukiant dirbtinį jūros vandenį ir šarminį natūralų jūros vandenį tiriant HER,

OER ir OWS reakcijas. Prieš kiekvieną matavimą elektrolitas buvo 20 min prisotinamas argonu (Ar), siekiant pašalinti ištirpusį deguonį.

Elektrokatalizatorių aktyvumas buvo vertinamas registruojant LSV kreives 25-75 °C temperatūros intervale. HER matavimams potencialas buvo keičiamas nuo atviros grandinės potencialo (OCP) iki -0,43 V (vs. RHE), o OER – nuo OCP iki 2,06 V (vs. RHE), abiem atvejais taikant 10 mV s⁻¹ elektrodo potencialo skleidimo greitį. OWS efektyvumas buvo vertinamas dviejų elektrodų celėje, naudojant šarminį jūros vandenį ir optimizuotus NiMn/Ti elektrokatalizatorius kaip anodą ir katodą. LSV kreivės buvo registruojamos 1,0-2,6 V įtampų intervale, taikant tą patį 10 mV s⁻¹ skleidimo greitį. Elektrochemiškai aktyvus paviršiaus plotas (ECSA) optimizuotam 3D NiMnCo/Ti-2 elektrokatalizatoriui buvo nustatytas pagal dvigubo sluoksniu talpą (C_{dl}), registruojant ciklines voltamperogramas (CV) 1,0 M KOH tirpale, esant skirtingiems elektrodo potencialo skleidimo greičiams (5-50 mV s⁻¹) nefaradėjiniėje srityje.

Stabilumo tyrimai.

Ilgalaikis optimizuotų elektrokatalizatorių stabilumas buvo vertinamas registruojant chronoamperometrines (CA) kreives esant pastoviam potencialui -0,23 V (HER) ir 1,81 V (OER) (vs. RHE), taip pat chronopotenciometrines (CP) kreives esant 10 mA cm⁻² srovės tankiui. Be to, buvo atlikta daugiaetapė CP analizė, taikant palaipsniui didėjančius, o vėliau mažėjančius srovės tankius nuo 20 mA cm⁻² iki 100 mA cm⁻², siekiant įvertinti optimizuoto 3D trinario NiMnCo/Ti-2 elektrodo, pasižyminčio išskirtinėmis HER elektrokatalizinėmis savybėmis, patikimumą ir ilgalaikį stabilumą.

Struktūrinė analizė.

Binarių ir trinarių elektrokatalizatorių mikrostruktūra ir paviršiaus morfologija buvo tiriama naudojant skenuojantį elektroninį mikroskopą Helios TM4000Plus (Hitachi, Tokijas, Japonija) su energijos dispersijos rentgeno spektrometru (AZtecOne, Oxford Instruments, Jungtinė Karalystė). Metalų kiekiai elektroduose buvo nustatyti taikant ICP-OES analizę, naudojant spektrometrą Optima 7000DV (Perkin Elmer, JAV), registruojant emisijos spektrus ties šiais bangos ilgiais:

Ni – 231,604 nm, Mo – 202,031 nm, Mn – 257,610 nm, Co – 228,616 nm.

REZULTATŲ APTARIMAS

3D NiMo/Ti elektrokatalizatorių morfologija.

Skenuojančiosios elektroninės mikroskopijos (SEM) vaizdai parodė, kad susintetintų 3D binarių NiMo/Ti-1 ir NiMo/Ti-2 elektrokatalizatorių paviršius buvo tolygiai padengtas be įtrūkimų, lygus ir vienodai pasiskirsčiusiomis nikelio ir molibdeno dalelėmis, tačiau morfologiškai neišsiskyrė. Tuo tarpu NiMo/Ti-3 elektrokatalizatorius, nusodintas iš tirpalo su didesne Ni^{2+} jonų koncentracija (1,0 M), suformavo unikalią, kedro lapus primenančią struktūrą, visiškai padengiančią titano paviršių. Šios kedro lapo formos Ni-Mo architektūros, stebimos esant didesniai didinimui, pasižymi netaisyklingai išsidėsčiusiomis, aiškiai apibrėžtomis struktūromis, kurios skiriasi dydžiu ir forma.

3D NiMo/Ti elektrokatalizatorių HER ir OER aktyvumo tyrimas.

Susintetintų NiMo/Ti elektrodų elektrokatalitinis aktyvumas buvo tirtas taikant LSV metodą, naudojant Ar prisotintą 1,0 M NaOH elektrolitą esant 25 °C temperatūrai. Optimizuotas NiMo/Ti-3 elektrokatalizatorius, gautas nusodinant iš tirpalo, kuriame buvo didesnė (1,0 M) Ni^{2+} jonų koncentracija, pasižymėjo pagerintu vandenilio išsiskyrimo reakcijos (HER) aktyvumu – norint pasiekti standartinį srovės tankį (10 mA cm^{-2}) šarminėje terpėje, reikėjo tik 288 mV viršįtampio. Deguonies išsiskyrimo reakcijos (OER) atveju šiam katalizatoriui buvo būdingas palyginti nedidelis 580 mV viršįtampis. Remiantis gautais voltamperogramų duomenimis, buvo sudarytos Tafel kreivės tiek HER, tiek OER analizei. Optimizuoto NiMo/Ti-3 elektrokatalizatoriaus stabilumas buvo vertintas taikant CA matavimą, palaikant -0,23 V (vs. RHE) potencialą HER reakcijai 2 valandas. Be to, ta pati CA analizė buvo atlikta palaikant 1,81 V (vs. RHE) potencialą per 2 valandas, siekiant įvertinti katalizatoriaus ilgaamžiškumą OER sąlygomis. Gauti voltamperogramų rezultatai ir kita susijusi informacija pateikiami 11 pav. ir 5 lentelėje (32 psl).

3D NiMn/Ti elektrokatalizatorių mikrostruktūra ir paviršiaus morfologija.

3D nikelio-mangano (NiMn) binarės dangos buvo susintetintos taikant dinaminio vandenilio burbulų šablono (DHBT) metodą. Siekiant sukurti efektyvų bifunkcinį elektrokatalizatorių su palankia paviršiaus morfologija, buvo naudotas $(\text{NH}_4)_2\text{SO}_4$ kaip dangos struktūros modifikatorius ir boro rūgštis (H_3BO_3) kaip pH stabilizatorius. Elektrokatalizatoriai buvo žymimi kaip NiMn/Ti- n ($n = 1, 2, 3, 4, 5$), priklausomai nuo $\text{Ni}^{2+}:\text{Mn}^{2+}$ molinių

santykių nusodinimo vonelėse (pvz., NiMn/Ti-1 ir NiMn/Ti-5 atitinkamai atitiko santykius 1:1 ir 1:5). NiMn/Ti-1 pasižymėjo tipiška globuline morfologija su smulkiomis granulėmis, tolygiai padengusiomis paviršių. Padidinus Mn kiekį ($\text{Ni}^{2+}:\text{Mn}^{2+} = 1:2$), NiMn/Ti-2 paviršiuje susiformavo didesnės granulės. NiMn/Ti-3 paviršius pasižymėjo nelygia, šiurkščia, plokštelių tipo heterostrukture morfologija. Pažymėtina, kad aukštesnės celės įtampos vertės buvo užfiksuotos elektrocheminio nusodinimo metu, kai vonelės tirpale buvo didesnis $\text{Ni}^{2+}:\text{Mn}^{2+}$ molinis santykis. Be to, NiMn dangų nusodinimas rūgštinėje terpėje buvo pasirinktas siekiant paskatinti intensyvių vandenilio burbuliukų susidarymą, o atlikus elektrolizę pastebėta, kad burbuliukų formavimasis nuosekliai intensyvėjo. Atsižvelgiant į šiuos veiksnius, galima manyti, kad Ni ir Mn dalelės pradėjo kauptis (aglomeruotis) ant titano paviršiaus, sudarydamos mažus iškilimus ar gūbrio formos darinius, kai buvo vykdoma NiMn/Ti-4 katalizatoriaus elektrocheminė danga. Galiausiai, taikant dinaminio vandenilio burbulų šablono metodiką, NiMn/Ti-5 elektrokatalizatoriaus paviršiaus morfologija virto unikalia mikrodrydžio porėta architektūra su įvairaus dydžio poromis, kurios pagerina elektrolito difuziją, elektronų pernašą ir padidina aktyvių vietų/centrų skaičių.

3D NiMn/Ti elektrokatalizatorių HER aktyvumo tyrimas.

Susintetintų 3D NiMn/Ti elektrokatalizatorių HER aktyvumas buvo tirtas užrašant LSV kreives 1,0 M KOH tirpale, dirbtiniame jūros vandenyje (1,0 M KOH + 0,5 M NaCl) ir šarminiame natūraliame jūros vandenyje (1,0 M KOH + natūralus jūros vanduo), esant 25 °C temperatūrai ir 10 mV s⁻¹ elektrodo potencialo skleidimo greičiui ir skleidžiant elektrodo potencialą. Kiekvienas elektrodas buvo paruoštas tris kartus, siekiant patikrinti rezultatų pakartojamumą. Iš visų tirtų elektrodų, 3D NiMn/Ti-5, turintis didžiausią Mn kiekį, parodė geriausią HER aktyvumą. Šis optimizuotas elektrokatalizatorius pasiekė 10 mA cm⁻² srovės tankį esant tik 127 mV viršįtampiui šarminėje terpėje, o tai buvo geresnis rezultatas nei NiMn/T-4 (145 mV) ir NiMn/Ti-3 (150 mV). Naudojant natūralų jūros vandenį iš Baltijos jūros (Klaipėdos pakrantė), NiMn/Ti-5 taip pat pademonstravo išskirtinį aktyvumą – reikėjo tik 79 mV viršįtampio. Dar geresnis rezultatas buvo pasiektas dirbtiniame jūros vandenyje – tik 64 mV viršįtampiu. Be to, šio elektrokatalizatoriaus stabilumas buvo tirtas visose trijose terpėse taikant CP metodą esant 10 mA cm⁻² srovės tankiui ir CA metodą esant -0,23 V (vs. RHE) potencialui 10 valandų trukmės testuose, esant 25 °C temperatūrai. Optimizuotas 3D NiMn/Ti-5 elektrokatalizatorius visose tirtose terpėse pasižymėjo tik nežymiais potencialo svyravimais (~15-57 mV), o CA analizė parodė aukštą srovės išlaikymą – virš 85% po analizės pabaigos.

3D NiMn/Ti elektrokatalizatorių OER aktyvumo tyrimas.

Susintetinti binariai 3D NiMn/Ti elektrokatalizatoriai buvo tirti siekiant įvertinti jų elektrokatalitinį aktyvumą (OER), registruojant LSV kreives visose trijose tiriamose terpėse: 1,0 M KOH, dirbtiniame ir natūraliame šarminiame jūros vandenyje, esant 25 °C temperatūrai. Kiekvieno tiriamo elektrodo OER aktyvumo pakartojamumas buvo patikrintas atliekant pakartotinius matavimus.

Iš vonelės su $\text{Ni}^{2+}:\text{Mn}^{2+}$ molinis santykis buvo 1:1, nusodintas 3D NiMn/Ti-1 elektrokatalizatorius parodė išskirtinį OER aktyvumą šarminėje terpėje – norint pasiekti 10 mA cm^{-2} srovės tankį, reikėjo tik 356 mV viršįtampio. Šis rezultatas buvo geresnis nei NiMn/Ti-2 (361 mV) ir NiMn/Ti-3 (371 mV) elektrodų. Pastebėta, kad OER aktyvumas mažėjo didėjant Mn kiekiui elektroduose, todėl trys geriausiai veikę NiMn/Ti OER elektrokatalizatoriai (NiMn/Ti-1, NiMn/Ti-2 ir NiMn/Ti-3) buvo nuodugniai ištirti atliekant LSV analizę esant skirtingai elektrolito temperatūrai. Optimizuotas NiMn/Ti-1 elektrokatalizatorius taip pat parodė gerą OER aktyvumą šarminiame jūros vandenyje – reikalingi viršįtampiai, norint pasiekti 10 mA cm^{-2} srovės tankį, buvo 388 mV dirbtiniame jūros vandenyje (ASW) ir 386 mV natūraliame šarminiame jūros vandenyje (SSW).

OER aktyvumo sumažėjimas ASW ir SSW terpėse paaiškinamas dviem pagrindinėmis priežastimis:

i) Chloro išsiskyrimo reakcija (CIER) – tai konkurencinė reakcija, vykstanti kartu su OER, kuri mažina srovės efektyvumą dėl hipohlorito ir kitų chloro junginių susidarymo aukšto pH terpėje.

ii) Natūraliame jūros vandenyje esantys Ca^{2+} , Mg^{2+} , Br^- , SO_4^{2-} jonai, bakterijos ir kietosios dalelės sukelia nuosėdų susidarymą, katalizatoriaus paviršiaus užteršimą, aktyvių vietų pasyvaciją ir išplovimą, dėl ko mažėja OER efektyvumas.

Be to, CP ir CA matavimai, atlikti su optimizuotu NiMn/Ti-1 elektrokatalizatoriumi, esant 1,81 V (vs. RHE) potencialui ir 10 mA cm^{-2} srovės tankiui, parodė ilgalaikį stabilumą visose tirtose terpėse – 1,0 M KOH, ASW ir SSW. Optimizuotas NiMn/Ti-1 elektrokatalizatorius pasižymėjo tik nežymiais potencialo svyravimais (apie 34-40 mV) SSW ir ASW terpėse, o CA analizė parodė išskirtinį srovės išlaikymą – apie 85-99% po 24 valandų trukmės analizės.

3D NiMn/Ti elektrokatalizatorių bendras jūros vandens skaidymo efektyvumas.

Išsamūs tyrimai parodė, kad susintetinti binariai 3D NiMn/Ti elektrokatalizatoriai pasižymi puikiais bifunkcinėmis savybėmis, tinkamomis bendram vandens skaidymui (OWS). NiMn/Ti-5 elektrokatalizatorius (suformuotas esant $\text{Ni}^{2+}:\text{Mn}^{2+}$ moliniam santykiui 1:5 dengimo elektrolite) pasižymėjo išskirtiniu HER aktyvumu, o NiMn/Ti-1 (suformuotas esant moliniam santykiui 1:1) – pakankamu OER efektyvumu ir ilgalaikiu stabilumu tiek ASW, tiek SSW terpėse. Kadangi vienas iš pagrindinių šio darbo tikslų buvo sukurti efektyvius elektrokatalizatorius atsinaujinančiai vandenilio gamybai iš jūros vandens – gausiausio pasaulio vandens šaltinio – optimizuoti NiMn/Ti-5 (HER) ir NiMn/Ti-1 (OER) elektrodai buvo sujungti į dviejų elektrodų elektrolizerį, skirtą bendram šarminio jūros vandens skaidymui.

Elektrolizeris, kuriame buvo naudojami abu optimizuoti elektrodai [NiMn/Ti-5₍₋₎||NiMn/Ti-1₍₊₎] ir ASW kaip elektrolitas, pasiekė 10 mA cm⁻² srovės tankį esant vos 1,619 V celės įtampai. Palyginimui, analogiškas elektrolizeris su Pt katodu (geometrinis plotas ~2 cm²) ir NiMn/Ti-1 anodu [Pt₍₋₎||NiMn/Ti-1₍₊₎] reikalavo 0,075 V didesnės celės įtampos (1,694 V). Užfiksuota mažesnė įtampa šiame 3D binariame bifunkciniame elektrolizės įrenginyje rodo jo konkurencingumą, palyginti su neseniai aprašytais medžiagomis, kuriose nenaudojami taurieji metalai ir kurios taikomos viso jūros vandens skaidymo (OWS) procesuose tiek sintetiname (SSW), tiek šarminiame (ASW) jūros vandenyje. Be to, 10 valandų nepertraukiamo stabilumo bandymo metu nustatyta, kad [NiMn/Ti-5₍₋₎||NiMn/Ti-1₍₊₎] elektrolizerio potencialas išliko stabilus – per visą analizės laikotarpį nepastebėta reikšmingo įtampos pokyčio.

3D NiMnCo/Ti elektrokatalizatorių mikrostruktūra ir paviršiaus morfologija.

Trinariai trimačiai nikelio-mangano-kobalto (NiMnCo) katalizatoriai buvo susintetinti taikant dinaminio vandenilio burbulų šablono (DHBT) metodą. Siekiant sukurti patobulintą ir efektyvų HER elektrokatalizatorių, tinkamą tiek gėlo, tiek jūrinio vandens skaidymui, buvo panaudoti du priedai: amonio sulfatas ((NH₄)₂SO₄) ir boro rūgštis (H₃BO₃). Amonio sulfatas veikė kaip elektrodo dangos morfologijos modifikatorius, o boro rūgštis – kaip žinomas tirpalo pH stabilizatorius. Susintetintų 3D NiMnCo/Ti elektrokatalizatorių ir analogiškų 3D binarinių katalizatorių paviršiaus morfologija pavaizduota 18 pav. Elektrokatalizatoriai buvo žymimi kaip NiMnCo/Ti-*n* (kur *n* = 1, 2),

atsižvelgiant į Co^{2+} jonų molinę koncentraciją nusodinimo vonelėse. Paprastumo dėlei katalizatoriai buvo žymimi sveikaisiais skaičiais: NiMnCo/Ti-1 buvo gauti iš tirpalo, kuriame Co^{2+} koncentracija siekė 0,1 M, o NiMnCo/Ti-2 – iš tirpalo su 0,2 M Co^{2+} koncentracija.

3D NiMnCo/Ti elektrokatalizatorių elektrocheminis aktyvumas HER.

Susintetintų 3D NiMnCo/Ti elektrokatalizatorių elektrocheminis aktyvumas HER buvo vertintas užrašant LSV 1,0 M KOH, SSW (1,0 M KOH + 0,5 M NaCl) ir ASW (1,0 M KOH + natūralus jūros vanduo) terpėse, esant 25 °C temperatūrai ir 10 mV s⁻¹ elektrodo potencialo skleidimo greičiui nuo atviros grandinės potencialo (OCP) iki -0,43 V (vs. RHE). Siekiant įvertinti rezultatų atkuriamumą, kiekvienam katalizatoriui buvo susintetinta po kelis elektrodus.

Pirmiausia buvo užrašytos 3D trinarių NiMnCo/Ti-1 ir NiMnCo/Ti-2 bei dviejų binarių (NiMn/Ti ir NiCo/Ti) elektrokatalizatorių poliarizacijos kreivės šarminėje terpėje (1,0 M KOH), siekiant įvertinti jų aktyvumą HER. Rezultatai parodė, kad 3D NiMnCo/Ti-2 elektrokatalizatorius pasižymėjo geriausiu HER aktyvumu – siekiant pasiekti etaloninį 10 mA cm⁻² srovės tankį, reikėjo vos 66 mV viršįtampio. Šis rezultatas reikšmingai pranoko kitus tirtus elektrodus: NiMnCo/Ti-1 (99 mV), NiMn/Ti (245 mV) ir NiCo/Ti (283 mV). Gauti rezultatai rodo, kad didesnė Co^{2+} jonų koncentracija nusodinimo vonelėje (0,2 M) turėjo teigiamą poveikį katalizinėms savybėms. Be to, trinarė katalizatoriaus sudėtis sukūrė sinergetinį efektą, reikšmingai padidinusį HER aktyvumą šarminėje terpėje.

Nustačius, kad NiMnCo/Ti-2 elektrodas pasižymi puikiu elektrokataliziniu aktyvumu šarminėje terpėje (1 M KOH), tolesni LSV tyrimai buvo atlikti SSW ir ASW terpėse, siekiant įvertinti vandenilio gamybos efektyvumą sąlygomis, kurioms būdinga didelė chloro ir teršalų koncentracija. Šios sąlygos imituoja praktinį jūros vandens skaidymo procesą. Visi susintetinti elektrodai buvo tiriami tomis pačiomis nepalankiomis sąlygomis. Trinaris 3D NiMnCo/Ti-2 elektrokatalizatorius parodė didžiausią HER aktyvumą tiek SSW, tiek ASW terpėse, palyginti su kitais tirtais katalizatoriais, patvirtindamas savo pranašumą ne tik laboratorinėmis, bet ir arčiau realių eksploatacinių sąlygų esančiomis sąlygomis. Susintetintas 3D NiMnCo/Ti-2 elektrokatalizatorius pasižymėjo itin žemais viršįtampiais – siekiant 10, 20 ir 50 mA cm⁻² srovės tankių ASW terpėje, reikėjo atitinkamai 59, 111 ir 210 mV. Dar mažesni viršįtampiai buvo užfiksuoti SSW terpėje – 29 mV (η_{10}), 84 mV (η_{20}) ir 195 mV (η_{50}). Be to, trinario 3D NiMnCo/Ti-1 elektrokatalizatoriaus aktyvumas taip pat buvo reikšmingas visose trijose tirtose elektrolitinėse terpėse. Etaloninis 10 mA cm⁻² srovės tankis buvo

pasiektas esant 99 mV viršįtampiiui 1,0 M KOH, 99 mV – ASW ir 89 mV – SSW terpėse. Optimizuoto 3D NiMnCo/Ti-2 elektrokatalizatoriaus elektrochemiškai aktyvus paviršiaus plotas (ECSA) siekė 297 cm², tai yra gerokai daugiau nei elektrodo geometrinis plotas. Šis padidėjęs ECSA rodo didelį aktyviųjų vietų kiekį, kuris reikšmingai prisideda prie pagerėjusio HER elektrocheminio aktyvumo.

Optimizuoto NiMnCo/Ti-2 elektrokatalizatoriaus stabilumas buvo įvertintas visose trijose elektrolito terpėse, taikant ilgalaikę CP analizę esant pastoviam 10 mA cm⁻² srovės tankiui ir CA analizę esant pastoviam -0,23 V (vs. RHE) potencialui 50 valandų, 25 °C temperatūroje. Be to, siekiant įrodyti susintetinto elektrokatalizatoriaus mechaninį tvirtumą ir ilgalaikį veikimo stabilumą, 1,0 M KOH ir SSW terpėse buvo atlikta daugiaetapė CP analizė, trunkanti 18 valandų.

Susintetintas 3D NiMnCo/Ti-2 elektrokatalizatorius parodė išskirtinį elektrokatalizinį stabilumą, kuris buvo įvertintas taikant CA analizę visose trijose tirtose elektrolito terpėse – apskaičiuotas srovės išlaikymas siekė apie 90-95%. CP analizės, atliktos su optimizuotu NiMnCo/Ti-2 elektrokatalizatoriumi, parodė nereikšmingas potencialo svyravimo amplitudes po 50 valandų trukmės tyrimo, patvirtindamos ilgalaikį elektrodo stabilumą. Be to, daugiaetapės CP analizės, taikant kintančius srovės tankius nuo 20 mA cm⁻² iki 100 mA cm⁻² 1,0 M KOH ir SSW terpėse, dar kartą patvirtino pagerintą susintetinto elektrokatalizatoriaus patvarumą ir ilgaamžiškumą.

IŠVADOS

- Netauriųjų pereinamųjų metalų pagrindu sukurti 3D NiMo/Ti elektrokatalizatoriai buvo sėkmingai susintetinti elektrocheminio nusodinimo metodu, taikant dinaminio vandenilio burbulo šablono (DHBT) techniką. Jų elektrokatalitinis aktyvumas HER ir OER reakcijoms buvo tirtas šarminėje terpėje (1,0 M NaOH). Susintetinti 3D NiMo/Ti elektrokatalizatoriai šioje terpėje parodė vidutinį HER ir OER aktyvumą.
- Susintetinti 3D NiMn/Ti elektrokatalizatoriai pasižymėjo pagerintu HER aktyvumu šarminėje terpėje, imituotame jūros vandenyje (SSW) ir šarminiame jūros vandenyje (ASW), o optimizuotas NiMn/Ti-5 elektrokatalizatorius parodė išskirtinius rezultatus. Esant etaloniniam 10 mA cm⁻² srovės tankiui, itin efektyvus NiMn/Ti-5 HER elektrokatalizatoriaus viršįtampis siekė tik 127 mV (1,0 M KOH), 79 mV (ASW) ir 64 mV (SSW). Tuo tarpu geriausiai veikiančiam 3D NiMn/Ti-1 OER elektrokatalizatoriui reikėjo palyginti nedidelių viršįtampių – 356 mV

(1,0 M KOH), 388 mV (ASW) ir 386 mV (SSW). Optimizuoti NiMn/Ti-5 HER ir NiMn/Ti-1 OER elektrokatalizatoriai buvo išbandyti ilgalaikio stabilumo testuose atitinkamai 10 ir 24 valandas, per kurias reikšmingas potencialų sumažėjimas nebuvo pastebėtas.

- Optimizuotas NiMn/Ti-5 elektrokatalizatorius parodė pagerintą HER aktyvumą visose trijose tirtose elektrolitų terpėse dėl unikalios porėtos paviršiaus morfologijos, kurioje gausu skirtingo dydžio porų. Šios tarpusavyje sujungtos poros padidina aktyviųjų vietų kiekį, sudaro daugiau kanalų elektrolito difuzijai ir paspartina elektronų pernašos efektyvumą.
- Geriausiai veikiančių 3D NiMn/Ti-5 ir NiMn/Ti-1 elektrokatalizatorių pora buvo panaudota kaip katodas ir anodas dviejų elektrodų šarminio jūros vandens (ASW) elektrolizeryje, siekiant įvertinti bendrą vandens skaidymo (OWS) našumą. Ši sistema [NiMn/Ti-5₍₋₎||NiMn/Ti-1₍₊₎] pasižymėjo puikiu OWS aktyvumu, pasiekdama 10 mA cm⁻² srovės tankį esant 1,619 V elemento įtampai, pranokdama tauriųjų metalų pagrindu veikiančią sistemą [Pt₍₋₎||NiMn/Ti-1₍₊₎] (1,694 V).
- Galiausiai elektrocheminio nusodinimo metodu, taikant DGBT techniką, buvo pagaminti tauriųjų 3D ternariniai NiMnCo/Ti elektrokatalizatoriai. Optimizuotas NiMnCo/Ti-2 elektrokatalizatorius, turintis žiedinio kopūsto mikroapvalią paviršiaus morfologiją, parodė išskirtinį ir itin efektyvų HER aktyvumą visose trijose tirtose elektrolitų terpėse. Itin maži viršįtampiai, reikalingi pasiekti etaloninį 10 mA cm⁻² srovės tankį, buvo 66 mV (1,0 M KOH), 59 mV (ASW) ir 29 mV (SSW). Optimizuotas 3D NiMnCo/Ti-2 elektrokatalizatorius pasižymėjo išskirtiniu stabilumu visose terpėse, srovės išlaikymas siekė apie 90-95%, o potencialo svyravimai po 50 valandų bandymų buvo nereikšmingi. Be to, NiMnCo/Ti-2 elektrokatalizatorius buvo tirtas daugiasluoksniu chronopotenciometrinio metodu keičiant srovės tankius nuo 20 iki 100 mA cm⁻² 1,0 M KOH ir SSW terpėse, išlaikant išskirtinį stabilumą viso eksperimento metu.
- Optimizuoto 3D NiMnCo/Ti-2 elektrokatalizatoriaus elektrochemiškai aktyvus paviršiaus plotas (ECSA) siekė 297 cm², tai yra maždaug 150 kartų didesnis už katalizatoriaus geometrinį paviršiaus plotą. Toks didelis ECSA rodiklis rodo didelį aktyviųjų vietų skaičių, kuris žymiai pagerina elektrokatalizinį aktyvumą HER. Todėl pagerėjęs ir išskirtinis elektrokatalizinis HER aktyvumas bei ilgaamžis stabilumas šarminio gėlo ir jūros vandens terpėse patvirtina susintetinto elektrokatalizatoriaus patvarumą, struktūrinį vientisumą ir tinkamumą praktiniam didelio masto vandenilio gamybai iš realaus jūros vandens.

REFERENCES

- [1] W. Yang, J. Bao, H. Liu, J. Zhang and L. Guo, Low-grade heat to hydrogen: Current technologies, challenges and prospective. *Renew. Sustain. Energy Rev.*, 2023, **188**, 113842. [DOI:10.1016/j.rser.2023.113842](https://doi.org/10.1016/j.rser.2023.113842)
- [2] Q. Hassan, A.Z. Sameen, H.M. Salman, M. Jaszczur and A.K. Al-Jiboory, Hydrogen energy future: Advancements in storage technologies and implications for sustainability. *J. Energy Storage*, 2023, **72**, 108404. [DOI:10.1016/j.est.2023.108404](https://doi.org/10.1016/j.est.2023.108404)
- [3] H.M. Zhang and J. Li, Strategies for overcoming seawater adverse effects on cathodic hydrogen evolution reaction electrocatalysts. *Fuel*, 2024, **367**, 131505. [DOI:10.1016/j.fuel.2024.131505](https://doi.org/10.1016/j.fuel.2024.131505)
- [4] X.W. Lv, W.W. Tian and Z.Y. Yuan, Recent advances in high-efficiency electrocatalytic water splitting systems. *Electrochem. Energy Rev.*, 2023, **6**, 23. [DOI:10.1007/s41918-022-00159-1](https://doi.org/10.1007/s41918-022-00159-1)
- [5] J.N. Bamba, A.T. Dumlao, R.M. Lazaro, D.D. Matienzo and J. Ocon, Green Hydrogen from Seawater Electrolysis: Recent Developments and Future Perspectives. *Curr. Opin. Electrochem.*, 2024, **48**, 101592. [DOI:10.1016/j.coelec.2024.101592](https://doi.org/10.1016/j.coelec.2024.101592)
- [6] B.S. Zainal, P.J. Ker, H. Mohamed, H.C. Ong, I.M.R. Fattah, S.M.A. Rahman, L.D. Nghiem and T.M.I. Mahlia, Recent advancement and assessment of green hydrogen production technologies. *Renew. Sustain. Energy Rev.*, 2024, **189**, 113941. [DOI:10.1016/j.rser.2023.113941](https://doi.org/10.1016/j.rser.2023.113941)
- [7] G. Lagioia, M.P. Spinelli and V. Amicarelli, Blue and green hydrogen energy to meet European Union decarbonisation objectives. An overview of perspectives and the current state of affairs. *Int. J. Hydrogen Energy*, 2023, **48**, 1304-1322. [DOI:10.1016/j.ijhydene.2022.10.044](https://doi.org/10.1016/j.ijhydene.2022.10.044)
- [8] P. Kumar, A. Date, N. Mahmood, R.K. Das and B. Shabani, Freshwater supply for hydrogen production: An underestimated challenge. *Int. J. Hydrogen Energy*, 2024, **78**, 202-217. [DOI:10.1016/j.ijhydene.2024.06.257](https://doi.org/10.1016/j.ijhydene.2024.06.257)
- [9] R.R. Beswick, A.M. Oliveira and Y. Yan, Does the green hydrogen economy have a water problem? *ACS Energy Lett.*, 2021, **6**, 3167-3169. [DOI:10.1021/acsenerylett.1c01375](https://doi.org/10.1021/acsenerylett.1c01375)
- [10] M. Chatenet, B.G. Pollet, D.R. Dekel, F. Dionigi, J. Deseure, P. Millet, R.D. Braatz, M.Z. Bazant, M. Eikerling, I. Staffell, P. Balcombe, Y. Shao-Horn, and H. Schäfer, Water electrolysis: from textbook knowledge to the latest scientific strategies and industrial developments. *Chem. Soc. Rev.*, 2022, **51**, 4583-4762. [DOI:10.1039/D0CS01079K](https://doi.org/10.1039/D0CS01079K)

- [11] K. Mazloomi and C. Gomes, Hydrogen as an energy carrier: Prospects and challenges. *Renew. Sustain. Energy Rev.*, 2012, **16**, 3024-3033.
[DOI:10.1016/j.rser.2012.02.028](https://doi.org/10.1016/j.rser.2012.02.028)
- [12] N. Nie, D. Zhang, Z. Wang, S. Ge, Y. Gu, B. Yang, J. Lai and L. Wang, Stable p-block metals electronic perturbation in PtM@CNT (M= Ga, In, Pb and Bi) for acidic seawater hydrogen production at commercial current densities. *Appl. Catal. B: Environ.*, 2023, **322**, 122100.
[DOI:10.1016/j.apcatb.2022.122100](https://doi.org/10.1016/j.apcatb.2022.122100)
- [13] J.N. Hansen, H. Prats, K.K. Toudahl, N.M. Secher, K. Chan, J. Kibsgaard and I. Chorkendorff, Is there anything better than Pt for HER? *ACS Energy Lett.*, 2021, **6**, 1175-1180. [DOI:10.1021/acscenergylett.1c00246](https://doi.org/10.1021/acscenergylett.1c00246)
- [14] L. Du, V. Prabhakaran, X. Xie, S. Park, Y. Wang, Y. Shao, Low-PGM and PGM-free catalysts for proton exchange membrane fuel cells: Stability challenges and material solutions. *Adv. Mater.*, 2021, **33**, 1908232.
[DOI:10.1002/adma.201908232](https://doi.org/10.1002/adma.201908232)
- [15] L. Tian, Z. Li, X. Xu, C. Zhang, Advances in noble metal (Ru, Rh, and Ir) doping for boosting water splitting electrocatalysis. *J. Mater. Chem. A*, 2021, **9**, 13459-13470. [DOI:10.1039/D1TA01108A](https://doi.org/10.1039/D1TA01108A)
- [16] J. Huang, B. Hu, J. Meng, T. Meng, W. Liu, Y. Guan, L. Jin and X. Zhang, Highly efficient sustainable strategies toward carbon-neutral energy production. *Energy Environ. Sci.*, 2024, **17**, 1007-1045.
[DOI:10.1039/D3EE03363E](https://doi.org/10.1039/D3EE03363E)
- [17] M.A.U. Din, M.R. Krishnan and E.H. Alsharaeh, Design strategies for cost-effective high-performance electrocatalysts in seawater electrolysis to produce hydrogen. *J. Energy Chem.*, 2024, **102**, 497-515.
[DOI:10.1016/j.jechem.2024.10.047](https://doi.org/10.1016/j.jechem.2024.10.047)
- [18] O.S. Ibrahim, A. Singlitico, R. Proskovics, S. McDonagh, C. Desmond and J.D. Murphy, Dedicated large-scale floating offshore wind to hydrogen: Assessing design variables in proposed typologies. *Renew. Sustain. Energy Rev.*, 2022, **160**, 112310. [DOI:10.1016/j.rser.2022.112310](https://doi.org/10.1016/j.rser.2022.112310)
- [19] IPCC (2021), Climate Change 2021 - The Physical Science Basis: Contribution of Working Group I to the Sixth Assessment Report of the Intergovernmental Panel on Climate Change, Cambridge University Press (2021), [DOI:10.1017/9781009157896](https://doi.org/10.1017/9781009157896)
- [20] IEA (2021), Net Zero by 2050: A roadmap for the global energy sector, IEA, Paris. Available at: <https://www.iea.org/reports/net-zero-by-2050>
- [21] M. Dvoynikov, G. Buslaev, A. Kunshin, D. Sidorov, A. Kraslawski and M. Budovskaya, New concepts of hydrogen production and storage in the Arctic region. *Resources*, 2021, **10**, 3. [DOI:10.3390/resources10010003](https://doi.org/10.3390/resources10010003)

- [22] F. Dawood, M. Anda and G.M. Shafiullah, Hydrogen production for energy: An overview. *Int. J. Hydrogen Energy*, 2020, **45**, 3847-3869. DOI:10.1016/j.ijhydene.2019.12.059
- [23] J. Diab, L. Fulcheri, V. Hessel, V. Rohani and M. Frenklach, Why turquoise hydrogen will Be a game changer for the energy transition. *Int. J. Hydrogen Energy*, 2022, **47**, 25831-25848. DOI:10.1016/j.ijhydene.2022.05.299
- [24] A.I. Osman, N. Mehta, A.M. Elgarahy, M. Hefny, A. Al-Hinai, A.A.H. Al-Muhtaseb and D.W. Rooney, Hydrogen production, storage, utilisation and environmental impacts: a review. *Environ. Chem. Lett.*, 2022, **20**, 153-188. DOI:10.1007/s10311-021-01322-8
- [25] World Energy Council (2019), New hydrogen economy: hope or hype? Available at: <https://www.worldenergy.org/assets/downloads/WEInnovation-Insights-Brief-New-Hydrogen-Economy-Hype-or-Hope.pdf>
- [26] IEA (2024), Global Hydrogen Review 2024, IEA, Paris. Available at: <https://iea.blob.core.windows.net/assets/89c1e382-dc59-46ca-aa47-9f7d41531ab5/GlobalHydrogenReview2024.pdf>
- [27] IEA (2024), Coal 2024, IEA, Paris. Available at: <https://iea.blob.core.windows.net/assets/a1ee7b75-d555-49b6-b580-17d64ccc8365/Coal2024.pdf>
- [28] N.A. Kelly, Hydrogen production by water electrolysis. In *Advances in hydrogen production, storage and distribution*, 2014, 159-185. Woodhead Publishing. DOI:10.1533/9780857097736.2.159
- [29] R. Sen, S. Das, A. Nath, P. Maharana, P. Kar, F. Verpoort, P. Liang, and S. Roy, Electrocatalytic water oxidation: An overview with an example of translation from lab to market. *Front. Chem.*, 2022, **10**, 861604. DOI:10.3389/fchem.2022.861604
- [30] B. You and Y. Sun, Innovative strategies for electrocatalytic water splitting. *Acc. Chem. Res.*, 2018, **51**, 1571-1580. DOI:10.1021/acs.accounts.8b00002
- [31] A. Mathur and C.E. Diesendruck, Advanced Device Architecture Strategies for Decoupled Water Splitting: A Review. *ACS Mater. Lett.*, 2024, **6**, 2725-2737. DOI:10.1021/acsmaterialslett.4c00745
- [32] S. Gupta, M.K., Patel, A. Miotello, and N. Patel, Metal boride-based catalysts for electrochemical water-splitting: a review. *Adv. Funct. Mater.*, 2020, **30**, 1906481. DOI:10.1002/adfm.201906481
- [33] A. Raveendran, M. Chandran, and R. Dhanusuraman, A comprehensive review on the electrochemical parameters and recent material development of electrochemical water splitting electrocatalysts. *RSC Adv.*, 2023, **13**, 3843-3876. DOI:10.1039/D2RA07642J

- [34] NT. Suen, SF. Hung, Q. Quan, N. Zhang, YJ. Xu and HM. Chen, Electrocatalysis for the oxygen evolution reaction: recent development and future perspectives. *Chem. Soc. Rev.*, 2017, **46**, 337-365. DOI:10.1039/C6CS00328A
- [35] T. Naito, T. Shinagawa, T. Nishimoto and K. Takanabe, Recent advances in understanding oxygen evolution reaction mechanisms over iridium oxide. *Inorg. Chem. Front.*, 2021, **8**, 2900-2917. DOI:10.1039/D0QI01465F
- [36] Q. Liang, G. Brocks and A. Bieberle-Hütter, Oxygen evolution reaction (OER) mechanism under alkaline and acidic conditions. *J. Phys. Energy*, 2021, **3**, 026001. DOI:10.1088/2515-7655/abdc85
- [37] X. Li, Z. Cheng and X. Wang, Understanding the mechanism of the oxygen evolution reaction with consideration of spin. *Electrochem. Energy Rev.*, 2021, **4**, 136-145. DOI:10.1007/s41918-020-00084-1
- [38] Y. Zhan, M. Lu, S. Yang, C. Xu, Z. Liu, and J.Y. Lee, Activity of transition-metal (manganese, iron, cobalt, and nickel) phosphates for oxygen electrocatalysis in alkaline solution. *ChemCatChem*, 2016, **8**, 372-379. DOI:10.1002/cctc.201500952
- [39] H. Osgood, S.V. Devaguptapu, H. Xu, J. Cho and G. Wu, Transition metal (Fe, Co, Ni, and Mn) oxides for oxygen reduction and evolution of bifunctional catalysts in alkaline media. *Nano Today*, 2016, **11**, 601-625. DOI:10.1016/j.nantod.2016.09.001
- [40] K.S. Exner, Design criteria for oxygen evolution electrocatalysts from first principles: introduction of a unifying material-screening approach. *ACS Appl. Energy Mater.*, 2019, **2**, 7991-8001. DOI:10.1021/acsaem.9b01480
- [41] M. Tahir, L. Pan, F. Idrees, X. Zhang, L. Wang, JJ. Zou and Z.L. Wang, Electrocatalytic oxygen evolution reaction for energy conversion and storage: A comprehensive review. *Nano Energy*, 2017, **37**, 136-157. DOI:10.1016/j.nanoen.2017.05.022
- [42] L. Jin, H. Xu, K. Wang, Y. Liu, X. Qian, H. Chen and G. He, Design strategies of electrocatalyst for improving durability and selectivity of seawater splitting. *Chem. Eng. J.*, 2025, **507**, 160362. DOI:10.1016/j.cej.2025.160362
- [43] J. Liang, Z. Li, X. He, Y. Luo, D. Zheng, Y. Wang, T. Li, B. Ying, S. Sun, Z. Cai, Q. Liu, B. Tang and X. Sun, Electrocatalytic seawater splitting: Nice designs, advanced strategies, challenges and perspectives. *Mater. Today*, 2023, **69**, 193-235. DOI:10.1016/j.mattod.2023.08.024
- [44] X. Liu, J. Chi, N. Mao and L. Wang, Principles of designing electrocatalyst to boost reactivity for seawater splitting. *Adv. Energy Mater.*, 2023, **13**, 2301438. DOI:10.1002/aenm.202301438

- [45] Y.S. Park, J. Lee, M.J. Jang, J. Yang, J. Jeong, J. Park, Y. Kim, M.S. Seo, Z. Chen and S.M. Choi, High-performance anion exchange membrane alkaline seawater electrolysis. *J. Mater. Chem. A*, 2021, **9**, 9586-9592. DOI:10.1039/D0TA12336F
- [46] The U.S. Geological Survey, Available at: <https://www.usgs.gov/special-topics/water-science-school/science/how-much-water-there-earth>
- [47] The U.S. Geological Survey, Available at: <https://www.usgs.gov/media/images/how-much-water-there-earth-1>
- [48] Igor Shiklomanov's chapter "World freshwater resources" in Peter H. Gleick (editor), 1993, *Water in Crisis: A Guide to the World's Freshwater Resources* (Oxford University Press, New York). Available at: <https://static1.squarespace.com/static/5eb18d627d53aa0e85b60c65/t/5eda4aab9295d05ffb9402ee/1591364273240/Gleick-Peter.-1993.-Water-in-crisis.pdf>
- [49] The U.S. Geological Survey. Available at: <https://www.usgs.gov/media/images/distribution-water-and-above-earth>
- [50] S. Dresp, F. Dionigi, M. Klingenhof and P. Strasser, Direct electrolytic splitting of seawater: opportunities and challenges. *ACS Energy Lett.*, 2019, **4**, 933-942. DOI:10.1021/acseenergylett.9b00220
- [51] J. Li, J. Sun, Z. Li, and X. Meng, Recent advances in electrocatalysts for seawater splitting in hydrogen evolution reaction. *Int. J. Hydrogen Energy*, 2022, **47**, 29685-29697. DOI:10.1016/j.ijhydene.2022.06.288
- [52] J. Liu, X. Liu, H. Shi, J. Luo, L. Wang, J. Liang, S. Li, L.M. Yang, T. Wang, Y. Huang and Q. Li, Breaking the scaling relations of oxygen evolution reaction on amorphous NiFeP nanostructures with enhanced activity for overall seawater splitting. *Appl. Catal. B: Environ.*, 2022, **302**, 120862. DOI:10.1016/j.apcatb.2021.120862
- [53] J. Liu, S. Duan, H. Shi, T. Wang, X. Yang, Y. Huang, G. Wu and Q. Li, Rationally designing efficient electrocatalysts for direct seawater splitting: challenges, achievements, and promises. *Angew. Chem.*, 2022, **134**, e202210753. DOI:10.1002/ange.202210753
- [54] H.Y. Wang, C.C. Weng, J.T. Ren and Z.Y. Yuan, An overview and recent advances in electrocatalysts for direct seawater splitting. *Front. Chem. Sci. Eng.*, 2021, **15**, 1408-1426. DOI:10.1007/s11705-021-2102-6
- [55] S. Bolar, S. Shit, N.C. Murmu and T. Kuila, Progress in theoretical and experimental investigation on seawater electrolysis: opportunities and challenges. *Sust. Energy Fuels*, 2021, **5**, 5915-5945. DOI:10.1039/D1SE01347E

- [56] S. Khatun, H. Hirani and P. Roy, Seawater electrocatalysis: activity and selectivity. *J. Mater. Chem. A*, 2021, **9**, 74-86. DOI:10.1039/D0TA08709B
- [57] Y. Yao, X. Gao and X. Meng, Recent advances on electrocatalytic and photocatalytic seawater splitting for hydrogen evolution. *Int. J. Hydrogen Energy*, 2021, **46**, 9087-9100. DOI:10.1016/j.ijhydene.2020.12.212
- [58] J.N. Hausmann, R. Schlögl, P.W. Menezes and M. Driess, Is direct seawater splitting economically meaningful? *Energy Environ. Sci.*, 2021, **14**, 3679-3685. DOI:10.1039/D0EE03659E
- [59] A.R. Jadhav, A. Kumar, J. Lee, T. Yang, S. Na, J. Lee, Y. Luo, X. Liu, Y. Hwang, Y. Liu and H. Lee, Stable complete seawater electrolysis by using interfacial chloride ion blocking layer on catalyst surface. *J. Mater. Chem. A*, 2020, **8**, 24501-24514. DOI:10.1039/D0TA08543J
- [60] D.W. Kirk and A.E. Ledas, Precipitate formation during sea water electrolysis. *Int. J. Hydrogen Energy*, 1982, **7**, 925-932. DOI:10.1016/0360-3199(82)90160-4
- [61] S.C. Ke, R. Chen, G.H. Chen and X.L. Ma, Mini review on electrocatalyst design for seawater splitting: recent progress and perspectives. *Energy Fuels*, 2021, **35**, 12948-12956. DOI:10.1021/acs.energyfuels.1c02056
- [62] W. Tong, M. Forster, F. Dionigi, S. Dresp, R.S. Erami, P. Strasser, A.J. Cowan and P. Farràs, Electrolysis of low-grade and saline surface water. *Nat. Energy*, 2020, **5**, 367-377. DOI:10.1038/s41560-020-0550-8
- [63] G. Liu, Y. Xu, T. Yang and L. Jiang, Recent advances in electrocatalysts for seawater splitting. *Nano Mater. Sci.*, 2023, **5**, 101-116. DOI:10.1016/j.nanoms.2020.12.003
- [64] IRENA (2020), Green Hydrogen Cost Reduction: Scaling up Electrolysers to Meet the 1.5°C Climate Goal, International Renewable Energy Agency, Abu Dhabi. Available at: https://www.irena.org/-/media/Files/IRENA/Agency/Publication/2020/Dec/IRENA_Green_hydrogen_cost_2020.pdf
- [65] European Commission (2020), Communication from the Commission to the EUROPEAN Parliament, the Council, the EUROPEAN economic and Social Committee and the Committee of the Regions: A hydrogen strategy for a climate-neutral Europe. Available at: https://energy.ec.europa.eu/system/files/2020-07/hydrogen_strategy_0.pdf
- [66] IRENA (2021), World Energy Transitions Outlook: 1.5°C Pathway, International Renewable Energy Agency, Abu Dhabi. Available at: https://www.irena.org/media/Files/IRENA/Agency/Publication/2021/Jun/IRENA_World_Energy_Transitions_Outlook_2021.pdf

- [67] British Petroleum (2020), Statistical review of world energy 2021. Available at: <https://www.bp.com/content/dam/bp/business-sites/en/global/corporate/pdfs/energy-economics/statistical-review/bp-stats-review-2021-full-report.pdf>
- [68] IRENA (2023), World Energy Transitions Outlook 2023: 1.5°C Pathway, International Renewable Energy Agency, Abu Dhabi. Available at: https://www.irena.org/-/media/Files/IRENA/Agency/Publication/2023/Jun/IRENA_World_energy_transitions_outlook_2023.pdf
- [69] U.S. Department of Energy (2024), Hydrogen Program Plan. Available at: <https://www.hydrogen.energy.gov/docs/hydrogenprogramlibraries/pdfs/hydrogen-program-plan-2024.pdf>
- [70] U.S. Department of Energy (2023), U.S. National Clean Hydrogen Strategy and Roadmap. Available at: <https://www.hydrogen.energy.gov/docs/hydrogenprogramlibraries/pdfs/us-national-clean-hydrogen-strategy-roadmap.pdf>
- [71] U.S. Department of Energy (2021), Hydrogen Shot Available at: <https://www.energy.gov/topics/hydrogen-shot>
- [72] H. Xu, Y. Zhao, G. He and H. Chen, Race on engineering noble metal single-atom electrocatalysts for water splitting. *Int. J. Hydrogen Energy*, 2022, **47**, 14257-14279. DOI:10.1016/j.ijhydene.2022.02.152
- [73] X. Guo, H. Zhang, Z. Shen, X. Liu, W. Xia, M. Ma and D. Cao, Construction and prospect of noble metal-based catalysts for proton exchange membrane water electrolyzers. *Small Struct.*, 2023, **4**, 2300081. DOI:10.1002/sstr.202300081
- [74] G. Gao, Z. Sun, X. Chen, G. Zhu, B. Sun, Y. Yamauchi and S. Liu, Recent advances in Ru/Ir-based electrocatalysts for acidic oxygen evolution reaction. *Appl. Catal. B: Environ.*, 2024, **343**, 123584. DOI:10.1016/j.apcatb.2023.123584
- [75] B. Sun, H. Cheng, K. Song, Z. Jiang, C. Shi, H. Liang, S. Ma and H. Hu, Iridium-based electrocatalysts for oxygen evolution reaction in acidic media: from in situ characterization to rational design. *J. Energy Chem.*, 2025, **107**, 472-494. DOI:10.1016/j.jechem.2025.03.067
- [76] Y. Yang, T. Zhou, Z. Zeng, Y. Hu, F. Yang, W. Sun and L. He, Novel sulfate solid supported binary Ru-Ir oxides for superior electrocatalytic activity towards OER and CER. *J. Colloid Interface Sci.*, 2024, **659**, 191-202. DOI:10.1016/j.jcis.2023.12.178
- [77] S.C. Jesudass, S. Surendran, D.J. Moon, S. Shanmugapriya, J.Y. Kim, G. Janani, K. Veeramani, S. Mahadik, I.G. Kim, P. Jung, G. Kwon, K. Jin, J.K. Kim, K. Hong, Y.I. Park, T.H. Kim, J. Heo and U. Sim, Defect engineered ternary metal spinel-type Ni-Fe-Co oxide as bifunctional electrocatalyst for

- overall electrochemical water splitting. *J. Colloid Interface Sci.*, 2024, **663**, 566-576. [DOI:10.1016/j.jcis.2024.02.042](https://doi.org/10.1016/j.jcis.2024.02.042)
- [78] Z. Luo, Q. Peng, Z. Huang, L. Wang, Y. Yang, J. Dong, T.T. Isimjan and X. Yang, Fine-tune d-band center of cobalt vanadium oxide nanosheets by N-doping as a robust overall water splitting electrocatalyst. *J. Colloid Interface Sci.*, 2023, **629**, 111-120. [DOI:10.1016/j.jcis.2022.09.069](https://doi.org/10.1016/j.jcis.2022.09.069)
- [79] Z. Gao, T. Wang, Z. Zeng, Z. Guo, X. Xu, Y. Li, L. Lin, R. Jia and S. Han, Effect of oxygen vacancy on electrochemical performance of NiCo-layered double oxides as water splitting electrocatalyst. *J. Alloys Compd.*, 2023, **963**, 171273. [DOI:10.1016/j.jallcom.2023.171273](https://doi.org/10.1016/j.jallcom.2023.171273)
- [80] M. Khairy and K.G. Mahmoud, In-situ growth of nanostructured nickel sulphides on nickel foam platform for boosting the electrocatalytic activity of overall water splitting. *J. Alloys Compd.*, 2023, **935**, 168056. [DOI:10.1016/j.jallcom.2022.168056](https://doi.org/10.1016/j.jallcom.2022.168056)
- [81] K. Premnath, J. Madhavan, S. Prasad, M.J. Aljaafreh, M.S. AlSalhi and S.P. Loke, Ultra-efficient, low-cost and carbon-supported transition metal sulphide as a platinum-free electrocatalyst towards hydrogen evolution reaction at alkaline medium. *Int. J. Hydrogen Energy*, 2022, **47**, 41974-41983. [DOI:10.1016/j.ijhydene.2021.09.120](https://doi.org/10.1016/j.ijhydene.2021.09.120)
- [82] Y. Lu, Z. Li, Y. Xu, L. Tang, S. Xu, D. Li, J. Zhu and D. Jiang, Bimetallic Co-Mo nitride nanosheet arrays as high-performance bifunctional electrocatalysts for overall water splitting. *Chem. Eng. J.*, 2021, **411**, 128433. [DOI:10.1016/j.cej.2021.128433](https://doi.org/10.1016/j.cej.2021.128433)
- [83] Q. Li, P. Yang, Y. Liu, W. Xiao, Z. Xiao, G. Xu, L. Wang, F. Liu and Z. Wu, In-situ construction of pomegranate-like nickel-vanadium nitride for hydrogen production through urea-assisted water-splitting. *J. Alloys Compd.*, 2023, **968**, 171861. [DOI:10.1016/j.jallcom.2023.171861](https://doi.org/10.1016/j.jallcom.2023.171861)
- [84] A. Li, L. Zhang, F. Wang, L. Zhang, L. Li, H. Chen and Z. Wei, Rational design of porous Ni-Co-Fe ternary metal phosphides nanobricks as bifunctional electrocatalysts for efficient overall water splitting. *Appl. Catal. B: Environ.*, 2022, **310**, 121353. [DOI:10.1016/j.apcatb.2022.121353](https://doi.org/10.1016/j.apcatb.2022.121353)
- [85] X. Wang, C. Wang, F. Lai, H. Sun, N. Yu and B. Geng, Self-supported CoFe-P nanosheets as a bifunctional catalyst for overall water splitting. *ACS Appl. Nano Mater.*, 2021, **4**, 12083-12090. [DOI:10.1021/acsanm.1c02607](https://doi.org/10.1021/acsanm.1c02607)
- [86] S. Rajalekshmi, S.M.S. Kumar and A. Pandikumar, Exploring transition metal hydroxides performance in membrane-free electrolyzer based decoupled water splitting for step-wise production of hydrogen and oxygen. *Chem. Eng. J.*, 2024, **496**, 154215. [DOI:10.1016/j.cej.2024.154215](https://doi.org/10.1016/j.cej.2024.154215)
- [87] S. Ge, X. Shen, J. Gao, K. Ma, H. Zhao, R. Fu, C. Feng, Y. Zhao, Q. Jiao and H. Li, Synergy of Mo doping and heterostructures in FeCo₂S₄@Mo-NiCo

- LDH/NF as durable and corrosion-resistant bifunctional electrocatalyst towards seawater electrolysis at industrial current density. *Chem. Eng. J.*, 2024, **485**, 150161. DOI:10.1016/j.cej.2024.150161
- [88] Y. Ma, L. Li, Y. Zhang, N. Jian, H. Pan, J. Deng and J. Li, Nickel foam supported Mn-doped NiFe-LDH nanosheet arrays as efficient bifunctional electrocatalysts for methanol oxidation and hydrogen evolution. *J. Colloid Interface Sci.*, 2024, **663**, 971-980. DOI:10.1016/j.jcis.2024.02.191
- [89] C. Zhang, Z. Xu, Y. Yu, A. Long, X. Ge, Y. Song, Y. An and Y. Gu, Ternary NiMoCo alloys and fluffy carbon nanotubes grown on ZIF-67-derived polyhedral carbon frameworks as bifunctional electrocatalyst for efficient and stable overall water splitting. *Electrochim. Acta*, 2022, **424**, 140613. DOI:10.1016/j.electacta.2022.140613
- [90] F. Yang, Z. Li, F. Zhu, X. Chen, S. Ge, F. Yin, F.F. Yang, R. Yang, Y. Liu, L. Gao, Q. Wang, R. Feng, B. Jin and P. Hu, Three-dimensional multi-channel structure NiCo alloy used for boosting efficient overall water splitting. *Fuel*, 2024, **364**, 131119. DOI:10.1016/j.fuel.2024.131119
- [91] Y. He, W. Liu and J. Liu, MOF-based/derived catalysts for electrochemical overall water splitting. *J. Colloid Interface Sci.*, 2024, **661**, 409-435. DOI:10.1016/j.jcis.2024.01.106
- [92] Y. Li, Z. Feng, X. Wang, X. Han, C. Li, J. Xia, J., S. Yin, and H. Li, MOFs-derived 3D hierarchical CoFe₂O₄/RuO₂ hollow nanosheet array for efficient overall water splitting. *Electrochim. Acta*, 2024, **503**, 144930. DOI:10.1016/j.electacta.2024.144930
- [93] P. Sharma, S. Kainth, O.P. Pandey and R. Mahajan, Customized synthesis of 2D Ti₃C₂ MXene for improved overall water splitting. *ACS Appl. Nano Mater.*, 2023, **6**, 21788-21802. DOI:10.1021/acsanm.3c03986
- [94] M. Molaei and M. Atapour, Nickel-based coatings as highly active electrocatalysts for hydrogen evolution reaction: a review on electroless plating cost-effective technique. *Sustain. Mater. Technol.*, 2024, **40**, e00991. DOI:10.1016/j.susmat.2024.e00991
- [95] Z. Cai, X. Bu, P. Wang, W. Su, R. Wei, J.C. Ho, J. Yang and X. Wang, Simple and cost effective fabrication of 3D porous core-shell Ni nanochains@NiFe layered double hydroxide nanosheet bifunctional electrocatalysts for overall water splitting. *J. Mater. Chem. A*, 2019, **7**, 21722-21729. DOI:10.1039/C9TA07282A
- [96] H. Fan, Y. Ma, W. Chen, Y. Tang, L. Li and J. Wang, Facile one-step electrodeposition of two-dimensional nickel-iron bimetallic sulfides for efficient electrocatalytic oxygen evolution. *J. Alloys Compd.*, 2022, **894**, 162533. DOI:10.1016/j.jallcom.2021.162533

- [97] H. Liu, H. Chen, S. Zhang, K. Wang, L. Yang, Y. Chen, H. Liu and H. Li, Simplified fast synthesis of strong-coupling composite supercapacitor materials by one-step bipolar pulse electrodeposition. *J. Mater. Chem. A*, 2022, **10**, 14954-14964. DOI:10.1039/D2TA03436K
- [98] H.Y. Wang, J.T. Ren, L. Wang, M.L. Sun, H.M. Yang, X.W. Lv and Z.Y. Yuan, Synergistically enhanced activity and stability of bifunctional nickel phosphide/sulfide heterointerface electrodes for direct alkaline seawater electrolysis. *J. Energy Chem.*, 2022, **75**, 66-73. DOI:10.1016/j.jechem.2022.08.019
- [99] W. Yuan, Z. Cui, S. Zhu, Z. Li, S. Wu and Y. Liang, Structure engineering of electrodeposited NiMo films for highly efficient and durable seawater splitting. *Electrochim. Acta*, 2021, **365**, 137366. DOI:10.1016/j.electacta.2020.137366
- [100] C. Özgür and M.E. Mert, Prediction and optimization of the process of generating green hydrogen by electrocatalysis: A study using response surface methodology. *Fuel*, 2022, **330**, 125610. DOI:10.1016/j.fuel.2022.125610
- [101] B.J. Plowman, L.A. Jones and S.K. Bhargava, Building with bubbles: the formation of high surface area honeycomb-like films via hydrogen bubble templated electrodeposition. *Chem. Commun.*, 2015 **51**, 4331-4346. DOI:10.1039/C4CC06638C
- [102] P. Wang and B. Wang, Designing self-supported electrocatalysts for electrochemical water splitting: Surface/interface engineering toward enhanced electrocatalytic performance. *ACS Appl. Mater. Interfaces*, 2021, **13**, 59593-59617. DOI:10.1021/acsami.1c17448
- [103] H. Jiang, N. Cong, H. Jiang, M. Tian, Z. Xie, H. Fang, J. Han, Z. Ren and Y. Zhu, Dynamic hydrogen bubble template electrodeposition of Ru on amorphous Co support for electrochemical hydrogen evolution. *Int. J. Hydrogen Energy*, 2023, **48**, 21599-21609. DOI:10.1016/j.ijhydene.2023.03.077
- [104] A.A. Abdelraouf, A.M. Abdelrahim, M.G. Abd El-Moghny and M.S. El-Deab, Electrocatalysis by design: Enhanced bifunctional activity of exfoliated graphite rod modified with NiCo porous layers towards overall water splitting. *J. Environ. Chem. Eng.*, 2025, **13**, 117089. DOI:10.1016/j.jece.2025.117089
- [105] Z. Li, X. Zhang, C. Ou, Y. Zhang, W. Wang, S. Dong and X. Dong, Transition metal-based self-supported anode for electrocatalytic water splitting at a large current density. *Coord. Chem. Rev.*, 2023, **495**, 215381. DOI:10.1016/j.ccr.2023.215381

- [106] L. Hong, C. Jing, Y. Zhang, H. Huang, Q. Jiang and J. Tang, Heterostructures with transition metal sulfides and transition metal phosphide: NiMnS/FeP achieve efficient seawater OER. *J. Environ. Chem. Eng.*, 2025, **13**, 115224. DOI:10.1016/j.jece.2024.115224
- [107] J. Hao, K. Wu, C. Lyu, Y. Yang, H. Wu, J. Liu, N. Liu, W-M. Lau and J. Zheng, Recent advances in interface engineering of Fe/Co/Ni-based heterostructure electrocatalysts for water splitting. *Mater. Horiz.*, 2023, **10**, 2312-2342. DOI:10.1039/D3MH00366C
- [108] M. Salmi, N. Khossossi, Y. Boudad, C. Jama, F. Bentiss, Z. Zaroual and S. El Ghachtouli, Enhanced efficiency and durability of nickel sulfide catalyst integrated with reduced graphene oxide: Exploring hierarchically porous structures for methanol oxidation reaction. *Int. J. Hydrogen Energy*, 2025, **100**, 580-595. DOI:10.1016/j.ijhydene.2024.12.285
- [109] F. Arshad, A. Tahir, T.U. Haq, A. Munir, I. Hussain and F. Sher, Bubbles templated interconnected porous metallic materials: synthesis, surface modification, and their electrocatalytic applications for water splitting and alcohols oxidation. *ChemistrySelect*, 2022, **7**, e202202774. DOI:10.1002/slct.202202774
- [110] E. Cossar, M.S.E. Houache, Z. Zhang and E.A. Baranova, Comparison of electrochemical active surface area methods for various nickel nanostructures. *J. Electroanal. Chem.*, 2020, **870**, 114246. DOI:10.1016/j.jelechem.2020.114246
- [111] Y. Zhang, L. Chen, B. Yan, F. Zhang, Y. Shi and X. Guo, Regeneration of textile sludge into Cu₈S₅ decorated N, S self-doped interconnected porous carbon as an advanced bifunctional electrocatalyst for overall water splitting. *Chem. Eng. J.*, 2023, **451**, 138497. DOI:10.1016/j.cej.2022.138497
- [112] Y. Yu, J. Li, J. Luo, Z. Kang, C. Jia, Z. Liu, W. Huang, Q. Chen, P. Deng, Y. Shen and X. Tian, Mo-decorated cobalt phosphide nanoarrays as bifunctional electrocatalysts for efficient overall water/seawater splitting. *Mater. Today Nano*, 2022, **18**, 100216. DOI:10.1016/j.mtnano.2022.100216
- [113] M. Saquib, P. Arora and A. C. Bhosale, Nickel molybdenum selenide on carbon cloth as an efficient bifunctional electrocatalyst for alkaline seawater splitting. *Fuel*, 2024, **365**, 131251. DOI:10.1016/j.fuel.2024.131251
- [114] Y. Luo, P. Wang, G. Zhang, S. Wu, Z. Chen, H. Ranganathan, S. Sun and Z. Shi, Mn-doped nickel-iron phosphide heterointerface nanoflowers for efficient alkaline freshwater/seawater splitting at high current densities. *Chem. Eng. J.*, 2023, **454**, 140061. DOI:10.1016/j.cej.2022.140061
- [115] S. Gopalakrishnan, V. Saranya, S. Harish, E.S. Kumar and M. Navaneethan, Heterogeneous bimetallic oxysulfide nanostructure (Ni-Co) as hybrid bifunctional electrocatalyst for sustainable overall alkaline simulated

- seawater splitting. *J. Alloys Compd.*, 2023, **965**, 171124.
DOI:10.1016/j.jallcom.2023.171124
- [116] T. Yang, H. Lv, Q. Quan, X. Li, H. Lu, X. Cui, G. Liu and L. Jiang, Electronic structure modulation of MoO₂ via Er-doping for efficient overall water/seawater splitting and Mg/seawater batteries. *Appl. Surf. Sci.*, 2023, **615**, 156360. DOI:10.1016/j.apsusc.2023.156360
- [117] H. Wang, J. Ying, Y.X. Xiao, J.B. Chen, J.H. Li, Z.Z. He, H.J. Yang and X.Y. Yang, Ultrafast synthesis of Cu₂O octahedrons inlaid in Ni foam for efficient alkaline water/seawater electrolysis. *Electrochem. Commun.*, 2022, **134**, 107177. DOI:10.1016/j.elecom.2021.107177
- [118] J. Sun, J. Li, Z. Li, C. Li, G. Ren, Z. Zhang and X. Meng, Modulating the electronic structure on cobalt sites by compatible heterojunction fabrication for greatly improved overall water/seawater electrolysis. *ACS Sustain. Chem. Eng.*, 2022, **10**, 9980-9990. DOI:10.1021/acssuschemeng.2c02571
- [119] B. Debnath, S. Parvin, H. Dixit and S. Bhattacharyya, Oxygen-defect-rich cobalt ferrite nanoparticles for practical water electrolysis with high activity and durability. *ChemSusChem*, 2020, **13**, 3875-3886.
DOI:10.1002/cssc.202000932
- [120] Q. Zhang, K. Lian, Q. Liu, G. Qi, S. Zhang, J. Luo and X. Liu, High entropy alloy nanoparticles as efficient catalysts for alkaline overall seawater splitting and Zn-air batteries. *J. Colloid Interface Sci.*, 2023, **646**, 844-854.
DOI:10.1016/j.jcis.2023.05.074
- [121] M. Austeria, H.T. Dao, M. Mai and D.H. Kim, Dual-phase cobalt phosphide/phosphate hybrid interactions via iridium nanocluster interfacial engineering toward efficient overall seawater splitting. *Appl. Catal. B: Environ.*, 2023, **327**, 122467. DOI:10.1016/j.apcatb.2023.122467
- [122] C. Kim, S. Lee, S.H. Kim, J. Park, S. Kim, S.-H. Kwon, J.-S. Bae, Y.S. Park and Y. Kim, Cobalt-iron-phosphate hydrogen evolution reaction electrocatalyst for solar-driven alkaline seawater electrolyzer. *Nanomaterials*, 2021, **11**, 2989. DOI:10.3390/nano11112989
- [123] H. Jin, X. Wang, C. Tang, A. Vasileff, L. Li, A. Slattery and S.-Z. Qiao, Stable and highly efficient hydrogen evolution from seawater enabled by an unsaturated nickel surface nitride. *Adv. Mater.*, 2021, **33**, 2007508.
DOI:10.1002/adma.202007508

LISTS OF PUBLICATIONS

The main results of this doctoral thesis were published in 6 scientific publications (P: 1-6).

- P1. **S. Barua**, A. Balčiūnaitė, J. Vaičiūnienė, L. Tamašauskaitė-Tamašiūnaitė and E. Norkus, Three-dimensional Au(NiMo)/Ti catalysts for efficient hydrogen evolution reaction. *Materials*, 2022, **15**, 7901.
[DOI:10.3390/ma15227901](https://doi.org/10.3390/ma15227901)
- P2. **S. Barua**, A. Balčiūnaitė, J. Vaičiūnienė, L. Tamašauskaitė-Tamašiūnaitė and E. Norkus, Three-dimensional Au(NiMo)/Ti catalysts for efficient oxygen evolution reaction. *Chemija*, 2023, **34**, 32-40.
[DOI:10.6001/chemija.2023.34.1.4](https://doi.org/10.6001/chemija.2023.34.1.4)
- P3. **S. Barua**, A. Balčiūnaitė, J. Vaičiūnienė, L. Tamašauskaitė-Tamašiūnaitė and E. Norkus, Bimetallic 3D Nickel-Manganese/Titanium Bifunctional Electrocatalysts for Efficient Hydrogen and Oxygen Evolution Reaction in Alkaline and Acidic Media. *Coatings*, 2023, **13**, 1102.
[DOI:10.3390/coatings13061102](https://doi.org/10.3390/coatings13061102)
- P4. **S. Barua**, A. Balčiūnaitė, D. Upskuvienė, J. Vaičiūnienė, L. Tamašauskaitė-Tamašiūnaitė and E. Norkus, 3D Nickel-Manganese bimetallic electrocatalysts for an enhanced hydrogen evolution reaction performance in simulated seawater/alkaline natural seawater. *Int. J. Hydrogen Energy*, 2024, **79**, 1490-1500. [DOI:10.1016/j.ijhydene.2024.07.131](https://doi.org/10.1016/j.ijhydene.2024.07.131)
- P5. **S. Barua**, A. Balčiūnaitė, D. Upskuvienė, J. Vaičiūnienė, L. Tamašauskaitė-Tamašiūnaitė and E. Norkus, Bimetallic Ni-Mn Electrocatalysts for Stable Oxygen Evolution Reaction in Simulated/Alkaline Seawater and Overall Performance in the Splitting of Alkaline Seawater. *Coatings*, 2024, **14**, 1074.
[DOI:10.3390/coatings14081074](https://doi.org/10.3390/coatings14081074)




PUBLICATION IN PRESS

- P6. **S. Barua**, A. Balčiūnaitė, D. Upskuvienė, J. Vaičiūnienė, L. Tamašauskaitė-Tamašiūnaitė and E. Norkus, 3D NiMnCo electrocatalysts with cauliflower curd-shaped microspherical morphology for an efficient and sustainable hydrogen evolution reaction in alkaline freshwater/seawater media. (Submitted)

(No special permission is required to reuse all or part of articles published, including figures and tables as these are open access articles; published under an open access Creative Commons CC BY 4.0 license (MDPI and Chemija) and the author retains the right to include those Elsevier articles in a thesis or dissertation.)

Article

Three-Dimensional Au(NiMo)/Ti Catalysts for Efficient Hydrogen Evolution Reaction

Sukomol Barua , Aldona Balčiūnaitė *, Jūrate Vaičiūnienė, Loretta Tamašauskaitė-Tamašiūnaitė  and Eugenijus Norkus * 

Department of Catalysis, Center for Physical Sciences and Technology (FTMC), LT-10257 Vilnius, Lithuania

* Correspondence: aldonabalciaite@ftmc.lt (A.B.); eugenijus.norkus@ftmc.lt (E.N.)

Abstract: In this study, NiMo catalysts that have different metal loadings in the range of ca. 28–106 $\mu\text{g cm}^{-2}$ were electrodeposited on the Ti substrate followed by their decoration with a very low amount of Au-crystallites in the range of ca. 1–5 $\mu\text{g cm}^{-2}$ using the galvanic displacement method. The catalytic performance for hydrogen evolution reaction (HER) was evaluated on the NiMo/Ti and Au(NiMo)/Ti catalysts in an alkaline medium. It was found that among the investigated NiMo/Ti and Au(NiMo)/Ti catalysts, the Au(NiMo)/Ti-3 catalyst with the Au loading of 5.2 $\mu\text{g cm}^{-2}$ gives the lowest overpotential of 252 mV for the HER to reach a current density of 10 mA cm^{-2} . The current densities for HER increase ca. 1.1–2.7 and ca. 1.1–2.2 times on the NiMo/Ti and Au(NiMo)/Ti catalysts, respectively, at -0.424 V, with an increase in temperature from 25 °C to 75 °C.

Keywords: gold; nickel; molybdenum; electrodeposition; galvanic displacement; hydrogen evolution reaction



Citation: Barua, S.; Balčiūnaitė, A.; Vaičiūnienė, J.; Tamašauskaitė-Tamašiūnaitė, L.; Norkus, E. Three-Dimensional Au(NiMo)/Ti Catalysts for Efficient Hydrogen Evolution Reaction. *Materials* **2022**, *15*, 7901. <https://doi.org/10.3390/ma15227901>

Academic Editors: Soo Young Kim and Laura Calvillo

Received: 31 August 2022

Accepted: 5 November 2022

Published: 9 November 2022

Publisher's Note: MDPI stays neutral with regard to jurisdictional claims in published maps and institutional affiliations.

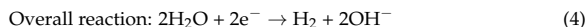
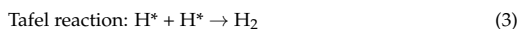
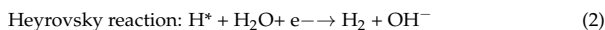
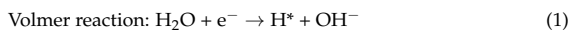


Copyright: © 2022 by the authors. Licensee MDPI, Basel, Switzerland. This article is an open access article distributed under the terms and conditions of the Creative Commons Attribution (CC BY) license (<https://creativecommons.org/licenses/by/4.0/>).

1. Introduction

Although fossil fuels, such as coal, oil, and natural gas, are the main energy sources and are widely used to meet energy needs, the increasing emissions of pollutants, carbon dioxide (CO_2), and other greenhouse gases require the development of sustainable technologies to meet ever-increasing energy needs. Among various candidates to fulfill energy demands, hydrogen (H_2) can be a potential substitute fuel for effective energy production and storage. H_2 is a clean, economical renewable energy source and an excellent energy storage medium with excellent energy conversion efficiency, higher gravimetric energy density than gasoline (120 vs. 44 MJ kg^{-1}), eco-friendliness, and zero carbon dioxide emission [1–4]. H_2 , an important chemical feedstock widely used in petroleum refining and ammonia synthesis, is industrially produced via coal gasification and steam reforming reaction under harsh conditions, resulting in the emission of greenhouse gases and micro-pollutants [5,6]. Among the various available methods, electrocatalytic water splitting is one of the most promising alternatives for H_2 production that gained intense research interest in the last decades, as electricity-driven water splitting generates green H_2 .

It is well-known that H_2 production by electrocatalytic water splitting in alkaline media is limited by the sluggish hydrogen evolution reaction (HER) kinetics and enormous electricity consumption. The HER mechanism of electrocatalytic water splitting includes three main steps, i.e., Volmer, Heyrovsky, and Tafel reactions, as shown below, in alkaline media [7]:



The sluggish HER kinetics in alkaline media is mainly due to the fact that in the Volmer reaction, the proton source comes from the water molecule instead of H_3O^+ in the acid electrolyte, which involves additional energy to break the H–O–H bond [7]. To date, platinum (Pt) is the most effective and benchmark electrocatalyst for HER to achieve the lowest overpotential in both acidic and alkaline mediums, but unfortunately, because of the high production costs and the scarcity of resources, the use of Pt or other noble metals for electrodes for the water splitting process is not economically feasible [8,9]. In this context, it is the pursuit of most researchers to find an efficient, cost-effective and stable non-noble metal electrocatalyst for alkaline media to accelerate the Volmer step. Recent studies demonstrated that a number of non-noble transition metal-based materials, including nickel, molybdenum [10–16], cobalt [17–19], iron [20,21], tungsten [22,23], and transition metal compounds (TMCs), such as carbides [23–25], phosphide [26–28], nitrides [29], and sulfides [30], were investigated as electrocatalysts for HER to achieve excellent chemical stability due to their low cost and sufficient corrosion resistance under alkaline media. Additionally, low-cost transition metals, especially nickel-based electrocatalysts, received noticeable attention as supercapacitor electrodes and bifunctional electrocatalysts due to their abundant reserves, intrinsic high catalytic activity, excellent corrosion resistance, and high electrical conductivity [31]. A number of methods, such as spontaneous galvanic displacement [32], electrochemical deposition [13,33,34], hydrothermal synthesis, etc., were developed to explore and enhance the HER activity of Ni-based bi- and tri-metallic alloy catalysts Ni-M (M = Fe, Co, Mn, Mo, Cr, etc.) and Ni-M bimetallic oxides (BOs).

According to Engel–Brewer valence bond theory, whenever metals of the left half of the transition series (such as Ni and Co) are alloyed with metals of the right half of the transition series metals (Mo or W), a synergistic effect can be anticipated in terms of hydrogen evolution activity [35]. The synergistic effect between Mo and Ni in the effect of hydrogen binding energy (HBE) is noteworthy, as the HBE between Ni and H is slightly weaker, whereas it is stronger enough between Mo and H. Therefore, the HBE can be controlled to a relatively moderate value by chemically coupling Ni and Mo, which can contribute to balancing the thermodynamics between hydrogen adsorption and desorption [36]. Moreover, enhanced HER activity demonstrated by a self-supported Ni–Mo–P ternary alloy coating on a three-dimensional (3D) Ni foam substrate (Ni–Mo–P/NF) were reported at a current density of $-10 \text{ mA}\cdot\text{cm}^{-2}$ at a small overpotential of -63 mV in 1 M KOH electrolyte [13]. Heterostructured Ni–Mo–N composite nanoparticles, decorated on nitrogen-doped reduced graphene oxide (Ni–Mo–N/NG), also reported an excellent HER electrocatalytic activity with zero onset potential and 46.6 and 159.8 mV overpotentials for 10 and $100 \text{ mA}\cdot\text{cm}^{-2}$, respectively, in 1 M potassium hydroxide (KOH) solution [14].

This study presents a simple and low-cost procedure to fabricate efficient catalysts for HER. Three-dimensional (3D) binary Ni–Mo catalysts with different total metal loadings supported on a titanium (Ti) surface (denoted as NiMo/Ti) were prepared via the electrodeposition method, whereas for the decoration of the prepared NiMo/Ti catalysts with a small amount of Au crystallites, the galvanic displacement method was used.

2. Materials and Methods

2.1. Chemicals

Titanium foil (99.7% purity) and HAuCl_4 (99.995%) were purchased from Sigma-Aldrich (Saint Louis, MO, USA) Supply. H_2SO_4 (96%), HCl (35–38%), nickel sulfate hexahydrate ($\text{NiSO}_4\cdot 6\text{H}_2\text{O}$, >98%), sodium molybdate dihydrate ($\text{Na}_2\text{MoO}_4\cdot 2\text{H}_2\text{O}$, >99.5%), and NaOH (98.8%) were purchased from Chempur Company (Karlsruhe, Germany). Ultra-pure water with a resistivity of $18.2 \text{ M}\Omega\cdot\text{cm}^{-1}$ was used for preparing the solutions. All chemicals were of analytical grade and used directly without further purification.

2.2. Fabrication of Catalysts

The catalysts were prepared by a facile, two-step process that involves electrodeposition of Ni^{2+} and Mo^{6+} ion on the surface of the Ti electrode, followed by a spontaneous

Au displacement from the Au (III)-containing solution. Before the deposition of the NiMo catalysts, the Ti plates were pretreated in diluted H_2SO_4 (1:1 vol) at 70°C for 3 s. NiMo catalysts were electroplated on the Ti surface (1×1 cm) from a bath containing 0.03 M Na_2MoO_4 along with 0.1, 0.2, and 1.0 M NiSO_4 in an acidic condition (1.5 M H_2SO_4 and 1 M HCl). The chronopotentiometry was used for the NiMo coatings deposition on the Ti surface. The plating of coatings was carried out at the current of 0.1 mA and 1 mA for 3 min at each current. The Au crystallites were deposited on the prepared NiMo/Ti electrodes by their immersion into 1 mM HAuCl_4 + 0.1 M HCl solution for 10 s. After plating, the samples were taken out, thoroughly rinsed with deionized water, and air-dried at room temperature.

2.3. Characterization of Catalysts

The morphology and composition of the prepared catalysts were investigated by scanning electron microscopy (SEM) TM 4000 Plus (HITACHI, Tokyo, Japan).

XRD patterns of pure Ti sheet, Ni-Mo/Ti, and Au-Ni-Mo/Ti catalysts were measured using an X-ray diffractometer D2 PHASER (Bruker, Karlsruhe, Germany). The measurements were conducted in the 2θ range of 10 – 90° .

The metal loadings were determined by inductively coupled plasma optical emission spectrometry (ICP–OES) analysis. The ICP–OES spectra were recorded using an Optima 7000DV spectrometer (Perkin Elmer, Waltham, MA, USA) at wavelengths of λ_{Ni} 231.604 nm, λ_{Mo} 202.031 nm, and λ_{Au} 267.595 nm.

2.4. Electrochemical Measurements

A conventional three-electrode electrochemical cell was used for electrochemical measurements. The fabricated NiMo/Ti and Au(NiMo)/Ti catalysts were employed as working electrodes, a Pt sheet was used as a counter electrode, and a calomel electrode was used as a reference. All potentials in this work were converted to the reversible hydrogen electrode (RHE) scale using the following Equation (5):

$$E_{\text{RHE}} = E_{\text{SCE}} + 0.242 \text{ V} + 0.059 \text{ V} \times \text{pH}_{\text{solution}}. \quad (5)$$

Current densities were calculated using the electrodes' geometric area of 2 cm^2 . Linear sweep voltammograms were recorded in a 1 M NaOH solution and always deaerated by argon (Ar) for 20 min prior to measurements. HER polarization curves were recorded from the open circuit potential (OCP) to -0.42 V (vs. RHE) at a polarization rate of $10 \text{ mV} \cdot \text{s}^{-1}$. Polarization curves were recorded at several temperatures from 25 to 75°C , and temperatures were set with a water jacket connected to a LAUDA Alpha RA 8 thermostat. Stability was studied by recording chronoamperometry (CA) curves for HER at a potential of -0.22 V (vs. RHE) for half an hour. All electrochemical measurements were performed with a Metrohm Autolab potentiostat (PGSTAT302, Utrecht, The Netherlands) using the Electrochemical Software (Nova 2.1.4).

3. Results

In this study, we investigated the electrocatalytic activity of prepared 3D binary NiMo/Ti and ternary Au(NiMo)/Ti catalysts for HER. These catalysts were deposited on the Ti surface (1×1 cm) using an electrochemical bath. The optimal conditions for different 3D binary catalyst depositions were determined and are given in Table 1. The electrochemical deposition was carried out by applying the constant current of 0.1 mA and 1 mA for 3 min at each current. The Au crystallites were deposited on the prepared NiMo/Ti electrodes by their immersion into 1 mM HAuCl_4 + 0.1 M HCl solution for 10 s at room temperature.

Table 1. Composition of the electrochemical bath.

Catalysts	Concentration in Mol dm ^{−3}	
	Ni ²⁺	Mo ⁶⁺
NiMo/Ti-1	0.1	0.03
NiMo/Ti-2	0.2	0.03
NiMo/Ti-3	1.0	0.03

The morphology and composition of the prepared catalysts were studied by SEM. Figure 1 shows SEM images of the prepared different compositions 3D NiMo/Ti and Au(NiMo)/Ti catalysts. The low magnification SEM image of the 3D NiMo/Ti-3 catalyst (Figure 1c) proves the formation of many cedar leaf-like Ni-Mo alloy structures in a large area, in which leaf-like Ni-Mo alloy is uniformly dispersed on the Ti foil. These cedar leaf-like structures still retain much space among the leaves, forming a porous morphology that can be expected to facilitate electrolyte penetration. Many nanoparticles can be seen in Figure 1c, and they irregularly stack together, forming a cedar leaf-like structure. When Au crystallites were deposited on the prepared NiMo/Ti-3 electrode by being immersed into 1 mM HAuCl₄ + 0.1 M HCl solution for 10 s, the porous leaf-like alloy structure was immediately covered with a tiny globular surface (Figure 1f). The mass of the elements (metal loadings) on the Ti substrate surface was determined by ICP-OES analysis (Table 2).

Table 2. The metal loading in the catalysts was determined by ICP-OES analysis and metal mass weight ratio.

Catalyst	Ni Loadings (μg _{Ni} cm ^{−2})	Mo Loadings (μg _{Mo} cm ^{−2})	Auloadings (μg _{Au} cm ^{−2})	Total Metal Loading (μg _{metal} cm ^{−2})	Mass Weight Ratio	
					Mo:Ni	Au:NiMo
NiMo/Ti-1	23.4	4.9		28.3	1:4.78	
NiMo/Ti-2	29.6	5.3		34.9	1:5.58	
NiMo/Ti-3	99.5	6.7		106.2	1:14.85	
Au(NiMo)/Ti-1	18.3	4.4	1.2	23.9	1:4.16	1:18.92
Au(NiMo)/Ti-2	25.4	4.6	1.7	31.7	1:5.52	1:17.65
Au(NiMo)/Ti-3	81.4	6.0	5.2	92.6	1:13.57	1:16.81

It can be seen that the formed 3D binary NiMo/Ti catalysts contained ca. 82.8–93.7 wt.% of Ni, whereas those 3D ternaries Au(NiMo)/Ti catalysts possessed 76.6–87.9 wt.% of Ni. The total metal loadings (μg_{metal}cm^{−2}) in the prepared catalysts are quite different and vary from 23.9 up to 106.2 μg_{metal}cm^{−2}. It should be noted that Ni and Mo amounts increase in the NiMo coatings by increasing the Ni²⁺ concentration in the plating solution, whereas the Mo amount was kept the same. Calculated Mo:Ni and Au:NiMo mass weight ratios are given in Table 2.

As seen from the data in Table 2, mass weight ratios Mo:Ni for NiMo/Ti increase due to the rise of Ni²⁺ concentration in the plating solution. A similar phenomenon is observed in the case of Au crystallite-modified NiMo/Ti catalysts. Mass ratios Mo:Ni also increase with the increase in the Ni²⁺ concentration in the plating solution (Table 2). Moreover, Au loadings in the AuNiMo/Ti-1, AuNiMo/Ti-2, and AuNiMo/Ti-3 catalysts increased while the deposition times of Au crystallites were the same—10 s. The mass ratio Au:NiMo slightly decreases. The increased Ni amount in the catalysts allows for achieving a higher Au loading in the ones.

Figure 2 shows XRD patterns for a pure Ti sheet (lower curve) and NiMo/Ti-3 and Au(NiMo)/Ti-3 catalysts (upper curves). Symbols indicate the positions of the XRD peaks of Ti (ICDD card no 00-044-1294).

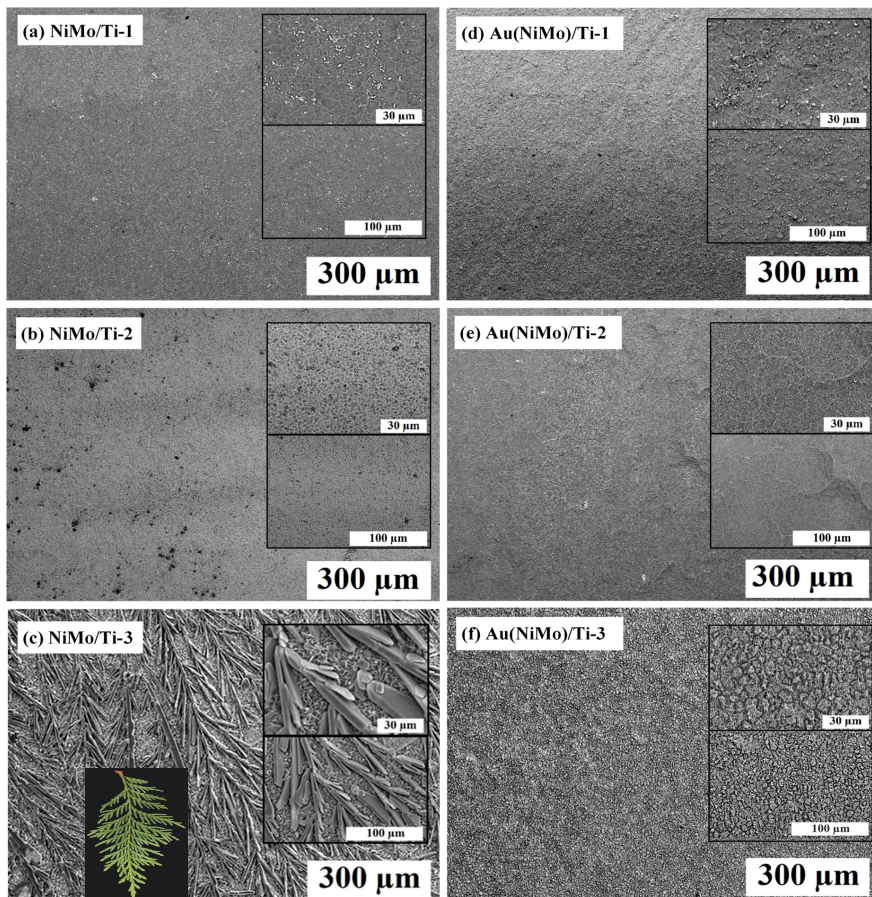


Figure 1. SEM views of NiMo/Ti (a–c) and Au(NiMo)/Ti (d–f) catalysts mentioned in Table 2. (c) The inset represents a photo of a cedar leaf.

The lowest XRD pattern (a) in Figure 2 contains sharp XRD peaks of the Ti sheet corresponding to the hexagonal structure of Ti. In the case of NiMo/Ti-3 and Au(NiMo)/Ti-3 catalysts, XRD peaks corresponding to Mo (110) and Mo (200) are shifted towards higher diffraction angles with respect to the positions of Mo presented in ICDD card no 00-044-1120. Additionally, the body-centered cubic lattice parameter decreases from 3.147 to 3.093 Å. This is the result of the formation of a solid solution of Ni (ICDD # 00-004-0850) with a small amount of Mo and Mo-Ni solid solution. There are no visible changes in the XRD patterns for NiMo/Ti-3 and Au(NiMo)/Ti-3 (Figure 2, b,c curves) as the Au (ICDD # 00-004-0784) peaks can be amorphous or crystalline with low intensity.

The electrocatalytic properties of the prepared catalysts were investigated by recording LSVs in 1.0 M NaOH solution at a potential scan rate of 10 mV·s^{−1} in a potential range from open-circuit potential (OCP) up to −0.42 V (vs. RHE) for HER, at several temperatures from 25 up to 75 °C (Figure 3). Ternary Au(NiMo)/Ti-3 coating exhibited the highest

current density (j), followed by Au(NiMo)/Ti-2 and Au(NiMo)/Ti-1, and the fabricated binary (NiMo/Ti) catalysts exhibited notably lower current density, in mutual comparison for HER (Figure 3). For those binary NiMo/Ti catalysts, the current density increases ca. 1.2–2.7 times with an increase in temperature from 25 up to 75 °C, whereas fabricated 3D ternary Au(NiMo)/Ti catalysts exhibit ca. 1.1–2.2 times higher current density for HER.

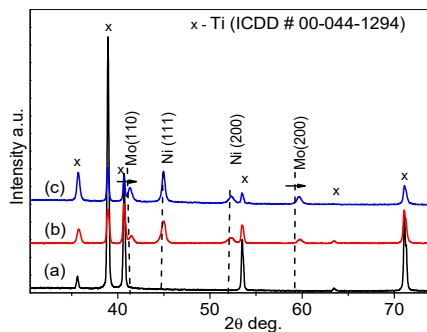


Figure 2. XRD patterns of Ti sheet (a), Ni-Mo/Ti-3 (b), and Au(Ni-Mo)/Ti-3 (c) catalysts.

The electrocatalytic properties of the prepared catalysts were investigated by recording LSVs in 1.0 M NaOH solution at a potential scan rate of 10 mV·s^{−1} in a potential range from open-circuit potential (OCP) up to −0.42 V (vs. RHE) for HER, at several temperatures from 25 up to 75 °C (Figure 3). Ternary Au(NiMo)/Ti-3 coating exhibited the highest current density (j), followed by Au(NiMo)/Ti-2 and Au(NiMo)/Ti-1, and the fabricated binary (NiMo/Ti) catalysts exhibited notably lower current density, in mutual comparison for HER (Figure 3). For those binary NiMo/Ti catalysts, the current density increases ca. 1.2–2.7 times with an increase in temperature from 25 up to 75 °C, whereas fabricated 3D ternary Au(NiMo)/Ti catalysts exhibit ca. 1.1–2.2 times higher current density for HER.

For instance, the current densities of −49.84, −40.73, and −36.58 mA·cm^{−2} were reached at −0.424 V (vs. RHE) using Au-decorated ternary Au(NiMo)/Ti-3, Au(NiMo)/Ti-2, and Au(NiMo)/Ti-1 catalysts, and relatively lower −34.81, −26.5, and −21.75 mA·cm^{−2} current densities were recorded at the same potential via using 3D binary NiMo/Ti-3, NiMo/Ti-2, and NiMo/Ti-1 catalysts at 25 °C, respectively (Figure 4a,b, Table 3). Overpotentials (vs. RHE) to reach the current density of 10 mA·cm^{−2} (η_{10}) were found in a gradual increasing order for both Au(NiMo)/Ti and NiMo/Ti catalysts as follows:

$$\text{Au(NiMo)/Ti-3 (−252 mV)} < \text{Au(NiMo)/Ti-2 (−298 mV)} < \text{Au(NiMo)/Ti-1 (−308 mV)} \\ \text{NiMo/Ti-3 (−288 mV)} < \text{NiMo/Ti-2 (−344 mV)} < \text{NiMo/Ti-1 (−349 mV)}.$$

It was determined that mass weight ratios Mo:Ni for NiMo/Ti catalysts increase due to the increased Ni²⁺ concentration in the plating solution (Table 2). A higher mass-weight ratio Mo:Ni induces a more pronounced activity of the NiMo/Ti catalyst for HER. Additionally, the increased amount of Ni in the NiMo/Ti catalysts allows for achieving higher Au loading in the Au(NiMo)/Ti catalysts. This is the main factor that influences the lowering overpotential at Au(NiMo)/Ti catalysts compared with NiMo/Ti catalysts. The higher activity of Au crystallite-modified NiMo/Ti catalysts may be related with the synergetic effect of Au, Ni, and Mo [35].

HER polarization curves were then further used for constructing the Tafel plots and calculating the Tafel slope. Tafel slope values of 99.6, 100.5, and 130.4 mV·dec^{−1} were found for HER at NiMo/Ti-1, NiMo/Ti-2, and NiMo/Ti-3 catalysts, respectively. For those 3D ternary Au(NiMo)/Ti catalysts, Tafel slope values of 143.8, 98.7, and 131.2 mV·dec^{−1} were determined at Au(NiMo)/Ti-1, Au(NiMo)/Ti-2, and Au(NiMo)/Ti-3 catalysts, respectively (Figure 4a',b', Table 3). The determination of the Tafel slope explores the HER kinetics

by measuring the increase in current density with the increase in overpotential, whereas the exchange current density (j_0) reflects the electrode's intrinsic activity for HER. The exchange current density (j_0) was calculated for HER at all six catalysts by extrapolating the Tafel plots, η vs. $\log j$. Thus, the j_0 value of 0.144, 0.011, 0.076, 0.075, 0.006, and 0.005 $\text{mA}\cdot\text{cm}^{-2}$ were calculated for Au(NiMo)/Ti-3, Au(NiMo)/Ti-2, Au(NiMo)/Ti-1, NiMo/Ti-3, NiMo/Ti-2, and NiMo/Ti-1 catalysts, respectively (Table 3). It is worth noting that the j_0 value determined for HER at the Au(NiMo)/Ti-3 coating was ca. 2–28 times higher than that determined for the rest of the studied catalysts.

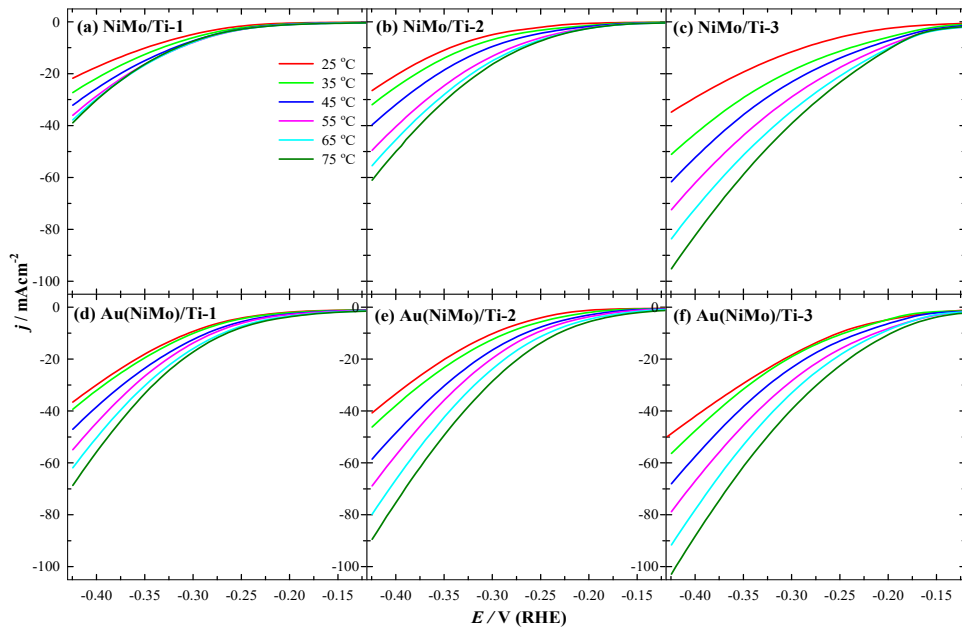


Figure 3. HER polarization curves of 3D NiMo/Ti (a–c) and Au(NiMo)/Ti (d–f) catalysts in 1 M NaOH solution at a $10 \text{ mV}\cdot\text{s}^{-1}$ potential scan rate and a temperature range (25–75 °C).

Table 3. Electrochemical performance of the tested catalysts toward HER in alkaline media.

Catalysts	j ($\text{mA}\cdot\text{cm}^{-2}$) in Different Temperatures (°C) at -0.424 V						Tafel Slope ($\text{mV}\cdot\text{dec}^{-1}$)	η_{10}^* (mV)	j_0 ($\text{mA}\cdot\text{cm}^{-2}$)
	25	35	45	55	65	75			
NiMo/Ti-1	−21.75	−27.25	−32.14	−35.99	−37.83	−38.91	99.6	−349	0.005
NiMo/Ti-2	−26.5	−31.94	−39.72	−49.53	−55.44	−61.05	100.5	−344	0.006
NiMo/Ti-3	−34.81	−51.09	−61.63	−72.42	−83.62	−95.19	130.4	−288	0.075
Au(NiMo)/Ti-1	−36.58	−39.32	−47.04	−54.93	−61.86	−68.68	143.8	−308	0.076
Au(NiMo)/Ti-2	−40.73	−46.19	−58.55	−68.86	−79.8	−89.45	98.7	−298	0.011
Au(NiMo)/Ti-3	−49.84	−56.38	−68	−78.81	−91.6	−102.86	131.2	−252	0.144

* Overpotential at $10 \text{ mA}\cdot\text{cm}^{-2}$.

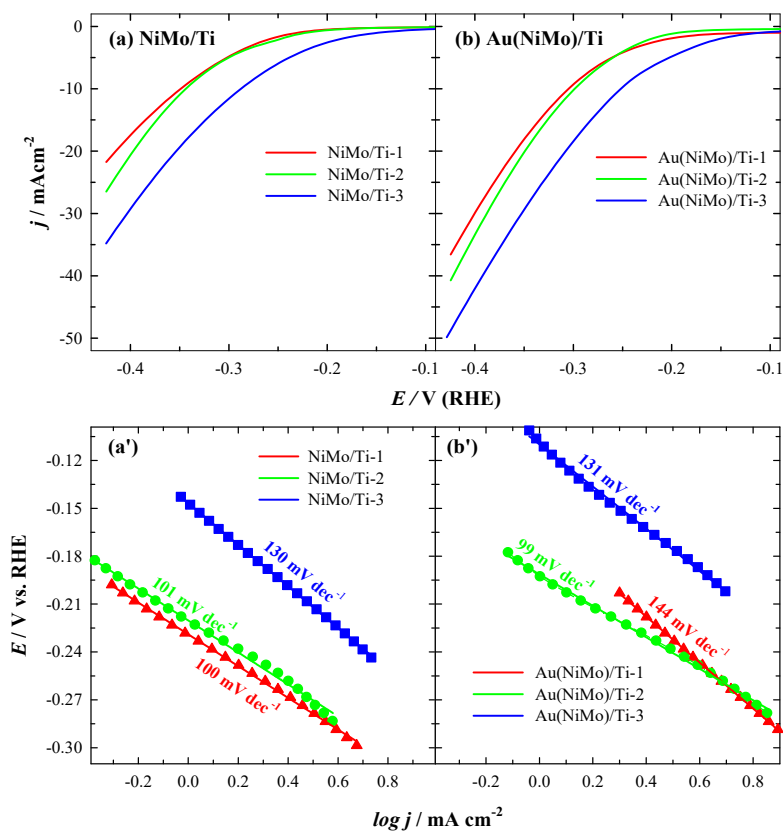


Figure 4. HER polarization curves of 3D NiMo/Ti (a) and Au(NiMo)/Ti (b) catalysts in 1 M NaOH solution at a potential scan rate of $10 \text{ mV} \cdot \text{s}^{-1}$ and 25°C temperature and corresponding Tafel plots (a',b').

Another crucial criterion for an advanced electrode material is its electrochemical stability. Chronoamperometric measurements with all six catalysts were carried out in 1 M NaOH at -0.22 V for 2 h. Initially, in the first 50–200 s, a decrease in current density was observed for all investigated catalysts. However, after approximately 500 s, the current densities settled down and remained apparently parallel throughout the experiments. CA results confirm the result of LSV analysis in terms of the ternary Au(NiMo)/Ti-3 catalyst, giving the highest current density during HER ($-10.36 \text{ mA} \cdot \text{cm}^{-2}$ at 50 s) (Figure 5). A more than 2.5 times lower current density was obtained with Au(NiMo)/Ti-2 ($-3.81 \text{ mA} \cdot \text{cm}^{-2}$) and ca. 5 times lower with Au(NiMo)/Ti-1 catalysts ($-2.02 \text{ mA} \cdot \text{cm}^{-2}$). In the case of the binary NiMo/Ti-3 catalyst, a comparatively lower current density was recorded ($-6.13 \text{ mA} \cdot \text{cm}^{-2}$ at 50 s) along with a 3–5 times lower value for NiMo/Ti-2 ($-2.06 \text{ mA} \cdot \text{cm}^{-2}$) and NiMo/Ti-1 ($-1.23 \text{ mA} \cdot \text{cm}^{-2}$) catalysts.

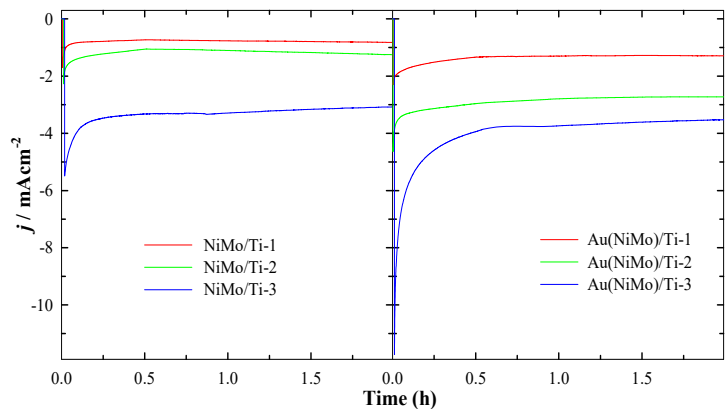


Figure 5. Chronoamperometric data of the investigated NiMo/Ti and Au(NiMo)/Ti catalysts in 1 M NaOH solution at the potential value of -0.22V (vs. RHE), $t = 2\text{ h}$.

A comparison of HER parameters generated using herein-tested NiMo/Ti and Au(NiMo)/Ti catalysts in an alkaline medium with some electrodes reported in the literature is given in Table 4.

Table 4. The electrochemical performance of herein tested catalysts towards HER in alkaline media and compared with that of transition metal-based electrodes reported in the literature.

Catalyst	Overpotential η_{10}^{**} (mV)	Tafel Slope (mV·dec ⁻¹)	Temperature (°C)	Electrolyte	Ref.
Au(NiMo)/Ti-3	−252	131.2	25	1 M NaOH	This work
NiMo/Ti-3	−288	130.4	25	1 M NaOH	This work
Au(NiMo)/Ti-2	−298	98.7	25	1 M NaOH	This work
NiMo/Ti-2	−344	100.5	25	1 M NaOH	This work
Au(NiMo)/Ti-1	−308	143.8	25	1 M NaOH	This work
NiMo/Ti-1	−349	99.6	25	1 M NaOH	This work
Ni-Mo-O MCFs	−222.8	141.6	-	1 M KOH	[33]
NiFeCMo-30	−254	163.9	-	30% KOH	[34]
NiS ₂ /MoS ₂ HNW	−204	65	-	1 M KOH	[37]
Ni-Cr-Mo-Fe, Ni-Cr-Mo, Ni-Cr alloy	−232 −249 −255	57.7 61.1 62.3	25	1 M KOH	[38]
Ni-Mo/WC 1, Ni-Mo/WC 2, Ni-Mo/WC 3	−411 −262 −134	208 153 163	25	1 M KOH	[39]
Ni/TM-360 s	−205	104	-	1 M KOH	[40]
NiCu _{0.57} /Ni ₃ S ₂ /TM, Ni/Ni ₃ S ₂ /TM	−239 −441	86 195	-	1 M KOH	[41]
Ni ₃ Te ₂ -Ni foam	−212	126.2	-	1 M KOH	[42]
Ni ₃ Te ₂ -Au glass	−237	73.1	-	1 M KOH	[42]
Ni ₃ Te ₂ -Hydrothermal	−304	94.2	-	1 M KOH	[42]
NiTe ₂ -nanosheet	−256	98	-	1 M KOH	[43]

Table 4. Cont.

Catalyst	Overpotential η_{10} ** (mV)	Tafel Slope (mV·dec ⁻¹)	Temperature (°C)	Electrolyte	Ref.
NiTeNR/NF	−248	185	-	1 M KOH	[44]
NiTe ₂	−520	188.3	-	1 M KOH	[45]

MCFs—mesoporous composite films, HNW—hybrid nanowire, WC—tungsten carbide, TM—Ti mesh, and NR/NF—nanorods/Ni foam. ** Overpotential at 10 mA·cm⁻².

4. Conclusions

In summary, NiMo and Au(NiMo) catalysts supported on a titanium surface were studied as electrocatalysts for HER in an alkaline medium. NiMo/Ti catalysts with different total metal loadings in the range of ca. 28–106 $\mu\text{g cm}^{-2}$ were prepared using a simple and low-cost metal electrodeposition method. The decoration of the prepared NiMo/Ti catalysts with a small amount of Au-crystallites in the range of ca. 1–5 $\mu\text{g cm}^{-2}$ was carried out using the galvanic displacement method.

It was determined that, among the investigated catalysts, the Au(NiMo)/Ti-3 catalyst with the Au loading of 5.2 $\mu\text{g cm}^{-2}$ exhibits the highest current density, as well as exchange current density during HER in a 1 M NaOH solution. Moreover, the Au(NiMo)/Ti-3 catalyst also displays excellent HER performance with an overpotential of 252 mV at a current density of 10 mA·cm⁻².

Author Contributions: Conceptualization, A.B. and E.N.; methodology, J.V. and S.B.; formal analysis, S.B.; investigation, S.B. and J.V.; data curation, L.T.-T.; writing—original draft preparation, A.B. and S.B.; writing—review and editing, E.N. and A.B.; visualization, L.T.-T. All authors have read and agreed to the published version of the manuscript.

Funding: This research is funded by the European Social Fund under Measure No. 09.3.3-LMT-K-712-19-0138 ‘Development of Competences of Scientists, other Researchers and Students through Practical Research Activities’.

Institutional Review Board Statement: Not applicable.

Informed Consent Statement: Not applicable.

Data Availability Statement: Not applicable.

Conflicts of Interest: The authors declare no conflict of interest.

References

- Wang, W.; Xu, M.; Xu, X.; Zhou, W.; Shao, Z. Perovskite oxide-based electrodes for high-performance photoelectrochemical water splitting: A review. *Angew. Chem. Int. Ed.* **2020**, *59*, 136–152. [\[CrossRef\]](#) [\[PubMed\]](#)
- Ye, S.; Luo, F.; Zhang, Q.; Zhang, P.; Xu, T.; Wang, Q.; He, D.; Guo, L.; Zhang, Y.; He, C.; et al. Highly stable single Pt atomic sites anchored on aniline-stacked graphene for hydrogen evolution reaction. *Energy Environ. Sci.* **2019**, *12*, 1000–1007. [\[CrossRef\]](#)
- Wang, X.; Zhuang, L.; Jia, Y.; Liu, H.; Yan, X.; Zhang, L.; Yang, D.; Zhu, Z.; Yao, X. Plasma-triggered synergy of exfoliation, phase transformation, and surface engineering in cobalt diselenide for enhanced water oxidation. *Angew. Chem. Int. Ed.* **2018**, *57*, 16421–16425. [\[CrossRef\]](#)
- Wu, W.; Niu, C.; Wei, C.; Jia, Y.; Li, C.; Xu, Q. Activation of MoS₂ basal planes for hydrogen evolution by zinc. *Angew. Chem. Int. Ed.* **2019**, *58*, 2029–2033. [\[CrossRef\]](#)
- Lin, L.; Sherrell, P.; Liu, Y.; Lei, W.; Zhang, S.; Zhang, H.; Wallace, G.G.; Chen, J. Engineered 2D transition metal dichalcogenides—A vision of viable hydrogen evolution reaction catalysis. *Adv. Energy Mater.* **2020**, *10*, 1903870. [\[CrossRef\]](#)
- Zhang, S.; Zhang, X.; Rui, Y.; Wang, R.; Li, X. Recent advances in non-precious metal electrocatalysts for pH-universal hydrogen evolution reaction. *Green Energy Environ.* **2021**, *6*, 458–478. [\[CrossRef\]](#)
- Luo, W.; Wang, Y.; Cheng, C. Ru-based electrocatalysts for hydrogen evolution reaction: Recent research advances and perspectives. *Mater. Chem. Phys.* **2020**, *15*, 100274.
- Chen, Y.; Zheng, Y.; Yue, X.; Huang, S. Hydrogen evolution reaction in full pH range on nickel doped tungsten carbide nanocubes as efficient and durable non-precious metal electrocatalysts. *Int. J. Hydrogen Energy* **2020**, *45*, 8695–8702. [\[CrossRef\]](#)
- Chao, T.; Hu, Y.; Hong, X.; Li, Y. Design of noble metal electrocatalysts on an atomic level. *ChemElectroChem* **2019**, *6*, 289–303. [\[CrossRef\]](#)

10. Yan, Y.; Wang, P.; Lin, J.; Cao, J.; Qi, J. Modification strategies on transition metal-based electrocatalysts for efficient water splitting. *J. Energy Chem.* **2021**, *58*, 446–462. [\[CrossRef\]](#)
11. Mohammed-Ibrahim, J.; Sun, X. Recent progress on earth abundant electrocatalysts for hydrogen evolution reaction (HER) in alkaline medium to achieve efficient water splitting—A review. *J. Energy Chem.* **2019**, *34*, 111–160. [\[CrossRef\]](#)
12. Qian, G.; Chen, J.; Yu, T.; Liu, J.; Luo, L.; Yin, S. Three-phase heterojunction NiMo-based nano-needle for water splitting at industrial alkaline conditions. *Nano-Micro Lett.* **2022**, *14*, 20. [\[CrossRef\]](#) [\[PubMed\]](#)
13. Toghrayi, A.; Shahrabi, T.; Darband, G.B. Electrodeposition of self-supported Ni-Mo-P film on Ni foam as an affordable and high-performance electrocatalyst toward hydrogen evolution reaction. *Electrochim. Acta* **2020**, *335*, 135643. [\[CrossRef\]](#)
14. Xue, S.; Zhang, W.; Zhang, Q.; Du, J.; Cheng, H.M.; Ren, W. Heterostructured Ni-Mo-N nanoparticles decorated on reduced graphene oxide as efficient and robust electrocatalyst for hydrogen evolution reaction. *Carbon* **2020**, *165*, 122–128. [\[CrossRef\]](#)
15. Lu, X.; Cai, M.; Huang, J.; Xu, C. Ultrathin and porous Mo-doped Ni nanosheet arrays as high-efficient electrocatalysts for hydrogen evolution reaction. *J. Colloid Interface Sci.* **2020**, *562*, 307–312. [\[CrossRef\]](#)
16. Mei, M.; Xu, X.; Wang, Y.; Wang, X.; Huo, Y. Three-dimensional supramolecular phosphomolybdate architecture-derived Mo-based electrocatalytic system for overall water splitting. *Inorg. Chem. Front.* **2018**, *5*, 819–826. [\[CrossRef\]](#)
17. Liu, Y.; Yang, F.; Qin, W.; Yang, G. Co₂P@NiCo₂O₄ bi-functional electrocatalyst with low overpotential for water splitting in wide range pH electrolytes. *J. Colloid Interface Sci.* **2019**, *534*, 55–63. [\[CrossRef\]](#)
18. Cai, Z.; Li, A.; Zhang, W.; Zhang, Y.; Cui, L.; Liu, J. Hierarchical Cu@Co-decorated CuO@Co₃O₄ nanostructure on Cu foam as efficient self-supported catalyst for hydrogen evolution reaction. *J. Alloys Compd.* **2021**, *882*, 160749. [\[CrossRef\]](#)
19. Milikić, J.; Balčiūnaitė, A.; Sukackienė, Z.; Mladenović, D.; Santos, D.M.; Tamašauskaitė-Tamašiūnaitė, L.; Šljukić, B. Bimetallic Co-based (CoM, M= Mo, Fe, Mn) coatings for high-efficiency water splitting. *Materials* **2020**, *14*, 92. [\[CrossRef\]](#)
20. Gong, Y.; Pan, H.; Xu, Z.; Yang, Z.; Lin, Y.; Wang, J. Crossed FeCo₂S₄ nanosheet arrays grown on 3D nickel foam as high-efficiency electrocatalyst for overall water splitting. *Int. J. Hydrogen Energy* **2018**, *43*, 17259–17264. [\[CrossRef\]](#)
21. Liu, X.; Yin, Y.; Xiong, K.; Li, M. Facile synthesis of low-cost Fe₃C-nitrogen and phosphorus co-doped porous carbon nanofibers: The efficient hydrogen evolution reaction catalysts. *J. Alloys Compd.* **2021**, *856*, 156213. [\[CrossRef\]](#)
22. Lv, F.; Feng, J.; Wang, K.; Dou, Z.; Zhang, W.; Zhou, J.; Yang, C.; Luo, M.; Yang, Y.; Li, Y.; et al. Iridium-tungsten alloy nanodendrites as pH-universal water-splitting electrocatalysts. *ACS Cent. Sci.* **2018**, *4*, 1244–1252. [\[CrossRef\]](#) [\[PubMed\]](#)
23. Su, W.; Yan, P.; Wei, X.; Zhu, X.; Zhou, Q. Facile one-step synthesis of nitrogen-doped carbon sheets supported tungsten carbide nanoparticles electrocatalyst for hydrogen evolution reaction. *Int. J. Hydrogen Energy* **2020**, *45*, 33430–33439. [\[CrossRef\]](#)
24. Huang, J.; Hong, W.; Liu, W. Molybdenum carbide nanosheets decorated with Ni(OH)₂ nanoparticles towards efficient hydrogen evolution reaction in alkaline media. *Appl. Surf. Sci.* **2022**, *579*, 152152. [\[CrossRef\]](#)
25. Kim, S.K.; Qiu, Y.; Zhang, Y.J.; Hurt, R.; Peterson, A. Nanocomposites of transition-metal carbides on reduced graphite oxide as catalysts for the hydrogen evolution reaction. *Appl. Catal. B Environ.* **2018**, *235*, 36–44. [\[CrossRef\]](#)
26. Li, X.; Liu, Y.; Wu, Y.; Li, S.; Dai, Y.; Guan, J.; Zhang, M. Vanadium doped nickel cobalt phosphide as an efficient and stable electrode catalyst for hydrogen evolution reaction. *J. Electroanal. Chem.* **2021**, *902*, 115812. [\[CrossRef\]](#)
27. Thi, M.L.N.; Tran, T.H.; Anh, P.H.; Nhac-Vu, H.T.; Bui, Q.B. Hierarchical zinc-nickel phosphides nanosheets on 3D nickel foam as self-supporting electrocatalysts for hydrogen evolution reaction. *Polyhedron* **2019**, *168*, 80–87. [\[CrossRef\]](#)
28. Lu, Z.P.; Sepunaru, L. Electrodeposition of iron phosphide film for hydrogen evolution reaction. *Electrochim. Acta* **2020**, *363*, 137167. [\[CrossRef\]](#)
29. Chen, P.; Ye, J.; Wang, H.; Ouyang, L.; Zhu, M. Recent progress of transition metal carbides/nitrides for electrocatalytic water splitting. *J. Alloys Compd.* **2021**, *883*, 160833. [\[CrossRef\]](#)
30. Gao, T.; Nie, M.; Luo, J.; Huang, Z.; Sun, H.; Guo, P.; Xue, Z.; Liao, J.; Li, Q.; Teng, L. Nickel sulfides supported by carbon spheres as efficient catalysts for hydrogen evolution reaction. *Electrochem. Commun.* **2021**, *129*, 107076. [\[CrossRef\]](#)
31. Wang, L.; Fan, J.; Liu, Y.; Chen, M.; Lin, Y.; Bi, H.; Liu, B.; Shi, N.; Xu, D.; Bao, J.; et al. Phase-modulation of iron/nickel phosphides nanocrystals “Armored” with porous P-doped carbon and anchored on P-doped graphene nanohybrids for enhanced overall water splitting. *Adv. Funct. Mater.* **2021**, *31*, 2010912. [\[CrossRef\]](#)
32. Papaderakis, A.; Mintsouli, I.; Georgieva, J.; Sotiropoulos, S. Electrocatalysts prepared by galvanic replacement. *Catalysts* **2017**, *7*, 80. [\[CrossRef\]](#)
33. Zhao, X.; He, B.; Zhang, J.; Du, C.; Ye, Q.; Liu, S. Electrodeposition of mesoporous Ni-Mo-O composite films for hydrogen evolution reaction. *Vacuum* **2022**, *198*, 110888. [\[CrossRef\]](#)
34. Wu, Y.; He, H. Electrodeposited nickel-iron-carbon-molybdenum film as efficient bifunctional electrocatalyst for overall water splitting in alkaline solution. *Int. J. Hydrogen Energy* **2019**, *44*, 1336–1344. [\[CrossRef\]](#)
35. Bodnarova, R.; Kozeljova, M.; Latyshev, V.; Vorobiov, S.; Lisnichuk, M.; You, H.; Gregor, M.; Komanicky, V. Study of synergistic effects and compositional dependence of hydrogen evolution reaction on Mo_xNi_y alloy thin films in alkaline media. *Mol. Catal.* **2022**, *528*, 112481. [\[CrossRef\]](#)
36. Li, M.; Zhu, Y.; Wang, H.; Wang, C.; Pinna, N.; Lu, X. Ni strongly coupled with Mo₂C encapsulated in nitrogen-doped carbon nanofibers as robust bifunctional catalyst for overall water splitting. *Adv. Energy Mater.* **2019**, *9*, 1803185. [\[CrossRef\]](#)
37. Kuang, P.; Tong, T.; Fan, K.; Yu, J. In situ fabrication of Ni-Mo bimetal sulfide hybrid as an efficient electrocatalyst for hydrogen evolution over a wide pH range. *ACS Catal.* **2017**, *7*, 6179–6187. [\[CrossRef\]](#)

38. Nady, H.; El-Rabiei, M.M.; Samy, M.; Deyab, M.A.; Abd El-Hafez, G.M. Novel Ni–Cr-based alloys as hydrogen fuel sources through alkaline water electrolytes. *Int. J. Hydrogen Energy* **2021**, *46*, 34749–34766. [[CrossRef](#)]
39. Laszczyńska, A.; Tylus, W.; Szczygieł, I. Electrocatalytic properties for the hydrogen evolution of the electrodeposited Ni–Mo/WC composites. *Int. J. Hydrogen Energy* **2021**, *46*, 22813–22831. [[CrossRef](#)]
40. Wang, J.; Wang, Y.; Xie, T.; Deng, Q. Facile and fast synthesis of Ni composite coating on Ti mesh by electrodeposition method for high-performance hydrogen production. *Mater. Lett.* **2019**, *245*, 138–141. [[CrossRef](#)]
41. Wang, J.; Wang, Y.; Yao, Z.; Xie, T.; Deng, Q.; Jiang, Z.; Zhu, Q.; Liu, S.; Peng, Y.; Zhang, X. Enhanced hydrogen evolution activity of Ni/Ni₃S₂ nanosheet grown on Ti Mesh by Cu Doped Ni. *J. Electrochem. Soc.* **2019**, *166*, F168. [[CrossRef](#)]
42. De Silva, U.; Masud, J.; Zhang, N.; Hong, Y.; Liyanage, W.P.; Zaeem, M.A.; Nath, M. Nickel telluride as a bifunctional electrocatalyst for efficient water splitting in alkaline medium. *J. Mater. Chem. A* **2018**, *6*, 7608–7622. [[CrossRef](#)]
43. Ge, Y.; Gao, S.P.; Dong, P.; Baines, R.; Ajayan, P.M.; Ye, M.; Shen, J. Insight into the hydrogen evolution reaction of nickel dichalcogenide nanosheets: Activities related to non-metal ligands. *Nanoscale* **2017**, *9*, 5538–5544. [[CrossRef](#)] [[PubMed](#)]
44. Yang, L.; Xu, H.; Liu, H.; Cheng, D.; Cao, D. Active site identification and evaluation criteria of in situ grown CoTe and NiTe nanoarrays for hydrogen evolution and oxygen evolution reactions. *Small Methods* **2019**, *3*, 1900113. [[CrossRef](#)]
45. Nappini, S.; B'Olimpio, G.; Zhang, L.; Ghosh, B.; Kuo, C.-N.; Zhu, H.; Cheng, J.; Nardone, M.; Ottaviano, L.; Mondal, D.; et al. Transition-metal dichalcogenide NiTe₂: An ambient-stable material for catalysis and nanoelectronics. *Adv. Funct. Mater.* **2020**, *30*, 2000915. [[CrossRef](#)]

Three-dimensional Au(NiMo)/Ti catalysts for efficient oxygen evolution reaction

Sukomol Barua,

Aldona Balčiūnaitė*,

Jūratė Vaičiūnienė,

Loreta Tamašauskaitė-Tamašiūnaitė,

Eugenijus Norkus

*Department of Catalysis,
Center for Physical Sciences
and Technology (FTMC),
3 Saulėtekio Avenue,
10257 Vilnius, Lithuania*

In this study, three-dimensional gold-nickel-molybdenum (Au(NiMo)) catalysts have been studied as catalysts for the oxygen evolution reaction (OER). The catalysts have been deposited on a titanium surface using electroplating and galvanic displacement techniques. The modification of NiMo with a low amount of Au crystallites in a range of 1.2–5.2 $\mu\text{g}_{\text{Au}} \text{ cm}^{-2}$ results in enhanced activity for OER in the alkaline medium compared to respective binary un-modified NiMo catalysts. The current densities for OER increase ca. 1.2–7.3 and 1.3–5.1 times with an increase in temperature from 25 up to 75°C using the prepared 3D binary NiMo/Ti and Au(NiMo)/Ti catalysts, respectively.

Keywords: gold, nickel, molybdenum, three-dimensional catalysts, oxygen evolution reaction

INTRODUCTION

To address the ever-increasing energy demands and rapid depletion of fossil fuels and, at the same time, global warming and environmental emission, it is urgently important to exploit more and more clean and renewable alternative energy resources, e.g. solar, wind, geothermal energy, and bioenergy for a sustainable world. Research has shown that among those above-mentioned renewable fuels, hydrogen, the most abundant element on earth, can also be considered to be the most efficient main medium for energy storage in the future due to its excellent energy conversion efficiency, higher gravimetric energy density than gasoline (120 vs 44 MJ kg⁻¹), eco-friendliness, high-energy density, recyclability, as well as zero-emission of greenhouse gases [1–5].

Electrocatalytic water splitting has gained much research interest as one of the most promising methods for hydrogen production, as high pure hydrogen can be produced by electrochemical wa-

ter splitting as an environment-friendly method [6, 7]. The electrochemical water splitting incorporates two half-reactions, namely the hydrogen evolution reaction (HER) and oxygen evolution reaction (OER) on the cathode and anode, respectively. Compared to HER, OER is the main bottleneck for electrocatalytic water splitting due to its dual influence of sluggish reaction kinetics with multiple proton-couple electron transfer reactions and thermodynamics. As water electrolysis is thermodynamically hindered at standard temperature and pressure and more potential is required in addition to the standard thermodynamic potential (1.23 V), it is necessary to fabricate efficient catalysts for OER to overcome the resistance and barriers of hydrogen production by OER overpotentials. In this scenario, material selection and design are the key factors for exploring high-active electrocatalysts substantiating their cost, stability, efficiency and earth-abundance [8–11].

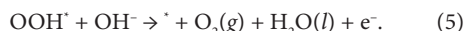
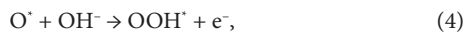
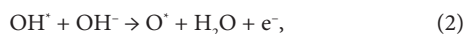
As it is well established that water electrolysis in acidic electrolytes has higher energy efficiency and production rate compared to alkaline electrolytes, albeit the harsh corrosive acidic environment

* Corresponding author. Email: aldona.balciunaite@ftmc.lt

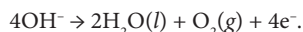
allows some noble metal-based catalysts only for both electrodes. At present, platinum (Pt) is the benchmark electrocatalyst for HER [12] and noble metals iridium (Ir), ruthenium (Ru) and their oxides (IrO_2 and RuO_2) have been regarded as promising excellent electrocatalysts for OER [13, 14], but their high production costs and low reserve limit the industrial application of noble metal catalysts for electrocatalytic water splitting. Therefore, due to the less corrosion ability of alkali, researchers have unveiled the engineering of non-noble metal electrocatalysts with a high activity and durability, and a low cost in recent years to promote the industrial development of alkaline water splitting.

In recent decades, researchers have developed several reaction mechanisms, such as the adsorbate evolution mechanism (AEM) [15] and lattice oxygen oxidation mechanism (LOM) [16], to fundamentally understand the reaction mechanisms and find the origin of the reaction overpotential at the active site of different materials. Using these discovered mechanisms as the guidelines, it is possible to design more efficient OER electrocatalysts by increasing the exposure of electrochemically active sites by reducing the particle size, engineering morphology of the catalyst, and promoting the surface reconstruction of the catalysts into the active species [17].

The OER mechanism involves the breaking of the O–H bond and the formation of the O–O bond and changes according to the pH of the electrolyte. In alkaline electrolytes, oxygen molecules are produced by the conversion of the OH^- through four-electron transfer steps. The mechanism of OER has been shown in Eqs. (1)–(5) for the alkaline medium [18–19]:



The total response is the following:



Undoubtedly, over the past years, abundant low-cost transition metals on the earth (Ni, Fe, Mo, Co, Mn, Cu, etc.), their compounds and alloys with different elemental compositions have gained extensive attention as OER electrocatalysts to replace noble IrO_2 and RuO_2 electrodes. These electrocatalysts include monometallic [20, 21], bimetallic [22, 23] and trimetallic [24–26] transition metals as well as their carbides [27–29], nitrides [27, 30, 31], phosphides [32–34], sulphides [35, 36], etc. Studies revealed that in order to act as an electrocatalyst with an excellent electrocatalytic activity, the electrode must have a high surface active area as well as a high intrinsic electrocatalytic activity along with durability. The intrinsic electrocatalytic activity can be achieved by alloying various transition metals instead of using pure metal(s) and the electrochemically active surface area can be enhanced by fabricating different nanostructures such as nanowires [37, 38] nanosheets [4, 33, 39], nanocones [40], nanostars [9], etc. Other studies have demonstrated that binary, ternary and multinary alloying of transition metals such as Ni–Co [41], Ni–Mn [42], Mn–Co–Ni [43], Ni–Fe–Mo–Cu [44], etc. exhibit improved electrocatalytic activity for water splitting in different compositions. Among these transition metals, nickel can be considered to be an excellent candidate as an electrocatalyst because of its less free energy to absorb hydrogen and Ni– Mo_2C -embedded N-doped carbon nanofibers (Ni/ Mo_2C -NCNFs) demonstrated as an excellent bifunctional electrocatalyst for overall water splitting delivering low overpotentials of 143 mV for HER and 288 mV for OER to attain current density of 10 mA cm^{-2} [45]. The synergistic effect between Ni and Mo is noteworthy here as the hydrogen binding energy (HBE) between Ni and H is slightly weaker, whereas it is stronger enough between Mo_2C and H. Thus, the HBE can be controlled to a relatively moderate value by chemically coupling Ni and Mo_2C , which could contribute to balance the thermodynamics between hydrogen adsorption and desorption [45, 46]. Nickel molybdenum nitride nanorods grown on Ni foam ($\text{Ni}_{\text{foam}}@(\text{Ni}-\text{Ni}_{0.2}\text{Mo}_{0.8}\text{N})$) exhibit an excellent electrocatalytic performance in 1.0 M KOH with low overpotentials of 15 and 218 mV for HER and OER, respectively, at a current density of 10 mA cm^{-2} [31]. Furthermore, a unique fabrication of Ni–Mo nanostars by the electrochemical deposition method also resulted in an excellent

electrocatalytic behaviour where a minimum value of 60 mV and 225 mV overpotential were required for generating the current density of 10 mA cm^{-2} in the HER and OER process, respectively, in the alkaline medium (1.0 M KOH) [9].

Inspired by the above-mentioned reports, herein we apply the widely used simple, fast and inexpensive electrodeposition technique to fabricate a low-cost, binderless and thin-layer three-dimensional (3D) binary Ni-Mo catalysts supported on titanium (Ti) surface (denoted as NiMo/Ti) followed by decoration with a very low amount of Au-crystallites (denoted as Au(NiMo)/Ti) for investigating their electrocatalytic OER performance in the alkaline medium (1.0 M NaOH).

EXPERIMENTAL

Chemicals

Titanium foil (99.7% purity) and HAuCl_4 (99.995%) were purchased from Sigma-Aldrich Supply. H_2SO_4 (96%), HCl (35–38%), nickel sulfate hexahydrate ($\text{NiSO}_4 \cdot 6\text{H}_2\text{O}$, >98%), sodium molybdate dihydrate ($\text{Na}_2\text{MoO}_4 \cdot 2\text{H}_2\text{O}$, >99.5%) and NaOH (98.8%) were purchased from Chempur Company. Ultra-pure water with a resistivity of $18.2 \text{ M}\Omega \cdot \text{cm}^{-1}$ was used for preparing the solutions. All chemicals were of analytical grade and used directly without further purification.

Fabrication of catalysts

The catalysts were prepared by a facile, two-step process that involves electrodeposition of the Ni-Mo layer on the surface of the titanium (Ti) electrode followed by a galvanic displacement from the Au(III)-containing solution. Prior to the deposition of the NiMo catalysts, the titanium plates were pretreated in diluted H_2SO_4 (1:1 vol) at 70°C for 3 s. NiMo catalysts were electroplated on the Ti surface ($1 \times 1 \text{ cm}$) from a bath containing 0.03 M Na_2MoO_4 along with 0.1, 0.2 and 1.0 M NiSO_4 in an acidic medium (1.5 M H_2SO_4 and 1 M HCl). The process of electrochemical deposition was carried out at the constant current of 0.1 and 1 mA for 3 min at each current. The Au crystallites were deposited on the prepared NiMo/Ti electrodes by their immersion into 1 mM HAuCl_4 + 0.1 M HCl solution for 10 s. After plating, the samples were taken out, thoroughly rinsed with deionized water and air-dried at room temperature.

Characterization of catalysts

The morphology and composition of the prepared catalysts were investigated by scanning electron microscopy (SEM) using an SEM workstation SEM TM 4000 Plus (HITACHI). The metal loadings were determined by inductively coupled plasma optical emission spectrometry (ICP-OES) analysis. The ICP-OES spectra were recorded using an Optima 7000 DV spectrometer (Perkin Elmer, Waltham, MA, USA) at wavelengths of λ_{Ni} 231.604 nm, λ_{Mo} 202.031 nm and λ_{Au} 267.595 nm.

Electrochemical measurements

To investigate the electrochemical properties of our fabricated catalysts, a conventional three-electrode electrochemical cell was used and those fabricated NiMo/Ti and Au(NiMo)/Ti catalysts were employed as working electrodes, a Pt sheet was used as a counter electrode, and a calomel electrode was used as a reference. All potentials in this work were converted to the reversible hydrogen electrode (RHE) scale using the following equation (6):

$$E_{\text{RHE}} = E_{\text{SCE}} + 0.242 \text{ V} + 0.059 \text{ V} \times \text{pH}_{\text{solution}} \quad (6)$$

Current densities were calculated using the electrode geometric area of 2 cm^2 . 1 M NaOH solution was used as an alkaline medium (working electrolyte) and always deaerated by argon (Ar) for 20 min before recording each linear sweep voltammograms (LSVs). The OER polarization curves were recorded from the open circuit potential (OCP) to 2.08 V (vs RHE) at a potential scan rate of $10 \text{ mV} \cdot \text{s}^{-1}$. Polarization curves were recorded at several temperatures from 25 up to 75°C , setting the temperature with a water jacket connected to a LAUDA Alpha RA 8 thermostat. Chronoamperometry (CA) curves were recorded for 2 h at a potential of 1.83 V (vs RHE) for investigating the stability of those fabricated catalysts. All electrochemical measurements were performed with a Metrohm Autolab potentiostat (PGSTAT302) using the Electrochemical Software (Nova 2.1.4).

RESULTS AND DISCUSSION

This study presents the preparation of 3D-structured binary NiMo/Ti and ternary Au(NiMo)/Ti catalysts and their electrocatalytic performance was investigated for OER. The composition of the plating

solutions for fabricating 3D binary NiMo/Ti catalysts is listed in Table 1, and the fabrication was carried out using the electrochemical deposition method as described in the Section ‘Fabrication of catalysts’. As mentioned in Table 1, the $\text{Ni}^{2+}/\text{Mo}^{6+}$ ratio of the plating solutions was varied by changing the concentration of NiSO_4 , while the concentration of Na_2MoO_4 was kept constant. The morphology and composition of the prepared six catalysts have been characterized by SEM and ICP-OES techniques and are presented in Fig. 1 and Table 2. Figure 1a–c shows the SEM images of the NiMo layers electrodeposited on the Ti surface and as a function of the adjacent $\text{Ni}^{2+}/\text{Mo}^{6+}$ ratio, both the surfaces of NiMo/Ti-1 and NiMo/Ti-2 catalysts are smooth and not well-distinctive with a porous architecture Fig. (1a, b). In the case of the NiMo/Ti-3 catalyst, the lower magnification SEM image depicts the wide-ranging cedar leaf-like Ni-Mo alloy structure that grows in a large area on the Ti surface as a function of the $\text{Ni}^{2+}/\text{Mo}^{6+}$ ratio. Those leaf-like Ni-Mo alloy architectures have been uniformly dispersed on the Ti surface and the higher magnification portraits an irregular

stack of well-defined randomly distributed particles forming a cedar leaf-like structure. Figure 1f depicts the surface of Au(NiMo)/Ti-3 electrode, where Au crystallites were deposited on the prepared NiMo/Ti-3 electrode after immersing into 1 mM HAuCl_4 + 0.1 M HCl solution for 10 s. The mass of the elements (metal loadings) deposited onto the Ti substrate surface was determined by ICP-OES analysis (Table 2). It was found that the formed 3D binary NiMo/Ti catalysts contained ca. 83–94 wt.% of Ni, whereas those 3D ternary Au(NiMo)/Ti catalysts possessed ca. 77–88 wt.% of Ni, 6–18 wt.% of Mo and 5–6 wt.% of Au. The total metal loadings ($\mu\text{g}_{\text{metal}}\text{cm}^{-2}$) in the prepared catalysts are quite different and vary from 24 up to $106\mu\text{g}_{\text{metal}}\text{cm}^{-2}$.

Table 1. Composition of the electrochemical bath

Catalysts	Concentration in $\text{mol}\cdot\text{dm}^{-3}$	
	Ni^{2+}	Mo^{6+}
NiMo/Ti-1	0.1	0.03
NiMo/Ti-2	0.2	0.03
NiMo/Ti-3	1.0	0.03

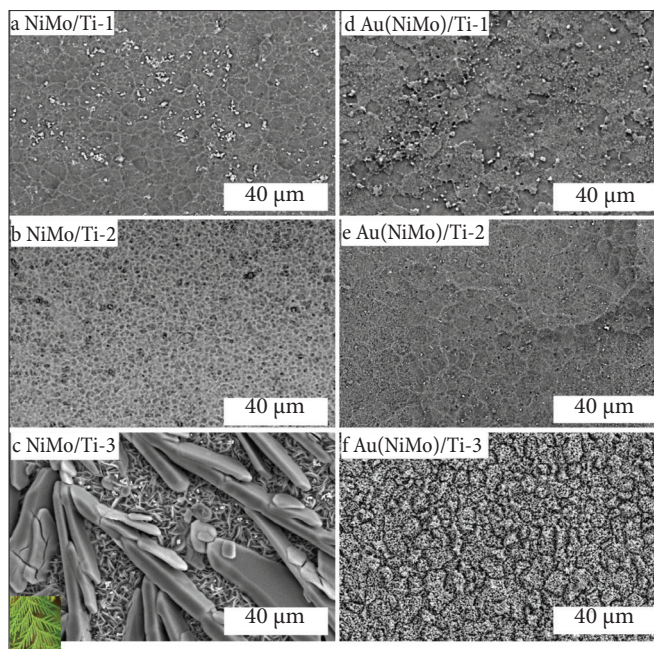


Fig. 1. SEM views of NiMo/Ti (a–c) and Au(NiMo)/Ti (d–f) catalysts mentioned in Table 2. (c) The inset represents the photo of a cedar leaf

Table 2. The metal loading in the catalysts determined by ICP-OES analysis

Catalyst	Ni loadings, $\mu\text{g}_{\text{Ni}}\text{cm}^{-2}$	Mo loadings, $\mu\text{g}_{\text{Mo}}\text{cm}^{-2}$	Au loadings, $\mu\text{g}_{\text{Au}}\text{cm}^{-2}$	Total metal loading, $\mu\text{g}_{\text{metal}}\text{cm}^{-2}$
NiMo/Ti-1	23.4	4.9		28.3
NiMo/Ti-2	29.6	5.3		34.9
NiMo/Ti-3	99.5	6.7		106.2
Au(NiMo)/Ti-1	18.3	4.4	1.2	23.9
Au(NiMo)/Ti-2	25.4	4.6	1.7	31.7
Au(NiMo)/Ti-3	81.4	6.0	5.2	92.6

The investigation of the electrocatalytic OER performance of the prepared catalysts was performed by recording LSVs in 1.0 M NaOH solution at a potential scan rate of $10\text{ mV}\cdot\text{s}^{-1}$ in several temperatures from 25 up to 75°C and the potential range from the open-circuit potential (OCP) up to 2.08 V (vs RHE). Ternary Au(NiMo)/Ti-3 catalyst exhibited the highest current density (j), followed by Au(NiMo)/Ti-2 and Au(NiMo)/Ti-1. For instance, Au-decorated ternary Au(NiMo)/Ti-3, Au(NiMo)/Ti-2 and Au(NiMo)/Ti-1 catalysts reached the current densities up to 71, 37 and $21\text{ mA}\cdot\text{cm}^{-2}$ at 25°C . On the contrary, that fabricated binary (NiMo/Ti)

catalysts exhibited comparatively lower (from 1.2 to 3 times lower) current densities with a mutual comparison for OER (Fig. 2). It has been observed that the current densities increase gradually with an increase of temperature from 25 up to 75°C and for binary NiMo/Ti catalysts, j increases ca. 1.2–7.3 times higher, whereas ca. 1.3–5.1 times higher values were recorded for Au(NiMo)/Ti catalysts. Figure 3a, b depicted the current densities of 3D binary NiMo/Ti and Au-decorated ternary Au(NiMo)/Ti catalysts at 25°C , respectively.

An overpotential to reach a current density of $10\text{ mA}\cdot\text{cm}^{-2}$ (η_{10}) was found to be similar for

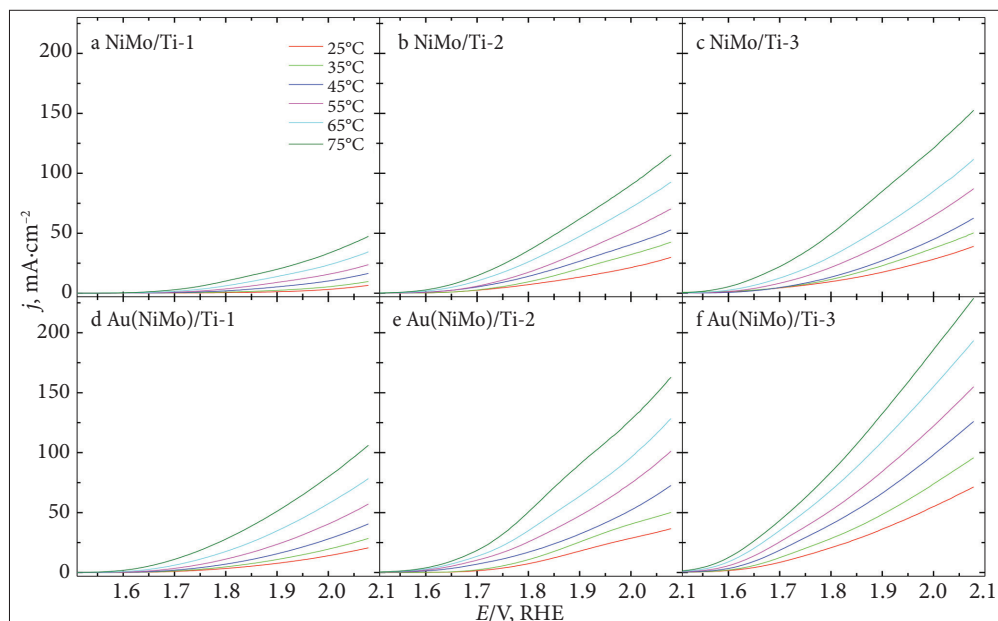


Fig. 2. OER polarization curves of 3D NiMo/Ti (a–c) and Au(NiMo)/Ti (d–f) catalysts in 1 M NaOH solution at $10\text{ mV}\cdot\text{s}^{-1}$ potential scan rate and $25\text{--}75^\circ\text{C}$ temperature range

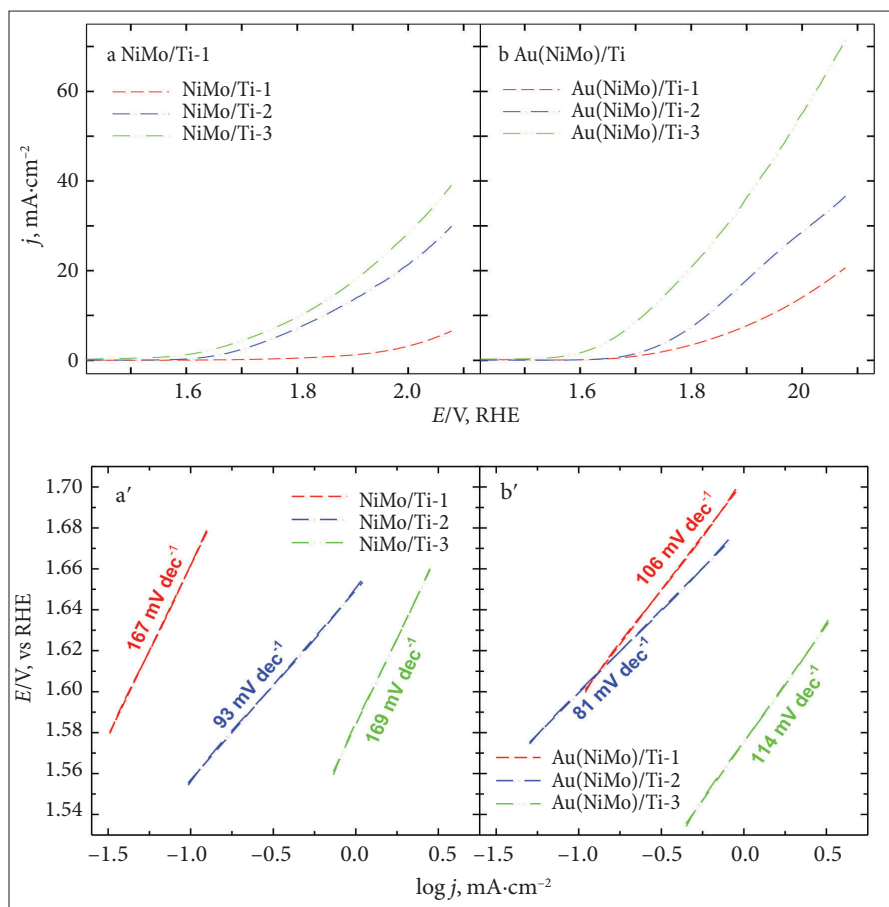


Fig. 3. OER polarization curves of 3D NiMo/Ti (a) and Au(NiMo)/Ti (b) catalysts in 1 M NaOH solution at 10 mV·s⁻¹ potential scan rate and 25°C temperature and the corresponding Tafel plots (a', b')

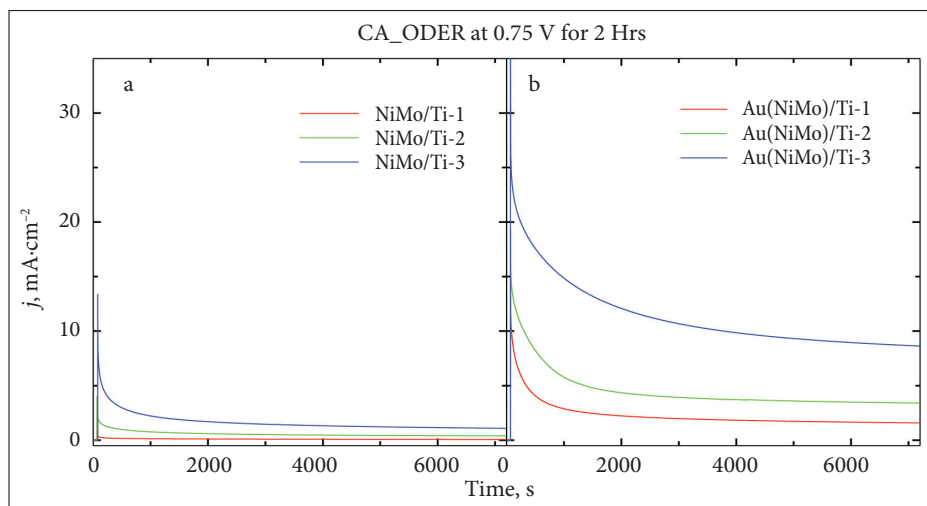
Au(NiMo)/Ti-2 (1.83 V), NiMo/Ti-3 (1.81 V) and NiMo/Ti-2 (1.85 V) and ca. 0.11 V higher for Au(NiMo)/Ti-1 (1.94 V) catalyst (Table 3). Au(NiMo)/Ti-3 catalyst demonstrates as the superior among all as required the lowest overpotential of 1.71 V. The current density at NiMo/Ti-1 catalyst did not reach a value of 10 mA·cm⁻² in the investigated potential range; it reached a value of only 6.52 mA·cm⁻² at 2.08 V and 25°C. The Tafel plots were constructed by using the OER polarization curves and the resultant Tafel slopes were demonstrated in Fig. 3 (a', b'). The Tafel slope values of 167, 93 and 169 mV·dec⁻¹ were obtained for OER at NiMo/Ti-1, NiMo/Ti-2 and NiMo/Ti-3 catalysts, respectively, and the evaluated

Tafel slope values for those Au-decorated ternary Au(NiMo)/Ti-1, Au(NiMo)/Ti-2 and Au(NiMo)/Ti-3 catalysts were, respectively, 106, 81 and 114 mV·dec⁻¹.

Another crucial criterion for an advanced electrode material is its electrochemical stability. To further explore and elucidate the OER activities, the durability of all six catalysts was evaluated by chronoamperometric (CA) measurements in 1 M NaOH at 1.83 V (vs RHE) for 2 h (Fig. 4). For binary NiMo/Ti catalysts, a sharp decrease in current densities was observed, while the Au(NiMo)/Ti catalysts show much higher stability for OER

Table 3. Electrochemical performance of the tested catalysts toward OER in alkaline media

Catalysts	j (mA·cm ⁻²) in different temperatures (°C) at 2.08 V						Tafel slope, mV·dec ⁻¹	η_{10}^* , V
	25	35	45	55	65	75		
NiMo/Ti-1	6.52	9.76	16.5	23.77	34.5	47.45	167	–
NiMo/Ti-2	29.91	42.62	52.75	70.28	92.62	115.31	93	1.85
NiMo/Ti-3	39.05	50.34	62.55	87.13	111.65	152.53	169	1.81
Au(NiMo)/Ti-1	20.63	28.46	40.59	57.16	78.34	106.14	106	1.94
Au(NiMo)/Ti-2	36.61	50.16	72.65	101.24	128.39	162.8	81	1.83
Au(NiMo)/Ti-3	71.37	95.73	126.0	154.94	193.31	228.63	114	1.71

* Overpotential at 10 mA·cm⁻².Fig. 4. Chronoamperometric data of the investigated NiMo/Ti and Au(NiMo)/Ti catalysts in 1 M NaOH solution at the potential value of 1.83 V (vs RHE), $t = 2$ h (7200 s)

in alkaline media. The CA results confirmed the result obtained by LSV analysis in terms of Au(NiMo)/Ti-3 catalyst giving the highest catalytic activity (current density) for OER (Fig. 4b). More than 2.5 times lower current density was obtained with Au(NiMo)/Ti-2 (3.39 mA·cm⁻²) and ca. 5.5 times lower with Au(NiMo)/Ti-1 catalysts (1.57 mA·cm⁻²) in CAs after 2 h. In the case of binary NiMo/Ti-3 coating, a comparatively lower current density was recorded (1.1 mA·cm⁻²) along with 2.8 and more than 17 times lower value for NiMo/Ti-2 (0.39 mA·cm⁻²) and NiMo/Ti-1 (0.06 mA·cm⁻²) catalysts. The attained current densities after 0.5 h and after 2 h for OER are 1.3–1.8 times lower for all the prepared catalysts.

CONCLUSIONS

The binary Ni-Mo alloy coatings were successfully deposited on the Ti substrate through the electro-deposition method and subsequently decorated with a very low amount of Au-crystallites from the gold-containing solution to investigate their enhanced catalytic performance by comparing with those respective bare NiMo/Ti catalysts for oxygen evolution reaction. These fabricated binder-free electrodes exhibited a good stability, which could be ascribed to the high intrinsic activity between Ni and Mo as well as their uniformly dispersed large specific surface area. The Au(NiMo)/Ti catalysts with the low Au loadings in a range of 1.2–5.2 $\mu\text{g}_{\text{Au}}\text{cm}^{-2}$ possess ca. 1.2–3.2 times higher

electrocatalytic activity towards the oxygen evolution reaction in the alkaline medium as compared to the respective binary NiMo/Ti catalysts and seem to be promising anode materials for OER. The best electrochemical activity for OER in alkaline media was obtained using Au(NiMo)/Ti-3 catalysts with the Au loading of $5.2 \mu\text{g}_{\text{Au}} \text{cm}^{-2}$.

Received 3 December 2022

Accepted 14 December 2022

References

- W. Wang, M. Xu, X. Xu, W. Zhou, Z. Shao, *Angew. Chem. Int. Ed.*, **59**, 136 (2020).
- Y. Xie, Y. Liu, Z. Yang, *Int. J. Hydrogen Energy*, **45**, 6500 (2020).
- Y. Chen, Y. Zheng, X. Yue, S. Huang, *Int. J. Hydrogen Energy*, **45**, 8695 (2020).
- M. A. Ashraf, C. Li, B. T. Pham, D. Zhang, *Int. J. Hydrogen Energy*, **45**, 24670 (2020).
- M. I. Jamesh, X. Sun, *J. Energy Chem.*, **34**, 111 (2019).
- J. Hou, Y. Wu, B. Zhang, S. Cao, Z. Li, L. Sun, *Adv. Funct. Mater.*, **29**, 1808367 (2019).
- B. You, M. T. Tang, C. Tsai, F. Abild-Pedersen, X. Zheng, H. Li, *Adv. Mater.*, **31**, 1807001 (2019).
- J. Song, C. Wei, Z. F. Huang, et al., *Chem. Soc. Rev.*, **49**, 2196 (2020).
- D. Zhang, M. A. Ashraf, *Int. J. Hydrogen Energy*, **45**, 30533 (2020).
- J. Ma, A. Cai, X. Guan, et al., *Int. J. Hydrogen Energy*, **45**, 9583 (2020).
- C. Wei, R. R. Rao, J. Peng, et al., *Adv. Mater.*, **31**, 1806296 (2019).
- S. L. Zhang, X. F. Lu, Z. P. Wu, D. Luan, X. W. Lou, *Angew. Chem. Int. Ed.*, **60**, 19068 (2021).
- X. J. Cui, P. J. Ren, C. Ma, *Adv. Mater.*, **32**, 1908126 (2020).
- J. Yin, J. Jin, M. Lu, et al., *J. Am. Chem. Soc.*, **142**, 18378 (2020).
- L. Gao, X. Cui, C. D. Sewell, J. Li, Z. Lin, *Chem. Soc. Rev.*, **50**, 8428 (2021).
- Y. Tian, S. Wang, E. Velasco, et al., *Science*, **23**, 100756 (2020).
- W. H. Lee, M. H. Han, Y. J. Ko, B. K. Min, K. H. Chae, H. S. Oh, *Nat. Commun.*, **13**, 1 (2022).
- C. Feng, M. B. Faheem, J. Fu, Y. Xiao, C. Li, Y. Li, *ACS Catal.*, **10**, 4019 (2020).
- Y. Gong, J. Yao, P. Wang, Z. Li, H. Zhou, C. Xu, *Chin. J. Chem. Eng.*, **43**, 282 (2022).
- L. Peng, J. Shen, X. Zheng, *J. Catal.*, **369**, 345 (2019).
- H. Liang, M. Xu, E. Asselin, *J. Power Sources*, **510**, 230387 (2021).
- C. Shuai, Z. Mo, X. Niu, et al., *J. Alloy. Compd.*, **847**, 156514 (2020).
- F. Zheng, Z. Zhang, D. Xiang, et al., *J. Colloid Interface Sci.*, **555**, 541 (2019).
- Y. Huang, S. L. Zhang, X. F. Lu, Z. P. Wu, D. Luan, X. W. Lou, *Angew. Chem.*, **133**, 11947 (2021).
- X. Luo, Q. Shao, Y. Pi, X. Huang, *ACS Catal.*, **9**, 1013 (2018).
- Y. Yang, L. Dang, M. J. Shearer, et al., *Adv. Energy Mater.*, **8**, 1703189 (2018).
- P. Chen, J. Ye, H. Wang, L. Ouyang, M. Zhu, *J. Alloy. Compd.*, **883**, 160833 (2021).
- H. Sun, Z. Yan, F. Liu, W. Xu, F. Cheng, J. Chen, *Adv. Mater.*, **32**, 1806326 (2020).
- Y. Yu, J. Zhou, Z. Sun, *Adv. Funct. Mater.*, **30**, 2000570 (2020).
- A. K. Tareen, G. S. Priyanga, K. Khan, E. Pervaiz, T. Thomas, M. Yang, *Chem. Sus. Chem.*, **12**, 3941 (2019).
- J. Jia, M. Zhai, J. Lv, B. Zhao, H. Du, J. Zhu, *ACS Appl. Mater. Interfaces*, **10**, 30400 (2018).
- Y. Liu, N. Ran, R. Ge, et al., *Chem. Eng. J.*, **425**, 131642 (2021).
- S. Chen, J. Dai, F. Ren, H. Xu, Y. Du, *J. Colloid Interface Sci.*, **536**, 71 (2019).
- C. Zhou, J. Mu, Y. F. Qi, Q. Wang, X. J. Zhao, E. C. Yang, *Int. J. Hydrogen Energy*, **44**, 8156 (2019).
- P. Ganesan, A. Sivanantham, S. Shanmugam, *J. Mater. Chem. A*, **4**, 16394 (2016).
- Y. Guo, T. Park, J. W. Yi, et al., *Adv. Mater.*, **31**, 1807134 (2019).
- J. He, Z. Hu, J. Zhao, et al., *Chem. Eng. Sci.*, **243**, 116774 (2021).
- S. Kocabas, A. Cetin, A. M. Önal, E. N. Esenturk, *J. Nanopart. Res.*, **21**, 1 (2019).
- Y. M. Chai, X. Y. Zhang, J. H. Lin, et al., *Int. J. Hydrogen Energy*, **44**, 10156 (2019).
- X. Zhang, Y. Li, Y. Guo, et al., *Int. J. Hydrogen Energy*, **44**, 29946 (2019).
- G. Wu, S. Liu, G. Cheng, H. Li, Y. Liu, *Appl. Surf. Sci.*, **545**, 148975 (2021).
- S. Xu, Y. Du, X. Liu, et al., *J. Alloy. Compd.*, **826**, 154210 (2020).
- J. F. Qin, M. Yang, T. S. Chen, et al., *Int. J. Hydrogen Energy*, **45**, 2745 (2020).
- M. F. Khan, A. Qurashi, *Electrochim. Acta*, **400**, 139345 (2021).
- M. Li, Y. Zhu, H. Wang, C. Wang, N. Pinna, X. Lu, *Adv. Energy Mater.*, **9**, 1803185 (2019).
- P. Quaino, F. Juarez, E. Santos, W. Schmickler, *Beilstein J. Nanotechnol.*, **5**, 846 (2014).

Sukomol Barua, Aldona Balčiūnaitė, Jūratė Vaičiūnienė,
Loreta Tamašauskaitė-Tamašiūnaitė, Eugenijus Norkus




3D STRUKTŪROS Au(NiMo)/Ti KATALIZATORIAI EFEKTYVIAI DEGUONIES IŠSISKYRIMO REAKCIJAI

Santrauka

3D struktūros aukso-nikelio-molibdeno (Au(NiMo)) katalizatorių aktyvumas tirtas deguonies išsiskyrimo reakcijai (OER). Katalizatoriai buvo nusodinti ant titano paviršiaus naudojant elektrocheminį metalų nusodinimo bei galvaninio pakeitimo metodus. Au(NiMo)/Ti katalizatoriai, kuriuose nusodinto Au kiekis yra nuo 1,2 iki 5,2 $\mu\text{g}_{\text{Au}}\text{cm}^{-2}$, pasižymėjo ~1,2–3,2 karto didesniu elektrokataliziniu aktyvumu deguonies išsiskyrimo reakcijai šarminėje terpėje, palyginti su atitinkamais NiMo/Ti katalizatoriais. Didinant temperatūrą nuo 25 iki 75 °C, deguonies išsiskyrimo srovės tankio vertės padidėja 1,2–7,3 ir ~1,3–5,1 karto, naudojant, atitinkamai, 3D NiMo/Ti ir Au(NiMo)/Ti katalizatorius.

Article

Bimetallic 3D Nickel-Manganese/Titanium Bifunctional Electrocatalysts for Efficient Hydrogen and Oxygen Evolution Reaction in Alkaline and Acidic Media

Sukomol Barua , Aldona Balčiūnaitė ^{*}, Jūrate Vaičiūnienė, Loretta Tamašauskaitė-Tamašiūnaitė  and Eugenijus Norkus 

Department of Catalysis, Center for Physical Sciences and Technology (FTMC), LT-10257 Vilnius, Lithuania; sukamol.barua@ftmc.lt (S.B.); jurate.vaiciuniene@ftmc.lt (J.V.); loretta.tamasauskaite@ftmc.lt (L.T.-T.); eugenijus.norkus@ftmc.lt (E.N.)

^{*} Correspondence: aldonabalcunaite@ftmc.lt

Abstract: In this work, 3D nickel-manganese (NiMn) bimetallic coatings have been studied as electrocatalysts for both hydrogen evolution reaction (HER) and oxygen evolution reaction (OER) in alkaline (1.0 M KOH) media and the HER in acidic (0.5 M H₂SO₄) media. The catalysts have been deposited on a titanium substrate (1 × 1 cm²) using low-cost and facile electrochemical deposition method through a dynamic hydrogen bubble template technique. The electrocatalytic performance of these fabricated catalysts was investigated by using Linear Sweep Voltammetry (LSV) for HER and OER at different temperatures ranging from 25 up to 75 °C and also was characterized by scanning electron microscopy (SEM) and inductively coupled plasma optical emission spectroscopy (ICP-OES). It was found that fabricated NiMn/Ti-5 electrocatalyst with Ni²⁺/Mn²⁺ molar ratio of 1:5 exhibits excellent HER activity in alkaline media with overpotential of 127.1 mV to reach current density of 10 mA cm^{−2}. On the contrary, NiMn/Ti-1 electrocatalyst that fabricated with Ni²⁺/Mn²⁺ molar proportion of 1:1 and lowest Mn-loading of 13.43 μgcm^{−2} demonstrates exceptional OER activity with minimum overpotential of 356.3 mV to reach current density of 10 mA cm^{−2}. The current densities increase ca. 1.8–2.2 times with an increase in temperature from 25 °C to 75 °C for both HER and OER investigation. Both catalysts also have exhibited excellent long-term stability for 10 h at constant potentials as well as constant current density of 10 mA cm^{−2} that assure their robustness and higher durability regarding alkaline water splitting.

Keywords: nickel; manganese; bifunctional electrocatalyst; electrodeposition; hydrogen evolution reaction; oxygen evolution reaction



Citation: Barua, S.; Balčiūnaitė, A.; Vaičiūnienė, J.; Tamašauskaitė-Tamašiūnaitė, L.; Norkus, E. Bimetallic 3D Nickel-Manganese/Titanium Bifunctional Electrocatalysts for Efficient Hydrogen and Oxygen Evolution Reaction in Alkaline and Acidic Media. *Coatings* **2023**, *13*, 1102. <https://doi.org/10.3390/coatings13061102>

Academic Editor: Rosalba Passalacqua

Received: 15 May 2023

Revised: 9 June 2023

Accepted: 13 June 2023

Published: 15 June 2023



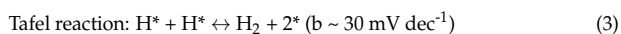
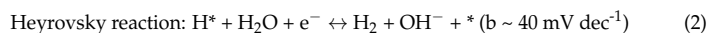
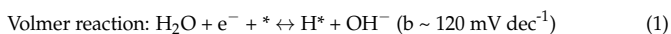
Copyright: © 2023 by the authors. Licensee MDPI, Basel, Switzerland. This article is an open access article distributed under the terms and conditions of the Creative Commons Attribution (CC BY) license (<https://creativecommons.org/licenses/by/4.0/>).

1. Introduction

Over the last decade, a substantial research focusing on uninterrupted supply of renewable and clean energy has become a key issue due to alarming environmental threat and rapid depletion of fossil fuels [1–4]. In order to find potential substitutes, hydrogen is considered the most promising alternative to fossil fuels because of its advantages of zero carbon emissions, high gravimetric energy density (140 MJ·Kg^{−1}), and high efficiency [5–10]. Comparing with major methods for industrial hydrogen production e.g., coal gasification and steam methane reforming, the electrocatalytic water splitting in large-scale can also be considered as the most prospecting method [11]. This is not only due to the low conversion efficiency of methane and coal steam into H₂ and CO₂, and their consequences of carbon-emissions and global climate warming but also the advantageous feature of high purity industrial-level H₂ production from abundant natural resource with free-carbon emission and sustainability. This promising method of green H₂ production can also be the most convenient way to store the intermittent renewable energy like solar and wind energy by converting the electricity into H₂ fuels [12].

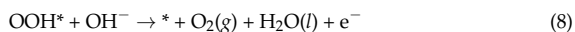
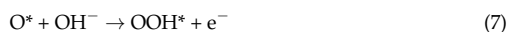
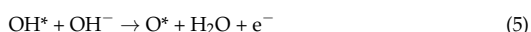
Electrocatalytic water splitting is regarded as a propitious approach for hydrogen production that consists of two half reactions: the anodic oxygen evolution reaction (OER) and the cathodic hydrogen evolution reaction (HER). The overall electrocatalytic water splitting under standard condition is a thermodynamically unfavorable uphill reaction that requires a thermodynamic Gibbs free energy of $237.2 \text{ kJ mol}^{-1}$, corresponding to the theoretical limit of 1.23 V. However, to drive the reaction at a practical rate, total energy of $285.8 \text{ kJ mol}^{-1}$ is required that when converted to potential becomes 1.48 V, which is called the overpotential. Thus, practical real-world water splitting processes are limited by the high overpotential and can only be occurred by exceeding this barrier [13]. Nevertheless, two half-cell reactions of water splitting, i.e., HER and OER require large amount of energy to initiate and high individual overpotential to overcome sluggish multi-electron transfer kinetics, which leads to energy waste [14,15]. To overcome lethargic kinetics and for reducing high overpotential values of complex electron transfer pathways, currently, Pt-group and Pt-based materials (e.g., Pt/C) are considered as benchmark catalysts for HER and Ir/Ru-based ($\text{IrO}_2/\text{RuO}_2$) materials are considered the highly efficient commercially available catalysts for OER [16–19]. However, their low natural reserves and high cost restrict the large-scale industrial application of these catalysts and hinder the production and commercialization of hydrogen by electrocatalytic water splitting. Therefore, the designing and development of a cost-efficient, stable and highly efficient bifunctional electrocatalyst is the key factor to breaking the technical bottleneck of renewable green hydrogen production from overall water splitting [20,21].

In electrocatalytic water splitting, the mechanism of cathodic HER involves three main steps, i.e., Volmer, Heyrovsky and Tafel reactions, as shown below, in alkaline media, where the asterisk (*) represents the active sites on the surface of the electrocatalyst [22]:



where b is the Tafel slope obtained from the HER polarization curves.

On the other hand, in alkaline electrolytes, the anodic OER mechanism involves the breaking of the O—H bond and the formation of the O—O bond and progresses through four electron transfer steps. The mechanism of OER has been shown in Equations (4)–(8) for alkaline medium [23].



In a quest to get over these energy consuming slothful multi-electron transfer kinetics and to promote potential substitutes of high-cost, noble metal-based electrocatalysts, an intense research interest has been paid on various transition metals based materials for exploring high-active electrocatalysts substantiating their cost, stability, efficiency and earth-abundance. In recent years, many non-noble transition metal-based compounds (especially 3d-block transition metals such as Ni, Co, Fe, Mo, Mn etc.) and their alloys [24–28], ox-

ides [29–32], hydroxides/layered double hydroxide (LDH) [33–36], oxyhydroxides [37–39], phosphides [40–44], sulfides [45–48] etc. have been explored and demonstrated excellent individual HER or OER performance as well as unique superior bifunctional electrocatalytic activity.

Among these electrocatalysts, nickel-based materials especially nickel-based bi- or trimetallic and multicomponent alloy electrocatalysts can be considered as potential substitutes for noble metal catalysts due to their abundant reserves, low cost, unique electronic interaction, diversity of modification by optimizing the electronic structure, high electrical conductivity, excellent corrosion resistance, optimal stability, and excellent performance for the production of hydrogen in alkaline media [49–53]. In addition, nickel doping or alloying with other non-precious metals improve the electronic structure of the electrodes and proven as one of the most promising strategies for enhancement of electrocatalytic activity. For example, the addition of iron to the Ni–Mo electrodeposition bath leads to a synergistic effect on the deposition of molybdenum and the amount of molybdenum on the electrode surface increased from 9.3 to 37.4 atomic percent. The as-fabricated ($\text{Ni}_{52.3}\text{Mo}_{37.4}\text{Fe}_{10.2}$) electrocatalyst with optimal composition exhibits a small overpotential of 65 mV and 344 mV for delivering current density of 10 mA cm^{-2} on HER and OER, respectively in alkaline media [54]. An enhanced HER and OER activity have been demonstrated by Cu-doped Ni bifunctional electrocatalysts as require minimum overpotential of 76 mV and 290 mV, respectively to the current density of 10 mA cm^{-2} [55]. Gao et al. reported a ternary Ni–Fe–Mo alloy nanowire electrocatalyst ($\text{Ni}_{0.8}\text{Fe}_{0.15}\text{Mo}_{0.05}$) which exhibits prominently improved OER catalytic performance achieving an optimal overpotential of 300 mV at 50 mA cm^{-2} with corresponding Tafel slope value of 42.4 mV dec^{-1} [56]. All of these studies have shown that metal alloying prompts to improve electrocatalytic activity. In addition, Mn as one of the first-row transition metal element has received tremendous attention as dopant to decorate high-performance alloy electrocatalysts for overall water splitting [57]. Luo et al. synthesized Mn–Fe bimetallic oxide heterostructures on nickel foam by adjusting the molar ratio of Fe:Mn [58]. The MnFeO–NF-0.4 electrocatalyst with Fe:Mn ratio of 0.4:1 exhibited outstanding performance with ultralow overpotential of 157 mV for the OER while the MnFeO–NF-0.8 (Fe:Mn ratio of 0.8:1) demonstrated superior HER performance with only 64 mV overpotential to achieve a current density of 10 mA cm^{-2} . Xu et al. designed Mn-doped Ni_2P microflowers with optimal Mn/Ni ratio of 0.053 which outperforms many commercially used electrocatalysts exhibiting low overpotentials of 205 mV for HER and 330 mV for OER to achieve a current density of 100 mA cm^{-2} [59].

Moreover, another favorable approach to improve the electrocatalytic performance of catalysts is to increase the active surface area by creating a three-dimensional structure. Electrocatalyst in the form of three-dimensional coating is more suitable for practical application in comparison with powder as polymer binders are used to adhere powder electrocatalysts to the conducting surface, whereas, the catalyst on self-supporting electrodes are easy to operate and remain in direct contact with electrolytes, which can increase the conductivity and accelerate electron transfer. Additionally, the 3D interconnected network structure of the self-supporting electrode substrate is more favorable for the release of hydrogen and oxygen [60–62]. Answering above phenomena, the electrochemical deposition method is the facile, cost-effective, binder-free, template-free, versatile method to fabricate highly active electrocatalysts with desired composition and morphology.

To our knowledge, a number of NiMn LDH-based catalysts [34,63–69], their phosphides [70], phosphates [71], selenides [72] and composites [73] have been reviewed and investigated with different composition, morphology and fabrication conditions but only few works carried out on nickel-manganese bi- or, trimetallic alloy catalysts for electrocatalytic water splitting.

In this study, we report an affordable and facile fabrication of bimetallic NiMn alloy electrocatalysts demonstrating their superior bifunctional electrocatalytic performance for hydrogen evolution reaction in both alkaline and acidic media (1 M KOH and 0.5 M H_2SO_4) and the oxygen evolution reaction in alkaline media with excellent long-term stability.

2. Materials and Methods

2.1. Chemicals

Titanium foil (99.7% purity) and stainless steel foil (0.2 mm, Type 304) were purchased from Sigma-Aldrich (Saint Louis, MO, USA) Supply and Alfa Aesar (Karlsruhe, Germany) GmbH & Co., respectively. H_2SO_4 (96%), HCl (35–38%), nickel sulfate hexahydrate ($\text{NiSO}_4 \cdot 6\text{H}_2\text{O}$, >98%), manganese chloride tetrahydrate ($\text{MnCl}_2 \cdot 4\text{H}_2\text{O}$, >99%), ammonium sulfate ($(\text{NH}_4)_2\text{SO}_4$, >99%), boric acid (H_3BO_3 , >99.5%) and KOH (98.8%) were purchased from Chempur Company (Karlsruhe, Germany). Ultrapure water with a resistivity of $18.2 \text{ M}\Omega \text{ cm}^{-1}$ was used for preparing the solutions. All chemicals were of analytical grade and used directly without further purification.

2.2. Fabrication of Catalysts

In this study, titanium sheets were used as substrates to fabricate the bimetallic nickel-manganese alloy electrocatalysts with different compositions. The catalysts were prepared by a facile, low-cost electrochemical deposition method on Ti surface ($1 \times 1 \text{ cm}^2$) through a dynamic hydrogen bubble template technique. Initially, the titanium sheets were pretreated in diluted H_2SO_4 (1:1 vol.) at 70°C for 3 s, then rinsed with distilled water and finally immersed into the electrochemical deposition bath. The composition of the coating bath for NiMn/Ti electrocatalysts included $\text{NiSO}_4 \cdot 6\text{H}_2\text{O}$ ($52.57 \text{ g}\cdot\text{L}^{-1}$), $\text{MnCl}_2 \cdot 4\text{H}_2\text{O}$ (39.60 to $197.92 \text{ g}\cdot\text{L}^{-1}$), $(\text{NH}_4)_2\text{SO}_4$ ($66.07 \text{ g}\cdot\text{L}^{-1}$) and H_3BO_3 ($18.55 \text{ g}\cdot\text{L}^{-1}$) dissolved in distilled water at acidic condition (1.5 M H_2SO_4 and 1 M HCl). Also, $52.57 \text{ g}\cdot\text{L}^{-1}$ of $\text{NiSO}_4 \cdot 6\text{H}_2\text{O}$ and $197.92 \text{ g}\cdot\text{L}^{-1}$ of $\text{MnCl}_2 \cdot 4\text{H}_2\text{O}$ were used separately with aforementioned other reagents to prepare Ni/Ti and Mn/Ti catalyst samples, respectively, for comparing performances with fabricated catalysts. The composition of the electrochemical bath and electroplating conditions used for coating treatment are presented in Table 1. Electrochemical deposition was implemented in a two-electrode cell in which a stainless steel sheet ($40 \times 25 \times 0.2 \text{ mm}$) was used as the anode. The fabrication procedure was carried out under the applied current density and duration time conditions of 50 mA cm^{-2} for 3 min and 500 mA cm^{-2} for another 3 min. After coating, the samples were taken out, thoroughly rinsed with deionized water, air-dried at room temperature and preserved for further investigations.

Table 1. The composition of the electrochemical bath with plating condition parameters.

Catalysts	Concentration (M)				Plating Conditions	
	$\text{NiSO}_4 \cdot 6\text{H}_2\text{O}$	$\text{MnCl}_2 \cdot 4\text{H}_2\text{O}$	$(\text{NH}_4)_2\text{SO}_4$	H_3BO_3	Parameters	Values
Ni/Ti	0.2	-	0.5	0.3	Current densities	50 mA cm^{-2}
Mn/Ti	-	1.0	0.5	0.3		500 mA cm^{-2}
NiMn/Ti-1	0.2	0.2	0.5	0.3	Time	3 min
NiMn/Ti-2	0.2	0.4	0.5	0.3		
NiMn/Ti-3	0.2	0.6	0.5	0.3	Temperature	25°C
NiMn/Ti-4	0.2	0.8	0.5	0.3		
NiMn/Ti-5	0.2	1.0	0.5	0.3	pH	~1

2.3. Characterization of Catalysts

The morphology and composition of the prepared Ni/Ti sample and NiMn/Ti catalysts were investigated by scanning electron microscopy (SEM) using a SEM workstation SEM TM 4000 Plus (HITACHI) with an energy dispersive X-ray (EDX) spectrometer.

The metal loadings were determined by inductively coupled plasma optical emission spectroscopy (ICP-OES) analysis. The ICP-OES spectra were recorded using an Optima 7000DV spectrometer (Perkin Elmer, Waltham, MA, USA) at wavelengths of λ_{Ni} 231.604 nm and λ_{Mn} 257.610 nm.

2.4. Electrochemical Measurements

The electrocatalytic activity of bimetallic nickel-manganese electrocatalysts towards HER and OER was evaluated by linear sweep voltammetry (LSV) using a potentiostat PGSTAT302 (Metrohm Autolab B.V., Utrecht, The Netherlands) through Electrochemical Software (Nova 2.1.4). A standard three-electrode electrochemical cell was used during the investigation and the fabricated NiMn/Ti catalysts with a geometric area of 2 cm² were employed as working electrodes, a Pt sheet was used as a counter electrode and a saturated calomel electrode (SCE) was used as a reference. All potentials in this work were converted to the reversible hydrogen electrode (RHE) scale using the following equation:

$$E_{\text{RHE}} = E_{\text{SCE}} + 0.242 \text{ V} + 0.059 \text{ V} \times \text{pH}_{\text{solution}} \quad (9)$$

LSVs were recorded in an Ar-saturated 1 M KOH solution at the temperature range from 25 °C to 75 °C, setting the temperature with a water jacket connected to a LAUDA Alpha RA 8 thermostat. HER and OER polarization curves were recorded from the open circuit potential (OCP) to −0.432 V (vs. RHE) and OCP to 2.068 V (vs. RHE), respectively, at a potential scan rate of 10 mV s^{−1}. The HER polarization curves in acidic media (0.5 M H₂SO₄) were recorded from the OCP to −0.958 V (vs. RHE) at a potential scan rate of 10 mV s^{−1}. Also, in order to evaluate the long-term stability of the fabricated catalysts, the chronopotentiometric curves were recorded at a constant current density of 10 mA cm^{−2} in 1.0 M KOH solution for 10 h. Moreover, the chronoamperometry (CA) curves were also studied after 10 h continuous electrolysis in alkaline environment at a potential of −0.232 V (vs. RHE) for HER and at a potential of 1.818 V (vs. RHE) for OER.

3. Results and Discussions

3.1. Microstructure and Morphology Studies

In this study, the electrocatalytic performance of 3D bimetallic nickel-manganese alloy electrocatalysts were evaluated for HER and OER in the alkaline (1.0 M KOH) medium as well as the HER activity in acidic (0.5 M H₂SO₄) medium. The coatings' surface morphology was studied by scanning electron microscopy (SEM). Figure 1 depicted the SEM images of the prepared Ni/Ti (a) sample and NiMn/Ti-1 (b), NiMn/Ti-2 (c), NiMn/Ti-3 (d), NiMn/Ti-4 (e) NiMn/Ti-5 (f) catalysts. The surface morphology of Ni/Ti sample is observed to be compact, smooth and crack-free where the Ni particles are seem to be uniformly distributed. The top side views of NiMn/Ti catalysts demonstrate a typical globular morphology consisting of smaller nodules in Figure 1b. The size of nodules enlarged with increase of Mn-content on the catalyst and started to cover the surface of substrate (Figure 1c,d). With higher Mn-content, the catalysts turned into a unique porous architecture with abundant pores of different sizes, which can provide more channels for electrolyte diffusion, accelerate the efficiency of electron transport and increase numerous active sites (Figure 1e,f).

Mass of the elements (metal loadings) deposited onto the Ti substrate surface was determined by ICP-OES analysis (Table 2). It can be seen that the fabricated bimetallic NiMn/Ti electrocatalysts possessed ca. 44–86.6 wt% of Ni and ca. 13.4–56 wt.% of Mn. The total metal loadings (μg_{metal}cm^{−2}) in the prepared catalysts were gradually uplifted with increase of Mn-concentration and vary from ca. 100 up to 1223.5 μg_{metal}cm^{−2}.

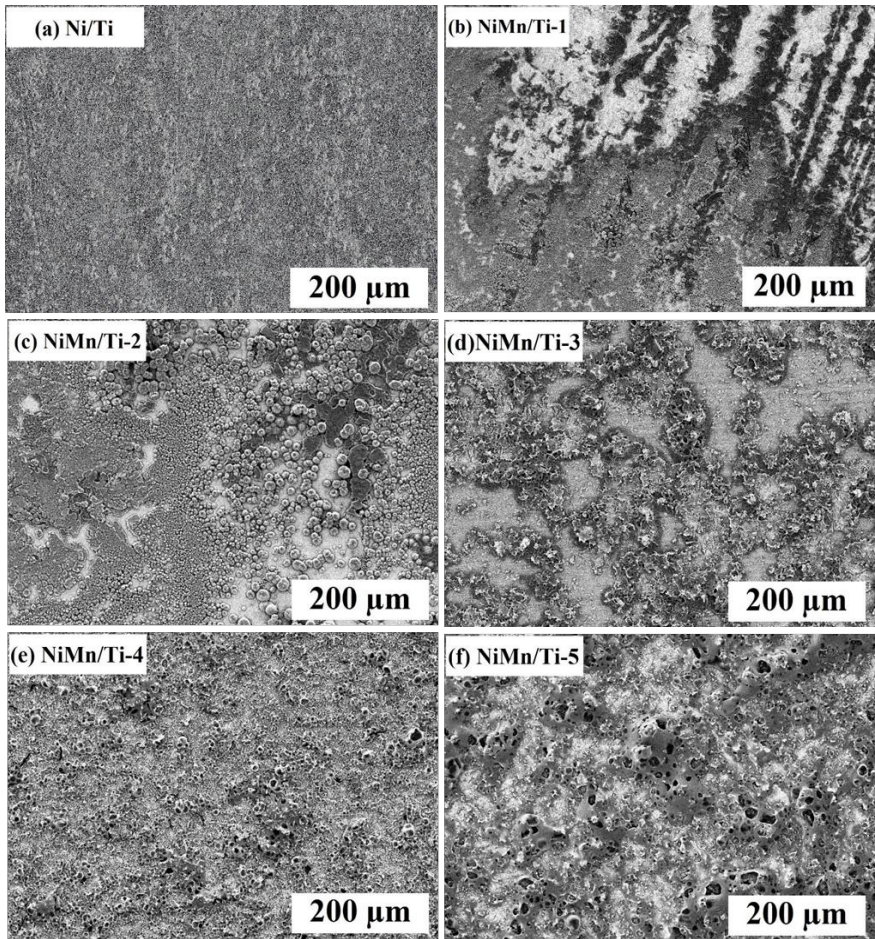


Figure 1. SEM views of Ni/Ti sample (a) and bimetallic NiMn/Ti catalysts (b–f).

Table 2. The metal loading in the catalysts as determined by ICP-OES analysis.

Catalyst	Ni Loading ($\mu\text{g}_{\text{Ni}}\text{cm}^{-2}$)	Mn Loading ($\mu\text{g}_{\text{Mn}}\text{cm}^{-2}$)	Total Metal Loading ($\mu\text{g}_{\text{metal}}\text{cm}^{-2}$)	Wt. %	
				Ni	Mn
Mn/Ti	-	21.5	21.5	-	100
Ni/Ti	300.25	-	300.25	100	-
NiMn/Ti-1	86.55	13.43	99.98	86.56	13.44
NiMn/Ti-2	126.4	40.55	166.95	75.71	24.29
NiMn/Ti-3	269.7	105.25	374.95	71.93	28.07
NiMn/Ti-4	448.45	374.4	822.85	54.49	45.51
NiMn/Ti-5	538	685.5	1223.5	43.97	56.03

3.2. Electrocatalytic Activity towards HER

The electrocatalytic performance of the prepared catalysts for HER was investigated by recording LSVs in 1.0 M KOH solution at a potential scan rate of $10 \text{ mV} \cdot \text{s}^{-1}$ from OCP up to -0.432 V (vs. RHE), at temperature from 25 up to 75°C . The current density increases ca. 1.85–2.25 times with an increase in temperature from 25 up to 75°C using the fabricated 3D NiMn/Ti catalysts for HER. The LSV curves are shown in Figure 2 at the range of investigated temperatures and the polarization curves of fabricated catalysts at only 25°C are discretely demonstrated in Figure 3a with prepared bare Ni/Ti and Mn/Ti catalysts from Ni and Mn-solution.

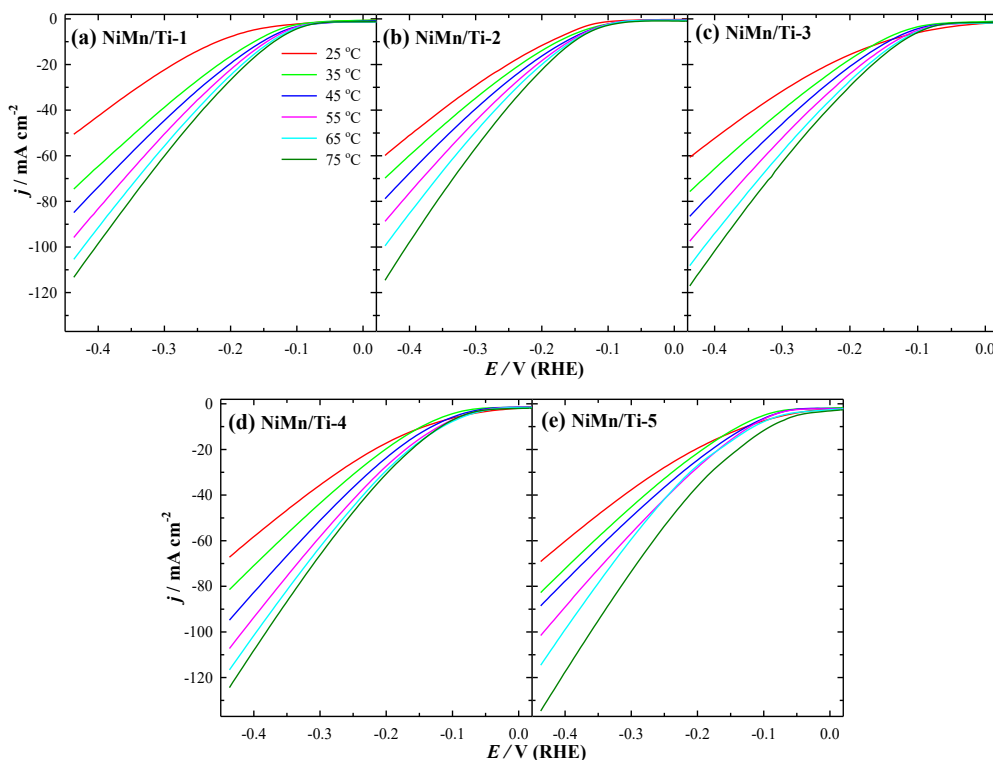


Figure 2. HER polarization curves of 3D NiMn/Ti catalysts in 1 M KOH solution at $10 \text{ mV} \cdot \text{s}^{-1}$ potential scan rate and a temperature range from 25 up to 75°C .

As shown in Figure 3a, all fabricated NiMn/Ti catalysts exhibit remarkable HER catalytic activities surpassing those of Ni/Ti and Mn/Ti samples. It is worth mentioning that via alloying Ni to Mn with different molar ratio enhanced the electrocatalytic activity and the overpotential values at 10 mA cm^{-2} (η_{10}) were considerably reduced from 424.2 mV for Mn/Ti sample to 220.3 mV for NiMn/Ti-1 catalyst. The bimetallic NiMn/Ti-5 delivers superior catalytic activity with a low overpotential of 127.1 mV to achieve 10 mA cm^{-2} relative to the NiMn/Ti-4 (144.8 mV) and NiMn/Ti-3 (149.8 mV) catalysts (Table 3). The obtained results show that the overpotential for HER in alkaline media is shifted to a more positive potential region with the increase of Mn in the coatings.

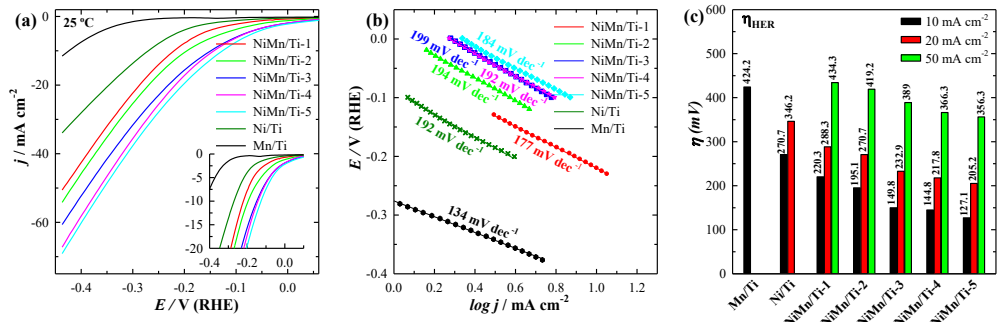


Figure 3. HER polarization curves in 1 M KOH solution at 10 mV s^{-1} potential scan rate and at 25 °C temperature (a) with corresponding extracted Tafel plots (b) and required overpotentials to reaching the current densities of 10, 20 and 50 mA cm^{-2} (c).

Table 3. Electrochemical parameters of the investigated catalysts toward HER in alkaline media.

Catalysts	j (mA cm^{-2}) in Different Temperatures (°C) at −0.432 V(vs. RHE)						j ($\text{mA } \mu\text{g}^{-1}$) at 25 °C	η_{10} (mV) at 25 °C	Tafel Slope (mV dec^{-1})
	25	35	45	55	65	75			
Mn/Ti	11.53	-	-	-	-	-	0.54	424.2	134
Ni/Ti	33.95	-	-	-	-	-	0.11	270.7	192
NiMn/Ti-1	50.58	74.57	84.92	95.81	105.39	113.28	0.51	220.3	177
NiMn/Ti-2	59.85	69.79	78.84	88.75	99.49	114.56	0.36	195.1	194
NiMn/Ti-3	60.65	75.68	86.56	97.46	108.15	117.03	0.16	149.8	199
NiMn/Ti-4	67.25	81.47	94.82	107.25	116.65	124.41	0.08	144.8	192
NiMn/Ti-5	69.12	82.75	88.56	101.6	114.59	134.67	0.06	127.1	184

To reveal the HER kinetics behavior, the NiMn/Ti electrocatalysts were investigated using Tafel plots. The Tafel equation (Equation (10)) was used for the determination of the kinetic parameters for the HER:

$$\eta = a + b \log j \tag{10}$$

where, η (V), a (V), b (V dec^{-1}) and j (A cm^{-2}) represent the applied overpotential, the curve intercept, the Tafel slope and the resulting current density, respectively. Tafel slope values were found to be 177, 194, 199, 192, and 184 mV dec^{-1} (Figure 3b and Table 3) for the prepared 3D bimetallic NiMn/Ti-1, NiMn/Ti-2, NiMn/Ti-3, NiMn/Ti-4, and NiMn/Ti-5 catalysts, respectively, implying that HER might occur through the Volmer–Heyrovsky mechanism. To evaluate the electrocatalytic activity of catalysts, it is important to compare the required overpotential to reach a current density of 10 mA cm^{-2} (η_{10}) that considered a benchmark in many studies. The magnitude of overpotentials required to reach current densities of 10, 20 and 50 mA cm^{-2} were shown in Figure 3c. It has been seen that alloying Ni to Mn with higher concentrations prompt to enhance the electrocatalytic activity and lowering overpotentials for HER, thus, the η_{10} , η_{20} and η_{50} values have followed a sequential downward order from NiMn/Ti-1 to NiMn/Ti-5.

Subsequently, the electrocatalytic activities of the prepared 3D NiMn/Ti catalysts for HER were also investigated in acidic media (0.5 M H_2SO_4) at a potential scan rate of 10 mV s^{-1} from OCP up to -0.958 V (vs. RHE). As evident from LSVs shown in Figure 4a, all studied catalysts exhibited excellent HER performance at 25 °C in comparison with prepared samples, while an optimal HER catalytic activity was observed on NiMn/Ti-5

with minimum overpotential of 102.1 mV to reach current density of 10 mA cm⁻², followed by NiMn/Ti-4 (160.1 mV) and NiMn/Ti-3 (177.7 mV).

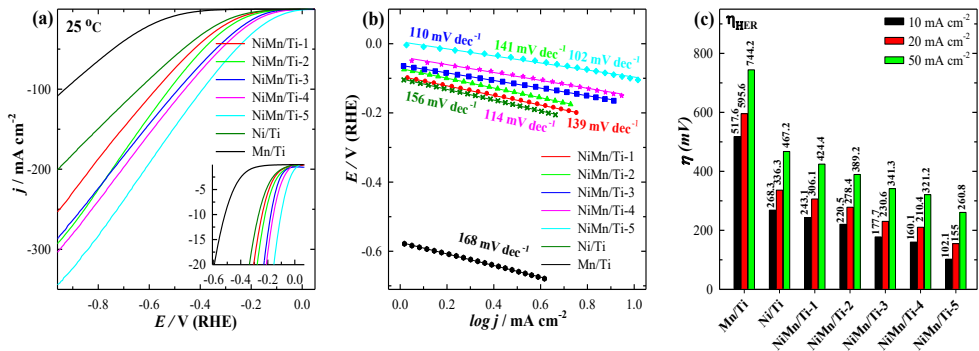


Figure 4. HER polarization curves of 3D NiMn/Ti catalysts in 0.5 M H₂SO₄ solution at a potential scan rate of 10 mV s⁻¹ and 25 °C temperature (a). with corresponding extracted Tafel plots (b) and required overpotentials to reaching the current densities of 10, 20 and 50 mA cm⁻² (c).

The polarization curves were then used for constructing the Tafel plots and calculating the Tafel slopes. The lowest Tafel slope value of 102 mV dec⁻¹ was found for NiMn/Ti-5 electrocatalyst. Higher values of 114, 110, 141, and 139 mV dec⁻¹ were determined at NiMn/Ti-4, NiMn/Ti-3, NiMn/Ti-2 and NiMn/Ti-1, respectively (Figure 4b and Table 4). The overpotentials required to reach current density of 10 mA cm⁻² for all catalysts were shown in Figure 4c and Table 4 and all values followed the similar lowering order likewise as alkaline media from NiMn/Ti-1 to NiMn/Ti-5 catalysts.

Table 4. Electrochemical parameters of the investigated catalysts toward HER in acidic media.

Catalysts	<i>j</i> (mA cm ⁻²) at 25 °C	<i>j</i> (mA μg ⁻¹) at 25 °C	η ₁₀ (mV) at 25 °C	Tafel Slope (mV dec ⁻¹)
Mn/Ti	108.67	5.05	517.6	168
Ni/Ti	201.13	0.67	268.3	156
NiMn/Ti-1	253.59	2.54	243.1	139
NiMn/Ti-2	293.17	1.76	220.5	141
NiMn/Ti-3	286.79	0.77	177.7	110
NiMn/Ti-4	303.79	0.37	160.1	114
NiMn/Ti-5	344.59	0.28	102.1	102

3.3. Electrocatalytic Activity towards OER

The electrocatalytic OER performance of fabricated 3D bimetallic NiMn/Ti catalysts was also thoroughly investigated in the alkaline (1.0 M KOH) electrolyte. The polarization curves were recorded in 1.0 M KOH solution at a potential scan rate of 10 mV·s⁻¹ from OCP up to 2.068 V (vs. RHE) in the temperature range of 25–75 °C (Figure 5). The current densities increased ca. 1.77–2.21 times within this investigated range of temperature and it was observed that NiMn/Ti-1 exhibits much higher OER activity, needing a low overpotential of 356.3 mV at 10 mA cm⁻² as compared to the NiMn/Ti-2 (361.4 mV) and NiMn/Ti-3 (371.4 mV) catalysts.

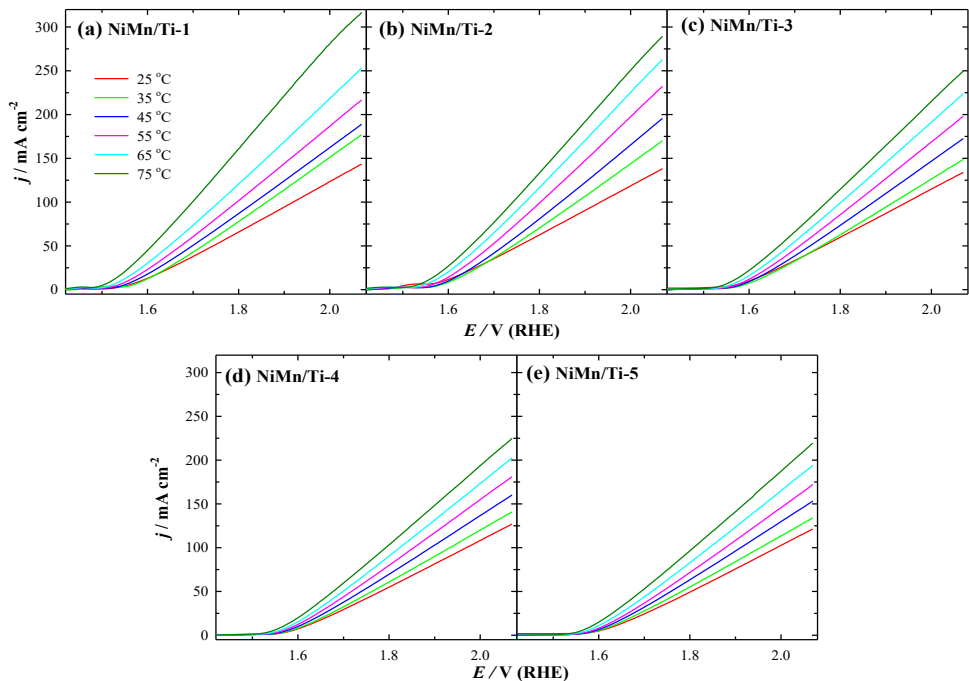


Figure 5. OER polarization curves of 3D NiMn/Ti catalysts in 1 M KOH solution at 10 mV s^{−1} potential scan rate and a temperature range from 25 up to 75 °C.

Figure 6a demonstrates the OER activity of all fabricated catalysts at 25 °C and it was observed that the catalysts prepared via alloying Ni to Mn with different proportion ratios notably prompt to enhance their electrocatalytic activity. The achieved overpotentials value at 10 mA cm^{−2} (η_{10}) of the prepared NiMn/Ti catalysts were remarkably reduced from Ni/Ti (449.5 mV) and Mn/Ti (671.1 mV) samples.

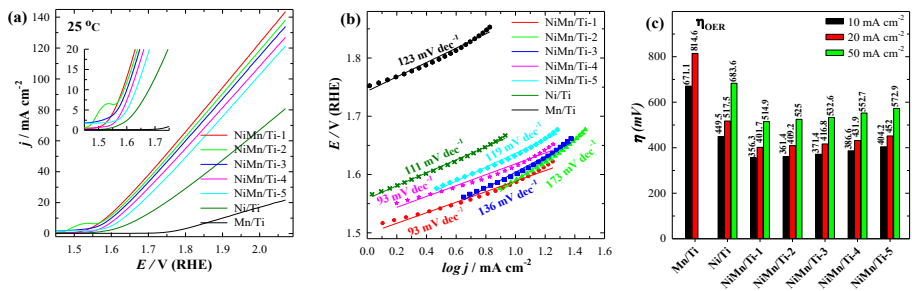


Figure 6. OER polarization curves at 25 °C temperature (a) with corresponding extracted Tafel plots (b) and required overpotentials to reaching the current densities of 10, 20 and 50 mA cm^{−2} (c).

The OER LSVs at 25 °C were then further used for constructing the Tafel plots and calculating the Tafel slopes. The Tafel slope for NiMn/Ti-1 was 93 mV dec⁻¹, which is lower than NiMn/Ti-2 (173 mV dec⁻¹), NiMn/Ti-3 (136 mV dec⁻¹) and NiMn/Ti-5 (119 mV dec⁻¹) (Figure 6b and Table 5).

Table 5. Electrochemical parameters of the investigated catalysts toward OER in alkaline media.

Catalysts	<i>j</i> (mA cm ⁻²) in Different Temperatures (°C) at 2.068 V						<i>j</i> (mA μg ⁻¹) at 25 °C	<i>η</i> ₁₀ (mV) at 25 °C	Tafel Slope (mV·dec ⁻¹)
	25	35	45	55	65	75			
Mn/Ti	21.64	-	-	-	-	-	1.0	671.1	123
Ni/Ti	80.89	-	-	-	-	-	0.27	449.5	111
NiMn/Ti-1	143.54	177.03	188.96	216.81	253.04	316.7	1.44	356.3	93
NiMn/Ti-2	138.28	170.03	195.53	232.16	262.74	289.38	0.83	361.4	173
NiMn/Ti-3	133.94	148.77	172.7	198.04	223.88	249.68	0.36	371.4	136
NiMn/Ti-4	126.97	140.93	160.16	181.08	202.56	224.84	0.15	386.6	93
NiMn/Ti-5	121.35	134.16	153.26	172.24	194.09	219.53	0.1	404.2	119

Moreover, the overpotentials to reach current densities of 10, 20 and 50 mA cm⁻² at 25 °C were also shown in Figure 6c and Table 5 and the *η*₁₀, *η*₂₀ and *η*₅₀ values have found to follow a sequential upward order from NiMn/Ti-1 to NiMn/Ti-5 catalysts. For instance, the *η*₁₀, *η*₂₀ and *η*₅₀ values were 356.3 mV, 401.7 mV and 514.9 mV for NiMn/Ti-1 as compared to 404.2 mV, 452 mV and 572.9 mV for NiMn/Ti-5, respectively, which certainly indicate the superior catalytic activity and favorable OER kinetics of NiMn/Ti-1 over the NiMn/Ti-5 electrocatalyst. A recent study also revealed that the OER performance of Ni_x/Mn_{1-x}O/CNTs electrocatalysts is significantly dependent on the content ratios of Ni and Mn. When the content of Mn element was more than 17%, the overpotential of catalyst increases, i.e., lowering Mn content notably improved the OER activity [74].

Furthermore, in order to compare the electrocatalytic activity of the prepared 3D bimetallic NiMn/Ti catalysts, the current density values were normalized in reference to the metals loadings for each catalyst to represent the mass activity of catalysts towards the HER and OER at 25 °C temperature (Tables 3–5). The highest mass electrocatalytic activity has been exhibited by NiMn/Ti-1 catalyst for HER in both acidic (2.54 mA μg⁻¹) and alkaline (0.51 mA μg⁻¹) media as well as for OER in alkaline (1.44 mA μg⁻¹) media with minimum metal loading of 99.98 μg cm⁻². It is worth mentioning that the mass activity of catalysts for both HER and OER has gradually declined with increase of Mn-loadings on prepared catalysts as higher Mn-concentration in coating bath favors the alloying of metals (Ni and Mn) via electrodeposition process and enriched the total metal loadings.

3.4. Electrocatalytic Stability Studies for HER and OER

To investigate the practical application and efficiency of any fabricated electrocatalysts, the desired electrocatalytic performance is not sufficient enough, and in addition, the electrocatalytic activity must be sustainable as long-term stability directly determines whether the materials can be developed for practical applications. Electrocatalytic stability is also directly related to the lifetime of the electrodes that regulates the production cost of hydrogen.

As the above mentioned investigations in alkaline and acidic media revealed that prepared bimetallic NiMn/Ti-5 electrocatalyst has excellent HER catalytic activity in both electrolytes and fabricated NiMn/Ti-1 electrocatalyst exhibits superior OER performance in alkaline media, thus in this section, the electrocatalytic stability of these two electrodes was investigated using different electrochemical methods. At first, the electrocatalytic durability was studied by Chronopotentiometry (CP) for 10 h. CP investigations were performed in 1.0 M KOH at a current density of 10 mA cm⁻² at 25 °C (Figure 7).

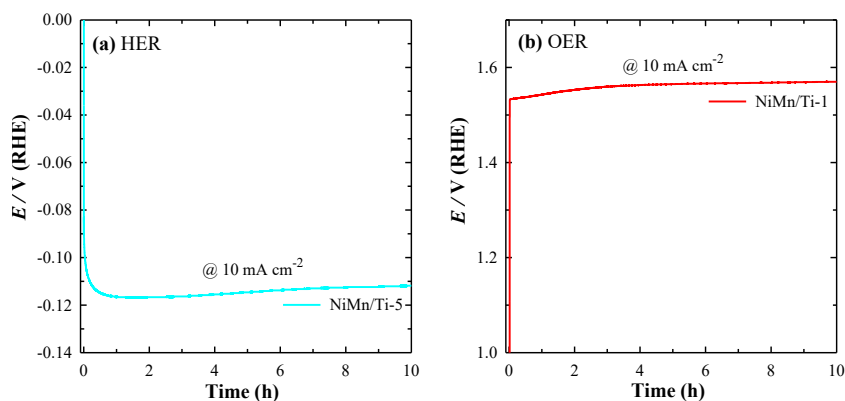


Figure 7. CP curves in 1.0 M KOH solution at a constant current density of 10 mA cm^{-2} at 25°C of the investigated NiMn/Ti-5 for HER (a) and NiMn/Ti-1 for OER (b) electrocatalysts.

It was observed that the potential of ca. 115 mV of NiMn/Ti-5 as HER electrocatalyst (Figure 7a) and of ca. 335 mV of NiMn/Ti-1 as OER electrocatalyst (Figure 7b) was achieved at current density of 10 mA cm^{-2} . The CP curves did not deteriorate significantly after 10 h continuous HER and OER electrolysis at a static current density of 10 mA cm^{-2} , proving their good electrocatalytic stability for HER and OER in an alkaline environment.

Additionally, the electrocatalytic stability of these two catalysts has been examined by CA as well. CA investigations were carried out in 1.0 M KOH at -0.232 V (vs. RHE) and 1.818 V (vs. RHE) at 25°C for the NiMn/Ti-5 and NiMn/Ti-1 electrocatalysts, respectively (Figure 8).

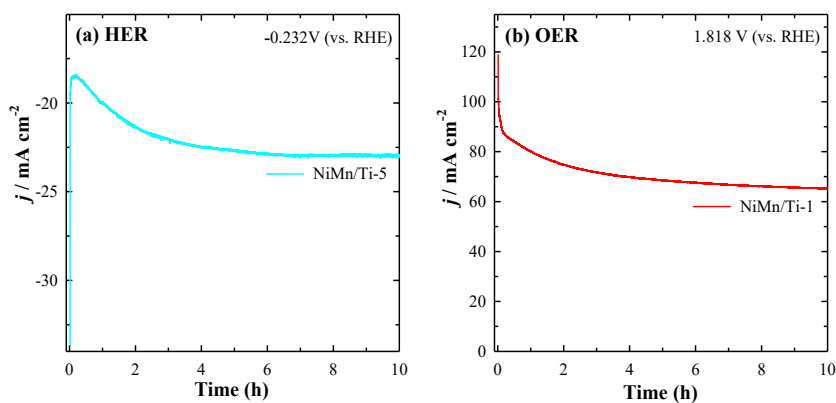


Figure 8. CA curves of the investigated NiMn/Ti-5 (a) and NiMn/Ti-1 (b) electrocatalysts in 1.0 M KOH solution at 25°C at the potential values of -0.232 V (vs. RHE) and 1.818 V (vs. RHE), respectively.

In this test, the electrocatalytic durability of both catalysts was studied by constant applied potential to the electrode and then the current density was monitored over time. After 10 h of investigation, approx. 6% degradation of current density was observed for NiMn/Ti-5 catalyst and the NiMn/Ti-1 catalyst has found to retain more than 92% of

its current, indicating their quite reasonable electrocatalytic stability in alkaline media as cathodic and anodic materials, respectively.

A comparison of HER and OER performance using herein-tested NiMn/Ti catalysts with some of the transition metal-based electrodes reported in the literature (Tables 6 and 7) demonstrates that these bimetallic catalysts exhibit comparable overpotentials and Tafel slopes for HER and OER.

Table 6. Electrochemical performance of herein tested catalysts towards HER in alkaline and acidic media with comparison of transition metal-based electrodes reported in the literatures.

Catalysts	Overpotential@Current Density (mV@mA cm ⁻²)	Tafel Slope (mV dec ⁻¹)	Temperature (°C)	Electrolyte	Ref.
Ni-Mn/Cu	101@10	118	-	1 M KOH	[28]
Ni-Fe-Mn/Cu	64@10	68			
Ni-Fe/NF	142@10	133.3	-	1 M KOH	[52]
Ni ₁ Mn ₁ P	160@10	109	-	1 M KOH	[70]
Ni ₂ Mn ₁ P	120@10	82			
Ni ₃ Mn ₁ P	140@10	93			
Mn-doped Ni ₂ P	160@10	124.27	-	1 M KOH	[75]
Mn-doped Fe ₂ P	136@10	142.34			
Mn-doped Ni ₂ P/Fe ₂ P	90@10	115.41			
Mn-Ni(OH) ₂	197@10	134.5	-	1 M KOH	[76]
NiS _x	172@10	111.9			
Mn-NiS _x	94.2@10	71.5			
Ni-Fe/Cu	124@10	114	-	1 M KOH	[77]
(Co,Fe)PO ₄	122@10	71	-	1 M KOH	[78]
NiFe ₁₀ Se ₁₀ @NF	154@10	129.3	-	1 M KOH	[79]
FeSe ₂ -MoSe ₂ (1-1)/rGO	178@10	80		1 M KOH	[80]
Ni-Mo/WC 3	134@10	163	25	1 M KOH	[81]
Ni-Co-Se@NiCo-LDH/NF	189@10	124.09	-	1 M KOH	[82]
Ni-Co-Fe-Se@NiCo-LDH/NF	113@10	44.87			
NC-1@CoO/NF	241@10	155	-	1 M KOH	[83]
NC-2@CoO/NF	139@10	96			
NC-3@CoO/NF	192@10	189			
NC-4@CoO/NF	196@10	141			
NiMo/FTO	154@10	152	25	1 M KOH	[84]
W ₂ C@CNT	125@10	104	-	1 M KOH	[85]
Mo ₂ C@CNT	118@10	92			
Ni-GF/VC	128@10	80	-	1 M KOH	[86]
Ni-GF/Fe ₃ C	93@10	63			
NiMn/Ti-1	220.3@10	177	25	1 M KOH	This work
NiMn/Ti-2	195.1@10	194			
NiMn/Ti-3	149.8@10	199			
NiMn/Ti-4	144.8@10	192			
NiMn/Ti-5	127.1@10	184			
NiMn/Ti-1	243.1@10	139	25	0.5 M H ₂ SO ₄	This Work
NiMn/Ti-2	220.5@10	141			
NiMn/Ti-3	177.7@10	110			
NiMn/Ti-4	160.1@10	114			
NiMn/Ti-5	102.1@10	102			

Table 6. Cont.

Catalysts	Overpotential@Current Density (mV@mA cm ⁻²)	Tafel Slope (mV dec ⁻¹)	Temperature (°C)	Electrolyte	Ref.
NiMo/FTO	140@20	118	25	0.5 M H ₂ SO ₄	[84]
W ₂ C@CNT	155@10	85	-	0.5 M H ₂ SO ₄	[85]
Mo ₂ C@CNT	121@10	77		0.5 M H ₂ SO ₄	
Ni-GF/VC	111@10	86	-	0.5 M H ₂ SO ₄	[86]
Ni-GF/Fe ₃ C	112@10	97		0.5 M H ₂ SO ₄	
Mo ₂ C-RGO (3.0 wt %)	125@10	89	25	0.5 M H ₂ SO ₄	[87]
Mo ₂ C P/Mo ₂ C F	118@10	48.6	-	0.5 M H ₂ SO ₄	[88]
Ni-Pt nanofilm	90@10	49	25	0.5 M H ₂ SO ₄	[89]
MoP	115@10	87	-	0.5 M H ₂ SO ₄	[90]
FeS-MoP	89@10	70		0.5 M H ₂ SO ₄	
MnS-MoP	88@10	68		0.5 M H ₂ SO ₄	
Mo ₂ N-Mo ₂ C/NC	114@10	62	-	0.5 M H ₂ SO ₄	[91]

NF—nickel foam, rGO—reduced graphene oxide, WC—tungsten carbide, CNT—carbon nanotube, LDH/NF—Layered double hydroxide/nickel foam, FTO—F-doped SnO₂, Ni-GF—Ni foam coated with graphene, F—microflower, NC—N-doped carbon framework.

Table 7. Electrochemical performance of herein tested catalysts towards OER in alkaline media with comparison of transition metal-based electrodes reported in the literatures.

Catalysts	Overpotential@Current Density (mV@mA cm ⁻²)	Tafel Slope (mV dec ⁻¹)	Electrolyte	Ref.
CoNi ₂ S ₄ (GCN)30/NF	340@30	93.21	1.0 M KOH	[48]
CoNi ₂ S ₄ (GCN)50/NF	310@30	49.86		
CoNi ₂ S ₄ (GCN)100/NF	350@30	109.01		
NMF-6 (Ni _{52.3} Mo _{37.4} Fe _{10.2})	344@10	-	1.0 M KOH	[54]
Ni ₁ Mn ₁ LDH	420@10	41	1.0 M KOH	[64]
Ni ₃ Mn ₁ LDH	350@10	40		
Ni ₅ Mn ₁ LDH	390@10	40		
NiMn LDH/NiCo ₂ O ₄	310@10	99	1.0 M KOH	[67]
Ni-Mn LDH	385@10	80	1.0 M KOH	[68]
21.1% Co-doped Ni-Mn LDH	310@10	59		
Ni ₁ Mn ₁ P	250@20	63	1.0 M KOH	[70]
Ni ₂ Mn ₁ P	340@20	93		
Ni ₃ Mn ₁ P	330@20	89		
Ni _{0.95} Mn _{0.05} O/CNT	293@10	55.6	1.0 M KOH	[74]
Ni _{0.83} Mn _{0.17} O/CNT	316@10	63.5		
NC-1@CoO/NF	340@10	93	1.0 M KOH	[83]
NC-2@CoO/NF	290@10	82		
NC-3@CoO/NF	335@10	127		
NC-4@CoO/NF	370@10	91		

Table 7. Cont.

Catalysts	Overpotential@Current Density (mV@mA cm ⁻²)	Tafel Slope (mV dec ⁻¹)	Electrolyte	Ref.
Ni _{1.5} Co _{1.5} P/MF	314@10	71	1.0 M KOH	[92]
Ni ₂ Co ₁ P/MF	342@10	83		
Ni ₁ Co ₂ P/MF	387@10	114		
Ni ₃ S ₂ /NF	362@10	56.5	1.0 M KOH	[93]
Cu ₂ S-Ni ₃ S ₂ /NF	329@10	44.11		
MCS@a-Ni ₃ S ₂	333@10	150.1	1.0 M KOH	[94]
Ni ₃ S ₂ @3-D GNS	305@10	50	1.0 M KOH	[95]
NiMn/Ti-1	356.3@10	93	1.0 M KOH at 25 °C	This work
NiMn/Ti-2	361.4@10	173		
NiMn/Ti-3	371.4@10	136		
NiMn/Ti-4	386.6@10	93		
NiMn/Ti-5	404.2@10	119		

GCN/NF—graphitic carbon nitride/nickel foam, LDH—layered double hydroxide, MF—microflower, MCS@a-Ni₃S₂—Mn-Cd-S@amorphous-Ni₃S₂, 3-D GNS—3-D graphene nanosheets, CNT—carbon nanotube.

4. Conclusions

In summary, a set of self-supported three-dimensional bimetallic NiMn alloy catalysts with various Ni:Mn molar ratios have been successfully synthesized through electrochemical deposition technique and their electrocatalytic activity for HER and OER was studied. The surface morphology demonstrates a unique 3D porous architecture that could avail numerous active sites and channels for electrolyte/gas diffusion. Electrochemical performance results manifested that the amalgamation of Mn element with Ni remarkably enhanced the electrocatalytic activity of the catalysts for HER and OER. The NiMn/Ti-5 electrocatalyst exhibited excellent HER activity with a low overpotential of 102.1 mV in acidic media and 127.1 mV in alkaline media to generate current densities of 10 mA cm⁻², respectively. On the contrary, NiMn/Ti-1 electrocatalyst with least Mn-content exhibits superior OER activity with a small overpotential of 356.3 mV to reach 10 mA cm⁻². Furthermore, the present electrocatalysts also demonstrated outstanding electrocatalytic long-term durability in an alkaline environment as the recorded potentials did not change significantly after 10 h continuous HER and OER electrolysis at a constant current density of 10 mA cm⁻².

This work tends to highlight the fabrication of Mn-containing bimetallic alloy catalysts as well as prioritize to increase the electrochemical active surface area of catalysts via 3D structure formation. The intrinsic activity of these 3D alloy catalysts will provide a strong guide for manufacturing bifunctional electrocatalysts for water splitting application with excellent comprehensive performance and the synergistic effects between transition elements may surpass the heteroatom doping strategy for enhancing the electrocatalytic performance.

Author Contributions: Conceptualization, A.B. and E.N.; methodology, S.B. and J.V.; formal analysis, S.B.; investigation, S.B. and J.V.; data curation, L.T.-T.; writing—original draft preparation, S.B. and A.B.; writing—review and editing, E.N. and A.B.; visualization, L.T.-T.; supervision, A.B. All authors have read and agreed to the published version of the manuscript.

Funding: This research received no external funding.

Institutional Review Board Statement: Not applicable.

Informed Consent Statement: Not applicable.

Data Availability Statement: The data presented in this study are available on request from the corresponding author.

Conflicts of Interest: The authors declare no conflict of interest.

References

1. Zhou, Z.; Pei, Z.; Wei, L.; Zhao, S.; Jian, X.; Chen, Y. Electrocatalytic hydrogen evolution under neutral pH conditions: Current understandings, recent advances, and future prospects. *Energy Environ. Sci.* **2020**, *13*, 3185–3206. [\[CrossRef\]](#)
2. Zhu, L.; Li, C.; Li, H.; Li, H.; Wu, Z.; Huang, Y.; Zhu, X.; Sun, Y. Adjustable antiperovskite cobalt-based nitrides as efficient electrocatalysts for overall water splitting. *J. Mater. Chem. A* **2022**, *10*, 15520–15527. [\[CrossRef\]](#)
3. Ali, A.; Long, F.; Shen, P.K. Innovative strategies for overall water splitting using nanostructured transition metal electrocatalysts. *Electrochem. Energy Rev.* **2022**, *5*, 1. [\[CrossRef\]](#)
4. Yan, Y.; Wang, P.; Lin, J.; Cao, J.; Qi, J. Modification strategies on transition metal-based electrocatalysts for efficient water splitting. *J. Energy Chem.* **2021**, *58*, 446–462. [\[CrossRef\]](#)
5. Cao, X.; Wang, T.; Jiao, L. Transition-metal (Fe, Co, and Ni)-based nanofiber electrocatalysts for water splitting. *Adv. Fiber Mater.* **2021**, *3*, 210–228. [\[CrossRef\]](#)
6. Guo, Y.; Park, T.; Yi, J.W.; Henzie, J.; Kim, J.; Wang, Z.; Jiang, B.; Bando, Y.; Sugahara, Y.; Tang, J.; et al. Nanoarchitectonics for transition-metal-sulfide-based electrocatalysts for water splitting. *Adv. Mater.* **2019**, *31*, 1807134. [\[CrossRef\]](#)
7. Yu, Y.; Zhou, J.; Sun, Z. Novel 2D Transition-Metal Carbides: Ultrahigh Performance Electrocatalysts for Overall Water Splitting and Oxygen Reduction. *Adv. Funct. Mater.* **2020**, *30*, 2000570. [\[CrossRef\]](#)
8. Su, H.; Jiang, J.; Song, S.; An, B.; Li, N.; Gao, Y.; Ge, L. Recent progress on design and applications of transition metal chalcogenide-associated electrocatalysts for the overall water splitting. *Chin. J. Catal.* **2023**, *44*, 7–49. [\[CrossRef\]](#)
9. Peng, X.; Yan, Y.; Jin, X.; Huang, C.; Jin, W.; Gao, B.; Chu, P.K. Recent advance and perspectives of electrocatalysts based on transition metal selenides for efficient water splitting. *Nano Energy* **2020**, *78*, 105234. [\[CrossRef\]](#)
10. Ali, A.; Shen, P.K. Nonprecious metal's graphene-supported electrocatalysts for hydrogen evolution reaction: Fundamentals to applications. *Carbon Energy* **2020**, *2*, 99–121. [\[CrossRef\]](#)
11. Sun, H.; Xu, X.; Kim, H.; Jung, W.; Zhou, W.; Shao, Z. Electrochemical water splitting: Bridging the gaps between fundamental research and industrial applications. *Energy Environ. Mater.* **2022**, *2022*, e12441. [\[CrossRef\]](#)
12. Fu, H.C.; Varadhan, P.; Tsai, M.L.; Li, W.; Ding, Q.; Lin, C.H.; Bonifazi, M.; Fratolocchi, A.; Jin, S.; He, J.H. Improved performance and stability of photoelectrochemical water-splitting Si system using a bifacial design to decouple light harvesting and electrocatalysis. *Nano Energy* **2020**, *70*, 104478. [\[CrossRef\]](#)
13. Kumar, M.; Meena, B.; Subramanyam, P.; Suryakala, D.; Subrahmanyam, C. Recent trends in photoelectrochemical water splitting: The role of cocatalysts. *NPG Asia Mater.* **2022**, *14*, 88. [\[CrossRef\]](#)
14. Wang, S.; Yang, P.; Sun, X.; Xing, H.; Hu, J.; Chen, P.; Cui, Z.; Zhu, W.; Ma, Z. Synthesis of 3D heterostructure Co-doped Fe₂P electrocatalyst for overall seawater electrolysis. *Appl. Catal. B Environ.* **2021**, *297*, 120386. [\[CrossRef\]](#)
15. Zhao, Y.; You, J.; Wang, L.; Bao, W.; Yao, R. Recent advances in Ni₃S₂-based electrocatalysts for oxygen evolution reaction. *Int. J. Hydrogen Energy* **2021**, *46*, 39146–39182. [\[CrossRef\]](#)
16. Li, Y.; Sun, Y.; Qin, Y.; Zhang, W.; Wang, L.; Luo, M.; Yang, H.; Guo, S. Recent advances on water-splitting electrocatalysis mediated by noble-metal-based nanostructured materials. *Adv. Energy Mater.* **2020**, *10*, 1903120. [\[CrossRef\]](#)
17. Xu, H.; Zhao, Y.; He, G.; Chen, H. Race on engineering noble metal single-atom electrocatalysts for water splitting. *Int. J. Hydrogen Energy* **2022**, *47*, 14257–14279. [\[CrossRef\]](#)
18. Zhang, J.; Lian, J.; Jiang, Q.; Wang, G. Boosting the OER/ORR/HER activity of Ru-doped Ni/Co oxides heterostructure. *Chem. Eng. J.* **2022**, *439*, 135634. [\[CrossRef\]](#)
19. Lin, S.; Yu, Y.; Sun, D.; Meng, F.; Chu, W.; Huang, L.; Ren, J.; Su, Q.; Ma, S.; Xu, B. FeNi₂P three-dimensional oriented nanosheet array bifunctional catalysts with better full water splitting performance than the full noble metal catalysts. *J. Colloid Interface Sci.* **2022**, *608*, 2192–2202. [\[CrossRef\]](#)
20. Sun, H.; Xu, X.; Song, Y.; Zhou, W.; Shao, Z. Designing high-valence metal sites for electrochemical water splitting. *Adv. Funct. Mater.* **2021**, *31*, 2009779. [\[CrossRef\]](#)
21. Chatenet, M.; Pollet, B.G.; Dekel, D.R.; Dionigi, F.; Deseure, J.; Millet, P.; Braatz, R.D.; Bazant, M.Z.; Eikerling, M.; Staffell, I.; et al. Water electrolysis: From textbook knowledge to the latest scientific strategies and industrial developments. *Chem. Soc. Rev.* **2022**, *51*, 4583–4762. [\[CrossRef\]](#) [\[PubMed\]](#)
22. Luo, W.; Wang, Y.; Cheng, C. Ru-based electrocatalysts for hydrogen evolution reaction: Recent research advances and perspectives. *Mater. Today Phys.* **2020**, *15*, 100274. [\[CrossRef\]](#)
23. Gong, Y.; Yao, J.; Wang, P.; Li, Z.; Zhou, H.; Xu, C. Perspective of hydrogen energy and recent progress in electrocatalytic water splitting. *Chin. J. Chem. Eng.* **2022**, *43*, 282–296. [\[CrossRef\]](#)
24. Darband, G.B.; Aliofkhazraei, M.; Rouhaghdam, A.S.; Kiani, M.A. Three-dimensional Ni-Co alloy hierarchical nanostructure as efficient non-noble-metal electrocatalyst for hydrogen evolution reaction. *Appl. Surf. Sci.* **2019**, *465*, 846–862. [\[CrossRef\]](#)
25. Darband, G.B.; Aliofkhazraei, M.; Rouhaghdam, A.S. Facile electrodeposition of ternary Ni-Fe-Co alloy nanostructure as a binder free, cost-effective and durable electrocatalyst for high-performance overall water splitting. *J. Colloid Interface Sci.* **2019**, *547*, 407–420. [\[CrossRef\]](#)
26. Nie, M.; Sun, H.; Gao, Z.D.; Li, Q.; Xue, Z.H.; Luo, J.; Liao, J.M. Co-Ni nanowires supported on porous alumina as an electrocatalyst for the hydrogen evolution reaction. *Electrochem. Commun.* **2020**, *115*, 106719. [\[CrossRef\]](#)

27. Xu, Y.; Dong, X.; Miao, J.; Wang, S.; Liu, Z.; Zhai, Z.; Zhang, L.; Liu, Z. Facile preparation of Ni, Co-alloys supported on porous carbon spheres for supercapacitors and hydrogen evolution reaction application. *Int. J. Hydrogen Energy* **2020**, *45*, 1466–1476. [\[CrossRef\]](#)
28. Ashraf, M.A.; Li, C.; Pham, B.T.; Zhang, D. Electrodeposition of Ni–Fe–Mn ternary nanosheets as affordable and efficient electrocatalyst for both hydrogen and oxygen evolution reactions. *Int. J. Hydrogen Energy* **2020**, *45*, 24670–24683. [\[CrossRef\]](#)
29. Zhou, J.; Xiao, H.; Weng, W.; Gu, D.; Xiao, W. Interfacial confinement of Ni–V₂O₃ in molten salts for enhanced electrocatalytic hydrogen evolution. *J. Energy Chem.* **2020**, *50*, 280–285. [\[CrossRef\]](#)
30. Browne, M.P.; Sofer, Z.; Pumera, M. Layered and two dimensional metal oxides for electrochemical energy conversion. *Energy Environ. Sci.* **2019**, *12*, 41–58. [\[CrossRef\]](#)
31. Li, C.; Zhang, B.; Li, Y.; Hao, S.; Cao, X.; Yang, G.; Wu, J.; Huang, Y. Self-assembled Cu–Ni bimetal oxide 3D in-plane epitaxial structures for highly efficient oxygen evolution reaction. *Appl. Catal. B Environ.* **2019**, *244*, 56–62. [\[CrossRef\]](#)
32. Yu, M.; Budiyo, E.; Tüysüz, H. Principles of water electrolysis and recent progress in cobalt-, nickel-, and iron-based oxides for the oxygen evolution reaction. *Angew. Chem. Int. Ed.* **2022**, *61*, e202103824.
33. Ma, X.; Wei, P.; Yang, Y.; Kang, H.; Guo, D.; Liu, L. One-pot synthesis of Ni–Co layered double hydroxide nanosheets as efficient catalysts for oxygen evolution reaction. *Mater. Today Commun.* **2019**, *20*, 100596. [\[CrossRef\]](#)
34. Gao, G.; Wang, K.; Wang, X. Peony flower-like Cu_xS@NiMn LDH heterostructure as an efficient electrocatalyst for the oxygen evolution reaction. *Int. J. Hydrogen Energy* **2023**, *48*, 1347–1359. [\[CrossRef\]](#)
35. Li, H.; Wang, X.; Wang, T.; Xiao, F. A facile, green and time-saving method to prepare partially crystalline NiFe layered double hydroxide nanosheets on nickel foam for superior OER catalysis. *J. Alloys Compd.* **2020**, *844*, 156224. [\[CrossRef\]](#)
36. Zhu, W.; Chen, W.; Yu, H.; Zeng, Y.; Ming, F.; Liang, H.; Wang, Z. NiCo/NiCo–OH and NiFe/NiFe–OH core shell nanostructures for water splitting electrocatalysis at large currents. *Appl. Catal. B Environ.* **2020**, *278*, 119326. [\[CrossRef\]](#)
37. Li, L.F.; Li, Y.F.; Liu, Z.P. Oxygen evolution activity on NiOOH catalysts: Four-coordinated Ni cation as the active site and the hydroperoxide mechanism. *ACS Catal.* **2020**, *10*, 2581–2590. [\[CrossRef\]](#)
38. Ullah, H.; Loh, A.; Trudgeon, D.P.; Li, X. Density functional theory study of NiFeCo ternary oxy-hydroxides for an efficient and stable oxygen evolution reaction catalyst. *ACS Omega* **2020**, *5*, 20517–20524. [\[CrossRef\]](#)
39. Vandichel, M.; Laasonen, K.; Kondov, I. Oxygen evolution and reduction on Fe-doped NiOOH: Influence of solvent, dopant position and reaction mechanism. *Top. Catal.* **2020**, *63*, 833–845. [\[CrossRef\]](#)
40. Pi, C.; Huang, C.; Yang, Y.; Song, H.; Zhang, X.; Zheng, Y.; Gao, B.; Fu, J.; Chu, P.K.; Huo, K. In situ formation of N-doped carbon-coated porous MoP nanowires: A highly efficient electrocatalyst for hydrogen evolution reaction in a wide pH range. *Appl. Catal. B Environ.* **2020**, *263*, 118358. [\[CrossRef\]](#)
41. Yan, Q.; Chen, X.; Wei, T.; Wang, G.; Zhu, M.; Zhuo, Y.; Cheng, K.; Ye, K.; Zhu, K.; Yan, J.; et al. Hierarchical edge-rich nickel phosphide nanosheet arrays as efficient electrocatalysts toward hydrogen evolution in both alkaline and acidic conditions. *ACS Sustain. Chem. Eng.* **2019**, *7*, 7804–7811. [\[CrossRef\]](#)
42. Ma, B.; Yang, Z.; Chen, Y.; Yuan, Z. Nickel cobalt phosphide with three-dimensional nanostructure as a highly efficient electrocatalyst for hydrogen evolution reaction in both acidic and alkaline electrolytes. *Nano Res.* **2019**, *12*, 375–380. [\[CrossRef\]](#)
43. Ge, R.; Huo, J.; Liao, T.; Liu, Y.; Zhu, M.; Li, Y.; Zhang, J.; Li, W. Hierarchical molybdenum phosphide coupled with carbon as a whole pH-range electrocatalyst for hydrogen evolution reaction. *Appl. Catal. B Environ.* **2020**, *260*, 118196. [\[CrossRef\]](#)
44. Zhou, M.; Sun, Q.; Shen, Y.; Ma, Y.; Wang, Z.; Zhao, C. Fabrication of 3D microporous amorphous metallic phosphides for high-efficiency hydrogen evolution reaction. *Electrochim. Acta* **2019**, *306*, 651–659. [\[CrossRef\]](#)
45. Zhu, L.; Liu, L.; Huang, G.; Zhao, Q. Hydrogen evolution over N-doped CoS₂ nanosheets enhanced by superaerophobicity and electronic modulation. *Appl. Surf. Sci.* **2020**, *504*, 144490. [\[CrossRef\]](#)
46. Guo, X.; Liu, Z.; Liu, F.; Zhang, J.; Zheng, L.; Hu, Y.; Mao, J.; Xue, Y.; Tang, C. Sulfur vacancy-tailored NiCo₂S₄ nanosheet arrays for the hydrogen evolution reaction at all pH values. *Catal. Sci. Technol.* **2020**, *10*, 1056–1065. [\[CrossRef\]](#)
47. Chen, S.; Liang, W.; Wang, X.; Zhao, Y.; Wang, S.; Li, Z.; Wang, S.; Hou, L.; Jiang, Y.; Gao, F. P-doped MOF-derived CoNi bimetallic sulfide electrocatalyst for highly-efficiency overall water splitting. *J. Alloys Compd.* **2023**, *931*, 167575. [\[CrossRef\]](#)
48. Zahra, R.; Pervaiz, E.; Baig, M.M.; Rabi, O. Three-dimensional hierarchical flowers-like cobalt-nickel sulfide constructed on graphitic carbon nitride: Bifunctional non-noble electrocatalyst for overall water splitting. *Electrochim. Acta* **2022**, *418*, 140346. [\[CrossRef\]](#)
49. Wang, J.; Shao, H.; Ren, S.; Hu, A.; Li, M. Fabrication of porous Ni–Co catalytic electrode with high performance in hydrogen evolution reaction. *Appl. Surf. Sci.* **2021**, *539*, 148045. [\[CrossRef\]](#)
50. Pan, Q.Q.; Xu, C.Y.; Li, X.; Zhang, J.F.; Hu, X.L.; Geng, Y.; Su, Z.M. Porous Ni–Mo bimetallic hybrid electrocatalyst by intermolecular forces in precursors for enhanced hydrogen generation. *Chem. Eng. J.* **2021**, *405*, 126962. [\[CrossRef\]](#)
51. Ros, C.; Murcia-López, S.; García, X.; Rosado, M.; Arbiol, J.; Llorca, J.; Morante, J.R. Facing seawater splitting challenges by regeneration with Ni–Mo–Fe bifunctional electrocatalyst for hydrogen and oxygen evolution. *ChemSusChem* **2021**, *14*, 2872–2881. [\[CrossRef\]](#)
52. Zhang, Z.; Wu, Y.; Zhang, D. Potentiostatic electrodeposition of cost-effective and efficient Ni–Fe electrocatalysts on Ni foam for the alkaline hydrogen evolution reaction. *Int. J. Hydrogen Energy* **2022**, *47*, 1425–1434. [\[CrossRef\]](#)
53. Sun, J.; Yu, B.; Tan, F.; Cheng, W.; Cheng, G.; Zhang, Z. High throughput preparation of Ni–Mo alloy thin films as efficient bifunctional electrocatalysts for water splitting. *Int. J. Hydrogen Energy* **2022**, *47*, 15764–15774. [\[CrossRef\]](#)

54. Badrnezhad, R.; Nasri, F.; Pourfarzad, H.; Jafari, S.K. Effect of iron on Ni–Mo–Fe composite as a low-cost bifunctional electrocatalyst for overall water splitting. *Int. J. Hydrogen Energy* **2021**, *46*, 3821–3832. [\[CrossRef\]](#)
55. Niu, J.; Yue, Y.; Yang, C.; Wang, Y.; Qin, J.; Zhang, X.; Wu, Z.S. Ultrarapid synthesis Ni–Cu bifunctional electrocatalyst by self-etching electrodeposition for high-performance water splitting reaction. *Appl. Surf. Sci.* **2021**, *561*, 150030. [\[CrossRef\]](#)
56. Gao, W.; Zou, Y.; Zang, Y.; Zhao, X.; Zhou, W.; Dai, Y.; Liu, H.; Wang, J.J.; Ma, Y.; Sang, Y. Magnetic-field-regulated Ni–Fe–Mo ternary alloy electrocatalysts with enduring spin polarization enhanced oxygen evolution reaction. *Chem. Eng. J.* **2023**, *455*, 140821. [\[CrossRef\]](#)
57. Yuan, H.; Zheng, S.; Sang, S.; Yang, J.; Sun, J.; Ma, Z.; Wang, X. Three-dimensional hierarchical nanoporous (Mn, Ni)-Doped Cu₂S architecture towards high-efficiency overall water splitting. *Int. J. Hydrogen Energy* **2022**, *47*, 11827–11840. [\[CrossRef\]](#)
58. Luo, J.; Guo, W.H.; Zhang, Q.; Wang, X.H.; Shen, L.; Fu, H.C.; Wu, L.L.; Chen, X.H.; Luo, H.Q.; Li, N.B. One-pot synthesis of Mn–Fe bimetallic oxide heterostructures as bifunctional electrodes for efficient overall water splitting. *Nanoscale* **2020**, *12*, 19992–20001. [\[CrossRef\]](#)
59. Xu, P.; Qiu, L.; Wei, L.; Liu, Y.; Yuan, D.; Wang, Y.; Tsiakaras, P. Efficient overall water splitting over Mn doped Ni₂P microflowers grown on nickel foam. *Catal. Today* **2020**, *355*, 815–821. [\[CrossRef\]](#)
60. Li, Y.; Dong, Z.; Jiao, L. Multifunctional transition metal-based phosphides in energy-related electrocatalysis. *Adv. Energy Mater.* **2020**, *10*, 1902104. [\[CrossRef\]](#)
61. Gbadamasi, S.; Mohiuddin, M.; Krishnamurthi, V.; Verma, R.; Khan, M.W.; Pathak, S.; Kalantar-Zadeh, K.; Mahmood, N. Interface chemistry of two-dimensional heterostructures—fundamentals to applications. *Chem. Soc. Rev.* **2021**, *50*, 4684–4729. [\[CrossRef\]](#) [\[PubMed\]](#)
62. Xu, X.; Tian, X.; Zhong, Z.; Kang, L.; Yao, J. In-situ growth of iron/nickel phosphides hybrid on nickel foam as bifunctional electrocatalyst for overall water splitting. *J. Power Sources* **2019**, *424*, 42–51. [\[CrossRef\]](#)
63. Sahoo, D.P.; Das, K.K.; Mansingh, S.; Sultana, S.; Parida, K. Recent progress in first row transition metal Layered double hydroxide (LDH) based electrocatalysts towards water splitting: A review with insights on synthesis. *Coord. Chem. Rev.* **2022**, *469*, 214666. [\[CrossRef\]](#)
64. Sumboja, A.; Chen, J.; Zong, Y.; Lee, P.S.; Liu, Z. NiMn layered double hydroxides as efficient electrocatalysts for the oxygen evolution reaction and their application in rechargeable Zn–air batteries. *Nanoscale* **2017**, *9*, 774–780. [\[CrossRef\]](#)
65. Wang, P.; Qi, J.; Li, C.; Li, W.; Wang, T.; Liang, C. Hierarchical CoNi₂S₄@NiMn-layered double hydroxide heterostructure nanoarrays on superhydrophilic carbon cloth for enhanced overall water splitting. *Electrochim. Acta* **2020**, *345*, 136247. [\[CrossRef\]](#)
66. Wang, P.; Qi, J.; Chen, X.; Li, C.; Li, W.; Wang, T.; Liang, C. Three-dimensional heterostructured NiCoP@NiMn-layered double hydroxide arrays supported on Ni foam as a bifunctional electrocatalyst for overall water splitting. *ACS Appl. Mater. Interfaces* **2019**, *12*, 4385–4395. [\[CrossRef\]](#)
67. Yang, L.; Chen, L.; Yang, D.; Yu, X.; Xue, H.; Feng, L. NiMn layered double hydroxide nanosheets/NiCo₂O₄ nanowires with surface rich high valence state metal oxide as an efficient electrocatalyst for oxygen evolution reaction. *J. Power Sources* **2018**, *392*, 23–32. [\[CrossRef\]](#)
68. Wang, Y.; Liu, X.; Zhang, N.; Qiu, G.; Ma, R. Cobalt-doped Ni–Mn layered double hydroxide nanoplates as high-performance electrocatalyst for oxygen evolution reaction. *Appl. Clay Sci.* **2018**, *165*, 277–283. [\[CrossRef\]](#)
69. Khan, R.; Mehran, M.T.; Baig, M.M.; Sarfraz, B.; Naqvi, S.R.; Niazi, M.B.K.; Khan, M.Z.; Khoja, A.H. 3D hierarchical Heterostructured LSTN@NiMn-layered double hydroxide as a bifunctional water splitting electrocatalyst for hydrogen production. *Fuel* **2021**, *285*, 119174. [\[CrossRef\]](#)
70. Jiang, D.; Ma, W.; Yang, R.; Quan, B.; Li, D.; Meng, S.; Chen, M. Nickel–manganese bimetallic phosphides porous nanosheet arrays as highly active bifunctional hydrogen and oxygen evolution electrocatalysts for overall water splitting. *Electrochim. Acta* **2020**, *329*, 135121. [\[CrossRef\]](#)
71. Zhang, G.; Ge, H.; Zhao, L.; Liu, J.; Wang, F.; Fan, S.; Li, G. NiMn_{1.5}PO₄ thin layer supported on Ni foam as a highly efficient bifunctional electrocatalyst for overall water splitting. *Electrochim. Acta* **2021**, *367*, 137567. [\[CrossRef\]](#)
72. Maleki, M.; Darband, G.B.; Rouhaghdam, A.S.; Andaveh, R.; Kazemi, Z.M. Mn-incorporated nickel selenide: An ultra-active bifunctional electrocatalyst for hydrogen evolution and urea oxidation reactions. *Chem. Commun.* **2022**, *58*, 3545–3548. [\[CrossRef\]](#) [\[PubMed\]](#)
73. Taherinia, D.; Hatami, H.; Valadi, F.M. Trimetallic Co–Ni–Mn metal–organic framework as an efficient electrocatalyst for alkaline oxygen evolution reaction. *J. Electroanal. Chem.* **2022**, *922*, 116720. [\[CrossRef\]](#)
74. Luo, L.; Huang, H.; Yang, G.; Gong, S.; Li, Y.; Wang, Y.; Luo, W.; Li, Z. Nickel and manganese oxide heterostructure nanoparticles supported by carbon nanotube for highly efficient oxygen evolution reaction catalysis. *Appl. Surf. Sci.* **2022**, *575*, 151699. [\[CrossRef\]](#)
75. Luo, Y.; Wang, P.; Zhang, G.; Wu, S.; Chen, Z.; Ranganathan, H.; Sun, S.; Shi, Z. Mn-doped nickel–iron phosphide heterointerface nanoflowers for efficient alkaline freshwater/seawater splitting at high current densities. *Chem. Eng. J.* **2023**, *454*, 140061. [\[CrossRef\]](#)
76. Huang, H.; Hu, X.; Hou, Z.; Yang, D.; Xiang, D.; Hu, L. Interfacial construction and lattice distortion-triggered bifunctionality of Mn–NiS/Mn–Ni₃S₄ for H₂ production. *Fuel* **2022**, *328*, 125337. [\[CrossRef\]](#)
77. Hatami, E.; Toghræi, A.; Darband, G.B. Electrodeposition of Ni–Fe micro/nano urchin-like structure as an efficient electrocatalyst for overall water splitting. *Int. J. Hydrogen Energy* **2021**, *46*, 9394–9405. [\[CrossRef\]](#)

78. Kim, C.; Lee, S.; Kim, S.H.; Park, J.; Kim, S.; Kwon, S.H.; Bae, J.S.; Park, Y.S.; Kim, Y. Cobalt-iron-phosphate hydrogen evolution reaction electrocatalyst for solar-driven alkaline seawater electrolyzer. *Nanomaterials* **2021**, *11*, 2989. [\[CrossRef\]](#)
79. Sun, Y.Y.; Jiang, M.Y.; Wu, L.K.; Hou, G.Y.; Tang, Y.P.; Liu, M. Ultra-thin NiFeSe nanosheets as a highly efficient bifunctional electrocatalyst for overall water splitting. *Sustain. Energy Fuels* **2020**, *4*, 582–588. [\[CrossRef\]](#)
80. Zhu, M.; Bai, X.; Yan, Q.; Yan, Y.; Zhu, K.; Ye, K.; Yan, J.; Cao, D.; Huang, X.; Wang, G. Iron molybdenum selenide supported on reduced graphene oxide as an efficient hydrogen electrocatalyst in acidic and alkaline media. *J. Colloid Interface Sci.* **2021**, *602*, 384–393. [\[CrossRef\]](#)
81. Laszczyńska, A.; Tylus, W.; Szczygieł, I. Electrocatalytic properties for the hydrogen evolution of the electrodeposited Ni–Mo/WC composites. *Int. J. Hydrogen Energy* **2021**, *46*, 22813–22831. [\[CrossRef\]](#)
82. Dai, Z.; Du, X.; Zhang, X. The synthesis of Ni-Co-Fe-Se@NiCo-LDH nanoarrays on Ni foam as efficient overall water splitting electrocatalyst. *J. Alloys Compd.* **2023**, *946*, 169451. [\[CrossRef\]](#)
83. Van Phuc, T.; Jana, J.; Ravi, N.; Kang, S.G.; Chung, J.S.; Choi, W.M.; Hur, S.H. Highly active Ni/Co-metal organic framework bifunctional electrocatalyst for water splitting reaction. *Int. J. Hydrogen Energy* **2022**, *47*, 22787–22795. [\[CrossRef\]](#)
84. Bao, F.; Kemppainen, E.; Dorbandt, I.; Bors, R.; Xi, F.; Schlattmann, R.; van de Krol, R.; Calnan, S. Understanding the Hydrogen Evolution Reaction Kinetics of Electrodeposited Nickel-Molybdenum in Acidic, Near-Neutral, and Alkaline Conditions. *ChemElectroChem* **2021**, *8*, 195–208. [\[CrossRef\]](#)
85. Hussain, S.; Rabani, I.; Vikraman, D.; Feroze, A.; Karuppasamy, K.; Haq, Z.U.; Seo, Y.S.; Chun, S.H.; Kim, H.S.; Jung, J. Hybrid design using carbon nanotubes decorated with Mo₂C and W₂C nanoparticles for supercapacitors and hydrogen evolution reactions. *ACS Sustain. Chem. Eng.* **2020**, *8*, 12248–12259. [\[CrossRef\]](#)
86. Yang, C.; Zhao, R.; Xiang, H.; Wu, J.; Zhong, W.; Li, W.; Zhang, Q.; Yang, N.; Li, X. Ni-activated transition metal carbides for efficient hydrogen evolution in acidic and alkaline solutions. *Adv. Energy Mater.* **2020**, *10*, 2002260. [\[CrossRef\]](#)
87. Caliskan, S.; Wang, A.; Qin, F.; House, S.D.; Lee, J.K. Molybdenum Carbide-Reduced Graphene Oxide Composites as Electrocatalysts for Hydrogen Evolution. *ACS Appl. Nano Mater.* **2022**, *5*, 3790–3798. [\[CrossRef\]](#)
88. Sun, Y.; Peng, F.; Zhang, L.; Jiang, B.; Dou, H.; Zhang, N.; Xu, M.; Yang, N. Hierarchical Nitrogen-doped Mo₂C Nanoparticle-in-microflower Electrocatalyst: In Situ Synthesis and Efficient Hydrogen-evolving Performance in Alkaline and Acidic Media. *ChemCatChem* **2020**, *12*, 6040–6049. [\[CrossRef\]](#)
89. Eiler, K.; Suriñach, S.; Sort, J.; Pellicer, E. Mesoporous Ni-rich Ni–Pt thin films: Electrodeposition, characterization and performance toward hydrogen evolution reaction in acidic media. *Appl. Catal. B Environ.* **2020**, *265*, 118597. [\[CrossRef\]](#)
90. El-Refaei, S.M.; Russo, P.A.; Schultz, T.; Koch, N.; Pinna, N. Dual doping of MoP with M (Mn, Fe) and S to achieve high hydrogen evolution reaction activity in both acidic and alkaline media. *ChemCatChem* **2021**, *13*, 4392–4402. [\[CrossRef\]](#)
91. Song, H.; Guo, S.; Zhang, X.; Yang, Y.; Gao, B.; Pi, Y.; Pi, C.; Chu, P.K.; Huo, K. In-Situ and controllable construction of Mo₂N embedded Mo₂C nanobelts as robust electrocatalyst for superior pH-universal hydrogen evolution reaction. *J. Alloys Compd.* **2022**, *918*, 165611. [\[CrossRef\]](#)
92. Chen, T.; Qian, M.; Tong, X.; Liao, W.; Fu, Y.; Dai, H.; Yang, Q. Nanosheet self-assembled NiCoP microflowers as efficient bifunctional catalysts (HER and OER) in alkaline medium. *Int. J. Hydrogen Energy* **2021**, *46*, 29889–29895. [\[CrossRef\]](#)
93. Bhat, K.S.; Nagaraja, H.S. In situ synthesis of copper sulfide-nickel sulfide arrays on three-dimensional nickel foam for overall water splitting. *ChemistrySelect* **2020**, *5*, 2455–2464. [\[CrossRef\]](#)
94. Li, Z.; Wang, X.; Wang, X.; Lin, Y.; Meng, A.; Yang, L.; Li, Q. Mn-Cd-S@amorphous-Ni₃S₂ hybrid catalyst with enhanced photocatalytic property for hydrogen production and electrocatalytic OER. *Appl. Surf. Sci.* **2019**, *491*, 799–806. [\[CrossRef\]](#)
95. Li, B.; Li, Z.; He, F.; Pang, Q.; Shen, P. One-pot preparation of Ni₃S₂@3-D graphene free-standing electrode by simple Q-CVD method for efficient oxygen evolution reaction. *Int. J. Hydrogen Energy* **2019**, *44*, 30806–30819. [\[CrossRef\]](#)

Disclaimer/Publisher's Note: The statements, opinions and data contained in all publications are solely those of the individual author(s) and contributor(s) and not of MDPI and/or the editor(s). MDPI and/or the editor(s) disclaim responsibility for any injury to people or property resulting from any ideas, methods, instructions or products referred to in the content.



3D Nickel–Manganese bimetallic electrocatalysts for an enhanced hydrogen evolution reaction performance in simulated seawater/alkaline natural seawater

S. Barua, A. Balčiūnaitė^{*}, D. Upskuvienė, J. Vaičiūnienė, L. Tamašauskaitė-Tamašiūnaitė, E. Norkus

Department of Catalysis, Center for Physical Sciences and Technology, Saulėtekio Ave. 3, LT-10257, Vilnius, Lithuania

ARTICLE INFO

Handling Editor: Dr J Lobato

Keywords:

Hydrogen evolution reaction (HER)
Catalyst
Seawater
Nickel
Manganese

ABSTRACT

In this paper, we report an inexpensive one-step synthesis of self-supported 3D nickel-manganese (NiMn) bimetallic coatings and their application for the hydrogen evolution reaction in simulated seawater (1 M KOH + 0.5 M NaCl) and alkaline natural seawater (1 M KOH + natural seawater). These binary coatings were electrodeposited on a titanium substrate using a facile electrochemical deposition method by a dynamic hydrogen bubble template technique. The as-deposited NiMn coatings with variable Mn amounts produce typical globular and unique porous architecture with abundant pores of different sizes. The activity of these fabricated catalysts towards the hydrogen evolution reaction was investigated by linear sweep voltammetry towards simulated seawater and alkaline natural seawater at different temperatures. The surface morphology and composition of the catalysts were also characterized by scanning electron microscopy and inductively coupled plasma optical emission spectroscopy. The as-prepared NiMn/Ti electrocatalyst, which was electrodeposited using a chemical bath containing Ni^{2+} and Mn^{2+} ions with a molar ratio of $\text{Ni}^{2+}:\text{Mn}^{2+} = 1:5$, exhibits excellent hydrogen evolution activity in simulated seawater with an ultra-low overpotential of 64.2 mV to reach a current density of 10 mA cm^{-2} . It is noteworthy that this NiMn/Ti electrocatalyst also achieves a current density of 10 mA cm^{-2} in alkaline natural seawater with a comparably low overpotential of 79.3 mV. The current densities increase by ca. 1.75–2.35 times with an increase in temperature from 25 °C to 75 °C for hydrogen evolution in both electrolytes. This bimetallic catalyst has shown excellent long-term stability at a constant potential of -0.23 V (vs. RHE) and a constant current density of 10 mA cm^{-2} for 10 h, which ensures higher durability and robustness for practical application of seawater splitting technology.

1. Introduction

The ever-increasing population growth and industrialization, together with the resulting depletion of natural resources and the alarming threat of a global environmental crisis, constrain us to explore green and sustainable alternatives to replace fossil fuels [1–6]. In order to address the global energy crisis and consider environmental challenges for sustainability, contemporary research and development mostly emphasizes on sustainable energy conversion and storage technologies. In this aspect, hydrogen (H_2) has received tremendous attention in recent decades as an environmentally friendly and sustainable energy carrier with high energy density (142.35 MJ kg^{-1}), abundant elemental abundance on Earth, and carbon-free emission during the

combustion process [7–10]. Green H_2 production from water electrolysis powered by renewable sources, such as wind, solar, geothermal, and bioenergy, can be considered as a promising alternative to traditional hydrocarbon fuels in the future for large-scale production of high-purity H_2 with zero carbon emissions [11–15]. According to the International Renewable Energy Agency (IRENA), the total H_2 feedstock market is estimated to be worth \$115 billion and the market value would increase up to \$155 billion by 2022, but unfortunately more than 95% of current H_2 production is based on fossil fuels (steam methane reforming, oil and coal gasification, etc.) and only ca. 4% of the global H_2 supply is produced by electrolysis [16–18].

To achieve global targets for carbon neutrality and to outperform traditional petrochemical techniques in terms of renewable

^{*} Corresponding author.

E-mail address: aldona.balciunaite@fmcc.lt (A. Balčiūnaitė).

<https://doi.org/10.1016/j.ijhydene.2024.07.131>

Received 30 April 2024; Received in revised form 21 June 2024; Accepted 9 July 2024

Available online 15 July 2024

0360-3199/© 2024 Hydrogen Energy Publications LLC. Published by Elsevier Ltd. All rights are reserved, including those for text and data mining, AI training, and similar technologies.

Table 1

The composition of the plating bath with plating condition parameters.

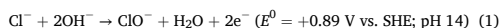
Catalysts	Concentration (M)				Plating conditions	
	NiSO ₄ ·6H ₂ O	MnCl ₂ ·4H ₂ O	(NH ₄) ₂ SO ₄	H ₃ BO ₃	Parameters	Values
NiMn/Ti-3	0.2	0.6	0.5	0.3	Current densities	50 mA cm ⁻² 500 mA cm ⁻²
NiMn/Ti-4	0.2	0.8	0.5	0.3	Time	3 min
NiMn/Ti-5	0.2	1.0	0.5	0.3	Temperature	25 °C
					pH ^a	~1

^a 1.5 M H₂SO₄ and 1 M HCl.

compatibility, electrochemical water splitting is one of the most benign approaches to H₂ production, consisting of two half-reactions: the cathodic H₂ evolution reaction (HER) and the anodic oxygen evolution reaction (OER) [19–26]. The overall electrocatalytic water splitting under standard conditions is a thermodynamically unfavourable uphill reaction that requires some external energy, namely overpotential. The sluggish kinetics of OER due to its inherent four-electron coupling proton transfer steps (1.23 V vs. RHE), which contribute to relatively higher overpotentials, is considered to be the bottleneck for the overall electrochemical water splitting. Practical, real-world water splitting can only occur by overcoming this barrier [27–30]. The water electrolysis process requires a minimum energy of 39.4 kWh kg⁻¹ to produce H₂ at 100% efficiency, while a typical electrocatalytic water splitting can only occur by overcoming this barrier [27–30]. The water electrolysis process requires a minimum energy of 39.4 kWh kg⁻¹ to produce H₂ at 100% efficiency, while a typical electrocatalytic water splitting can only occur by overcoming this barrier [27–30]. The water electrolysis process requires a minimum energy of 39.4 kWh kg⁻¹ to produce H₂ at 100% efficiency, while a typical electrocatalytic water splitting can only occur by overcoming this barrier [27–30].

The availability of global freshwater sources is also very limited and large-scale commercial H₂ production by water splitting consumes scarce freshwater resources, which account for only 2.5% of the world's total water resources. Thus, large-scale freshwater electrolysis would place a critical burden on vital freshwater resources in the context of gradually increasing population growth and industrial sustainability [32–34]. Compared to freshwater, seawater is the most abundant water source on the planet, accounting for ~96.5% of the world's total water resources. Using abundant seawater as an electrolyte instead of freshwater is not only the most promising strategy for sustainable H₂ production, but also reduces the overall production cost [35,36]. The high ionic conductivity of seawater (33.9 mS cm⁻¹ at 25 °C), which is equivalent to 0.5 M NaCl solution, can also play an advantageous role by reducing the use of additional acid and alkali for electrolysis [36–38].

Despite the abundant availability of seawater on our planet, industrial-scale production of high-purity H₂ from direct or selective electrolytic splitting of seawater remains a major challenge, in particular the chlorine evolution reaction (CER) and the formation of hypochlorite (ClO⁻) at the anode compete with the OER, resulting in low anode current efficiency. Chlorine electro-oxidation is a complicated reaction that depends on many factors, such as electrolyte pH, temperature, applied potential, and many others [39]. The Pourbaix diagram for the artificial seawater model at standard ambient temperature and chloride concentration of 0.5 M (similar to typical seawater) shows that at pH 0 the potential difference for chlorine and oxygen evolution is 130 mV, whereas at pH above 7.5 the potential difference is 480 mV. Since the potential difference between CER and OER is only 480 mV, hypochlorite (ClO⁻) formation via chloride (Cl⁻) oxidation could become the main reaction as shown in Eq. (1) [39,40].



Furthermore, the natural presence of abundant aggressive chloride (Cl⁻) ions (~0.5 M) is also highly corrosive to transition metal electrocatalysts, and the presence of unavoidable interfering ions (Na⁺, Ca²⁺, Mg²⁺, Br⁻, and SO₄²⁻), as well as impurities, microorganisms, and small particles in seawater cause poisoning and corrosion of the

electrode and significantly reduce the catalytic performance and durability of the electrocatalyst [41–48]. The commercialization prospect of seawater splitting is negatively affected by the formation of insoluble precipitates, such as Ca(OH)₂, Mg(OH)₂, etc. on the electrode surface, blocking the active sites [49–55]. The filtration and pre-treatment of natural seawater would be very effective in improving the performance and durability of seawater electrolysis. Thus, the design and fabrication of highly efficient and robust electrocatalysts with high corrosion resistance, high catalytic activity, and long-term stability for natural seawater splitting remains a challenge.

Currently, Pt and Pt-based materials are known as state-of-the-art HER electrocatalysts, although their high cost, natural scarcity, and long-term instability limit their economic feasibility. Non-noble metal bifunctional electrocatalysts could be a pathfinder for practical applications of both reactions by reducing the cost of water splitting for large-scale applications [56–59]. Many low-cost bifunctional electrocatalysts, synthesized by various methods, have been investigated and reported for freshwater/seawater electrolysis, demonstrating excellent catalytic performance and long-term stability. Among them, electrocatalysts synthesized by the electrodeposition method have some exceptional features, such as large electrochemically active surface area and strong corrosion resistance of the catalysts, together with a simple, low-cost, and controlled approach to develop binder-free electrodes at ambient temperature, minimizing the cost of high temperature and time [60–64]. In addition to its simplicity and controllability, this strategy also allows the direct growth of materials in size and structure on the substrates, which can be achieved by optimizing conditions such as deposition time, deposition potential, and precursor concentrations [65,66]. For example, Yuan et al. synthesized two hybrid NiMo films on nickel foam using different electrolytes with ultra-low overpotentials of 36.8 and 31.8 mV to reach a current density of 10 mA cm⁻² in alkaline (1 M KOH) and simulated seawater (1 M KOH+0.5 M NaCl) media, respectively [67]. These fabricated catalysts also achieved a lower cell voltage of only 1.563 V to reach the current density of 10 mA cm⁻² at room temperature in simulated seawater [67]. Liu et al. studied Fe(OH)₃/MoNiO_x and Mo_{0.84}Ni_{0.16}/MoNiO_x electrocatalysts that required only 1.54 V and 1.575 V to drive the current density of 10 mA cm⁻² in 1 M KOH and 1 M KOH + seawater, respectively [68]. The elegance of this work is the remarkable stability over 120 h at 100 mA cm⁻² in both electrolytes. Vijayapradeep et al. reported a noble Pt-carbon core-shell coated CoMo₂S₄ electrocatalyst that showed excellent electrochemical HER performance in alkaline media, requiring an overpotential of only 27 mV to achieve the benchmark current density of 10 mA cm⁻² [69]. According to the literature, as mentioned above, metal alloy electrodes fabricated by electrodeposition technique have excellent stability and very low overpotential for seawater splitting.

Our previous publication showed that these 3D bimetallic NiMn coatings electrodeposited on Ti substrate have efficient bifunctional activity with comprehensive HER performance and long-term durability for freshwater splitting in both alkaline and acidic media [70]. They are potential candidates with the added advantage of low fabrication cost. As it has been shown that binary, ternary, or multimetallic coatings have high efficiency for water splitting reactions as electrocatalysts [71], it was therefore decided to continue the scientific investigation focusing

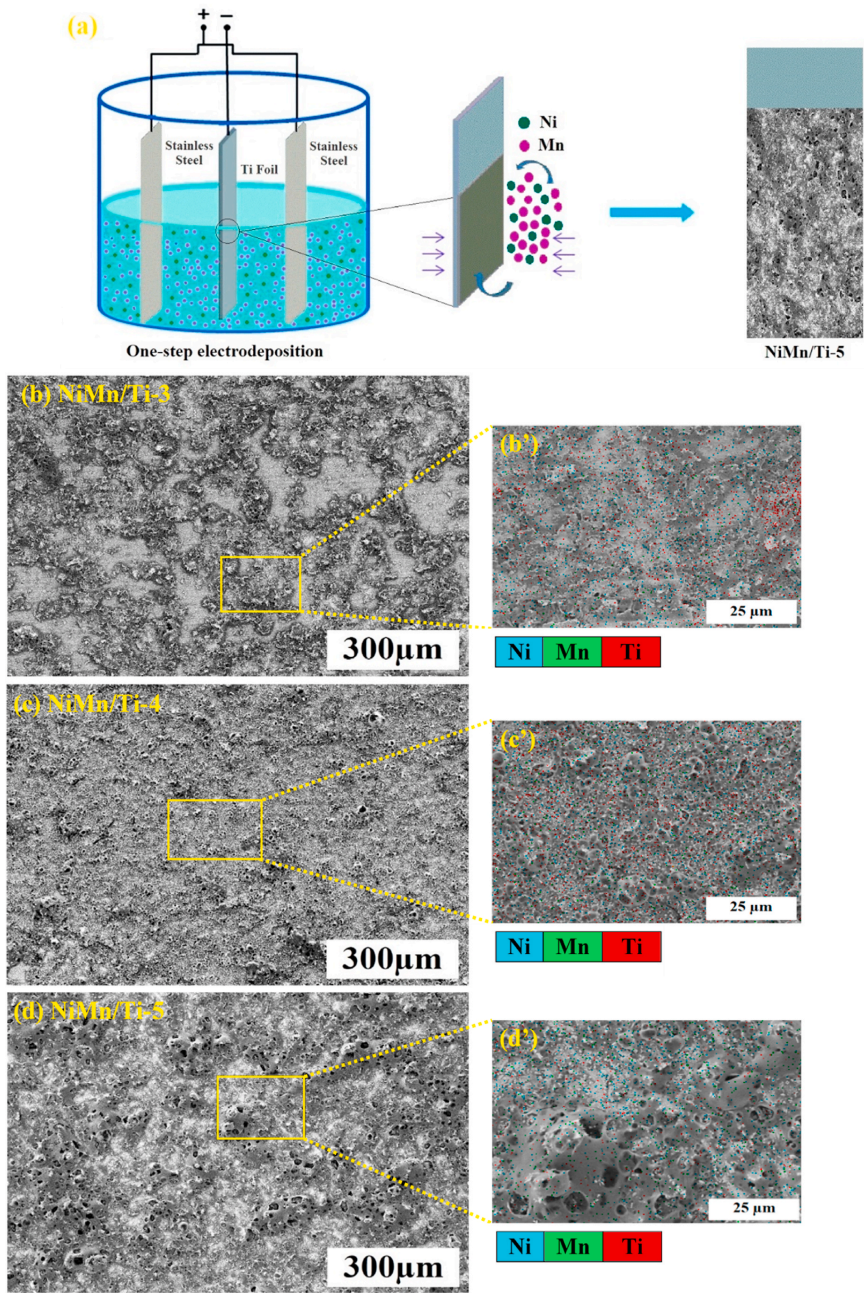


Fig. 1. (a) The schematic illustration of the preparation route of NiMn/Ti electrocatalysts. SEM views of bimetallic NiMn/Ti catalysts obtained in the plating solution, then the molar ratio of $\text{Ni}^{2+}:\text{Mn}^{2+}$ was equal to 1:3 (b), 1:4 (c), and 1:5 (d), along with elemental mapping for Ni, Mn and Ti (b'-d').

Table 2
The ICP-OES results of the studied electrocatalysts.

Catalyst	Ni loading ($\mu\text{g}/\text{cm}^2$)	Mn loading ($\mu\text{g}/\text{cm}^2$)	Total metal loading ($\mu\text{g}/\text{cm}^2$)	Wt. %	
				Ni	Mn
NiMn/Ti-3	269.7	105.25	374.95	71.93	28.07
NiMn/Ti-4	448.45	374.4	822.85	54.49	45.51
NiMn/Ti-5	538	685.5	1223.5	43.97	56.03

on these bifunctional electrocatalysts to investigate their electrocatalytic performance and long-term durability for HER in simulated seawater (SSW) and alkaline natural seawater (ASW).

2. Materials and method

Chemicals. Titanium foil (thickness 0.127 mm, 99.7% purity) and stainless steel foil (thickness 0.2 mm, type 304) were purchased from Sigma-Aldrich (Saint Louis, MO, USA) and Alfa Aesar (Karlsruhe, Germany, GmbH & Co.) suppliers, respectively. Nickel sulfate hexahydrate ($\text{NiSO}_4 \cdot 6\text{H}_2\text{O}$, >98%), manganese chloride tetrahydrate ($\text{MnCl}_2 \cdot 4\text{H}_2\text{O}$, >99%), ammonium sulfate ($(\text{NH}_4)_2\text{SO}_4$, >99%), boric acid (H_3BO_3 , >99.5%), H_2SO_4 (96%), HCl (35–38%), and KOH (98.8%) were purchased from Chempur Company (Karlsruhe, Germany). Ultrapure water with a resistivity of 18.2 $\text{M}\Omega \text{ cm}$ was used for the preparation of the

solutions. Natural seawater was collected from the Baltic Sea in the Klaipėda coastal region of Lithuania. All chemicals were of analytical grade and were used directly without further purification.

Fabrication of catalysts. In this study, the catalysts were fabricated by a facile, low-cost electrochemical deposition method using a dynamic hydrogen bubble template technique. The Ti sheets ($1 \times 1 \text{ cm}$) were first degreased with ethanol, followed by their activation and removal of possible oxides/hydroxides by pre-treatment in diluted H_2SO_4 (1:1 vol) at 70 °C. The Ti sheets were then rinsed with distilled water and immersed in the plating bath. The composition of the plating bath and the electroplating conditions are given in Table 1. The plating bath used consisted of NiSO_4 and MnCl_2 , serving as sources of nickel (Ni^{2+}) and manganese (Mn^{2+}) ions, respectively. In addition, $(\text{NH}_4)_2\text{SO}_4$ was used as a modifier of the coating morphology, while H_3BO_3 acted as a pH stabilizer. The concentrations of NiSO_4 , $(\text{NH}_4)_2\text{SO}_4$, and H_3BO_3 were

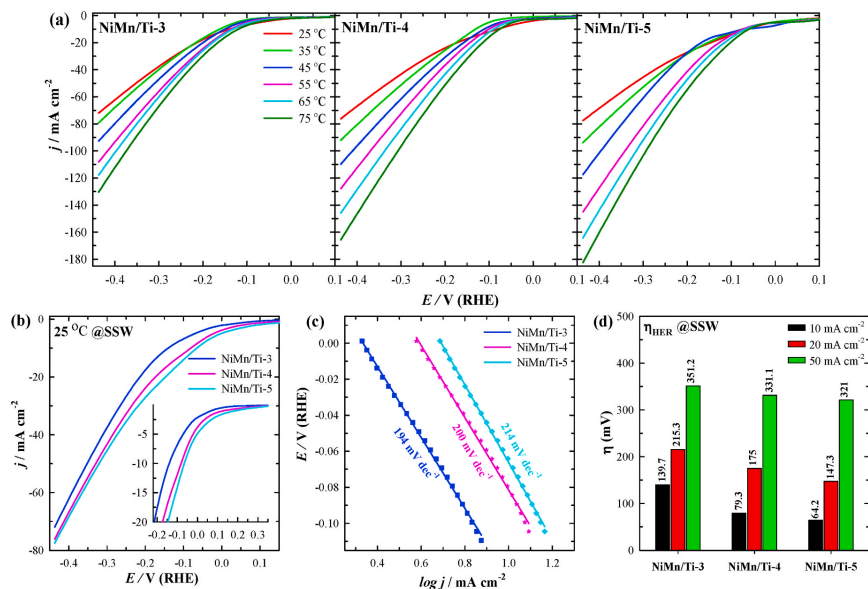


Fig. 2. HER polarization curves of 3D NiMn/Ti catalysts in SSW at 10 mV s^{-1} potential scan rate and 25–75 °C temperature range (a), at only 25 °C temperature (b) with corresponding extracted Tafel plots (c) and required overpotentials to reaching the current densities of 10, 20 and 50 mA cm^{-2} (d).

Table 3
Summarized electrochemical data of the investigated catalysts toward HER in simulated seawater.

Catalysts	j (mA cm^{-2}) at different temperatures (°C) at -0.43 V (vs. RHE)						η_{10} (mV) at 25 °C	Tafel slope (mV dec^{-1})
	25	35	45	55	65	75		
NiMn/Ti-3	71.95	79.13	92.69	108.1	117.72	130.3	139.7	194
NiMn/Ti-4	76.12	92.08	109.69	127.8	145.78	165.61	79.3	200
NiMn/Ti-5	77.49	93.78	117.4	144.97	164.2	182.41	64.2	214

Table 4

Comparison of the HER performance of as-synthesized electrocatalyst in simulated seawater electrolytes with other non-noble metal electrodes reported in the literature.

Catalysts	Overpotential@Current density (mV@mA cm ⁻²)	Tafel slope (mV dec ⁻¹)	Ref.
NiMn/Ti-5	64.2@10	214	This work
NiFeP-NS	83@10	97	[43]
CoS _x /CuS _x /NF	113.2@10	218.7	[64]
NiPS/NF	177@100	–	[66]
NiMo/NF (denoted as A3)	31.8@10	33.1	[67]
Mn-doped Ni ₂ P/Fe ₂ P	308@100	–	[79]
FMCO/NF	248@50	–	[81]
Co ₂ O ₄ /NF	342@50	–	
Zn–NiCoP	160@10	132.86	[82]
NMN-NF	99@10	48	[83]
Ni ₃ S ₂ -NF	109@10	52	
S–NiMoO ₄ @NiFe-LDH	46@10	69	[84]
	170@100		
Ni@CNTs-Mo ₃ C/Ni ₂ P	65.4@10	–	[86]
Co–Ni–S/NF	239@20	137	[87]
	291@50		
Ti@NiB-1.5 h	149@10	118	[88]
	219@25		
NM/NCS/NS/NF	171@30	129	[89]
	204@50		
Co–P@NN	55@10	61.5	[90]
	298@500		
Ni–B@HP	32@10	134.76	[91]
Ni–B@NF	223@100	120.85	
	42@10		
	295@100		
oct-Cu ₂ O–NF	237@20	160	[93]
FeP@CoP/NF	147@50	–	[96]
	197@100		
CoFeOF/NF	164@10	90.43	[97]

NS – Nanosheet, NF – Ni foam, LDH – Layered double hydroxide, NN – Nickel net, HP – Hydrophilic filter paper.

kept constant, while the concentration of MnCl₂ was varied (Table 1). All reagents were dissolved in distilled water under acidic conditions (1.5 M H₂SO₄ and 1 M HCl).

A two-electrode cell with a pair of stainless steel sheets (40 × 25 × 0.2 mm) as the anode and Ti as the cathode was used to electrochemically deposit 3D bimetallic NiMn on the Ti surface. The plating bath was operated at 25 °C. NiMn electroplating on Ti was carried out at the applied current density of 50 mA cm⁻² for 3 min and 500 mA cm⁻² for another 3 min. After plating, the obtained NiMn/Ti electrocatalysts were removed, thoroughly rinsed with deionized water, air-dried at room temperature, and carefully stored for future investigations.

Characterization of Catalysts. The morphology and composition of the prepared Ni/Ti and NiMn/Ti catalysts were investigated by scanning electron microscopy (SEM) using an SEM workstation TM4000 Plus with an AZetecOne detector (Hitachi, Tokyo, Japan).

The metal loadings were determined by inductively coupled plasma optical emission spectrometry (ICP-OES) analysis. The ICP-OES spectra were recorded using an Optima 7000DV spectrometer (PerkinElmer, Waltham, MA, USA) at wavelengths of λ_{Ni} 231.604 nm and λ_{Mn} 257.610 nm.

Electrochemical Measurements. The electrocatalytic performance of fabricated bimetallic nickel-manganese electrocatalysts towards HER was evaluated by linear sweep voltammetry (LSV) using a PGSTAT302 potentiostat (Metrohm Autolab B.V., Utrecht, The Netherlands) through electrochemical software (Nova 2.1.4). The LSVs were recorded in Ar-saturated Simulated Seawater (1 M KOH + 0.5 M NaCl, SSW) and Alkaline Seawater (1 M KOH + natural seawater, ASW) at temperatures ranging from 25 °C to 75 °C.

A standard three-electrode electrochemical cell was used throughout the performance study, with the fabricated NiMn/Ti electrocatalysts with a geometric area of 2 cm² as working electrodes, a graphite rod as counter electrode, and a saturated calomel electrode (SCE) was used as reference. All potentials in this work were converted to the reversible hydrogen electrode (RHE) scale using the following equation:

$$E_{\text{RHE}} = E_{\text{SCE}} + 0.242 \text{ V} + 0.059 \text{ V} \times \text{pH}_{\text{solution}} \quad (2)$$

The HER polarization curves were recorded in both working electrolytes from the open circuit potential (OCP) to –0.43 V (vs. RHE) at a potential scan rate of 10 mV s⁻¹. Moreover, the long-term stability of the fabricated NiMn/Ti-5 electrocatalyst was evaluated by recording the chronopotentiometry (CP) curves at a constant current density of 10 mA cm⁻² and the chronoamperometry (CA) curves at a constant potential of –0.23 V (vs. RHE) for 10 h in SSW and ASW.

3. Results and discussion

Microstructure and Morphology Studies. As shown schematically in Fig. 1a, these 3D bimetallic NiMn/Ti electrocatalysts were synthesized via a facile one-step electrodeposition method using a dynamic hydrogen bubble template technique. The surface morphology of the fabricated catalysts was investigated by scanning electron microscopy (SEM), as depicted in Fig. 1 (b) NiMn/Ti-3, (c) NiMn/Ti-4, and (d) NiMn/Ti-5. The top side view of the NiMn/Ti-3 catalyst demonstrates an uneven, rough morphology because the NiMn coatings were electrodeposited on the Ti substrate by dynamic hydrogen bubble templating from an aqueous solution containing Ni²⁺ and Mn²⁺ ions in a molar ratio of 1:3 (Fig. 1b). As the NiMn films were deposited under acidic conditions to ensure the generation of vigorous hydrogen bubbles, the deposited Ni and Mn particles in the coating from the plating bath using a Ni²⁺:Mn²⁺ molar ratio of 1:4 started to agglomerate by forming smaller nodule-like structures covering the surface of the substrate as shown in Fig. 1c. Of course, the catalysts were synthesized using different chemical bath compositions with the Ni²⁺:Mn²⁺ molar ratios increasing in a sequential order (from 1:3 up to 1:5); meanwhile, it was observed that the cell voltage during the electrodeposition also increased accordingly. As a consequence, the nodule size increased and the catalyst (herein denoted to NiMn/Ti-5, according to the bath

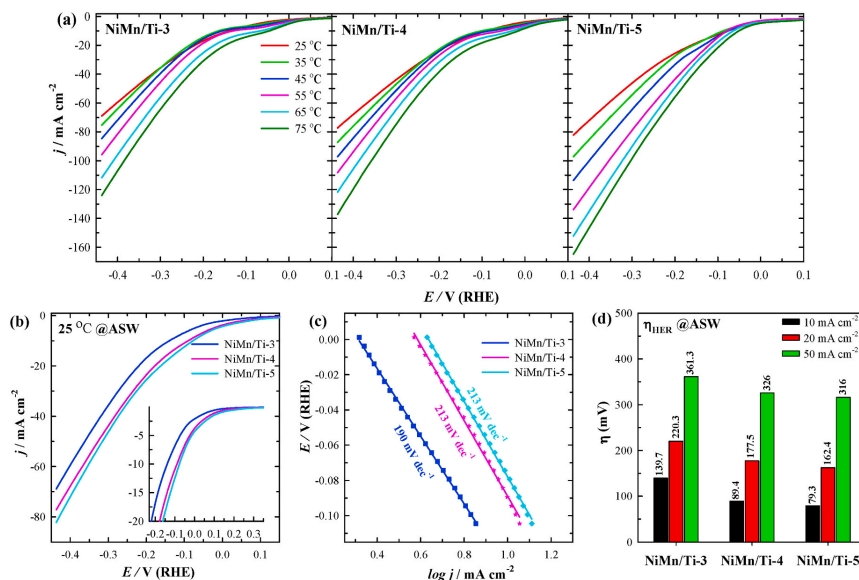


Fig. 3. HER polarization curves of 3D NiMn/Ti catalysts in ASW at a potential scan rate of 10 mV s⁻¹ and a temperature range of 25–75 °C (a), at a temperature of only 25 °C (b) with corresponding extracted Tafel plots (c) and overpotentials required to reach the current densities of 10, 20 and 50 mA cm⁻² (d).

Table 5

Summarized electrochemical data of the investigated catalysts toward HER in alkaline natural seawater.

Catalysts	<i>j</i> (mA cm ⁻²) at different temperatures (°C) at -0.43 V(vs. RHE)						η_{10} (mV) at 25 °C	Tafel slope (mV dec ⁻¹)
	25	35	45	55	65	75		
NiMn/Ti-3	68.92	75.24	84.58	95.78	111.77	124.05	139.7	190
NiMn/Ti-4	77.21	87.19	97.15	108.26	121.7	137.22	89.4	213
NiMn/Ti-5	82.17	97.15	113.59	133.93	152.15	164.7	79.3	213

composition of Ni²⁺:Mn²⁺ molar ratio) was turned into a unique porous architecture with an abundance of pores of distinctly different sizes by the dynamic hydrogen bubble template technique (Fig. 1d) [72,73]. It is expected that the presence of infinite pores of very large sizes on the synthesized NiMn/Ti-5 electrocatalyst will increase the number of active sites and thus facilitate the creation of more channels for electrolyte diffusion, which will accelerate the efficiency of electron transport [74–76]. The enlarged pictures of the EDS area show the elemental composition and the presence of Ni, Mn, and Ti components on the prepared electrodes, revealing a homogeneous dispersion of Ni and Mn particles on the Ti surface in relation to their bath compositions in Fig. 1 (b'–d'). These observations verified that the nickel-manganese architecture uniformly covered the entire surface of the substrate.

The data from the ICP-OES analysis of the deposited NiMn binary coatings are given in Table 2. These coatings were fabricated with different molar proportions of Ni:Mn. The amount of Ni varies from ca. 44–72 wt% in the synthesized catalysts, while the amount of deposited Mn is ca. 28–56 wt%. The total metal loadings were significantly increased with a gradual increase of the Mn concentration in the coating bath and varied from ca. 375 up to 1223.5 $\mu\text{g}_{\text{metal}}\text{cm}^{-2}$.

3.1. Electrocatalytic performance for HER in simulated seawater

The HER electrocatalytic activity of synthesized electrodes was investigated by the LSV method in an Ar-saturated simulated seawater

solution (a mixed solution of 1.0 M KOH and 0.5 M NaCl at pH 14, SSW). The LSVs of the as-fabricated electrocatalysts were recorded in SSW at a potential scan rate of 10 mV s⁻¹ from open-circuit potential (OCP) to -0.43 V (vs. RHE) in a temperature range from 25 °C up to 75 °C. To check the repeatability, each electrode was prepared three times and the LSVs were recorded for each electrode. Fig. 2a shows the corresponding polarization curves of the fabricated 3D NiMn/Ti catalysts for HER in SSW, where the catalytic activities were strongly affected by the different molar ratios of Ni and Mn elements and the current density increased by ca. 1.81–2.35 times with the temperature increase from 25 °C up to 75 °C. The polarization curves of the fabricated NiMn/Ti-3, NiMn/Ti-4, and NiMn/Ti-5 electrocatalysts recorded at 25 °C are shown separately in Fig. 2b with their corresponding extracted Tafel plots (Fig. 2c) and the overpotentials required to achieve the benchmark current densities (Fig. 2d). The HER polarization curves shown in Fig. 2b were used to extract the corresponding Tafel plots for the fabricated electrodes. The Tafel slope is a key parameter in electrochemical kinetics that reflects the rate-determining step of a reaction. For the hydrogen evolution reaction (HER), the Tafel slope provides insight into the mechanism of the reaction and the kinetics of the steps involved. As shown in Fig. 2c, the Tafel slope values were found to be 194, 200, and 214 mV dec⁻¹ for the prepared binary NiMn/Ti-3, NiMn/Ti-4, and NiMn/Ti-5 electrocatalysts, respectively. In addition, the amplitude of the overpotentials required to achieve current densities of 10, 20, and 50 mA cm⁻² were plotted (Fig. 2d). As can be observed, the NiMn/Ti-5

Table 6

A comparison of the HER performance of the as-synthesized electrocatalyst in alkaline natural seawater electrolytes with other non-noble metal electrodes reported in the literature.

Catalysts	Overpotential@Current density (mV@mA cm ⁻²)	Tafel slope (mV dec ⁻¹)	Ref.
NiMn/Ti-5	79.3@10	213	This work
NiPS/NF	188@100	–	[66]
NiMoN	82@100	–	[80]
FMCO/NF	250@50	–	[81]
S-NiMoO ₄ @NiFe-LDH	220@100	–	[84]
Ni-WO ₃ @NF	45.69@10	46	[85]
	125.81@100		
Ni@CNTs-Mo ₂ C/Ni ₂ P	65.9@10	–	[86]
Ni-SA/NC	139@10	123	[92]
Ni-NP/NC	151@10	201	
CoZnLDH-Cu ₂ SeS/NF	147@50	166.28	[94]
	197@100		
Mo-NiS@NiTe	57@10	57	[95]
	125@50		
FeP@CoP/NF	159@50	–	[96]
	205@100		
CoFeOF/NF	162@10	126.26	[97]
	269@100		
Mn _{0.25} Ni _{0.75} O	115@10	70	[98]

NF – Ni foam, LDH – Layered double hydroxide, SA/NC – single atom/nitrogen-doped carbon, NP/NC – nanoparticles/nitrogen-doped carbon.

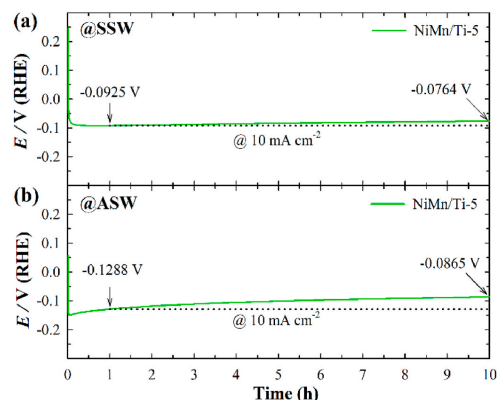


Fig. 4. Steady-state chronopotentiometry curves of the NiMn/Ti-5 electrocatalyst in SSW (a) and ASW (b) at a constant current density of 10 mA cm⁻² for 10 h.

electrocatalyst exhibits significantly enhanced HER activity with the lowest required overpotential of 64.2 mV to achieve the current density of 10 mA cm⁻², outperforming those of 79.3 and 139.7 mV for the NiMn/Ti-4 and NiMn/Ti-3 electrodes, respectively (Table 3). Notably that NiMn/Ti-5 electrocatalyst exhibiting the small overpotential of 64.2 mV at the same current density corresponds to a larger Tafel slope (214 mV dec⁻¹) as compared with other catalysts (Table 3). Typically, lower Tafel slopes are associated with faster reaction kinetics and thus higher activity. However, in some cases, the highest activity may correlate with the highest Tafel slope for several potential reasons. While a high Tafel slope generally indicates slower reaction kinetics, the overall activity of a catalyst for the HER can still be high due to factors such as surface properties, morphology, electronic effects, and mass transport considerations.

The as-fabricated 3D bimetallic NiMn/Ti electrocatalysts, especially NiMn/Ti-5, exhibited exceptional HER catalytic performance, which can reasonably outperform many currently reported non-noble metal

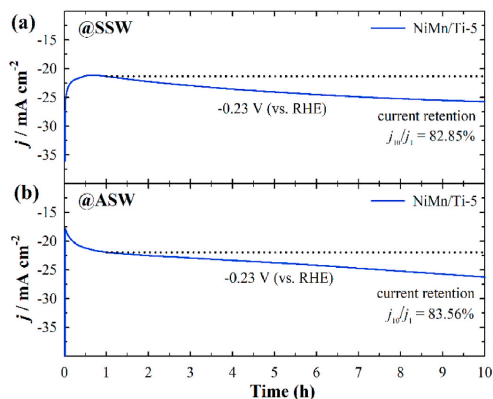


Fig. 5. Chronoamperometric curves of NiMn/Ti-5 electrocatalyst in simulated seawater (a) and natural alkaline seawater solution (b) at a constant potential of -0.23 V (vs. RHE) for 10 h.

electrocatalysts. The corresponding catalysts were also rationalised. The high activity of the NiMn/Ti-5 electrocatalyst can be related to the composition of the plating bath used for deposition as well as to the surface morphology obtained. It is evident that increasing the Mn²⁺ concentration in the plating solution, while keeping the other reagents and plating conditions the same, results in the deposition of a NiMn coating with nodular porous structures with significantly different pore sizes (Fig. 1d,d') compared to the NiMn coating obtained from the plating bath with the lowest Mn²⁺ concentration (Fig. 1b,b'). It is expected that an uneven and rough morphology of NiMn/Ti-5 and the presence of infinite pores of writ large sizes increases the number of active sites and thus increase the electrochemically active surface area of the catalyst, facilitates the creation of more channels for electrolyte diffusion, which accelerates the efficiency of electron transport as well as accelerating the adsorption of hydrogen atoms and making the combination with free hydrogen atoms faster and smoother [77,78]. Ni-Mn alloying also improves the intrinsic activity by optimizing the adsorption/desorption energy of intermediates in the HER process [79].

The obtained data mentioned above implies that the as-synthesized NiMn/Ti electrocatalysts, especially NiMn/Ti-5 are among the best Ni-based electrocatalysts for HER, as they outperform or are quite comparable to the latest non-precious metal-based HER catalysts in simulated seawater (Table 4).

3.2. Electrocatalytic performance for HER in alkaline natural seawater

Direct electrolysis of natural seawater (pH ≈ 8.2) results in the precipitation of various insoluble hydroxides, e.g., Mg(OH)₂ and Ca(OH)₂ due to the reaction with OH⁻ ions at the anode during electrolysis. These precipitates are deposited on the electrode surface, resulting in the blocking of active sites and consequently reducing the catalytic performance and durability of electrocatalysts, causing poisoning and corrosion. It is therefore essential to pre-treat these dissolved cations in natural seawater before electrolysis with a higher pH electrolyte. Natural seawater (pH ≈ 8.2) collected from the Baltic Sea near the Klaipėda coastal region of Lithuania was used, and 1.0 M equivalent solid KOH pellets were dissolved in the measured volume of collected seawater to convert it into the alkaline natural seawater electrolyte under investigation. A cloudy white layer of insoluble Mg/Ca hydroxides precipitates at the bottom of the volumetric flask overnight and is filtered off. The resulting filtrate (here the alkaline seawater, ASW) with a pH of ca.13.85 was collected, and the as-synthesized NiMn/Ti electrocatalysts were

further investigated in this alchemized electrolyte. The electrocatalytic HER activity was evaluated by recording the LSV polarization curves in an Ar-saturated aqueous saline electrolyte at a potential scan rate of 10 mV s^{-1} from open-circuit potential (OCP) up to -0.43 V (vs. RHE) at a temperature range of 25°C – 75°C . The HER corresponding polarization curves of the fabricated 3D NiMn/Ti catalysts in ASW are shown in Fig. 3a, where the current density increases ca. 1.77–2.0 times with an increase in temperature from 25°C up to 75°C . As evident from the LSVs shown in Fig. 3b, a negligible but certain decrease in the HER activity has occurred with respect to the fabricated NiMn/Ti catalysts in ASW due to their relative catalytic performance and the possible invasion of from bacteria/microbes, small particles, insoluble precipitates, and corrosion damage of active sites by aggressive Cl^- ions previously reported for natural seawater electrolysis on other electrodes [79,80].

As shown in Fig. 3b, the fabricated NiMn/Ti-5 electrocatalyst exceptionally possesses excellent HER catalytic activity in ASW, surpassing that of NiMn/Ti-4 and NiMn/Ti-3. Notably, the current density delivered by NiMn/Ti-5 in ASW (82.17 mA cm^{-2}) was also slightly higher than the value recorded in SSW (77.49 mA cm^{-2}). The Tafel slope values were found to be 190, 213, and 213 mV dec^{-1} (Fig. 3c and Table 5) for the as-synthesized 3D bimetallic NiMn/Ti-3, NiMn/Ti-4, and NiMn/Ti-5 electrocatalysts, respectively. Moreover, the overpotentials to reach current densities of 10, 20, and 50 mA cm^{-2} at 25°C were shown in Fig. 3d, and the η_{10} , η_{20} , and η_{50} values were found to follow a sequential downward order from NiMn/Ti-3 to NiMn/Ti-5 electrocatalysts. For example, the η_{10} , η_{20} , and η_{50} values were 139.7 mV, 220.3 mV, and 361.3 mV for NiMn/Ti-3 as compared to 89.4 mV, 177.5 mV, and 326 mV for NiMn/Ti-4 and 79.3 mV, 162.4 mV, and 316 mV for NiMn/Ti-5, respectively. The results obtained showed that the overpotentials for HER in AWS are shifted to the more positive potential region with increasing Mn content in the coatings.

A comparison of HER performance using the NiMn/Ti catalysts tested here shows that these non-noble bimetallic catalysts have great potential as a promising hydrogen evolution electrocatalyst for real seawater splitting technology (Table 6).

It was found that the higher HER current density values were obtained on the NiMn/Ti-5 in alkaline real seawater compared to simulated seawater. This phenomenon can be attributed to several factors: higher ionic strength and conductivity in real seawater allowing better ion mobility and lower resistance; potential catalytic effects of organic matter and microorganisms in real seawater (real seawater contains microorganisms that can form biofilms on electrode surfaces). These biofilms can either inhibit or enhance electrochemical reactions. In some cases, biofilms can act as biocatalysts, increasing the current density by

facilitating electron transfer processes); differences in the formation and stability of passive films on the electrode surface.

3.3. Electrocatalytic stability studies for HER

Stability assessment is another critically important criterion needed to study the electrocatalytic performance of cathodic HER electrocatalysts, especially for seawater electrolysis due to the presence of abundant corrosive Cl^- ions. The electrocatalytic activity of the catalysts needs to be sustainable in the long term to prove the practical applicability of seawater splitting technology. Therefore, according to the investigation, the durability of the optimal NiMn/Ti-5 electrocatalyst was studied through long-term operation tests in both SSW and ASW electrolytes by the method of chronopotentiometry (CP) at a fixed current density of 10 mA cm^{-2} and the chronoamperometry (CA) at a constant potential of -0.23 V (vs. RHE) for 10 h at 25°C . In Fig. 4a, the electrocatalytic stability of the NiMn/Ti-5 electrode was demonstrated using chronopotentiometry analysis at the current density of 10 mA cm^{-2} for 10 h. It is worth noting that in simulated seawater, the potential required for HER remains almost constant, with a negligible decrease of only 0.0161 V after 10 h of operation. On the contrary, the catalytic stability of the NiMn/Ti-5 electrocatalyst in alkaline natural seawater is slightly decreased at the beginning due to the obstruction of the active sites exposed in seawater, but it is believed that the unique porous architecture of the synthesized NiMn/Ti-5 electrocatalyst favours the rapid bubble overflow, which facilitates the electrolyte diffusion and electron transport. Thus, after 1 h of operation, due to the stabilization of the catalyst in ASW media, a slight fluctuation of the CP curve was recorded with a marginal decrease of the potential of only 0.042 V at the end of the continuous 10 h HER electrolysis (Fig. 4b).

In addition, the long-term stability of the optimal NiMn/Ti-5 electrocatalyst was also evaluated by conducting the chronoamperometric study in SSW and ASW at a constant potential of -0.23 V (vs. RHE) for 10 h. As shown in Fig. 5, the NiMn/Ti-5 electrode underwent a current density fluctuation in the first hour in both electrolytes, probably due to low the hydrogen evolution kinetics at the beginning of HER, i.e., generated hydrogen bubbles, which were unable to desorb from the electrode surface, blocking the electrode-electrolyte contact, etc. The initial lower current densities of NiMn/Ti-5 electrode have gradually recovered during the long-term operation, and corresponding to the improved current density obtained after 1 h, it was observed that the degradation of current density was approximately 17.2% in SSW (Fig. 5a) and only 16.4% current density degeneration was recorded in ASW (Fig. 5b) at the end of 10 h of continuous HER electrolysis.

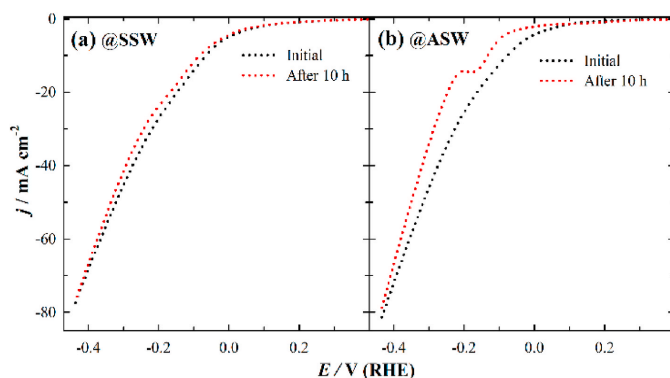


Fig. 6. HER polarization curves of 3D NiMn/Ti-5 electrocatalyst recorded before and after 10 h chronoamperometric measurement in SSW (a) and ASW (b) at 25°C temperature.

Furthermore, in order to address and verify the robustness and resistance of the synthesized electrocatalyst in Cl^- ion-rich seawater electrolysis, the comparison of the catalytic performance of the NiMn/Ti-5 electrode before and after 10 h chronoamperometric measurement in simulated seawater (Fig. 6a) and in alkaline natural seawater (Fig. 6b) was evaluated. After a continuous 10 h CA study, the recorded LSV curve shows a slight shift to a more negative potential zone, but the catalyst performed the same activity, demonstrating an excellent stability in SSW. Later on, the LSV curve recorded after 10 h continuous CA study shows a slight distortion, accompanied by a negligible decrease in current density from 82.2 to 79.9 mA cm^{-2} (a decrease of 2.8%) in ASW. This decrease can be attributed to the possible disruption of surface active sites and the formation of precipitates, which could hinder the exposure of active sites to seawater, as reported for natural seawater electrolysis [99].

4. Conclusions

In summary, we have successfully developed a novel, self-supported, bimetallic three-dimensional NiMn/Ti electrocatalysts for efficient and stable hydrogen evolution reaction by seawater splitting. The catalysts were fabricated with different Ni:Mn molar compositions via a facile, one-step electrochemical deposition method using a dynamic hydrogen bubble template technique, and their electrocatalytic activity and durability for HER in SSW and ASW were studied. Structure and surface morphology studies reveal a unique porous architecture with numerous active sites and uniform dispersion of Ni and Mn particles over the entire surface of the substrate.

The NiMn/Ti electrocatalyst, electroplated under optimal conditions using a chemical bath containing Ni^{2+} and Mn^{2+} ions with a molar ratio of $\text{Ni}^{2+}:\text{Mn}^{2+} = 1:5$, showed superior HER activity and stability, requiring ultra-low overpotentials of 64.2 and 79.3 mV to achieve the benchmark current density of 10 mA cm^{-2} in SSW and ASW, respectively, which are highly comparable to most of the non-noble metal based electrocatalysts reported in the recent past. The corresponding other catalysts prepared from the mentioned bath compositions have also exhibited remarkable HER activity with lower overpotentials required to drive the benchmark current densities. The composition of the plating solution plays a crucial role in regulating the morphology and structure of the synthesized NiMn/Ti catalysts, thereby enhancing their intrinsic catalytic activity. In addition, the high-performance optimal NiMn/Ti electrocatalyst also shows excellent long-term electrocatalytic durability in both working electrolytes as the recorded potentials remain almost unchanged with nominal degradation after 10 h of continuous HER operation.

The synthesis procedure of the NiMn/Ti electrocatalyst is simple, non-toxic, inexpensive, and time-saving. These features, together with the enhanced superior performance of the synthesized catalysts with robust nature, convincingly promised the promising potential of the NiMn/Ti electrocatalyst for real-life seawater splitting technology.

CRediT authorship contribution statement

S. Barua: Writing – original draft, Methodology, Investigation, Formal analysis. **A. Balciünaitė:** Writing – review & editing, Writing – original draft, Supervision, Conceptualization. **D. Upskuvienė:** Methodology, Investigation, Formal analysis, Data curation. **J. Vaičiūnienė:** Methodology, Investigation. **L. Tamašauskaitė-Tamašiūnaitė:** Visualization, Supervision, Data curation. **E. Norkus:** Writing – review & editing, Conceptualization.

Declaration of competing interest

The authors declare that they have no known competing financial interests or personal relationships that could have appeared to influence the work reported in this paper.

References

- [1] Feng C, Chen M, Yang Z, Xie Z, Li X, Li S, Abudula A, Guan G. Electrocatalytic seawater splitting for hydrogen production: recent progress and future prospects. *J Mater Sci Technol* 2023;162:203–26. <https://doi.org/10.1016/j.jmst.2023.03.058>.
- [2] Yan Y, Wang P, Lin J, Cao J, Qi J. Modification strategies on transition metal-based electrocatalysts for efficient water splitting. *J Energy Chem* 2021;58:446–62. <https://doi.org/10.1016/j.ijechem.2020.10.010>.
- [3] Sun H, Xu X, Kim H, Jung W, Zhou W, Shao Z. Electrochemical water splitting: Bridging the gaps between fundamental research and industrial applications. *Energy Environ. Mater.* 2022:e12441. <https://doi.org/10.1002/eeem2.12441>.
- [4] Hassan Q, Sameen AZ, Salman HM, Jaszczur M, Al-Jiboori AK. Hydrogen energy future: advancements in storage technologies and implications for sustainability. *J Energy Storage* 2023;72:108404. <https://doi.org/10.1016/j.est.2023.108404>.
- [5] Sui J, Chen Z, Wang C, Wang Y, Liu J, Li W. Efficient hydrogen production from solar energy and fossil fuel via water-electrolysis and methane-steam-reforming hybridization. *Appl Energy* 2020;276:115409. <https://doi.org/10.1016/j.apenergy.2020.115409>.
- [6] Yusuf BA, Yaseen W, Xie M, Zayyan RS, Muhammad AI, Nankya R, Xie J, Xu Y. Recent advances in understanding and design of efficient hydrogen evolution electrocatalysts for water splitting: a comprehensive review. *Adv Colloid Interface Sci* 2022;311:102811. <https://doi.org/10.1016/j.cis.2022.102811>.
- [7] Sun F, Qin J, Wang Z, Yu M, Wu X, Sun X, Qiu J. Energy-saving hydrogen production by chlorine-free hybrid seawater splitting coupling hydrazine degradation. *Nat Commun* 2021;12:4182. <https://doi.org/10.1038/s41467-021-24529-3>.
- [8] Yu ZY, Duan Y, Feng XY, Yu X, Gao MR, Yu SH. Clean and affordable hydrogen fuel from alkaline water splitting: past, recent progress, and future prospects. *Adv. Mater.* 2021;33:2007100. <https://doi.org/10.1002/adma.202007100>.
- [9] Li X, Zhao L, Yu J, Liu X, Zhang X, Liu H, Zhou W. Water splitting: from electrode to green energy system. *Nano-Micro Lett* 2020;12:1–29. <https://doi.org/10.1007/s40820-020-00469-3>.
- [10] Ng KH, Lai SY, Cheng CK, Cheng YW, Chong CC. Photocatalytic water splitting for solving energy crisis: Myth, Fact or Bust? *Chem. Eng. J.* 2021;417:128847. <https://doi.org/10.1016/j.cej.2021.128847>.
- [11] Staffell I, Scamman D, Abad AV, Balcombe P, Dods PE, Ekins P, Shah N, Ward KR. The role of hydrogen and fuel cells in the global energy system. *Energy Environ Sci* 2019;12:463–91. <https://doi.org/10.1039/C8EE01157E>.
- [12] Gong Y, Yao J, Wang P, Li Z, Zhou H, Xu C. Perspective of hydrogen energy and recent progress in electrocatalytic water splitting. *Chin J Chem Eng* 2022;43:282–96. <https://doi.org/10.1016/j.cjche.2022.02.010>.
- [13] Lv XW, Tian WW, Yuan ZY. Recent advances in high-efficiency electrocatalytic water splitting systems. *Electrochem Energy Rev* 2023;6:23. <https://doi.org/10.1007/s41918-022-00159-1>.
- [14] Zhao Y, Niu Z, Zhao J, Xue L, Fu X, Long J. Recent advances in photoelectrochemical water splitting for hydrogen production. *Electrochem Energy Rev* 2023;6:14. <https://doi.org/10.1007/s41918-022-00153-7>.
- [15] Kakoulaki G, Kougias I, Taylor N, Dolci F, Moya J, Jäger-Waldau A. Green hydrogen in Europe-A regional assessment: substituting existing production with electrolysis powered by renewables. *Energy Convers Manag* 2021;228:113649. <https://doi.org/10.1016/j.enconman.2020.113649>.
- [16] IRENA. Hydrogen from renewable power: technology outlook for the energy transition. 2018. ISBN 978-92-9260-077-8. [Accessed 8 April 2024].
- [17] Wismann ST, Engbek JS, Vendelbo SB, Bendixen FB, Eriksen WL, Aasberg-Petersen K, Frandsen C, Chorkendorff I, Mortensen PM. Electrified methane reforming: a compact approach to greener industrial hydrogen production. *Science* 2019;364:756–9. <https://doi.org/10.1126/science.aaw8775>.
- [18] Abad AV, Dods PE. Green hydrogen characterisation initiatives: definitions, standards, guarantees of origin, and challenges. *Energy Pol* 2020;138:111300. <https://doi.org/10.1016/j.enpol.2020.111300>.
- [19] Angeles-Olvera Z, Crespo-Yapur A, Rodríguez O, Choluta-Díaz JL, Martínez LM, Vide M. Nickel-based electrocatalysts for water electrolysis. *Energies* 2022;15:1609. <https://doi.org/10.3390/en15051609>.
- [20] Lei Y, Wang Y, Liu Y, Song C, Li Q, Wang D, Li Y. Designing atomic active centers for hydrogen evolution electrocatalysts. *Angew Chem Int Ed* 2020;59:20794–812. <https://doi.org/10.1002/ange.201914647>.
- [21] Yu L, Wu L, Song S, McElhenry B, Zhang F, Chen S, Ren Z. Hydrogen generation from seawater electrolysis over a sandwich-like NiCo/Ni₂P/NiCoNi microsheet array catalyst. *ACS Energy Lett* 2020;5:2681–9. <https://doi.org/10.1021/acsenenergylett.0c01244>.
- [22] Jiao Y, Yan H, Wang R, Wang X, Zhang X, Wu A, Tian C, Jiang B, Fu H. Porous plate-like MoP assembly as an efficient pH-universal hydrogen evolution electrocatalyst. *ACS Appl Mater Interfaces* 2020;12:49596–606. <https://doi.org/10.1021/acsaami.0c13533>.
- [23] Wu L, Yu L, Zhang F, McElhenry B, Luo D, Karim A, Chen S, Ren Z. Heterogeneous bimetallic phosphide Ni₂P-Fe₂P as an efficient bifunctional catalyst for water/seawater splitting. *Adv Funct Mater* 2021;31:2006484. <https://doi.org/10.1002/adfm.202006484>.
- [24] Wang P, Qi J, Li C, Li W, Wang T, Liang C. Hierarchical CoNi₂S₄@NiMn-layered double hydroxide heterostructure nanorings on superhydrophilic carbon cloth for enhanced overall water splitting. *Electrochim Acta* 2020;345:136247. <https://doi.org/10.1016/j.electacta.2020.136247>.
- [25] Maril M, Delplanck JL, Cisternas N, Tobosque P, Maril Y, Carrasco C. Critical aspects in the development of anodes for use in seawater electrolysis. *Int J*

- Hydrogen Energy 2022;47:3532–49. <https://doi.org/10.1016/j.ijhydene.2021.11.002>.
- [26] An L, Wei C, Lu M, Liu H, Chen Y, Scherer GG, Fisher AC, Xi P, Xu ZJ, Yan CH. Recent development of oxygen evolution electrocatalysts in acidic environment. *Adv. Mater.* 2021;33:2006328. <https://doi.org/10.1002/adma.202006328>.
- [27] Kumar M, Meena B, Subramanyam P, Suryakala D, Subrahmanyam C. Recent trends in photoelectrochemical water splitting: the role of cocatalysts. *NPG Asia Mater* 2022;14:88. <https://doi.org/10.1038/s41427-022-00436-x>.
- [28] Xu H, Zhao Y, He G, Chen H. Race on engineering noble metal single-atom electrocatalysts for water splitting. *Int J Hydrogen Energy* 2022;47:14257–79. <https://doi.org/10.1016/j.ijhydene.2022.02.152>.
- [29] Chatenet M, Pollet BG, Dekel DR, Dionigi F, Deseure J, Millet P, Braatz RD, Bazant MZ, Eikerling M, Staffell I, Balcombe P. Water electrolysis: from textbook knowledge to the latest scientific strategies and industrial developments. *Chem Soc Rev* 2022;51:4583–762. <https://doi.org/10.1039/D0CS01079K>.
- [30] Lee JE, Jeon KJ, Show PL, Jung SC, Choi YJ, Rhee GH, Lin KYA, Park YK. Mini review on H₂ production from electrochemical water splitting according to special nanostructured morphology of electrocatalysts. *Fuel* 2022;308:122048. <https://doi.org/10.1016/j.fuel.2021.122048>.
- [31] Mazloomi K, Gomes C. Hydrogen as an energy carrier: prospects and challenges. *Renew Sustain Energy Rev* 2012;16:3024–33. <https://doi.org/10.1016/j.rser.2012.02.028>.
- [32] Zhang DD, Shen JQ, Sun FH. Water resources liability measurement and the driving factors of water resources liability intensity. *Water Resour Manag* 2022;36:1553–69. <https://doi.org/10.1007/s11269-022-03101-8>.
- [33] Makanda K, Nzama S, Kanyeere T. Assessing the role of water resources protection practice for sustainable water resources management: a review. *Water* 2022;14:3153. <https://doi.org/10.3390/w14193153>.
- [34] Wang C, Shang H, Jin L, Xu H, Du Y. Advances in hydrogen production from electrocatalytic seawater splitting. *Nanoscale* 2021;13:7897–912. <https://doi.org/10.1039/D1NR00784J>.
- [35] Wang X, Zhai X, Yu Q, Liu X, Meng X, Wang X, Wang L. Strategies of designing electrocatalysts for seawater splitting. *J Solid State Chem* 2022;306:122799. <https://doi.org/10.1016/j.jssc.2021.122799>.
- [36] Sun F, Qin J, Wang Z, Yu M, Wu X, Sun X, Qiu J. Energy-saving hydrogen production by chlorine-free hybrid seawater splitting coupling hydrazine degradation. *Nat Commun* 2021;12:4182. <https://doi.org/10.1038/s41467-021-24529-3>.
- [37] Mohammed-Ibrahim J, Moussab H. Recent advances on hydrogen production through seawater electrolysis. *Mater. Sci. Energy Technol.* 2020;3:780–807. <https://doi.org/10.1016/j.mset.2020.09.005>.
- [38] Jiang S, Suo H, Zhang T, Liao C, Wang Y, Zhao Q, Lai W. Recent advances in seawater electrolysis. *Catalysts* 2022;12:123. <https://doi.org/10.3390/catal12020123>.
- [39] Tong W, Forster M, Dionigi F, Drepp S, Sadeghi Erami R, Strasser P, Cowan AJ, Farrás P. Electrolysis of low-grade and saline surface water. *Nat Energy* 2020;5:367–77. <https://doi.org/10.1038/s41560-020-0550-8>.
- [40] Dionigi F, Reier T, Pawolek Z, Glich M, Strasser P. Design criteria, operating conditions, and nickel-iron hydroxide catalyst materials for selective seawater electrolysis. *ChemSusChem* 2016;9:962–72. <https://doi.org/10.1002/cssc.201501581>.
- [41] Drepp S, Dionigi F, Klingenhof M, Strasser P. Direct electrolytic splitting of seawater: opportunities and challenges. *ACS Energy Lett* 2019;4:933–42. <https://doi.org/10.1021/acsenergylett.9b00220>.
- [42] Li J, Sun J, Li Z, Meng X. Recent advances in electrocatalysts for seawater splitting in hydrogen evolution reaction. *Int J Hydrogen Energy* 2022;47:29685–97. <https://doi.org/10.1016/j.ijhydene.2022.06.288>.
- [43] Liu J, Liu X, Shi H, Luo J, Wang L, Liang J, Li S, Yang LM, Wang T, Huang Y, Li Q. Breaking the scaling relations of oxygen evolution reaction on amorphous NiFeP nanostructures with enhanced activity for overall seawater splitting. *Appl Catal B Environ* 2022;302:120862. <https://doi.org/10.1016/j.apcatb.2021.120862>.
- [44] Liu J, Duan S, Shi H, Wang T, Yang X, Huang Y, Wu G, Li Q. Rationally designing efficient electrocatalysts for direct seawater splitting: challenges, achievements, and promises. *Angew Chem* 2022;134:e202210753. <https://doi.org/10.1002/ange.202210753>.
- [45] Wang HY, Weng CC, Ren JT, Yuan ZY. An overview and recent advances in electrocatalysts for direct seawater splitting. *Front Chem Sci Eng* 2021;15:1408–26. <https://doi.org/10.1007/s11705-021-2102-6>.
- [46] Bolar S. Progress in theoretical and experimental investigation on seawater electrolysis: opportunities and challenges. *Sustain Energy Fuels* 2021;5:5915–45. <https://doi.org/10.1039/D1SE01347E>.
- [47] Khatun S, Hirani H, Roy P. Seawater electrocatalysis: activity and selectivity. *J Mater Chem A* 2021;9:74–86. <https://doi.org/10.1039/D0TA08709B>.
- [48] Yao Y, Gao X, Meng X. Recent advances on electrocatalytic and photocatalytic seawater splitting for hydrogen evolution. *Int J Hydrogen Energy* 2021;46:9087–100. <https://doi.org/10.1016/j.ijhydene.2020.12.212>.
- [49] Hausmann JN, Schlögl R, Menezes PW, Driess M. Is direct seawater splitting economically meaningful? *Energy Environ Sci* 2021;14:3679–85. <https://doi.org/10.1039/D0EE03659E>.
- [50] Jadhav AR, Kumar A, Lee J, Yang T, Na S, Lee J, Luo Y, Liu X, Hwang Y, Liu Y, Lee H. Stable complete seawater electrolysis by using interfacial chloride ion blocking layer on catalyst surface. *J Mater Chem A* 2020;8:24501–14. <https://doi.org/10.1039/D0TA08543J>.
- [51] Kirk DW, Ledas AE. Precipitate formation during sea water electrolysis. *Int J Hydrogen Energy* 1982;7:925–32. [https://doi.org/10.1016/0360-3199\(82\)90160-4](https://doi.org/10.1016/0360-3199(82)90160-4).
- [52] Ke SC, Chen R, Chen GH, Ma XL. Mini review on electrocatalyst design for seawater splitting: recent progress and perspectives. *Energy Fuels* 2021;35:12948–56. <https://doi.org/10.1021/acs.energyfuels.1c02056>.
- [53] Lv Q, Han J, Tan X, Wang W, Cao L, Dong B. Featherlike NiCoP holey nanoarrays for efficient and stable seawater splitting. *ACS Appl Energy Mater* 2019;2:3910–7. <https://doi.org/10.1021/acsami.9b00599>.
- [54] Liu G, Xu Y, Yang T, Jiang L. Recent advances in electrocatalysts for seawater splitting. *Nano Mater.* Sci. 2023;5:101–16. <https://doi.org/10.1016/j.nanoms.2020.12.003>.
- [55] Dingenen F, Verbruggen SW. Tapping hydrogen fuel from the ocean: a review on photocatalytic, photoelectrochemical and electrolytic splitting of seawater. *Renew Sustain Energy Rev* 2021;142:110866. <https://doi.org/10.1016/j.rser.2021.110866>.
- [56] Wang C, Shang H, Xu H, Du Y. Nanoboxes endow non-noble-metal-based electrocatalysts with high efficiency for overall water splitting. *J Mater Chem A* 2021;9:857–74. <https://doi.org/10.1039/D0TA10596A>.
- [57] Yao Y, He J, Ma L, Wang J, Peng L, Zhu X, Li K, Qu M. Self-supported Co₉S₈-Ni₃S₂-CNTs/NF electrode with superwetting multistage micro-nano structure for efficient bifunctional overall water splitting. *J Colloid Interface Sci* 2022;616:287–97. <https://doi.org/10.1016/j.jcis.2022.02.071>.
- [58] Chinnadurai D, Rajendiran R, Kandasamy P. Bimetallic copper nickel sulfide electrocatalyst by one step chemical bath deposition for efficient and stable overall water splitting applications. *J Colloid Interface Sci* 2022;606:101–12. <https://doi.org/10.1016/j.jcis.2021.07.145>.
- [59] Poudel MB, Logeshwaran N, Kim AR, Karthikeyan SC, Vijayapradeep S, Yoo DJ. Integrated core-shell assembly of Ni₃S₂ nanowires and CoMoP nanosheets as highly efficient bifunctional electrocatalysts for overall water splitting. *J Alloys Compd* 2023;960:170678. <https://doi.org/10.1016/j.jallcom.2023.170678>.
- [60] Vijayapradeep S, Kumar RS, Shanmugam R, Yoo DJ. Constructing micro-nano rod-shaped iron-molybdenum oxide heterojunctions to enhance overall water electrolysis. *Mater Today Chem* 2024;36:101934. <https://doi.org/10.1016/j.mtchem.2024.101934>.
- [61] Cai Z, Bu X, Wang P, Su W, Wei R, Ho JC, Yang J, Wang X. Simple and cost effective fabrication of 3D porous core-shell Ni nanochains@NiFe layered double hydroxide nanosheet bifunctional electrocatalysts for overall water splitting. *J Mater Chem A* 2019;7:21722–9. <https://doi.org/10.1039/C9TA07282A>.
- [62] Fan H, Ma Y, Chen W, Tang Y, Li L, Wang J. Facile one-step electrodeposition of two-dimensional nickel-iron bimetallic sulfides for efficient electrocatalytic oxygen evolution. *J Alloys Compd* 2022;894:162533. <https://doi.org/10.1016/j.jallcom.2021.162533>.
- [63] Darband GB, Aliofkhazraei M, Rouhghafian AS, Kiani MA. Three-dimensional Ni-Co alloy hierarchical nanostructure as efficient non-noble-metal electrocatalyst for hydrogen evolution reaction. *Appl Surf Sci* 2019;465:846–62. <https://doi.org/10.1016/j.apsusc.2018.09.204>.
- [64] Mottakin M, Selvanathan V, Razali SA, Islam MA, Almomahadi H, Alharthi NH, Yoshimura S, Akhtaruzzaman M. Facile electrodeposition of biphasic Cu₂S/CoS₂ nanostructures as bifunctional electrocatalysts for seawater splitting. *Electrochim Acta* 2023;463:142861. <https://doi.org/10.1016/j.electacta.2023.142861>.
- [65] Zhang Y, Song X, Xue S, Liang Y, Jiang H. Fabrication of hierarchically structured S-doped NiFe hydroxide/oxyde electrodes for solar-assisted oxygen evolution reaction in seawater splitting. *Appl. Catal. A-Gen.* 2023;649:118965. <https://doi.org/10.1016/j.apcata.2022.118965>.
- [66] Wang HY, Ren JT, Wang L, Sun ML, Yang HM, Lv XW, Yuan ZY. Synergistically enhanced activity and stability of bifunctional nickel phosphide/sulfide heterointerface electrodes for direct alkaline seawater electrolysis. *J Energy Chem* 2022;75:66–73. <https://doi.org/10.1016/j.jechem.2022.08.019>.
- [67] Yuan W, Cui Z, Zhu S, Li Z, Wu S, Liang Y. Structure engineering of electrodeposited NiMo films for highly efficient and durable seawater splitting. *Electrochim Acta* 2021;365:137366. <https://doi.org/10.1016/j.electacta.2020.137366>.
- [68] Liu J, Huang J, Sun J, Song Y, Yang J, Chen Q, Zhang X, Zhang L. Rapid synthesis of NiMo-based electrocatalysts at room temperature for efficient oxygen and hydrogen evolution in seawater. *J Electroanal Chem* 2023;935:117311. <https://doi.org/10.1016/j.jelechem.2023.117311>.
- [69] Vijayapradeep S, Logeshwaran N, Ramakrishnan S, Kim AR, Sampath P, Kim DH, Yoo DJ. Novel Pt-carbon core-shell decorated hierarchical CoMoS₄ as efficient electrocatalysts for alkaline/seawater hydrogen evolution reaction. *Chem. Eng. J.* 2023;473:145348. <https://doi.org/10.1016/j.cej.2023.145348>.
- [70] Barua S, Balcinaitė A, Vaidienė J, Tamašauskaitė-Tamašienė L, Norkus E. Bimetallic 3D nickel-manganese/titanium bifunctional electrocatalysts for efficient hydrogen and oxygen evolution reaction in alkaline and acidic media. *Coatings* 2023;13:1102. <https://doi.org/10.3390/coatings13061102>.
- [71] Wang S, Lu A, Zhong CJ. Hydrogen production from water electrolysis: role of catalysts. *Nano Converg* 2021;8:1–23. <https://doi.org/10.1186/s40580-021-00254-x>.
- [72] Asnavandi M, Suryanto BH, Yang W, Bo X, Zhao C. Dynamic hydrogen bubble templated NiCu phosphide electrodes for pH-insensitive hydrogen evolution reactions. *ACS Sustainable Chem Eng* 2018;6:2866–71. <https://doi.org/10.1021/acssuschemeng.7b02492>.
- [73] Wang X, Bai J, Zhang M, Chen Y, Fan L, Yang Z, Zhang J, Guan R. A comparison between porous to fully dense electrodeposited CuNi films: insights on electrochemical performance. *Nanomaterials* 2023;13:491. <https://doi.org/10.3390/nano13030491>.
- [74] Zhang Y, Cui W, Li L, Zhan C, Xiao F, Quan X. Effect of aligned porous electrode thickness and pore size on bubble removal capability and hydrogen evolution

- reaction performance. *J Power Sources* 2023;580:233380. <https://doi.org/10.1016/j.jpowsour.2023.233380>.
- [75] Yu Y, Liu P, Dou M, Niu J, Zhang Z, Wang F. Promotion of hydrogen evolution catalysis by ordered hierarchically porous electrodes. *Catal Sci Technol* 2021;11:2997–3001. <https://doi.org/10.1039/D1CY00401H>.
- [76] Weber CC, Wrubel JA, Gubler L, Bender G, De Angelis S, Büchi FN. How the porous transport layer interface affects catalyst utilization and performance in polymer electrolyte water electrolysis. *ACS Appl Mater Interfaces* 2023;15:34750–63. <https://doi.org/10.1021/acsami.3c04151>.
- [77] Arabi M, Ghaffarinejad A, Darband GB. Electrodeposition of nanoporous nickel selenide on graphite rod as a bifunctional electrocatalyst for hydrogen and oxygen evolution reactions. *J Electroanal Chem* 2022;907:116066. <https://doi.org/10.1016/j.jelechem.2022.116066>.
- [78] Abdollahi A, Ghaffarinejad A, Arabi M. Electrodeposition of Ni-Fe on graphite rod as an efficient and binder-free electrocatalyst for oxygen and hydrogen evolution reactions. *J Alloys Compd* 2023;937:168400. <https://doi.org/10.1016/j.jallcom.2022.168400>.
- [79] Luo Y, Wang P, Zhang G, Wu S, Chen Z, Ranganathan H, Sun S, Shi Z. Mn-doped nickel-iron phosphide heterointerface nanoflowers for efficient alkaline freshwater/seawater splitting at high current densities. *Chem. Eng. J.* 2023;454:140061. <https://doi.org/10.1016/j.cej.2022.140061>.
- [80] Yu L, Zhu Q, Song S, McElhenny B, Wang D, Wu C, Qin Z, Bao J, Yu Y, Chen S, Ren Z. Non-noble metal-nitride based electrocatalysts for high-performance alkaline seawater electrolysis. *Nat Commun* 2019;10:5106. <https://doi.org/10.1038/s41467-019-13092-7>.
- [81] Liu W, Que W, Yin R, Dai J, Zheng D, Feng J, Xu X, Wu F, Shi W, Liu X, Cao X. Ferrum-molybdenum dual incorporated cobalt oxides as efficient bifunctional anti-corrosion electrocatalyst for seawater splitting. *Appl Catal B Environ* 2023;328:122488. <https://doi.org/10.1016/j.apcatb.2023.122488>.
- [82] Wang Q, Wang C, Du X, Zhang X. Controlled synthesis of M (M = Cr, Cu, Zn and Fe)-NiCoP hybrid materials as environmentally friendly catalyst for seawater splitting. *J Alloys Compd* 2023;966:171516. <https://doi.org/10.1016/j.jallcom.2023.171516>.
- [83] Li Y, Wu X, Wang J, Wei H, Zhang S, Zhu S, Li Z, Wu S, Jiang H, Liang Y. Sandwich structured $\text{Ni}_3\text{S}_2\text{-MoS}_2\text{-Ni}_3\text{S}_2$ @Ni foam electrode as a stable bifunctional electrocatalyst for highly sustained overall seawater splitting. *Electrochim Acta* 2021;390:138833. <https://doi.org/10.1016/j.electacta.2021.138833>.
- [84] Wang H, Chen L, Tan L, Liu X, Wen Y, Hou W, Zhan T. Electrodeposition of NiFe-layered double hydroxide layer on sulfur-modified nickel molybdate nanorods for highly efficient seawater splitting. *J Colloid Interface Sci* 2022;613:349–58. <https://doi.org/10.1016/j.jcis.2022.01.044>.
- [85] Liang W, Zhou M, Lin X, Xu J, Dong P, Le Z, Yang M, Chen J, Xie F, Wang N, Jin Y. Nickel-doped tungsten oxide promotes stable and efficient hydrogen evolution in seawater. *Appl Catal B Environ* 2023;325:122397. <https://doi.org/10.1016/j.apcatb.2023.122397>.
- [86] Wang J, Tran DT, Chang K, Prabhakaran S, Zhao J, Kim DH, Kim NH, Lee JH. Hierarchical Ni@CNTs-bridged $\text{Mo}_3\text{C}/\text{Ni}_2\text{P}$ heterostructure micro-pillars for enhanced seawater splitting and Mg/seawater battery. *Nano Energy* 2023;111:108440. <https://doi.org/10.1016/j.nanoen.2023.108440>.
- [87] Gopalakrishnan S, Saranya V, Harish S, Kumar ES, Navaneethan M. Heterogeneous bimetallic oxysulfide nanostructure (Ni-Co) as hybrid bifunctional electrocatalyst for sustainable overall alkaline simulated seawater splitting. *J Alloys Compd* 2023;965:171124. <https://doi.org/10.1016/j.jallcom.2023.171124>.
- [88] Zhang Y, Fu C, Fan J, Lv H, Hao W. Preparation of Ti@NiB electrode via electroless plating toward high-efficient alkaline simulated seawater splitting. *J Electroanal Chem* 2021;901:115761. <https://doi.org/10.1016/j.jelechem.2021.115761>.
- [89] Gopalakrishnan S, Harish S, Kumar ES, Navaneethan M. Interface engineering of heterogeneous NiMn layered double hydroxide/vertically aligned NiCo_2S_4 nanosheet as highly efficient hybrid electrocatalyst for overall seawater splitting. *Chemosphere* 2024;350:141016. <https://doi.org/10.1016/j.chemosphere.2023.141016>.
- [90] Liang R, Fan J, Lei F, Li P, Fu C, Lu Z, Hao W. Fabrication of ultra-stable and high-efficient CoP-based electrode toward seawater splitting at industrial-grade current density. *J Colloid Interface Sci* 2023;645:227–40. <https://doi.org/10.1016/j.jcis.2023.04.143>.
- [91] Zhou Z, Liang R, Weng S, Lei F, Qian Y, Yang Z, Yang H, Chen Z, Hao W. Construction of filterable and intelligent flexible NiB-Based catalytic electrode toward efficient overall seawater splitting. *Appl Surf Sci* 2023;640:158415. <https://doi.org/10.1016/j.apsusc.2023.158415>.
- [92] Zang W, Sun T, Yang T, Xi S, Waqar M, Kou Z, Lyu Z, Feng YP, Wang J, Pennycook SJ. Efficient hydrogen evolution of oxidized Ni-N₃ defective sites for alkaline freshwater and seawater electrolysis. *Adv. Mater.* 2021;33:2003846. <https://doi.org/10.1002/adma.202003846>.
- [93] Wang H, Ying J, Xiao YX, Chen JB, Li JH, He ZZ, Yang HJ, Yang XY. Ultrafast synthesis of Cu_2O octahedrons inlaid in Ni foam for efficient alkaline water/seawater electrolysis. *Electrochem Commun* 2022;134:107177. <https://doi.org/10.1016/j.elecom.2021.107177>.
- [94] Yang L, Zhao Y, Zhu L, Xia D. Rational construction of grille structured P-CoZnO- $\text{Cu}_2\text{SeS}/\text{NF}$ composite electrocatalyst for boosting seawater electrolysis and corrosion resistance. *Appl Surf Sci* 2023;631:157541. <https://doi.org/10.1016/j.apsusc.2023.157541>.
- [95] Zhang K, Yang E, Zheng Y, Yu D, Chen J, Lou Y. Robust and hydrophilic Mo-NiS@NiTe core-shell heterostructure nanorod arrays for efficient hydrogen evolution reaction in alkaline freshwater and seawater. *Appl Surf Sci* 2023;637:157977. <https://doi.org/10.1016/j.apsusc.2023.157977>.
- [96] Lyu C, Cheng J, Wu K, Wu J, Wang N, Guo Z, Hu P, Lau WM, Zheng J. Interfacial electronic structure modulation of CoP nanowires with FeP nanosheets for enhanced hydrogen evolution under alkaline water/seawater electrolytes. *Appl Catal B Environ* 2022;317:121799. <https://doi.org/10.1016/j.apcatb.2022.121799>.
- [97] Patil SA, Khot AC, Chavan VD, Rabani I, Kim DK, Jung J, Im H, Shrestha NK. Electrostatically robust CoFeOF nanosheet against chloride for green- H_2 production in alkaline seawater electrolysis. *Chem. Eng. J.* 2024;480:146545. <https://doi.org/10.1016/j.cej.2023.146545>.
- [98] Logeshwaran N, Vijayarapade S, Kim AR, Sampath P, Ramakrishnan S, Poudel MB, Kim DH, Yoo DJ. Study of engineering electronic structure modulated non-noble metal oxides for scaled-up alkaline blend seawater splitting. *J Energy Chem* 2023;86:167–79. <https://doi.org/10.1016/j.jechem.2023.06.039>.
- [99] Marimuthu T, Yuvakkumar R, Ravi G, Zheng Y, Bi Z, Xu X, Xu G, Velauthapillai D. One-step fabrication of copper sulfide catalysts for HER in natural seawater and their bifunctional properties in freshwater splitting. *Fuel* 2022;322:124073. <https://doi.org/10.1016/j.fuel.2022.124073>.

Article

Bimetallic Ni–Mn Electrocatalysts for Stable Oxygen Evolution Reaction in Simulated/Alkaline Seawater and Overall Performance in the Splitting of Alkaline Seawater

Sukomol Barua , Aldona Balčiūnaitė ^{*}, Daina Upskuvienė, Jūrate Vaičiūnienė, Loreta Tamašauskaitė-Tamašiūnaitė  and Eugenijus Norkus 

Department of Catalysis, Center for Physical Sciences and Technology (FTMC), LT-10257 Vilnius, Lithuania; sukomol.barua@ftmc.lt (S.B.); daina.upskuviene@ftmc.lt (D.U.); jurate.vaiciuniene@ftmc.lt (J.V.); loreta.tamasauskaite@ftmc.lt (L.T.-T.); eugenijus.norkus@ftmc.lt (E.N.)

^{*} Correspondence: aldona.balciunaite@ftmc.lt

Abstract: The perfect strategy for the generation of green and renewable hydrogen (H₂) fuels is the direct electrocatalytic splitting of plentiful seawater rather than scarce freshwater. One of the half-reactions taking place during the electrocatalytic splitting of seawater is oxygen evolution (OER). However, the OER is affected by slow four-electron transfer kinetics as well as competitive chlorine evolution reactions (CERs) in seawater. To overcome the kinematic and competitive barriers of seawater splitting and achieve an excellent overall performance of seawater splitting, we herein report a facile, low-cost, one-step fabrication procedure of 3D structured nickel–manganese (NiMn) coatings using a dynamic hydrogen bubble template (DHBT) technique. The electrocatalytic activities of the thus synthesized catalytic materials for OER in simulated seawater (0.5 M NaCl + 1 M KOH, denoted as SSW) and alkaline natural seawater (natural seawater + 1 M KOH, denoted as ASW) were investigated using linear sweep voltammetry (LSV) at varying temperatures from 25 to 75 °C. Scanning electron microscopy (SEM) and inductively coupled plasma–optical emission spectroscopy (ICP–OES) were used to examine the surface morphology and composition of the prepared catalysts. It was found that the prepared NiMn/Ti-1 catalyst in a plating bath containing a molar ratio of 1:1 Ni²⁺:Mn²⁺ and having the lowest Mn loading of 13.43 μg cm^{−2} exhibited quite reasonable activity for OER in Cl[−] ion rich SSW and ASW. To achieve the benchmark current density of 10 mA cm^{−2} in SSW and ASW, the NiMn/Ti-1 electrocatalyst requires overpotentials of 386 and 388 mV, respectively. In addition, this optimal bimetallic electrocatalyst also demonstrated superior long-run stability at 1.81 V (vs. RHE) and 10 mA cm^{−2} for 24 h in both working electrolytes. Impressively, the two-electrode electrolyzer—NiMn/Ti-5(−) || NiMn/Ti-1(+)—needs only 1.619 V to deliver 10 mA cm^{−2} current density for overall alkaline seawater electrolysis, which is even 0.075 V lower than the noble metal-based electrolyzer (Pt(−) || NiMn/Ti-1(+)).

Keywords: nickel; manganese; oxygen evolution reaction; alkaline natural seawater; simulated seawater; overall seawater splitting



Citation: Barua, S.; Balčiūnaitė, A.; Upskuvienė, D.; Vaičiūnienė, J.; Tamašauskaitė-Tamašiūnaitė, L.; Norkus, E. Bimetallic Ni–Mn Electrocatalysts for Stable Oxygen Evolution Reaction in Simulated/Alkaline Seawater and Overall Performance in the Splitting of Alkaline Seawater. *Coatings* **2024**, *14*, 1074. <https://doi.org/10.3390/coatings14081074>

Academic Editor: Jinyang Xu

Received: 12 July 2024

Revised: 7 August 2024

Accepted: 20 August 2024

Published: 22 August 2024



Copyright: © 2024 by the authors. Licensee MDPI, Basel, Switzerland. This article is an open access article distributed under the terms and conditions of the Creative Commons Attribution (CC BY) license (<https://creativecommons.org/licenses/by/4.0/>).

1. Introduction

Energy plays the most crucial role for the development and continuous growth of modern civilization in this era, maintaining the normal operation of the global economy. The dominance of fossil fuels, in particular natural gas, coal, and oil, in industrial energy consumption persists. However, the unending consumption of non-renewable fossil fuels has led to a global crisis of energy depletion and environmental threats. Hydrogen is a diverse energy bearer with the ability to address several critical energy challenges. In addition, hydrogen energy offers a number of advantages, including clean combustion products with zero pollution and zero CO₂ emissions, a high gravimetric energy density, renewable and plentiful resource reserves, and the potential to be considered one of the

best promising options to replace traditional fossil fuels [1–6]. The sources of hydrogen are diverse, and production processes can be classified into three categories: green hydrogen, blue hydrogen, and gray hydrogen, among others. Green hydrogen is obtained using electrochemical water splitting technology, which is environmentally friendly and effectively reduces the use of fossil fuels [7–9]. Consequently, green hydrogen has become a subject of considerable research interest.

Electrochemical water splitting comprises of two half-reactions: the cathodic hydrogen evolution reaction (HER) and the anodic OER. The four-electron transfer process ($4\text{OH}^- \rightarrow \text{H}_2\text{O} + \text{O}_2 + 4\text{e}^-$) of OER at the anode is considered the rate-limiting step for water splitting, exhibiting sluggish kinetics and necessitating a theoretical voltage equal to 1.23 V [10–13]. In recent decades, researchers have developed electrolyzers based on alkaline freshwater as the key source for water splitting. However, the limited availability of freshwater resources represents a significant challenge for the advancement of electrolyzer technology, particularly in light of the increasing global population and the associated demands of modern living standards. In comparison to the restricted availability of freshwater, seawater, which constitutes approximately 97% of the world's total water supply, can be regarded as an inexhaustible source. It is recommended that seawater splitting be considered as a more viable and sustainable option to freshwater electrolysis for hydrogen generation [14–17].

The industrial production of high-purity hydrogen from direct or selective electrolytic splitting of seawater remains a major challenge, despite the abundant availability of seawater on our planet. The presence of aggressive chloride anions (Cl^-), as well as other unfavorable ions including Ca^{2+} , Mg^{2+} , Na^+ , Br^- , and SO_4^{2-} , and a diverse range of bacteria, suspended solid microparticles, and other impurities, can cause the surface of electrocatalysts to become inactive and poisoned, ultimately leading to their deactivation and poisoning [18–20]. The CER that occurs at the anode represents the most critical encounter in the seawater electrolysis process. This reaction competes with the OER and forms aggressive substances: chloride products (e.g., HClO , Cl_2 , or ClO^-), which have the potential to degrade the electrolyte environment and result in low anode current efficiency. Moreover, the Pourbaix diagram indicates that OER is thermodynamically more favorable than CER across the whole pH region, with a constant potential difference of up to 480 mV remaining in the high pH region. Therefore, in an alkaline medium ($\text{pH} > 7.5$), electrocatalytic materials with an overpotential of less than 480 mV would be effective for splitting seawater without the occurrence of side-reactions caused by chloride ions [15,20–23]. Additionally, the disadvantage of high pH is the production of insoluble precipitates (e.g., $\text{Ca}(\text{OH})_2$ and $\text{Mg}(\text{OH})_2$), which lead to the poisoning of the catalytic sites in the natural seawater system.

Nevertheless, the high costs of green hydrogen energy remain a substantial obstacle to its widespread adoption, largely due to the inherent costs associated with the hydrogen production pathway. One of the principal factors contributing to this elevated cost is the electrocatalysts employed as electrodes in the water electrolyzers. The most advanced platinum group metal (PGM) catalysts demonstrate outstanding electrocatalytic activity for water splitting, while Pt-based catalysts are the leading electrocatalysts for HER. Ru- or Ir-based oxides exhibit the most efficient performances for OER [24–28]. However, the high costs and limited availability of precious PGM catalysts present significant obstacles to their large-scale commercial deployment. It is therefore anticipated that research into earth-abundant, inexpensive, highly efficient and durable electrocatalytic materials with the potential to reduce the energy barriers to hydrogen/oxygen evolution in HER/OER processes will be of significant interest.

In order to overcome the large overpotential associated with seawater splitting in OER, researchers have directed considerable attention toward cost-effective and earth-abundant transition metal-based electrocatalysts, which have emerged as promising options because of their active structural sites and near-optimal activity. Over the past decade, low-cost transition metals (TMs), including nickel-based [29–32], iron-based [33–37], and cobalt-based [38–42] sulfides [43–46], phosphides [47–50], nitrides [51–54], alloys [55,56], and

bimetallic LDHs [57–59], have emerged as alternative potential candidates for OER in alkaline freshwater/seawater and overall simulated/alkaline seawater splitting as replacements for precious metal catalysts. In order to identify the most catalytically efficient materials, two key properties must be considered: (i) the intrinsic activity of the substance, which directly regulates the chemical nature of the electrodes, and (ii) the active surface area of the catalysts. From among the early group of VIII B TMs, scientists have turned their attention to Ni-based electrodes due to the enhanced water splitting performance achieved through the formation of heterostructure hybrids and nanostructured composites, etc. with Fe, Co, and Mo [60–65]. In this context, another TM, namely Mn, has received increasing attention in recent years due to its optimal electronic configuration and higher M–H* bond strength [66,67]. Furthermore, Mn is capable of forming complexes with other metals by the splitting of the d-orbital, resulting in the creation of an electron-deficient eg-orbital. This change in the electronic level of the catalyst facilitates the exposure of additional active sites and enhances catalytic interactions [68]. Furthermore, Mn is recognized for its ability to reduce the overpotential in HER and OER electrolytic reactions, which makes it a highly promising candidate for the preparation of transition metal-based catalysts [69–73]. A recent published study by Priamushko et al. demonstrated that bimetallic oxides tailored by Mn exhibited enhanced OER kinetics due to increased active sites, catalyst stability, and current density [74]. Zhang et al. [75] showed that the incorporation of Mn as a dopant effectively enhanced the inherent activity and stability of Co–P nanosheets. Guo et al. reported a bimetallic MnCo–P/NF electrocatalyst [76] that exhibited excellent hydrogen catalytic activity, requiring an overpotential of 112 mV to achieve a higher current density of 100 mA cm^{−2} together with strong mechanical stability. A series of Mn-induced bimetallic and multicomponent alloy electrocatalysts have also been investigated for their potential in water electrolysis and other electrochemical reactions. These studies have demonstrated excellent catalytic activity, stability, selectivity, and protective properties against corrosion in seawater splitting [77–81].

In our previous publication, we demonstrated that those facile electrodeposited 3D NiMn coatings have superior bifunctional activity and long-term durability for HER and OER towards alkaline water electrolysis [82]. However, in the search for TM-based promising electrodes for a sustainable alternative to scarce freshwater, it was resolved to further investigate these low-cost catalysts to investigate their electrocatalytic performances and long-time durability for OER in alkaline natural seawater (ASW) and simulated seawater (SSW). To the extent of our knowledge, no publication has yet been reported on the catalytic activities of bimetallic Ni–Mn alloys as OER electrocatalysts for seawater splitting. However, in recent times, only a few publications have highlighted the applications of NiMn–LDH materials for overall alkaline freshwater/seawater electrolysis [57,83–85].

2. Materials and Methods

2.1. Chemicals

Titanium foil with a thickness of 0.127 mm thick and 99.7% purity (Sigma–Aldrich (Saint Louis, MO, USA)), stainless steel foil with a thickness of 0.2 mm (Type 304, Alfa Aesar (Karlsruhe, Germany) GmbH & Co.), nickel sulfate hexahydrate (NiSO₄·6H₂O, >98%, Chempur Company (Karlsruhe, Germany)), manganese chloride tetrahydrate (MnCl₂·4H₂O, >99%, Chempur Company (Karlsruhe, Germany)), boric acid (H₃BO₃, >99.5%, Chempur Company (Karlsruhe, Germany)), KOH (98.8%, Chempur Company (Karlsruhe, Germany)), ammonium sulfate ((NH₄)₂SO₄, >99%, Chempur Company (Karlsruhe, Germany)), H₂SO₄ (96%, Chempur Company (Karlsruhe, Germany)), and HCl (35–38%, Chempur Company (Karlsruhe, Germany)) were of analytical grade and were employed directly without any additional purification. All solutions were prepared using ultrapure water (18.2 MΩ·cm). The seawater was taken from the Baltic Sea in the Klaipėda coastal region of Lithuania.

2.2. Fabrication of Catalysts

The electrodes were fabricated via a one-step procedure as reported in our previous research [82]. In brief, the Ti sheets in the size of $1 \times 1 \text{ cm}^2$ were pretreated in dilute H_2SO_4 (1:1 vol.) at 70°C to activate and remove any possible oxides/hydroxides present on the surface. Following this, the sheets were rinsed with distilled water and subsequently immersed in the plating bath, which comprised 0.2 M NiSO_4 and 0.2 to 0.6 M MnCl_2 serving as the source of Ni^{2+} and Mn^{2+} ions, respectively. Then, 0.5 M $(\text{NH}_4)_2\text{SO}_4$ was used as a coating morphology modifier, while 0.3 M H_3BO_3 was employed as a pH stabilizer. All reagents were dissolved in ultrapure water under acid conditions, specifically 1 M HCl and 1.5 M H_2SO_4 . The composition and electroplating conditions of the plating baths used to prepare the electrodes are detailed in Table 1. After coating, the NiMn/Ti electrocatalysts were carefully washed with deionized water, dried in air at ambient temperature, and stored for future studies.

Table 1. The plating bath composition, along with the associated parameters of the plating condition.

Catalyst	Concentration (M)				Plating Conditions			
	NiSO_4	MnCl_2	$(\text{NH}_4)_2\text{SO}_4$	H_3BO_3	pH *	T ($^\circ\text{C}$)	j (mA cm^{-2})	t (min)
NiMn/Ti-1	0.2	0.2	0.5	0.3	~1	25	50	3
NiMn/Ti-2	0.2	0.4	0.5	0.3			500	3
NiMn/Ti-3	0.2	0.6	0.5	0.3				

* 1.5 M H_2SO_4 + 1 M HCl.

2.3. Characterization of Catalysts

An investigation into the composition and morphology of the fabricated NiMn/Ti catalysts was carried out using a TM4000Plus scanning electron microscope with an AZetecOne detector (Hitachi, Tokyo, Japan).

The loadings of Ni and Mn were identified using an Optima 7000DV inductively coupled plasma optical emission spectrometer (Perkin Elmer, Waltham, MA, USA). ICP–OES spectra were collected at λ_{Ni} 231.604 nm and λ_{Mn} 257.610 nm.

X-ray diffraction patterns were acquired using a D2 Phaser X-ray diffractometer with $\text{CuK}\alpha$ radiation (Bruker AXS, Karlsruhe, Germany). A step scan mode was used in the 2 θ from 10° to 90° . The step length was 0.04° and the count time was 1 s per step.

2.4. Electrochemical Measurements

The performances of the prepared NiMn catalysts were assessed through linear sweep voltammetry (LSV), employing a PGSTAT302 potentiostat (Metrohm Autolab B.V., Utrecht, The Netherlands). The LSVs were recorded in two different types of simulated seawater, namely Ar-deaerated simulated seawater (0.5 M NaCl + 1 M KOH) and alkaline seawater (natural seawater + 1 M KOH), at a range of temperatures from 25 to 75°C . A thermostatted electrochemical cell was utilized to evaluate the catalytic performance. The prepared NiMn/Ti catalysts (a geometric area of 2 cm^2) served as the working electrode, while a Pt sheet and a saturated calomel electrode (SCE) acted as the counter and the reference electrodes, respectively. If not indicated otherwise, all potential values were recalculated to the reversible hydrogen electrode (RHE) scale according to the following equation: $E_{\text{RHE}} = E_{\text{SCE}} + 0.242 \text{ V} + 0.059 \text{ V} \times \text{pH}_{\text{solution}}$.

The OER LSVs were obtained in the two operating electrolytes by scanning the electrode potential from the open circuit potential (OCP) to 2.06 V (vs. RHE) at 10 mV s^{-1} . Furthermore, the long-time durability of the prepared NiMn/Ti-1 catalyst was assessed through the collecting of the chronopotentiometric curves (CP) at a constant current density of 10 mA cm^{-2} . The chronoamperometric curves (CA) were collected at a constant potential of 1.81 V (vs. RHE) for 24 h in ASW and SSW. Moreover, the two-electrode seawater electrolyzer was assembled by employing the as-prepared optimal NiMn/Ti-1 electrocatalyst

as the anode and our previously reported efficient NiMn/Ti-5 HER electrocatalyst [82] as the cathode.

The electrochemically active surface area (ECSA) of the catalysts was determined using double layer capacitance (C_{dl}) measurements. CV curves were collected at varying scan rates within the non-faradaic region. Thereafter, the charging current, I_c , of the catalysts at each scan rate was calculated using the following Equation (1):

$$I_c [\text{mA}] = (I_{\text{anodic}} - I_{\text{cathodic}})_{\text{OCP}} \quad (1)$$

Then, the difference in anodic and cathodic current against the scan rate was plotted and the slope of the curve, which corresponds to the C_{dl} , was calculated [86–88] as demonstrated by Equation (2):

$$\text{Slope} = C_{dl} [\text{mF}] = \Delta I_c [\text{mA}] / \Delta v [\text{V s}^{-1}] \quad (2)$$

For the calculation of the ECSA values, the specific capacitance (C_s) of 0.040 mF cm^{-2} [86–88] was used in Equation (3):

$$\text{ECSA} [\text{cm}^2] = C_{dl} [\text{mF}] / C_s [\text{mF cm}^{-2}] \quad (3)$$

The roughness factor (R_f) for the catalysts was determined by the following Equation (4):

$$R_f = \text{ECSA} / S_{\text{geometric}} \quad (4)$$

3. Results and Discussion

3.1. Morphology and Microstructure Studies

Schematic fabrication of 3D NiMn/Ti catalysts via a straightforward one step electroplating approach is demonstrated in Figure 1a.

The surface morphology and structure of the NiMn/Ti-1, NiMn/Ti-2 and NiMn/Ti-3 catalysts was examined using scanning electron microscopy (SEM) as demonstrated in Figure 1b–d. The SEM micrograph demonstrated that the synthesized NiMn coating on the Ti, which was electrodeposited from an aqueous operating bath containing a molar ratio of 1:1 $\text{Ni}^{2+}:\text{Mn}^{2+}$ (denoted as NiMn/Ti-1), exhibited a typical globular morphology comprised of smaller nodules that grew with a uniform distribution, covering the Ti substrate (Figure 1b). The concentration of Mn^{2+} in the plating bath was found to be a determining factor in the size of the resulting nodules. As the $\text{Ni}^{2+}:\text{Mn}^{2+}$ ratio increased from 1:1 to 1:2, the nodules exhibited a notable enlargement in size (Figure 1c). As the concentration of Ni^{2+} remained constant (0.2 M) in all plating bath compositions, the as-synthesized NiMn/Ti-3 electrocatalyst formed an uneven, coarse, flake-like heterostructured surface as a result of a higher $\text{Ni}^{2+}:\text{Mn}^{2+}$ ratio of 1:3 in the plating bath and relatively higher cell voltage during electrodeposition, as depicted in Figure 1d.

The metal loadings deposited on the Ti surface were determined by ICP–OES analysis, the results of which are presented in Table 2. The catalysts were fabricated from different plating baths with varying molar ratios of Ni:Mn, resulting in variable Ni-loadings of ca. 72–86 wt% in the prepared catalysts, while the content of deposited Mn varied from ca. 13–28 wt%. It was vividly observed that the overall metal loadings increased significantly with higher concentration of Mn^{2+} in the plating bath, with a sum varying from ca. 100 up to $375 \mu\text{g}_{\text{metal}}\text{cm}^{-2}$.

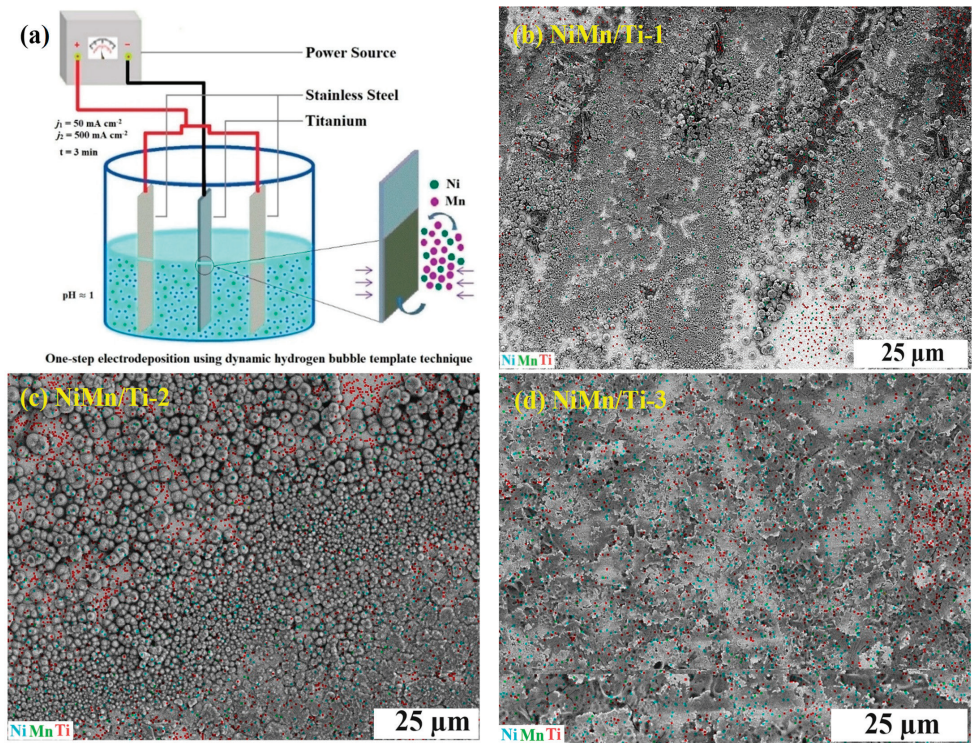


Figure 1. Illustration of the fabrication approach of NiMn/Ti catalysts (a) and the SEM mapping images of NiMn/Ti-1 (b), NiMn/Ti-2 (c), and NiMn/Ti-3 (d) catalysts.

Table 2. Metal loadings of various catalysts analyzed by ICP-OES.

Catalyst	Ni Loadings ($\mu\text{g}_{\text{Ni}}\text{cm}^{-2}$)	Mn Loadings ($\mu\text{g}_{\text{Mn}}\text{cm}^{-2}$)	Total Metal Loading ($\mu\text{g}_{\text{metal}}\text{cm}^{-2}$)	Wt%	
				Ni	Mn
NiMn/Ti-1	86.55	13.43	99.98	86.56	13.44
NiMn/Ti-2	126.4	40.55	166.95	75.71	24.29
NiMn/Ti-3	269.7	105.25	374.95	71.93	28.07

Figure 2 illustrates the XRD pattern of the NiMn catalyst deposited on the Ti surface. It can be seen that the major peaks align closely with the data provided for Ti according to COD No. 9016190. The most abundant phase, as determined by the XRD peak intensities, was hexagonal Ti, with diffraction peaks at 2θ approximately 35.0° , 38.4° , 40.1° , 53.0° , 62.9° , 76.2° , 77.3° and 82.3° , in good agreement with the phase of Ti (COD No. 9016190, $a = 2.95 \text{ \AA}$, $c = 4.68 \text{ \AA}$, space group $P 6_3/m m c$), which correspond to the lattice planes of (100), (002), (101), (102), (110), (112), (201), and (004), respectively.

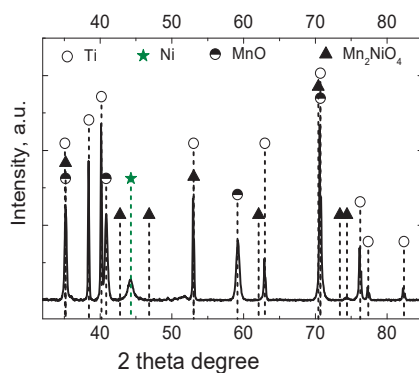


Figure 2. XRD patterns of NiMn/Ti-1. The symbols show the positions of the XRD peaks of Ti (COD No. 9016190), Ni (COD No. 2102269), MnO (COD No. 1010898), and Mn_2NiO_4 (COD No. 1530384).

Moreover, the pattern also displayed peaks corresponding to the phases of Ni, MnO, and Mn_2NiO_4 . The Ni peak was detected at 2θ approximately 44.3° , which is indexed to the (111) crystal plane (COD No. 2102269, $a = 3.5382 \text{ \AA}$, space group Fm-3m), while the MnO peaks were observed at 2θ approximately 35.1° , 40.8° , 59.1° , and 70.7° , indexed to the (111), (200), (220), and (311) crystal planes, respectively (COD No. 1010898, $a = 4.415 \text{ \AA}$, space group Fm-3m). The peak located at 35.2° may be assigned with the cubic phase of Mn_2NiO_4 (COD No. 1530384, $a = 8.45 \text{ \AA}$, space group Fd-3m), which correlates with the lattice plane of (311). It may be surmised that the NiMn catalyst exhibited a Ni phase with some MnO and Mn_2NiO_4 . Meanwhile, the Mn_2NiO_4 phase, which has a typical spinel structure, may prove to be a beneficial structure in enhancing the electrocatalytic activity of the prepared NiMn catalyst.

3.2. Electrocatalytic Activity for OER in SSW

To assess the OER performance of the prepared electrocatalysts, LSVs were obtained in an Ar-deaerated SSW solution of 0.5 M NaCl + 1.0 M KOH (resulting pH of 14) at $10 \text{ mV}\cdot\text{s}^{-1}$ from OCP up to 2.06 V, at a temperature range of 25 up to 75°C (Figure 3a). To ascertain the reproducibility, three electrodes were prepared and the LSVs were accounted for each electrode. As can be seen from the data presented in Figure 3a, ca. 1.57–1.72 times higher current density was attained on the investigated catalysts with an increase in temperature from 25 up to 75°C . Figure 3b shows the LSVs for all NiMn catalysts collected at a temperature of 25°C . It can be observed that the catalytic activity of the catalysts was significantly influenced by the varying molar ratio of $\text{Ni}^{2+}:\text{Mn}^{2+}$. Figure 3c shows the extracted Tafel plots for the aforementioned catalysts, while Figure 3d presents a summary of the overpotential values needed to reach the benchmark current density. Moreover, the slope of the Tafel is a pivotal parameter in the field of electrochemical kinetics and is used to reflect the rate-limiting step of a given reaction. With regard to the OER, the slope of the Tafel offers an insight into the underlying mechanism of the reaction and the kinetics of the steps involved.

Figure 3c shows that the Tafel slope values were 130, 120, and 86 mV dec^{-1} for the fabricated NiMn/Ti-1, NiMn/Ti-2 and NiMn/Ti-3 electrocatalysts, respectively. As depicted in Figure 3d, NiMn/Ti-1 requires overpotentials of 386, 423, and 509 mV to attain current densities of 10, 20 and 50 mA cm^{-2} , respectively, in SSW. These values are superior to those of NiMn/Ti-2 ($\eta_{10} = 413 \text{ mV}$, $\eta_{20} = 457 \text{ mV}$, and $\eta_{50} = 557 \text{ mV}$) and NiMn/Ti-3 ($\eta_{10} = 454 \text{ mV}$, $\eta_{20} = 497 \text{ mV}$, and $\eta_{50} = 603 \text{ mV}$). Table 3 summarizes the OER activity of the synthesized catalysts in SSW.

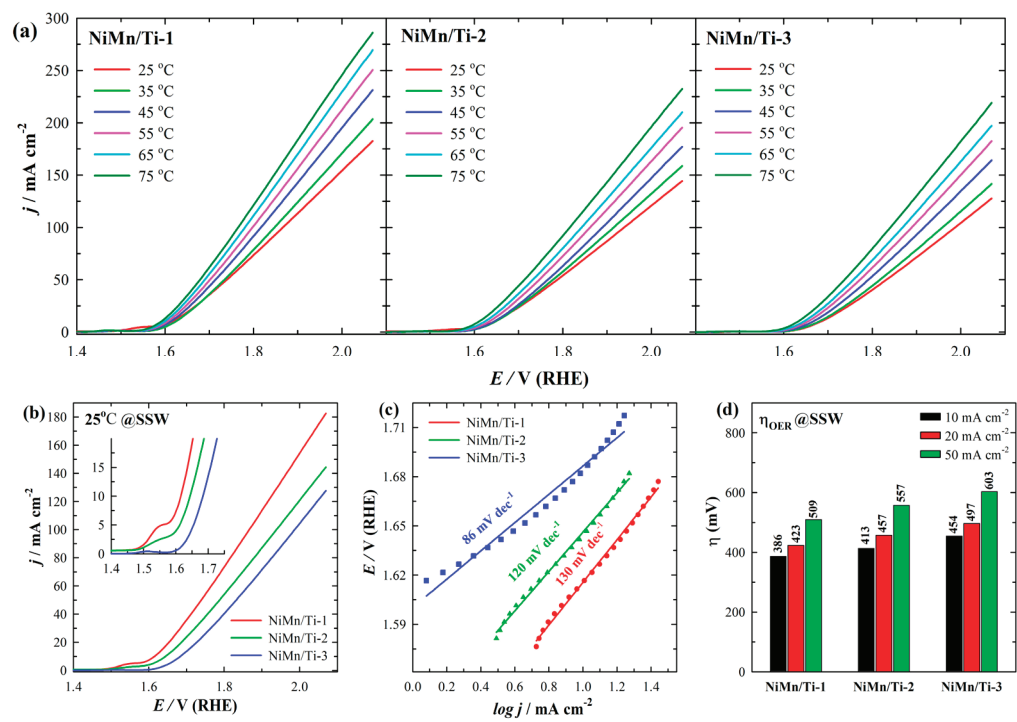


Figure 3. The OER polarization curves recorded on NiMn/Ti catalysts in SSW at 10 mV s^{−1} and a temperature range from 25 to 75 °C (a), LSVs obtained at 25 °C (b), the corresponding Tafel plots (c), and the overpotential values needed to achieve 10, 20, and 50 mA cm^{−2} current densities (d).

Table 3. Summary of electrochemical data of the catalysts under investigation for OER in SSW.

Catalysts	<i>j</i> at 2.06 V (mA cm ^{−2})						η_{10} at 25 °C (mV)	Tafel Slope (mV dec ^{−1})
	25 °C	35 °C	45 °C	55 °C	65 °C	75 °C		
NiMn/Ti-1	182.57	203.48	231.38	250.69	269.53	286.1	386	130
NiMn/Ti-2	144.36	158.77	177.15	195.43	210.07	232.39	413	120
NiMn/Ti-3	127.68	141.57	164.31	182.45	197.2	219.21	454	86

3.3. Electrocatalytic Performance for OER in ASW

Compared to fresh water, the availability of seawater could be the most sustainable resource for the implementation of electrocatalytic water electrolysis technology. However, natural seawater includes a large number of metal ions and radicals (e.g., Mg²⁺, Ca²⁺, Br[−], SO₄^{2−}, etc.), microbes, and solid particles that have the potential to precipitate during electrolysis and accumulate on the catalyst and electrode surface resulting in significant catalytic inefficiency. To explore the potential use of seawater, the seawater (pH ≈ 8.2) used in this study was taken from the Baltic Sea near the Klaipėda coastal region in Lithuania. To prepare the ASW, 1.0 M of KOH pellets were dissolved in the seawater. The precipitate, a white cloudy layer of insoluble metal hydroxides, was allowed to settle overnight and was then filtered from the solution. The clear filtrate was collected by decantation and filtration and was designated as ASW with a pH of ≈13.85.

The OER of the fabricated catalysts was evaluated by recording LSVs in an Ar-deaerated ASW electrolyte from OCP up to 2.06 V at 10 mV s^{-1} with temperatures ranging from 25 to 75 °C. Figure 4a displays the LSVs, which exhibited a significant enhancement in current density, reaching values between 1.65 and 1.75 times higher at elevated temperatures (25 up to 75 °C).

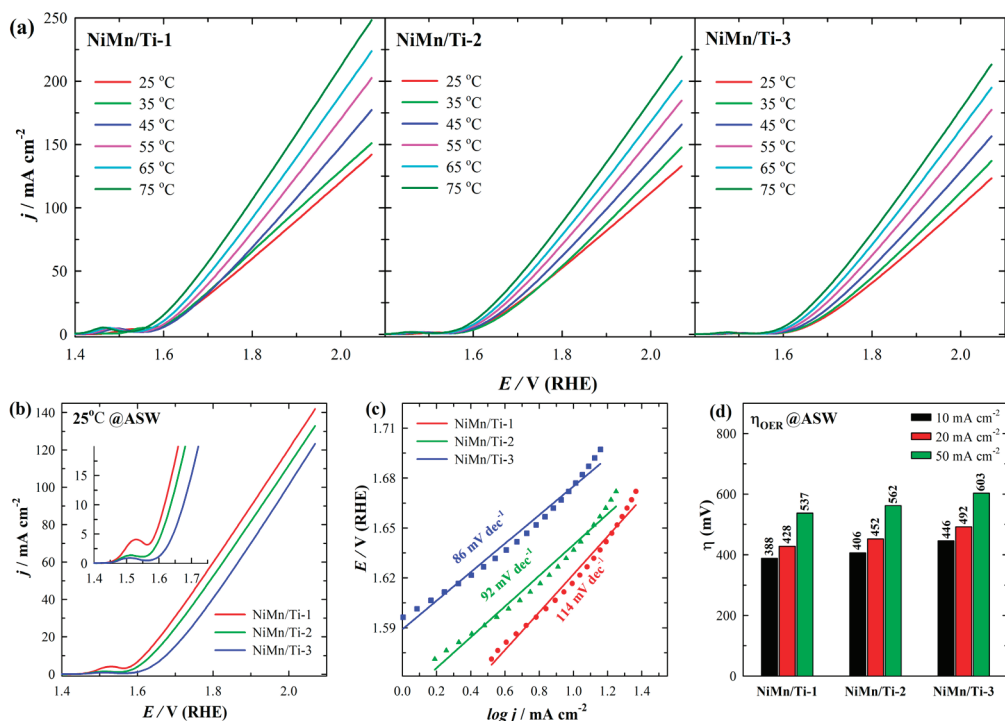


Figure 4. The OER LSVs recorded on NiMn/Ti catalysts in ASW at 10 mV s^{-1} and a temperature range of 25 to 75 °C (a), LSVs recorded at 25 °C (b), the corresponding Tafel plots (c), and the overpotential values needed to reach 10, 20, and 50 mA cm^{-2} current densities (d).

As illustrated in Figure 4b, the activity for OER of the prepared catalysts by varying the molar ratio of Ni to Mn exhibited a gradual decline in current density with increasing Mn concentrations. The anodic peak corresponding to the surface oxidation of Ni^{2+} to Ni^{3+} was found at approximately 1.55 V, indicating the creation of active sites for OER that enhanced the electrochemical process. This observation is in accordance with the findings of Luo et al., who demonstrated that the OER performance was significantly influenced by the Ni to Mn content ratios in the fabricated $\text{Ni}_x\text{Mn}_{1-x}\text{O}/\text{CNTs}$ electrocatalysts. It was reported that when the Mn content exceeded 17%, the overpotentials of the catalysts increased, indicating that a reduction in the Mn content resulted in a notable enhancement in OER activity [89]. However, the recorded current densities of the electrodes in ASW were also markedly lower than those observed in SSW. It is anticipated that the catalytic efficiency of the synthesized electrocatalysts in ASW will be appropriately decreased due to the existence of interfering ions and impurities in seawater. Subsequently, the OER LSV curves at 25 °C were employed to construct the Tafel plots and calculate the Tafel slopes. The values of the Tafel slope were determined to be 114, 92, and 86 mV dec^{-1} for the fabricated NiMn/Ti-1, NiMn/Ti-2 and NiMn/Ti-3 catalysts, respectively (Figure 4c and Table 4).

Table 4. Summary of electrochemical data of the catalysts under investigation for OER in ASW.

Catalysts	<i>j</i> at 2.06 V(mA cm ^{−2})						η_{10} at 25 °C(mV)	Tafel Slope (mV dec ^{−1})
	25 °C	35 °C	45 °C	55 °C	65 °C	75 °C		
NiMn/Ti-1	141.97	151.05	177.2	202.47	223.75	248.18	388	114
NiMn/Ti-2	132.92	147.65	165.8	184.67	200.39	219.45	406	92
NiMn/Ti-3	123.3	136.9	156.51	177.4	195	213.23	446	86

Furthermore, Figure 4d and Table 4 illustrate the overpotentials required to attain current densities of 10, 20, and 50 mA cm^{−2} at 25 °C. Notably, the NiMn/Ti-1 electrocatalyst exhibits relatively low overpotentials of 388, 428, and 537 mV, respectively, to drive current densities of 10, 20, and 50 mA cm^{−2} in the alkaline natural seawater. These values are superior to those of the NiMn/Ti-2 (η_{10} = 406 mV, η_{20} = 452 mV, and η_{50} = 562 mV) and NiMn/Ti-3 (η_{10} = 446 mV, η_{20} = 492 mV, and η_{50} = 603 mV) electrocatalysts.

The abovementioned data suggest that the as-synthesized NiMn bimetallic electrocatalyst, especially NiMn/Ti-1, exhibits promising OER performance, comparable to that of recent non-precious metal-based OER catalysts in alkaline media and simulated/alkaline seawater (Table 5).

Table 5. Comparison of the performances of OER electrocatalysts in neutral and simulated/alkaline seawater electrolytes reported in the literature.

Catalysts	η_{10} (mV)	Tafel Slope (mV dec ^{−1})	Electrolytes	Ref.
NiMn/Ti-1	386	130	1 M KOH + 0.5 M NaCl	This work
	388	114	1 M KOH + Seawater	
Co-CoO@C (denoted as ZIF67-600Ar/GF)	374	–	1 M KOH + Seawater	[90]
oct_Cu ₂ O-NF	354	90	1 M KOH + 0.5 M NaCl	[91]
CoSe/MoSe ₂ /NF	350	–	1 M KOH + Seawater	[92]
FTO/NiO	340	-	1 M KOH + 0.5 M NaCl	[93]
CoFe-LDH	530	–	Simulated seawater (pH 8.0)	[94]
Pb ₂ Ru ₂ O _{7−x}	500	~48	Natural simulated seawater (only 0.6 M NaCl)	[95]
Co ₃ O ₄	440	–	1 M PBS + 0.5 M NaCl	[96]
Co _{3−x} Pd _x O ₄	370			
CaFeO _x FePO ₄	~710	–	Phosphate-buffered (0.5 M, pH 7) seawater	[97]
Co(OH) ₃ Cl	379	–	1 M KOH + 0.6 M NaCl	[98]
ER-RP/P-SNCF-5	332	–	1 M KOH + 0.5 M NaCl	[99]
	346		1 M KOH + Seawater	

Furthermore, the ECSA of the NiMn/Ti-1 electrocatalyst was determined from the measurements of double layer capacitance (*C_{dl}*) by recording CV curves in the 1 M KOH solution at various scan rates (5–50 mVs^{−1}) in the non-faradaic region (Figure 5a).

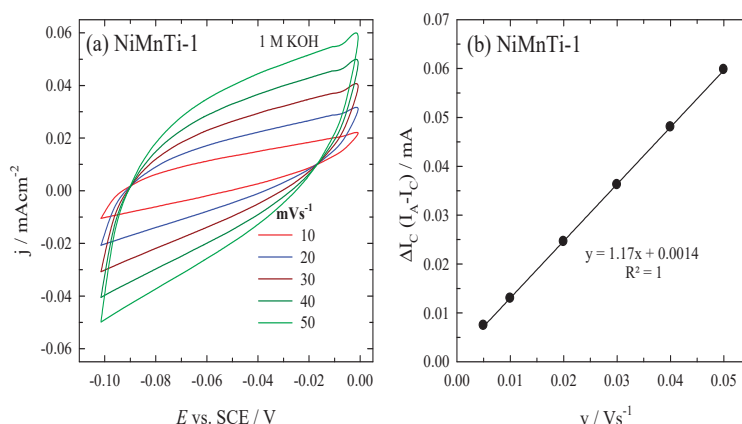


Figure 5. (a) CVs of NiMnTi-1 collected in N₂-deaerated 1 M KOH solution at varied scan rates. (b) Dependence of charging current on scan rate.

The plot of the charging current against the scan rate is depicted in Figure 5b. The C_{dl} for NiMnTi-1 was determined to be 1.17 mF, which yielded an estimated ECSA value of 29.25 cm². The roughness factor R_f for the NiMnTi-1 electrocatalyst is approximately 15, which indicates a high level of catalyst activity. Moreover, the R_f value obtained indicates that the actual surface area of the catalyst is 15 times higher than its geometric surface area. This increased surface area furnishes a larger number of active sites for the OER. As there are more sites where OER can occur simultaneously, an increased number of active sites can facilitate higher reaction rates. This can result in a higher current density for a given potential. Furthermore, with a larger number of active sites, the catalyst can operate with greater efficiency, potentially reducing the overpotential required for the OER to occur. This makes the process more energy efficient.

3.4. Electrocatalytic Stability Investigations for OER

An additional crucial factor to consider is the electrocatalytic stability of a catalyst, as this determines its practical utility and applicability. In the case of seawater splitting OER electrocatalysts, it is essential that the electrocatalytic activity is sustainable, given the presence of abundant corrosive Cl⁻ ions and competitive CER. Accordingly, the stability evaluation of the NiMn/Ti-1 catalyst was assessed by long-time operation assessments in both ASW and SSW electrolytes. This was conducted using the CP method at a fixed current density of 10 mA cm⁻² and the CA at a constant potential of 1.81 V at 25 °C for 24 h. The findings showed that the NiMn/Ti-1 electrocatalyst possesses superior long-lasting electrocatalytic stability in both investigating electrolytes.

Figure 6a demonstrates the electrocatalytic stability of the NiMn/Ti-1 catalyst by chronopotentiometric analysis at a constant current density of 10 mA cm⁻² for 24 h. After one hour of operation in both working electrolytes, the recorded potential remained almost constant throughout the progression of the OER process, exhibiting a marginal increase of only 34 mV in SSW and 40 mV in ASW. The remarkable stability of the synthesized NiMn/Ti-1 catalyst ensures enhanced structural integrity and significant chloride ion-resistivity, thereby conferring anti-corrosion properties that are beneficial for electrolysis of seawater.

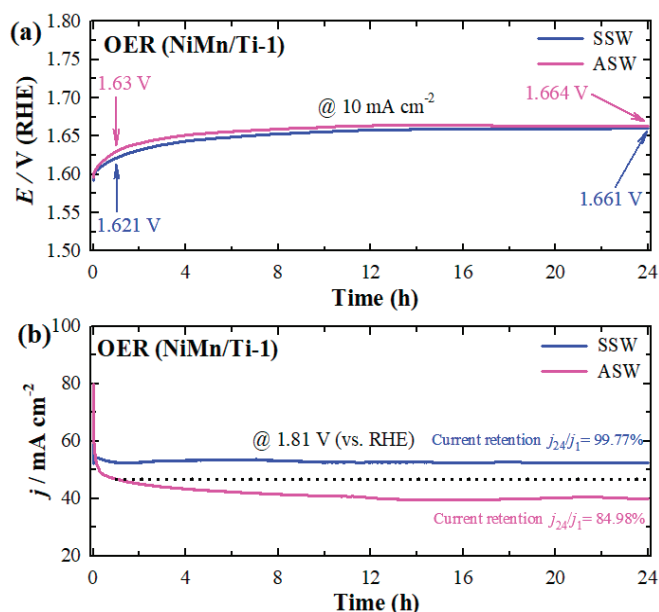


Figure 6. The chronopotentiometric (a) and chronoamperometric (b) curves of NiMn/Ti-1 in simulated seawater and alkaline natural seawater at a static current density of 10 mA cm^{-2} and a constant potential of 1.81 V for 24 h, respectively.

Furthermore, the catalytic stability of the as-synthesized NiMn/Ti-1 catalyst was also determined by the chronoamperometry at a constant potential of 1.81 V in SSW and ASW. As illustrated in Figure 6b, the NiMn/Ti-1 electrode exhibited an excellent current retention of ca. 100% in SSW, while displaying a relatively modest deviation in current density in ASW. Following a 24-h period of continuous OER electrolysis, a decline of approximately 15% in current density was monitored in comparison to the initial reading of the current density after one hour. The intrinsically stable electrochemical properties of the materials ensure the sustained performance of the OER after the completion of the stability tests. A higher roughness factor can contribute to the enhanced stability of the electrode by distributing stresses more evenly, enhancing the adherence of catalytic layers, and potentially aiding in the management of gas bubbles.

3.5. Performance of Overall Alkaline Seawater Splitting

In addition to exhibiting reasonable OER efficiency and outstanding long-time durability in both SSW and ASW, we conclude that the NiMn/Ti-1 electrocatalyst can be used as an effective and durable OER catalyst for OWS in seawater. Therefore, the optimal NiMn/Ti-1 electrocatalyst should be further investigated as an anode material for OWS in alkaline natural seawater solution. For the overall seawater-splitting performance, a two-electrode system was used, as illustrated schematically in Figure 7a. An electrolytic cell containing natural seawater and 1.0 M KOH was assembled with a synthesized NiMn/Ti-1 electrode together with our previously reported efficient NiMn/Ti-5 HER electrocatalyst [100] as the anode and cathode, respectively (Figure 7b). For comparison purposes, a two-electrode seawater electrolyzer was constructed using a fabricated NiMn/Ti-1 electrode and a Pt sheet ($\sim 2 \text{ cm}^2$) as the anode and cathode, respectively. It is noteworthy that the electrolyzer assembly, comprising the NiMn/Ti-5₍₋₎ || NiMn/Ti-1₍₊₎ catalysts, required a cell voltage of only 1.619 V to operate at a current density of 10 mA cm^{-2} at 25 °C. This voltage was 0.075 V

lower than that required by the electrolyzer employing Pt as the cathode: Pt₍₋₎ || NiMn/Ti-1₍₊₎ (Figure 7c). It is evident that the cell voltage of the NiMn/Ti-5₍₋₎ || NiMn/Ti-1₍₊₎ seawater electrolyzer is competitive with other recently reported non-precious metal-based materials for OWS performance in SSW/ASW, as illustrated in Figure 7d. The long-time stability of the electrolyzer NiMn/Ti-5₍₋₎ || NiMn/Ti-1₍₊₎ was also investigated in ASW. It was observed that the recorded potential remained relatively stable for the duration of the 10-h testing period (Figure 7e).

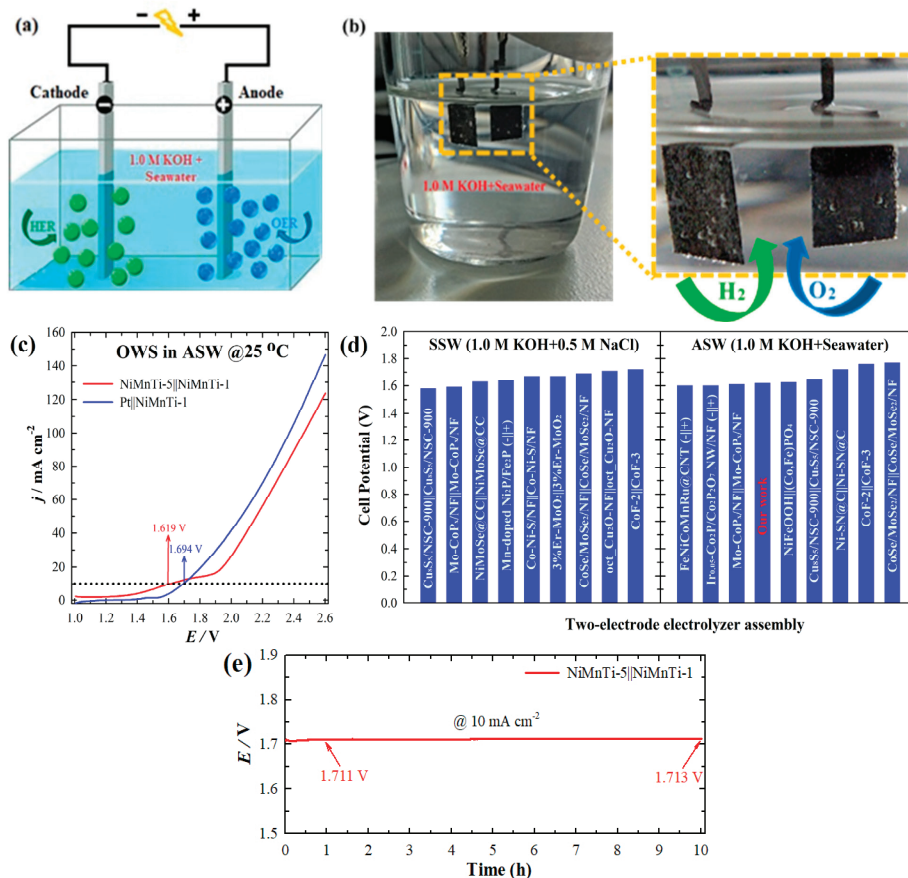


Figure 7. A schematic representation of the overall alkaline seawater splitting (a), a digital photograph of the assembled two-electrode NiMn/Ti-5₍₋₎ | NiMn/Ti-1₍₊₎ cell (left) and the bubbles on the electrodes (right) (b). LSVs for the overall alkaline seawater splitting at 25 °C (c). A comparison of activity of the assembled electrolyzer with that of recently reported catalysts (d) and a long-time durability test of the assembled NiMn/Ti-5₍₋₎ | NiMn/Ti-1₍₊₎ electrolyzer (e) for the overall alkaline natural seawater splitting.

A comparative analysis of the overall seawater splitting performance using the two-electrode seawater electrolyzer reported here shows that the composition of the synthesized bimetallic electrolyzer assembly as anode and cathode has great potential for the technology of seawater splitting (Table 6).

Table 6. Comparison of the performance of the two-electrode seawater electrolyzers assembled with the non-precious metal electrodes reported in the literature for SSW/ASW and natural seawater.

Electrodes (− +)	Potential@Current Density (V@mA cm ^{−2})	Electrolyte	Ref.
NiMn/Ti-5 NiMn/Ti-1 Pt NiMnTi-1	1.619@10 1.694@10	1 M KOH + Seawater	This work
FeNiCoMnRu@CNT (− +)	1.6@10	1 M KOH + Seawater	[56]
Pt/C/GF ZIF67-600Ar/GF	1.63@20	1 M KOH + Seawater	[90]
oct_Cu ₂ O-NF oct_Cu ₂ O-NF	1.71@10	1 M KOH + 0.5 M NaCl	[91]
CoSe/MoSe ₂ /NF CoSe/MoSe ₂ /NF	1.69@10 1.77@10	1 M KOH + 0.5 M NaCl 1 M KOH + Seawater	[92]
NiMoSe@CC NiMoSe@CC	1.63@10	1 M KOH + 0.5 M NaCl	[101]
3%Er-MoO ₂ 3%Er-MoO ₂	1.67@10	1.0 M KOH + 3.5% NaCl	[102]
Ir _{0.05} -Co ₂ P/Co ₂ P ₂ O ₇ NW/NF (− +)	1.6@10 1.67@10	1 M KOH + Seawater Seawater	[103]
CdFe-BDC CdFe-BDC	1.68@10	Seawater	[104]
Co-Ni-S/NF Co-Ni-S/NF	1.67@10	1 M KOH + 0.5 M NaCl	[105]
NiFeOOH (Co,Fe)PO ₄	1.625@10	1 M KOH + Seawater	[106]
Cu ₈ S ₅ /NSC-900 Cu ₈ S ₅ /NSC-900	1.58@10 1.65@10	1 M KOH + 0.5 M NaCl 1 M KOH + Seawater	[107]
NiCoN Ni _x P NiCoN S-(Ni,Fe)OOH	1.81@10	Seawater	[108]
Mn-doped Ni ₂ P/Fe ₂ P (− +)	1.64@10	1 M KOH + 0.5 M NaCl	[109]
RNPOH/NF RNPOH/NF	1.75@50	1 M KOH + Seawater	[110]
Mo-CoP _x /NF Mo-CoP _x /NF	1.59@10 1.61@10	1 M KOH + 0.5 M NaCl 1 M KOH + Seawater	[111]
CoF-2 CoF-3	1.72@10 1.76@10	1 M KOH + 0.6 M NaCl 1 M KOH + Seawater	[112]
Ni-SN@C Ni-SN@C	1.72@10	1 M KOH + Seawater	[113]

4. Conclusions

In conclusion, we successfully synthesized 3D NiMn/Ti electrocatalysts for stable oxygen evolution reactions by seawater splitting via a one-step and facile electrochemical deposition approach. The surface morphology of the NiMn/Ti-1 electrode exhibits a unique tiny nodule-like architecture covering the substrate, while the as-fabricated NiMn/Ti-3 electrocatalyst exhibits surface roughness with flake-like heterostructures. The optimal NiMn/Ti-1 electrocatalyst displayed excellent durability and quite reasonable OER activity in chloride ion-rich simulated seawater and alkaline seawater media. Moreover, a two-electrode seawater electrolyzer assembled with the as-prepared optimal NiMn/Ti-1 electrode and with an efficient NiMn/Ti-5 electrode, as the anode and cathode, respectively, requires only 1.619 V cell voltage to achieve a current density of 10 mA cm^{−2} at 25 °C. This NiMn/Ti-5(−)||NiMn/Ti-1(+) bimetallic seawater electrolyzer assembly was also subjected to a long-term durability study in ASW, and it demonstrated outstanding stability with no notable change in potential.

Author Contributions: Conceptualization, A.B. and E.N.; methodology, S.B. and J.V.; formal analysis, S.B.; investigation, S.B., D.U. and J.V.; data curation, L.T.-T.; writing—original draft preparation, S.B.; writing—review and editing, E.N. and A.B.; visualization, L.T.-T.; supervision, A.B. All authors have read and agreed to the published version of the manuscript.

Funding: This research received no external funding.

Institutional Review Board Statement: Not applicable.

Informed Consent Statement: Not applicable.

Data Availability Statement: The data presented in this study are available on request from the corresponding author.

Conflicts of Interest: The all authors declare no conflicts of interests.

References

- Yu, Z.Y.; Duan, Y.; Feng, X.Y.; Yu, X.; Gao, M.R.; Yu, S.H. Clean and affordable hydrogen fuel from alkaline water splitting: Past, recent progress, and future prospects. *Adv. Mater.* **2021**, *33*, 2007100. [\[CrossRef\]](#) [\[PubMed\]](#)
- Jiao, S.; Fu, X.; Wang, S.; Zhao, Y. Perfecting electrocatalysts via imperfections: Towards the large-scale deployment of water electrolysis technology. *Energy Environ. Sci.* **2021**, *14*, 1722–1770. [\[CrossRef\]](#)
- Wang, Y.; Vogel, A.; Sachs, M.; Sprick, R.S.; Wilbraham, L.; Moniz, S.J.; Godin, R.; Zwiijnenburg, M.A.; Durrant, J.R.; Cooper, A.I.; et al. Current understanding and challenges of solar-driven hydrogen generation using polymeric photocatalysts. *Nat. Energy* **2019**, *4*, 746–760. [\[CrossRef\]](#)
- Ma, T.; Lutkenhaus, J.L. Hydrogen power gets a boost. *Science* **2022**, *378*, 138–139. [\[CrossRef\]](#)
- Tanç, B.; Arat, H.T.; Baltacıoğlu, E.; Aydın, K. Overview of the next quarter century vision of hydrogen fuel cell electric vehicles. *Int. J. Hydrogen Energy* **2019**, *44*, 10120–10128. [\[CrossRef\]](#)
- Sun, H.; Xu, X.; Kim, H.; Jung, W.; Zhou, W.; Shao, Z. Electrochemical water splitting: Bridging the gaps between fundamental research and industrial applications. *Energy Environ. Mater.* **2023**, *6*, e12441. [\[CrossRef\]](#)
- Hassan, Q.; Sameen, A.Z.; Salman, H.M.; Jaszczur, M.; Al-Jiboori, A.K. Hydrogen energy future: Advancements in storage technologies and implications for sustainability. *J. Energy Storage* **2023**, *72*, 108404. [\[CrossRef\]](#)
- Guo, J.; Zheng, Y.; Hu, Z.; Zheng, C.; Mao, J.; Du, K.; Jaroniec, M.; Qiao, S.-Z.; Ling, T. Direct seawater electrolysis by adjusting the local reaction environment of a catalyst. *Nat. Energy* **2023**, *8*, 264–272. [\[CrossRef\]](#)
- Asghari, E.; Abdullah, M.I.; Foroughi, F.; Lamb, J.J.; Pollet, B.G. Advances, opportunities, and challenges of hydrogen and oxygen production from seawater electrolysis: An electrocatalysis perspective. *Curr. Opin. Electrochem.* **2022**, *31*, 100879. [\[CrossRef\]](#)
- Gao, X.; Li, X.; Yu, Y.; Kou, Z.; Wang, P.; Liu, X.; Zhang, J.; He, J.; Mu, S.; Wang, J. Synergizing aliovalent doping and interface in heterostructured NiV nitride@oxyhydroxide core-shell nanosheet arrays enables efficient oxygen evolution. *Nano Energy* **2021**, *85*, 105961. [\[CrossRef\]](#)
- Jiang, J.; Zhang, Y.-J.; Zhu, X.-J.; Lu, S.; Long, L.-L.; Chen, J.-J. Nanostructured metallic FeNi₂S₄ with reconstruction to generate FeNi-based oxide as a highly-efficient oxygen evolution electrocatalyst. *Nano Energy* **2021**, *81*, 105619. [\[CrossRef\]](#)
- Liu, J.; Zheng, M.; Li, J.; Yuan, Y.; Li, C.; Zhang, S.; Yang, L.; Bai, Z.; Lu, J. Lithiation-Induced Defect Engineering to Promote Oxygen Evolution Reaction. *Adv. Funct. Mater.* **2023**, *33*, 2209753. [\[CrossRef\]](#)
- Avci, Ö.N.; Sementa, L.; Fortunelli, A. Mechanisms of the oxygen evolution reaction on NiFe₂O₄ and CoFe₂O₄ Inverse-Spinel Oxides. *ACS Catal.* **2022**, *12*, 9058–9073. [\[CrossRef\]](#) [\[PubMed\]](#)
- Wang, C.; Shang, H.; Jin, L.; Xu, H.; Du, Y. Advances in hydrogen production from electrocatalytic seawater splitting. *Nanoscale* **2021**, *13*, 7897–7912. [\[CrossRef\]](#)
- Dresp, S.; Dionigi, F.; Klingenhof, M.; Strasser, P. Direct electrolytic splitting of seawater: Opportunities and challenges. *ACS Energy Lett.* **2019**, *4*, 933–942. [\[CrossRef\]](#)
- Liu, G.; Xu, Y.; Yang, T.; Jiang, L. Recent advances in electrocatalysts for seawater splitting. *Nano Mater. Sci.* **2023**, *5*, 101–116. [\[CrossRef\]](#)
- Wang, X.; Zhai, X.; Yu, Q.; Liu, X.; Meng, X.; Wang, X.; Wang, L. Strategies of designing electrocatalysts for seawater splitting. *J. Solid State Chem.* **2022**, *306*, 122799. [\[CrossRef\]](#)
- Wu, L.; Yu, L.; McElhenny, B.; Xing, X.; Luo, D.; Zhang, F.; Bao, J.; Chen, S.; Ren, Z. Rational design of core-shell-structured CoP_x@FeOOH for efficient seawater electrolysis. *Appl. Catal. B Environ.* **2021**, *294*, 120256. [\[CrossRef\]](#)
- Cui, B.; Shi, Y.; Li, G.; Chen, Y.; Chen, W.; Deng, Y.; Hu, W. Challenges and opportunities for seawater electrolysis: A mini-review on advanced materials in chlorine-involved electrochemistry. *Acta Phys.-Chim. Syn.* **2022**, *38*, 85–95. [\[CrossRef\]](#)
- Tong, W.; Forster, M.; Dionigi, F.; Dresp, S.; Sadeghi Erami, R.; Strasser, P.; Cowan, A.J.; Farràs, P. Electrolysis of low-grade and saline surface water. *Nat. Energy* **2020**, *5*, 367–377. [\[CrossRef\]](#)
- Dionigi, F.; Reier, T.; Pawolek, Z.; Glied, M.; Strasser, P. Design criteria, operating conditions, and nickel-iron hydroxide catalyst materials for selective seawater electrolysis. *ChemSusChem* **2016**, *9*, 962–972. [\[CrossRef\]](#) [\[PubMed\]](#)
- Jiang, S.; Liu, Y.; Qiu, H.; Su, C.; Shao, Z. High selectivity electrocatalysts for oxygen evolution reaction and anti-chlorine corrosion strategies in seawater splitting. *Catalysts* **2022**, *12*, 261. [\[CrossRef\]](#)
- Kim, D.; Choi, J.; Lee, K.; Kang, D.W.; Kwon, T. Emerging porous solids for electrocatalytic and photocatalytic seawater splitting. *Coord. Chem. Rev.* **2024**, *514*, 215935. [\[CrossRef\]](#)
- Wang, J.; Gao, Y.; Kong, H.; Kim, J.; Choi, S.; Ciucci, F.; Hao, Y.; Yang, S.; Shao, Z.; Lim, J. Non-precious-metal catalysts for alkaline water electrolysis: Operando characterizations, theoretical calculations, and recent advances. *Chem. Soc. Rev.* **2020**, *49*, 9154–9196. [\[CrossRef\]](#)

25. Du, L.; Prabhakaran, V.; Xie, X.; Park, S.; Wang, Y.; Shao, Y. Low-PGM and PGM-free catalysts for proton exchange membrane fuel cells: Stability challenges and material solutions. *Adv. Mater.* **2021**, *33*, 1908232. [\[CrossRef\]](#) [\[PubMed\]](#)
26. Xu, Y.; Liu, T.; Shi, K.; Yu, H.; Deng, K.; Wang, Z.; Li, X.; Wang, L.; Wang, H. Iridium-incorporated Co_3O_4 with lattice expansion for energy-efficient green hydrogen production coupled with glycerol valorization. *Chem. Commun.* **2023**, *59*, 1817–1820. [\[CrossRef\]](#)
27. Tian, L.; Li, Z.; Xu, X.; Zhang, C. Advances in noble metal (Ru, Rh, and Ir) doping for boosting water splitting electrocatalysis. *J. Mater. Chem. A* **2021**, *9*, 13459–13470. [\[CrossRef\]](#)
28. Gao, Y.; Xue, Y.; Qi, L.; Xing, C.; Zheng, X.; He, F.; Li, Y. Rhodium nanocrystals on porous graphdiyne for electrocatalytic hydrogen evolution from saline water. *Nat. Commun.* **2022**, *13*, 5227. [\[CrossRef\]](#)
29. Yu, Y.; Chen, X.; Li, J.; Xiao, Y.; Shi, X.; Rao, P.; Deng, P.; Wen, H.; Tian, X. Ni-based heterostructure with protective phosphide layer to enhance the oxygen evolution reaction for the seawater electrolysis. *Int. J. Hydrogen Energy* **2024**, *51*, 1373–1380. [\[CrossRef\]](#)
30. Xiao, X.; Wei, Y.; Song, S.; McElhenny, B.; Zhang, F.; Jiang, X.; Zhang, Y.; Chen, S.; Wang, M.; Shen, Y.; et al. Boosting oxygen evolution in seawater media at large current density via boron-doped (Ni, Fe) OOH grown on Ni_3N nanosheets. *Appl. Catal. B Environ. Energy* **2024**, *349*, 123871. [\[CrossRef\]](#)
31. Yang, X.; Bu, H.; Qi, R.; Ye, L.; Wang, C.; Gao, H.; Zhan, T.; Chen, Z. A highly efficient and long-term durable electrocatalyst for oxygen evolution in alkaline seawater by growing $\text{Ni}_{1.5}\text{Fe}_{1.5}\text{B}$ on the NiMoO_4 nanorods. *Mater. Today Chem.* **2024**, *35*, 101849. [\[CrossRef\]](#)
32. Wang, J.; Tran, D.T.; Chang, K.; Prabhakaran, S.; Zhao, J.; Kim, D.H.; Kim, N.H.; Lee, J.H. Hierarchical Ni@CNTs-bridged $\text{Mo}_3\text{C}/\text{Ni}_2\text{P}$ heterostructure micro-pillars for enhanced seawater splitting and Mg/seawater battery. *Nano Energy* **2023**, *111*, 108440. [\[CrossRef\]](#)
33. Fan, J.; Ma, X.; Xia, J.; Zhang, L.; Bi, Q.; Hao, W. Corrosion resistance and earth-abundance FeS-based heterojunction catalyst for seawater splitting at industrial grade density. *J. Colloid Interface Sci.* **2024**, *657*, 393–401. [\[CrossRef\]](#) [\[PubMed\]](#)
34. Gupta, A.; Allison, C.A.; Srivastava, R.; Kumar, A.; Sim, M.; Horinek, J.; Lin, W.; de Souza, F.M.; Mishra, S.R.; Perez, F.; et al. Nanoneedles like FeP engineered on Ni-foam as an effective catalyst towards overall alkaline freshwater, urea, and seawater splitting. *Fuel* **2024**, *369*, 131725. [\[CrossRef\]](#)
35. Li, L.; Zhang, G.; Wang, B.; Yang, S. Constructing the Fe/Cr double (oxy) hydroxides on Fe_3O_4 for boosting the electrochemical oxygen evolution in alkaline seawater and domestic sewage. *Appl. Catal. B Environ.* **2022**, *302*, 120847. [\[CrossRef\]](#)
36. Zhang, X.; Zhu, H.; Zuo, Z.; Jin, M.; Peng, O.; Lian, Q.; Huang, Y.; Cheng, P.; Ai, Z.; Xiang, S.; et al. Robust and efficient iron-based electrodes for hydrogen production from seawater at high current density above 1000 mA cm^{-2} . *Chem. Eng. J.* **2024**, *490*, 151705. [\[CrossRef\]](#)
37. Chen, J.; Wang, Y.; Qian, G.; Yu, T.; Wang, Z.; Luo, L.; Shen, F.; Yin, S. In situ growth of volcano-like FeIr alloy on nickel foam as efficient bifunctional catalyst for overall water splitting at high current density. *Chem. Eng. J.* **2021**, *421*, 129892. [\[CrossRef\]](#)
38. Chen, M.; Zhu, Z.; Li, X.; Li, J.; Shanguan, E.; Qi, J. Engineering heterostructured and hierarchical CoP/CoFeP nanosheet for effective oxygen evolution reaction in alkaline freshwater and seawater. *Int. J. Hydrogen Energy* **2024**, *71*, 1342–1350. [\[CrossRef\]](#)
39. Feng, S.; Rao, P.; Yu, Y.; Li, J.; Deng, P.; Kang, Z.; Wang, S.; Miao, Z.; Shen, Y.; Tian, X.; et al. Self-assembled heterojunction CoSe_2/CoO catalysts for efficient seawater electrolysis. *Electrochim. Acta* **2023**, *463*, 142870. [\[CrossRef\]](#)
40. Kim, S.; Ji, S.; Yang, H.; Son, H.; Choi, H.; Kang, J.; Li, O.L. Near surface electric field enhancement: Pyridinic-N rich few-layer graphene encapsulating cobalt catalysts as highly active and stable bifunctional ORR/OER catalyst for seawater batteries. *Appl. Catal. B Environ.* **2022**, *310*, 121361. [\[CrossRef\]](#)
41. Boakye, F.O.; Harrath, K.; Tabish, M.; Yasin, G.; Owusu, K.A.; Ajmal, S.; Zhang, W.; Zhang, H.; Wang, Y.-G.; Zhao, W. Phosphorus coordinated Co/Se₂ heterointerface nanowires: In-situ catalyst reconstruction towards efficient overall water splitting in alkaline and seawater media. *J. Alloys Compd.* **2023**, *969*, 172240. [\[CrossRef\]](#)
42. Khatun, S.; Roy, P. Cobalt chromium vanadium layered triple hydroxides as an efficient oxygen electrocatalyst for alkaline seawater splitting. *Chem. Commun.* **2022**, *58*, 1104–1107. [\[CrossRef\]](#)
43. Yang, J.; An, Y.; Guo, K.; Ren, X.; Jiang, B. Nitrogen doped FeCoNiS nanoparticles on N, S-co-doped vertical graphene as bifunctional electrocatalyst for water splitting. *Int. J. Hydrogen Energy* **2023**, *48*, 4143–4157. [\[CrossRef\]](#)
44. Ganesan, V.; Kim, J. Multi-shelled $\text{CoS}_2\text{--MoS}_2$ hollow spheres as efficient bifunctional electrocatalysts for overall water splitting. *Int. J. Hydrogen Energy* **2020**, *45*, 13290–13299. [\[CrossRef\]](#)
45. Hu, Y.; Zheng, Y.; Jin, J.; Wang, Y.; Peng, Y.; Yin, J.; Shen, W.; Hou, Y.; Zhu, L.; An, L.; et al. Understanding the sulphur-oxygen exchange process of metal sulphides prior to oxygen evolution reaction. *Nat. Commun.* **2023**, *14*, 1949. [\[CrossRef\]](#)
46. Pei, Z.; Qin, T.; Tian, R.; Ou, Y.; Guo, X. Construction of an amethyst-like $\text{MoS}_2/\text{Ni}_9\text{S}_8/\text{Co}_3\text{S}_4$ rod electrocatalyst for overall water splitting. *Nanomaterials* **2023**, *13*, 2302. [\[CrossRef\]](#)
47. Ding, X.; Uddin, W.; Sheng, H.; Li, P.; Du, Y.; Zhu, M. Porous transition metal phosphides derived from Fe-based Prussian blue analogue for oxygen evolution reaction. *J. Alloys Compd.* **2020**, *814*, 152332. [\[CrossRef\]](#)
48. Li, Q.; Dong, S.; Xie, H.; Ren, J.; Hu, X.; Li, Y.; Zhao, H.; Liu, Z.; Sun, F. Controllable synthesis of crystal-amorphous heterostructures in transition metal phosphide and enhancement mechanism for overall water splitting. *Appl. Surf. Sci.* **2024**, *647*, 158961. [\[CrossRef\]](#)
49. Wang, Q.; Wang, C.; Du, X.; Zhang, X. Controlled synthesis of M (M = Cr, Cu, Zn and Fe)-NiCoP hybrid materials as environmentally friendly catalyst for seawater splitting. *J. Alloys Compd.* **2023**, *966*, 171516. [\[CrossRef\]](#)

50. Zhang, X.; Sun, C.; Xu, S.; Huang, M.; Wen, Y.; Shi, X.-R. DFT-assisted rational design of CoM_xP/CC (M = Fe, Mn, and Ni) as efficient electrocatalyst for wide pH range hydrogen evolution and oxygen evolution. *Nano Res.* **2022**, *15*, 8897–8907. [\[CrossRef\]](#)
51. Xiong, T.; Li, J.; Roy, J.C.; Koroma, M.; Zhu, Z.; Yang, H.; Zhang, L.; Ouyang, T.; Balogun, M.-S.; Al-Mamun, M. Hetero-interfacial nickel nitride/vanadium oxytrichloride porous nanosheets as trifunctional electrodes for HER, OER and sodium ion batteries. *J. Energy Chem.* **2023**, *81*, 71–81. [\[CrossRef\]](#)
52. Liu, T.; Cai, S.; Zhao, G.; Gao, Z.; Liu, S.; Li, H.; Chen, L.; Li, M.; Yang, X.; Guo, H. Recycling valuable cobalt from spent lithium ion batteries for controllably designing a novel sea-urchin-like cobalt nitride-graphene hybrid catalyst: Towards efficient overall water splitting. *J. Energy Chem.* **2021**, *62*, 440–450. [\[CrossRef\]](#)
53. Zhu, J.; Du, Q.; Khan, M.A.; Zhao, H.; Fang, J.; Ye, D.; Zhang, J. 2D porous Co-Mo nitride heterostructures nanosheets for highly effective electrochemical water splitting. *Appl. Surf. Sci.* **2023**, *623*, 156989. [\[CrossRef\]](#)
54. Sinha, N.; Das, C.; Roy, P. Iron-doped cobalt nitride as an efficient electrocatalyst towards energy saving hydrazine assisted seawater splitting in near neutral to highly alkaline pH achieving industry level current density. *Int. J. Hydrogen Energy* **2024**, *51*, 1011–1021. [\[CrossRef\]](#)
55. Sharma, L.; Katiyar, N.K.; Parui, A.; Das, R.; Kumar, R.; Tiwary, C.S.; Singh, A.K.; Halder, A.; Biswas, K. Low-cost high entropy alloy (HEA) for high-efficiency oxygen evolution reaction (OER). *Nano Res.* **2022**, *15*, 4799–4806. [\[CrossRef\]](#)
56. Zhang, Q.; Lian, K.; Liu, Q.; Qi, G.; Zhang, S.; Luo, J.; Liu, X. High entropy alloy nanoparticles as efficient catalysts for alkaline overall seawater splitting and Zn-air batteries. *J. Colloid Interface Sci.* **2023**, *646*, 844–854. [\[CrossRef\]](#)
57. Wang, P.; Qi, J.; Li, C.; Li, W.; Wang, T.; Liang, C. Hierarchical CoNi₂S₄@NiMn-layered double hydroxide heterostructure nanoarrays on superhydrophilic carbon cloth for enhanced overall water splitting. *Electrochim. Acta* **2020**, *345*, 136247. [\[CrossRef\]](#)
58. He, S.; Yue, R.; Liu, W.; Ding, J.; Zhu, X.; Liu, N.; Guo, R.; Mo, Z. Nano-NiFe LDH assembled on CNTs by electrostatic action as an efficient and durable electrocatalyst for oxygen evolution. *J. Electroanal. Chem.* **2023**, *946*, 117718. [\[CrossRef\]](#)
59. Gupta, A.; Sadhanala, H.K.; Gedanken, A. Iron doped cobalt nickel layered double hydroxide supported on nickel foam as a robust electrocatalyst for highly efficient water oxidation in alkaline sea water. *Electrochim. Acta* **2023**, *470*, 143269. [\[CrossRef\]](#)
60. Luo, X.; Ji, P.; Wang, P.; Tan, X.; Chen, L.; Mu, S. Spherical Ni₃S₂/Fe-NiP_x Magic Cube with Ultrahigh Water/Seawater Oxidation Efficiency. *Adv. Sci.* **2022**, *9*, 2104846. [\[CrossRef\]](#)
61. Luo, X.; Ji, P.; Wang, P.; Cheng, R.; Chen, D.; Lin, C.; Zhang, J.; He, J.; Shi, Z.; Li, N.; et al. Interface engineering of hierarchical branched Mo-doped Ni₃S₂/Ni_xPy hollow heterostructure nanorods for efficient overall water splitting. *Adv. Energy Mater.* **2020**, *10*, 1903891. [\[CrossRef\]](#)
62. Bai, Y.; Wu, Y.; Zhou, X.; Ye, Y.; Nie, K.; Wang, J.; Xie, M.; Zhang, Z.; Liu, Z.; Cheng, T.; et al. Promoting nickel oxidation state transitions in single-layer NiFeB hydroxide nanosheets for efficient oxygen evolution. *Nat. Commun.* **2022**, *13*, 6094. [\[CrossRef\]](#)
63. Li, M.-X.; Xiao, B.; Zhao, Z.-Y.; Ma, Y.; Zhou, Y.-N.; Zhang, X.-Y.; Wang, F.-G.; Chai, Y.-M.; Dong, B. Morphology evolution regulation of dual-doped S, Fe-NiMoO₄ microrods based on precipitation-dissolution equilibrium for oxygen evolution. *Fuel* **2023**, *336*, 126769. [\[CrossRef\]](#)
64. Liu, Q.; Yan, Z.; Gao, J.; Wang, E. Surface-oxidized iron–cobalt–nickel alloy with continuous variable composition for hydrogen and oxygen evolution reaction. *ACS Sustain. Chem. Eng.* **2022**, *10*, 14926–14934. [\[CrossRef\]](#)
65. Jiang, S.; Zhu, L.; Yang, Z.; Wang, Y. Self-supported hierarchical porous FeNiCo-based amorphous alloys as high-efficiency bifunctional electrocatalysts towards overall water splitting. *Int. J. Hydrogen Energy* **2021**, *46*, 36731–36741. [\[CrossRef\]](#)
66. Chen, J.; Ling, Y.; Qu, D.; Huang, L.; Li, J.; Tang, P.; He, A.; Jin, X.; Zhou, Y.; Xu, M.; et al. Enhanced electrocatalysis of NiMnIn Heusler alloy films for hydrogen evolution reaction by magnetic field. *J. Alloys Compd.* **2021**, *877*, 160271. [\[CrossRef\]](#)
67. Ashraf, M.A.; Li, C.; Pham, B.T.; Zhang, D. Electrodeposition of Ni-Fe-Mn ternary nanosheets as affordable and efficient electrocatalyst for both hydrogen and oxygen evolution reactions. *Int. J. Hydrogen Energy* **2020**, *45*, 24670–24683. [\[CrossRef\]](#)
68. Srivastava, R.; Bhardwaj, S.; Kumar, A.; Robinson, A.N.; Sultana, J.; Mishra, S.R.; Perez, F.; Gupta, R.K. Bimetallic MnNi-hydroxide electrodeposited on Ni-foam for superior water-splitting and energy storage. *Int. J. Hydrogen Energy* **2024**, *49*, 971–983. [\[CrossRef\]](#)
69. Wang, Z.; Lu, L. The rise of manganese as catalysts for acidic water oxidation: A mini review. *Electrochem. Commun.* **2023**, *151*, 107505. [\[CrossRef\]](#)
70. Chang, S.-Q.; Cheng, C.-C.; Cheng, P.-Y.; Huang, C.-L.; Lu, S.-Y. Pulse electrodeposited FeCoNiMnW high entropy alloys as efficient and stable bifunctional electrocatalysts for acidic water splitting. *Chem. Eng. J.* **2022**, *446*, 137452. [\[CrossRef\]](#)
71. Huang, H.; Hu, X.; Hou, Z.; Yang, D.; Xiang, D.; Hu, L. Interfacial construction and lattice distortion-triggered bifunctionality of Mn-NiS/Mn-Ni₃S₄ for H₂ production. *Fuel* **2022**, *328*, 125337. [\[CrossRef\]](#)
72. Guo, M.; Zhang, B.; Zhang, Q. Deep eutectic solvent mediated synthesis of Mn-based hybrid electrocatalyst for oxygen evolution reaction: Insights into the effect of anion on the evolution of structure-activity. *Appl. Surf. Sci.* **2024**, *645*, 158843. [\[CrossRef\]](#)
73. Zhou, B.; Shao, Y.; Li, Z.; Yang, W.; Ren, X.; Hao, Y. Efficient energy-saving hydrogen production on binder-free electrodeposited hierarchical Ni-Mn-P@Ni-Co nanostructure. *Int. J. Hydrogen Energy* **2024**, *51*, 1022–1032. [\[CrossRef\]](#)
74. Priamushko, T.; Guggenberger, P.; Mautner, A.; Lee, J.; Ryoo, R.; Kleitz, F. Enhancing OER activity of Ni/Co oxides via Fe/Mn substitution within tailored mesoporous frameworks. *ACS Appl. Energy Mater.* **2022**, *5*, 13385–13397. [\[CrossRef\]](#)
75. Zhang, M.; Du, H.; Wei, Z.; Zhang, X.; Wang, R. Facile electrodeposition of Mn-CoP nanosheets on Ni foam as high-rate and ultrastable electrodes for supercapacitors. *ACS Appl. Energy Mater.* **2021**, *5*, 186–195. [\[CrossRef\]](#)
76. Guo, D.; Duan, D.; Gao, J.; Zhou, X.; Liu, S.; Wang, Y. Synthesis of nest-like porous MnCo-P electrocatalyst by electrodeposition on nickel foam for hydrogen evolution reaction. *Int. J. Hydrogen Energy* **2022**, *47*, 6620–6630. [\[CrossRef\]](#)

77. Aaboubi, O.; Ali-Omar, A.-Y.; Dzoyem, E.; Marthe, J.; Boudifa, M. Ni-Mn based alloys as versatile catalysts for different electrochemical reactions. *J. Power Sources* **2014**, *269*, 597–607. [\[CrossRef\]](#)
78. Xiao, T.; Sun, C.; Wang, R. Electrodeposited CrMnFeCoNi Oxy-carbide film and effect of selective dissolution of Cr on oxygen evolution reaction. *J. Mater. Sci. Technol.* **2024**, *200*, 176–184. [\[CrossRef\]](#)
79. Chinnadurai, D.; Rajendiran, R.; Li, O.L.; Prabakar, K. Mn-Co bimetallic phosphate on electrodeposited PANI nanowires with composition modulated structural morphology for efficient electrocatalytic water splitting. *Appl. Catal. B Environ.* **2021**, *292*, 120202. [\[CrossRef\]](#)
80. Wang, Y.; Dong, Q.; Du, X.; Zhang, X. Mn-doped nickel-copper phosphides as oxygen evolution reaction electrocatalyst in alkaline seawater solution. *Int. J. Hydrogen Energy* **2024**, *69*, 895–904. [\[CrossRef\]](#)
81. Zhao, Z.; Zhao, H.; Du, X.; Zhang, X. Fe, Mn-Ni₃S₂ directly grown on nickel foam as an environmentally friendly electrocatalyst for seawater splitting. *Surf. Interfaces* **2024**, *46*, 104079. [\[CrossRef\]](#)
82. Barua, S.; Balčiūnaitė, A.; Vaičiūnienė, J.; Tamašauskaitė-Tamašiūnaitė, L.; Norkus, E. Bimetallic 3D nickel-manganese/titanium bifunctional electrocatalysts for efficient hydrogen and oxygen evolution reaction in alkaline and acidic media. *Coatings* **2023**, *13*, 1102. [\[CrossRef\]](#)
83. Wang, P.; Qi, J.; Chen, X.; Li, C.; Li, W.; Wang, T.; Liang, C. Three-dimensional heterostructured NiCoP@NiMn-layered double hydroxide arrays supported on Ni foam as a bifunctional electrocatalyst for overall water splitting. *ACS Appl. Mater. Interfaces* **2020**, *12*, 4385–4395. [\[CrossRef\]](#) [\[PubMed\]](#)
84. Zhang, B.; Li, J.; Song, Q.; Liu, H. Double functionalization of Mo₂C and NiMn-LDH assembling g-C₃N₄ as efficient bifunctional electrocatalysts for selective electrocatalytic reactions and overall water splitting. *Int. J. Energy Res.* **2022**, *46*, 12406–12416. [\[CrossRef\]](#)
85. Gopalakrishnan, S.; Harish, S.; Kumar, E.S.; Navaneethan, M. Interface engineering of heterogeneous NiMn layered double hydroxide/vertically aligned NiCo₂S₄ nanosheet as highly efficient hybrid electrocatalyst for overall seawater splitting. *Chemosphere* **2024**, *350*, 141016. [\[CrossRef\]](#)
86. Anantharaj, S.; Ede, S.R.; Karthick, K.; Sam Sankar, S.; Sangeetha, K.; Karthik, P.E.; Subrata, K. Precision and correctness in the evaluation of electrocatalytic water splitting: Revisiting activity parameters with a critical assessment. *Energy Environ. Sci.* **2018**, *11*, 744–771. [\[CrossRef\]](#)
87. Cossar, E.; Houache, M.S.E.; Zhang, Z.; Baranova, E.A. Comparison of electrochemical active surface area methods for various nickel nanostructures. *J. Electroanal. Chem.* **2020**, *870*, 114246. [\[CrossRef\]](#)
88. Zabielaite, A.; Balciunaite, A.; Upskuvienė, D.; Simkunaite, D.; Levinas, R.; Niaura, G.; Vaiciuniene, J.; Jasulaitiene, V.; Tamasauskaite-Tamasuniute, L.; Norkus, E. Investigation of hydrogen and oxygen evolution on cobalt-nanoparticles-supported graphitic carbon nitride. *Materials* **2023**, *16*, 5923. [\[CrossRef\]](#) [\[PubMed\]](#)
89. Luo, L.; Huang, H.; Yang, Y.; Gong, S.; Li, Y.; Wang, Y.; Luo, W.; Li, Z. Nickel and manganese oxide heterostructure nanoparticles supported by carbon nanotube for highly efficient oxygen evolution reaction catalysis. *Appl. Surf. Sci.* **2022**, *575*, 151699. [\[CrossRef\]](#)
90. Sana Fathima, T.K.; Ghosh, A.; Ramaprabhu, S. ZIF67-derived Co-CoO/C nanocomposites as highly efficient and selective oxygen evolution reaction (OER) catalysts for seawater electrolysis. *Int. J. Hydrogen Energy* **2024**, *49*, 780–793. [\[CrossRef\]](#)
91. Wang, H.; Ying, J.; Xiao, Y.X.; Chen, J.B.; Li, J.H.; He, Z.Z.; Yang, H.J.; Yang, X.Y. Ultrafast synthesis of Cu₂O octahedrons inlaid in Ni foam for efficient alkaline water/seawater electrolysis. *Electrochim. Commun.* **2022**, *134*, 107177. [\[CrossRef\]](#)
92. Sun, J.; Li, J.; Li, Z.; Li, C.; Ren, G.; Zhang, Z.; Meng, X. Modulating the electronic structure on cobalt sites by compatible heterojunction fabrication for greatly improved overall water/seawater electrolysis. *ACS Sustain. Chem. Eng.* **2022**, *10*, 9980–9990. [\[CrossRef\]](#)
93. Juodkazytė, J.; Šebeka, B.; Savickaja, I.; Petrulevičienė, M.; Butkutė, S.; Jasulaitienė, V.; Selskis, A.; Ramanauskas, R. Electrolytic splitting of saline water: Durable nickel oxide anode for selective oxygen evolution. *Int. J. Hydrogen Energy* **2019**, *44*, 5929–5939. [\[CrossRef\]](#)
94. Cheng, F.; Feng, X.; Chen, X.; Lin, W.; Rong, J.; Yang, W. Synergistic action of Co-Fe layered double hydroxide electrocatalyst and multiple ions of sea salt for efficient seawater oxidation at near-neutral pH. *Electrochim. Acta* **2017**, *251*, 336–343. [\[CrossRef\]](#)
95. Gayen, P.; Saha, S.; Ramani, V. Selective seawater splitting using pyrochlore electrocatalyst. *ACS Appl. Energy Mater.* **2020**, *3*, 3978–3983. [\[CrossRef\]](#)
96. Wang, N.; Ou, P.; Hung, S.-F.; Huang, J.E.; Ozden, A.; Abed, J.; Grigioni, I.; Chen, C.; Miao, R.K.; Yan, Y.; et al. Strong-proton-adsorption Co-based electrocatalysts achieve active and stable neutral seawater splitting. *Adv. Mater.* **2023**, *35*, 2210057. [\[CrossRef\]](#)
97. Huang, W.-H.; Lin, C.-Y. Iron phosphate modified calcium iron oxide as an efficient and robust catalyst in electrocatalyzing oxygen evolution from seawater. *Farad. Disc.* **2019**, *215*, 205–215. [\[CrossRef\]](#)
98. Zhuang, L.; Li, J.; Wang, K.; Li, Z.; Zhu, M.; Xu, Z. Structural buffer engineering on metal oxide for long-term stable seawater splitting. *Adv. Funct. Mater.* **2022**, *32*, 2201127. [\[CrossRef\]](#)
99. Liu, F.; Hu, R.; Qiu, H.; Miao, H.; Wang, Q.; Yuan, J. Constructing high-activity cobalt-based perovskite hybrid by a top-down phase evolution method for the direct seawater electrolysis anode. *J. Alloys Compd.* **2022**, *913*, 165342. [\[CrossRef\]](#)

100. Barua, S.; Balčiūnaitė, A.; Upskuvienė, D.; Vaičiūnienė, J.; Tamašauskaitė-Tamašiūnaitė, L.; Norkus, E. 3D Nickel-manganese bimetallic electrocatalysts for an enhanced hydrogen evolution reaction performance in simulated seawater/alkaline natural seawater. *Int. J. Hydrogen Energy* **2024**, *79*, 1490–1500. [\[CrossRef\]](#)
101. Saquib, M.; Arora, P.; Bhosale, A.C. Nickel molybdenum selenide on carbon cloth as an efficient bifunctional electrocatalyst for alkaline seawater splitting. *Fuel* **2024**, *365*, 131251. [\[CrossRef\]](#)
102. Yang, T.; Lv, H.; Quan, Q.; Li, X.; Lu, H.; Cui, X.; Liu, G.; Jiang, L. Electronic structure modulation of MoO₂ via Er-doping for efficient overall water/seawater splitting and Mg/seawater batteries. *Appl. Surf. Sci.* **2023**, *615*, 156360. [\[CrossRef\]](#)
103. Austeria, M.; Dao, H.T.; Mai, M.; Kim, D.H. Dual-phase cobalt phosphide/phosphate hybrid interactions via iridium nanocluster interfacial engineering toward efficient overall seawater splitting. *Appl. Catal. B Environ.* **2023**, *327*, 122467. [\[CrossRef\]](#)
104. Luo, Y.; Yang, X.; He, L.; Zheng, Y.; Pang, J.; Wang, L.; Jiang, R.; Hou, J.; Guo, X.; Chen, L. Structural and electronic modulation of iron-based bimetallic metal-organic framework bifunctional electrocatalysts for efficient overall water splitting in alkaline and seawater environments. *ACS Appl. Mater. Interfaces* **2022**, *14*, 46374–46385. [\[CrossRef\]](#) [\[PubMed\]](#)
105. Gopalakrishnan, S.; Saranya, V.; Harish, S.; Kumar, E.S.; Navaneethan, M. Heterogeneous bimetallic oxysulfide nanostructure (Ni-Co) as hybrid bifunctional electrocatalyst for sustainable overall alkaline simulated seawater splitting. *J. Alloys Compd.* **2023**, *965*, 171124. [\[CrossRef\]](#)
106. Kim, C.; Lee, S.; Kim, S.H.; Park, J.; Kim, S.; Kwon, S.-H.; Bae, J.-S.; Park, Y.S.; Kim, Y. Cobalt-iron-phosphate hydrogen evolution reaction electrocatalyst for solar-driven alkaline seawater electrolyzer. *Nanomaterials* **2021**, *11*, 2989. [\[CrossRef\]](#) [\[PubMed\]](#)
107. Zhang, Y.; Chen, L.; Yan, B.; Zhang, F.; Shi, Y.; Guo, X. Regeneration of textile sludge into Cu₈S₅ decorated N, S self-doped interconnected porous carbon as an advanced bifunctional electrocatalyst for overall water splitting. *Chem. Eng. J.* **2023**, *451*, 138497. [\[CrossRef\]](#)
108. Yu, L.; Wu, L.; Song, S.; McElhenny, B.; Zhang, F.; Chen, S.; Ren, Z. Hydrogen generation from seawater electrolysis over a sandwich-like NiCoN/Ni₃P/NiCoN microsheet array catalyst. *ACS Energy Lett.* **2020**, *5*, 2681–2689. [\[CrossRef\]](#)
109. Luo, Y.; Wang, P.; Zhang, G.; Wu, S.; Chen, Z.; Ranganathan, H.; Sun, S.; Shi, Z. Mn-doped nickel-iron phosphide heterointerface nanoflowers for efficient alkaline freshwater/seawater splitting at high current densities. *Chem. Eng. J.* **2023**, *454*, 140061. [\[CrossRef\]](#)
110. Qian, L.; Zhu, Y.; Hu, H.; Zheng, Y.; Yuan, Z.; Dai, Y.; Zhang, T.; Yang, D.; Xue, S.; Qiu, F. Unique sandwich-cookie-like nanosheet array heterojunction bifunctional electrocatalyst towards efficient overall water/seawater splitting. *J. Colloid Interface Sci.* **2024**, *669*, 935–943. [\[CrossRef\]](#)
111. Yu, Y.; Li, J.; Luo, J.; Kang, Z.; Jia, C.; Liu, Z.; Huang, W.; Chen, Q.; Deng, P.; Shen, Y.; et al. Mo-decorated cobalt phosphide nanoarrays as bifunctional electrocatalysts for efficient overall water/seawater splitting. *Mater. Today Nano* **2022**, *18*, 100216. [\[CrossRef\]](#)
112. Debnath, B.; Parvin, S.; Dixit, H.; Bhattacharyya, S. Oxygen-defect-rich cobalt ferrite nanoparticles for practical water electrolysis with high activity and durability. *ChemSusChem* **2020**, *13*, 3875–3886. [\[CrossRef\]](#) [\[PubMed\]](#)
113. Jin, H.; Wang, X.; Tang, C.; Vasileff, A.; Li, L.; Slaterry, A.; Qiao, S.-Z. Stable and highly efficient hydrogen evolution from seawater enabled by an unsaturated nickel surface nitride. *Adv. Mater.* **2021**, *33*, 2007508. [\[CrossRef\]](#) [\[PubMed\]](#)

Disclaimer/Publisher's Note: The statements, opinions and data contained in all publications are solely those of the individual author(s) and contributor(s) and not of MDPI and/or the editor(s). MDPI and/or the editor(s) disclaim responsibility for any injury to people or property resulting from any ideas, methods, instructions or products referred to in the content.

3D NiMnCo electrocatalysts with cauliflower curd-shaped microspherical morphology for an efficient and sustainable hydrogen evolution reaction in alkaline freshwater/seawater media

Sukomol Barua, Aldona Balčiūnaitė, Daina Upskuvienė, Jūrate Vaičiūnienė, Loreta.

Tamašauskaitė-Tamašiūnaitė and Eugenijus Norkus

Department of Catalysis, Center for Physical Sciences and Technology (FTMC),

Saulėtekio ave. 3, LT-10257, Vilnius, Lithuania

E-mail: aldona.balciunaite@ftmc.lt

Abstract

Electrocatalytic seawater splitting is an ideal strategy for the large-scale production of green and renewable hydrogen energy. Compared to scarce freshwater, oceanic seawater electrolysis can be considered as a game-changer for the hydrogen economy. Herein, we report a cost-effective one-step synthesis of binder-free, self-supported 3D nickel-manganese-cobalt (NiMnCo) coatings on titanium (Ti) substrate and their electrocatalytic performance for the hydrogen evolution reaction was evaluated in alkaline media (1.0 M KOH), simulated seawater (SSW, 1.0 M KOH + 0.5 M NaCl) and alkaline natural seawater (ASW, 1.0 M KOH + natural seawater). These tri-component coatings have been electrodeposited on Ti substrate using an electrochemical deposition method through a dynamic hydrogen bubble template (DHBT) technique.

The reported ternary optimized NiMnCo/Ti-2 electrocatalyst exhibited an enhanced hydrogen evolution reaction (HER) through alkaline and seawater splitting with an ultra-low overpotential of 29, 59 and 66 mV to reach the benchmark current density of 10 mA cm⁻² in SSW, ASW and 1.0 M KOH, respectively. This efficient ternary NiMnCo/Ti-2 electrocatalyst exhibited a consistent long-term stability at a constant potential of -0.23 V (vs. RHE) and a constant current density of 10 mA cm⁻² for 50 hours without any significant degradation. Additionally, it demonstrated long-term stability in alkaline electrolyte and simulated seawater with a multi-step chronopotentiometric investigation through variable current densities from 20 mA cm⁻² to 100 mA cm⁻² for 18 hours. This superior performance can be accredited to the unique intermetallic structure and multi-component composition, which provides good Cl⁻ resistance, analytical stability and synergistic effects among its constituents. Therefore, the fabricated optimized NiMnCo/Ti-2 electrocatalyst can be considered as a promising candidate for realistic seawater electrolysis aiming of green hydrogen production.

Keywords: nickel; manganese; cobalt; electrocatalyst; hydrogen evolution reaction (HER); seawater electrolysis.

1. Introduction

Limited fossil fuel driven industrialization and the steadily increasing global energy demand due to burgeoning population growth resulting significant challenges for the existence of mankind as the vast consumption of fossil fuels not only depleting the natural resources but also aggravates environmental pollution and consequential global warming, climate change and other environmental complications [1-5]. Moreover, the fossil fuel reserves are also very inadequate and geospecific, thereby their drastic depletion could lead to energy shortfalls and geopolitical conflicts. In order to address both energy security and environmental sustainability by mitigating the emission of greenhouse gases, hydrogen (H_2) can be considered as a key emerging substitute for fossil fuels which definitely can serve as the most promising energy source by means of highest energy density ($\sim 142 \text{ MJ kg}^{-1}$) leaving zero carbon footprint, rich elemental abundance on Earth for scalability [6-10].

Hydrogen energy has received significant attention due to its numerous superiorities and can be produced from many different non-renewable conventional sources, e.g., coal, natural gas, biomass etc. To date, steam reforming of fossil fuels feasibly remains the most economical approach to produce hydrogen at a scale of $\sim \$2/\text{kg}$ [11], the primary global energy consumption by renewable energy increased from 28.82 EJ (Exajoule, 10^{18} Joules) in 2019 to 31.71 EJ in 2020, as reported by BP's statistical review [12]. However, the conventional steam reforming production pathway has a nominal conversion rate and leads to CO_2 emissions, CO intermediates and coke due to incomplete combustion which requires sophisticated technology and a lavish budget to mitigate through carbon capture and storage [13, 14]. Therefore, global energy utilization must be fully decarbonized to alleviate the negative environmental impacts caused by non-renewable energy carriers and to achieve the Paris Agreement target set for minimizing emissions by 2050 [15, 16]. The process of electrosynthesis of hydrogen through water electrolysis powered by renewable energy can be treated as a decarbonized energy source and green enough [17], and according to statistics, global hydrogen production stood at 90 Mt (million tons) in 2020 which is predicted to reach 530 Mt/year by 2050 to meet Net Zero Emission Scenario of International Energy Agency [18]. In the recent past, the U.S. Department of Energy also launched the

‘Hydrogen Shot’ program in June 2021 to restrain the cost of clean hydrogen to \$1 per 1 kilogram in 1 decade (“1 1 1”) [19, 20].

The process of green hydrogen production through water splitting comprises two key half-reactions: the anodic oxygen evolution reaction (OER) and the cathodic hydrogen evolution reaction (HER) whereas it requires ca. 9 L of pure water stoichiometrically to produce 1 kg of hydrogen [21-23]. The overall electrocatalytic water splitting reaction requires a theoretical voltage of 1.23 V, corresponding to the thermodynamic Gibbs free energy of $237.2 \text{ kJ mol}^{-1}$. However, the practical water electrolysis in standard conditions usually needs a higher input of 1.48 V and the process consumes additional energy to drive at a practical rate [24-28]. Therefore, the main technical bottleneck for the electrochemical water electrolysis is to achieve exceptional hydrogen conversion efficiency and overcoming the sluggish reaction kinetics of anodic OER which makes the overall water splitting more extortionate. The industrial commercialization of hydrogen production is also constrained by the consumption of a large volume of limited freshwater reserves but seawater is an ample natural resource covering ~97% of the total water reserve on Earth.

It is important to note that direct feed seawater electrolysis (DFSE) would be a more practical cost-effective approach for industrial-scale hydrogen production with high purity but commercialization of DFSE is limited due to the competing chlorine evolution reaction (CIER) in the anode [29-33]. According to the Pourbaix diagram for the artificial seawater model at standard ambient temperature, the formation of hypochlorite and other by-products might take place during CIER at higher pH values along with insoluble Mg/Ca hydroxide on the electrode surface which can hinder the long-term durability of electrocatalysts [32-34]. Therefore, in the last decades, tremendous breakthroughs have been made by the research and development to synthesize high-performance, durable electrocatalysts for electrocatalytic seawater splitting but today, for the commercialization of zero or low-carbon green hydrogen with renewability, it is important to focus on the development of electrocatalysts for seawater electrolysis with enhanced activity, selectivity, long-term stability along with anti-corrosion properties [35-38].

Nevertheless, the high cost of zero to low-carbon green hydrogen energy remains the primary hurdle in seawater splitting arising from the electrocatalysts employed as electrodes in water/seawater electrolyzers. The state-of-the-art platinum group metal (PGM) catalysts exhibit outstanding electrocatalytic activity for water electrolyzers, where Pt and Pt-based catalysts are the benchmark electrocatalysts for HER [39-43]. However, the scarcity and high cost of precious PGM

catalysts are the principal obstacles hindering their widespread application and large-scale commercialization. In recent years, the use of non-noble transition metal-based catalysts has been extended for HER in respect of water splitting and industrial electrolyzers including transition-metal-based oxides [44-46], LDHs and hydroxides [47-49], sulfides [50, 51], nitrides [52, 53], phosphides [54, 55], and alloys [56-58]. Among these, transition metal alloy electrocatalysts have drawn significant attention due to their ease of electronic and structural modification to improve the inherent electrocatalytic activity.

In general, several applicable techniques and methods have been used to synthesize electrocatalysts with enhanced electrocatalytic activity and structural integrity for long-term durability. The electrodeposition method is a facile, cost-effective method to fabricate binder-free 3D nano-micro architectures of different shapes and structural morphology, e.g., porous [59], nanosheets [60], nanotubes [61], nanocones [62] and nano-micro dendrites [63], etc. Such unique surface morphologies of electrocatalysts increase the active surface area and the number of active sites, resulting in the acceleration of electrolyte diffusion and improved electron transport efficiency [64, 65]. An attractive feature of the electrodeposition method is the dynamic hydrogen bubble template (DHBT) technique through which moderate-to-high controllable current density is usually applied to synthesize electrocatalysts and the formation of vigorous hydrogen bubbles acts as dynamic templates to regulate the surface and structural morphology [66]. For instance, Jiang et al. synthesized the trumpet-shaped Ru catalyst on amorphous cobalt support (T-Ru/a-Co) via the DHBT process which requires only 49 mV overpotential to obtain a current density of 10 mA cm^{-2} for HER in alkaline media (1.0 M KOH) [67]. Another study conducted by Hassanizadeh et al. shows that $\text{Ni}_3\text{S}_2@\text{Cu}@\text{NF}$ electrocatalyst synthesized via DHBT method, where copper and nickel sulfide coatings were electrodeposited at a constant current density of 6 A cm^{-2} for only 5 s forming a dendritic morphology with circular porous architecture with an average diameter of 9 μm in certain areas. Electrocatalysts fabricated by such a fast-forwarding, low-cost method also demonstrated enhanced HER activity in alkaline media with 98 mV overpotential to achieve a current density of 10 mA cm^{-2} [68]. Furthermore, a nanoflower-like NiFeCo catalyst fabricated by a facile one-step DHBT electrodeposition method on carbonized wood also exhibited remarkable HER activity in 1.0 M KOH solution requiring ultra-low overpotentials of 37 mV and 298 mV to achieve current densities of 10 mA cm^{-2} and 1000 mA cm^{-2} [69].

According to the aforementioned studies, cobalt (Co) can act as a promising transition metal for synthesizing alloyed electrocatalysts due to its large reserves and affordability. Moreover, Co possesses unpaired electrons in the outer $3d$ orbital which may pair easily with the $1s$ orbital of H atoms to form M-H bond and facilitate the HER process [70-72].

Our previous publications demonstrated the superior HER activity and sustainability of bimetallic 3D NiMn coatings electrodeposited by facile DHBT technique on Ti substrate towards alkaline media [73] and simulated/alkaline seawater [74]. Thus, it was decided to modify and synthesize our previous electrocatalyst via amalgamating with cobalt and resuming the scientific investigations and characterizations in a broad perspective to unfold the efficiency, durability and practical application of multicomponent electrodes for HER in alkaline media, simulated seawater (SSW) and alkaline seawater (ASW) electrolytes.

2. Experimental Section

2.1 Materials and Fabrication of Catalysts

All the chemicals used in the experiments were of analytical grade and used directly without further purification. Titanium (Ti) foils (0.127 mm thick) with size of (1×1 cm) were cut, sanded to 1000 grit and degreased with ethanol to remove the native surface oxide layer. Subsequently, the Ti plates were washed with deionized water (DI) followed by their activation via pretreatment in diluted H_2SO_4 (1:1 vol.) at 70°C. The electrocatalyst fabrication occurred via electrodeposition by DHBT technique in a two-electrode cell using a pair of wire-connected platinum sheets (55×35×1 mm) as the anode and Ti sheets as the cathode. To synthesize self-supported non-noble electrocatalysts, the chemical composition of the electrodeposition solution baths were composed of 0.2 M nickel sulfate hexahydrate ($\text{NiSO}_4 \cdot 6\text{H}_2\text{O}$, >98%) as a source of nickel ions, 1.0 M manganese chloride tetrahydrate ($\text{MnCl}_2 \cdot 4\text{H}_2\text{O}$, >99%) as a source of manganese ions, and variable concentrations of 0.1 M and 0.2 M cobalt nitrate hexahydrate [$\text{Co}(\text{NO}_3)_2 \cdot 6\text{H}_2\text{O}$, >98%] as a source of cobalt ions. Besides, 0.5 M $(\text{NH}_4)_2\text{SO}_4$ was added as a modifier of the coating morphology, and 0.5 M H_3BO_3 was used as a pH stabilizer during the preparation of each solution bath. H_2SO_4 (96%), HCl (35-38%), and KOH (85%) were purchased from Chempur Company (Karlsruhe, Germany). Moreover, two binary electrode compositions were also fabricated likewise to compare the catalytic activity as catalyst-samples. All reagents were dissolved in ultrapure DI water with a resistivity of 18.2 M Ω .cm at acidic conditions (1.5 M H_2SO_4 and 1 M HCl). The electrodeposition

temperature was maintained at 25°C and the pH of the solution was ca. 1. The compositions of formulated solution baths and the electroplating conditions used for the fabrication of catalysts and catalyst-samples are listed in Table 1.

After electroplating the electrodes, NiMnCo/Ti electrocatalysts were removed, thoroughly rinsed with deionized water, air-dried at room temperature, marked and carefully stored for subsequent investigations. The synthesized electrocatalysts were denominated as NiMnCo/Ti-*n* (*n*=1, 2), according to the molar concentrations of Co²⁺ ions in the solution baths (herein, we simplified the catalysts' acronyms with integer numbers. The 3D NiMnCo/Ti-1 and NiMnCo/Ti-2 electrodes were electrochemically synthesized from the bath solutions with Co²⁺ ion concentrations of 0.1 M and 0.2 M, respectively). The natural seawater was collected from the Baltic Sea coastline (Klaipėda seashore region, Lithuania, 55°42'45" N, 21°08'06" E).

Table 1. The composition of the electrochemical baths and electroplating condition parameters.

Catalysts	Concentration (M)					Plating conditions			
	Ni ²⁺ (aq)	Mn ²⁺ (aq)	Co ²⁺ (aq)	(NH ₄) ₂ SO ₄	H ₃ BO ₃	pH*	T, (°C)	<i>j</i> , (mA cm ⁻²)	<i>t</i> , (min)
NiCo/Ti	0.2	-	0.2	0.5	0.5	~1	25	50** 100***	10 5
NiMn/Ti	0.2	1.0	-	0.5	0.5	~1	25	50** 100***	10 5
NiMnCo/Ti-1	0.2	1.0	0.1	0.5	0.5	~1	25	50** 100***	10 5
NiMnCo/Ti-2	0.2	1.0	0.2	0.5	0.5	~1	25	50** 100***	10 5

* 1.5 M H₂SO₄ and 1 M HCl

** Current density during 1st step of electrodeposition

*** Current density during 2nd step of electrodeposition

2.2 Structural Characterization

To analyse the electrodes, scanning electron microscopy (SEM) using an SEM workstation, TM 4000 Plus, with an AZtecOne detector (HITACHI, Tokyo, Japan) was used to determine the microstructural surface morphology of the synthesized NiMnCo/Ti-1, NiMnCo/Ti-2 electrocatalysts and bimetallic catalyst-samples. The loadings of Ni, Mn and Co to Ti substrate were determined by inductively coupled plasma optical emission spectrometry (ICP-OES) analysis. The ICP-OES spectra were recorded using an Optima 7000DV spectrometer (Perkin

Elmer, Waltham, MA, USA) at wavelengths of λ_{Ni} 231.604 nm, λ_{Mn} 257.610 nm and λ_{Co} 228.616 nm.

2.3 Electrochemical Measurements

The electrochemical investigations have been carried out to determine the electrocatalytic HER performance via linear sweep voltammetry (LSV) using a potentiostat PGSTAT302 through Electrochemical Software (Nova 2.1.4, Metrohm Autolab B.V., Utrecht, The Netherlands). A three-electrode system consisting of a saturated calomel electrode (SCE) as a reference electrode, a graphite rod as a counter electrode and binder-free directly deposited NiMnCo/Ti electrocatalysts with a geometric area of 2 cm² were employed as working electrodes. All applied potentials in the three-electrode system corresponding to SCE were calibrated to the reversible hydrogen electrode (RHE) by using the following equation:

$$E_{\text{RHE}} = E_{\text{SCE}} + 0.242 \text{ V} + 0.059 \text{ V} \times \text{pH}_{\text{solution}} \quad (1)$$

The electrocatalytic activity of synthesized electrocatalysts was evaluated in alkaline media as well as simulated seawater (SSW) and alkaline natural seawater (ASW). The alkaline electrolyte was aqueous 1.0 M KOH solution prepared by weighing an equivalent amount of KOH pellets and dissolving in the required volume of DI water (pH ~14). Besides, SSW was prepared by weighing 0.5 M equivalent of NaCl salt and 1.0 M equivalent of KOH pellets and solvating together in a measured volume of DI water (pH ~14) whereas, the ASW was formulated by dissolving 1.0 M equivalent of KOH pellets in a certain volume of collected natural seawater, filtering out the cloudy insoluble metal hydroxides and collecting the clean filtrate (pH ~14).

The electrocatalytic activity for HER was evaluated by recording LSV polarization curves in all three electrolytes, 1.0 M KOH, SSW (1 M KOH + 0.5 M NaCl) and ASW (1 M KOH + natural seawater) at the temperature range from 25°C to 75°C. Prior to investigations, working electrolytes were deaerated with argon (Ar) for 20 min. The LSVs were recorded from the open circuit potential (OCP) to -0.43 V (vs. RHE) at a potential scan rate of 10 mV s⁻¹. Moreover, the long-term stability of the fabricated optimum NiMnCo/Ti-2 electrocatalyst was evaluated by recording the chronoamperometry (CA) curves at a constant potential of -0.23 V (vs. RHE) and chronopotentiometry (CP) curves at a constant current density of 10 mA cm⁻² for 50 hours. Moreover, the robustness and excellent durability of optimized NiMnCo/Ti-2 electrocatalyst was also evaluated by a multi-step chronopotentiometry test with current densities ranging from

20 mA cm⁻² to 100 mA cm⁻² in alkaline media and SSW, indicating sustainability, anti-corrosion property (resistance in Cl⁻ ion-rich seawater), structural integrity and suitability for use in practical seawater splitting applications.

Moreover, the electrochemically active surface area (ECSA) of NiMnCo/Ti-2 was determined by measuring the double layer capacitance (C_{dl}), as outlined in the reference [75]. In summary, CVs were recorded at different scan rates within the non-Faradaic region of a 1.0 M KOH solution.

3. Results and discussion

The enhanced electrocatalytic performance and superior long-term stability of the electrodes depend on the intrinsic and synergistic effects of the metal components, as well as their composition and the microstructural morphology of the electrocatalysts. The surface morphology of the optimized electrocatalyst was characterized by scanning electron microscopy (SEM), as shown in Fig. 1. The SEM image of the NiMnCo/Ti-2 electrocatalyst reveals a cauliflower curd-shaped microspherical architecture directly deposited on the conductive Ti substrate via a facile one-step electrodeposition method. These densely packed microspheres uniformly cover the entire substrate surface (Fig. 1a). A higher-magnification SEM image (Fig. 1a') further illustrates the distinct microspheres, each with diameters ranging from approximately 7-14 μ m, evenly distributed across the surface.

The NiMnCo/Ti-1 electrocatalyst also exhibits a similar microspherical morphology; however, the grains appear less well-defined and more integrated into larger chunks, as observed in Fig. 1b. In contrast, the bimetallic NiCo/Ti sample shows a rough and porous clustered surface morphology, with finer granularity within each cluster (Fig. 1c). Meanwhile, the NiMn/Ti electrode displays an uneven surface texture with noticeable variations in roughness (Fig. 1d).

The ICP-OES analysis was used to determine the metal loadings of the synthesized electrocatalysts, and the results are summarized in Table 2. The 3D ternary NiMnCo/Ti-1 and NiMnCo/Ti-2 electrocatalysts contained approximately 15.7–19.6 wt.% Ni, 20.4–27.8 wt.% Mn, and 52.6–63.8 wt.% Co.

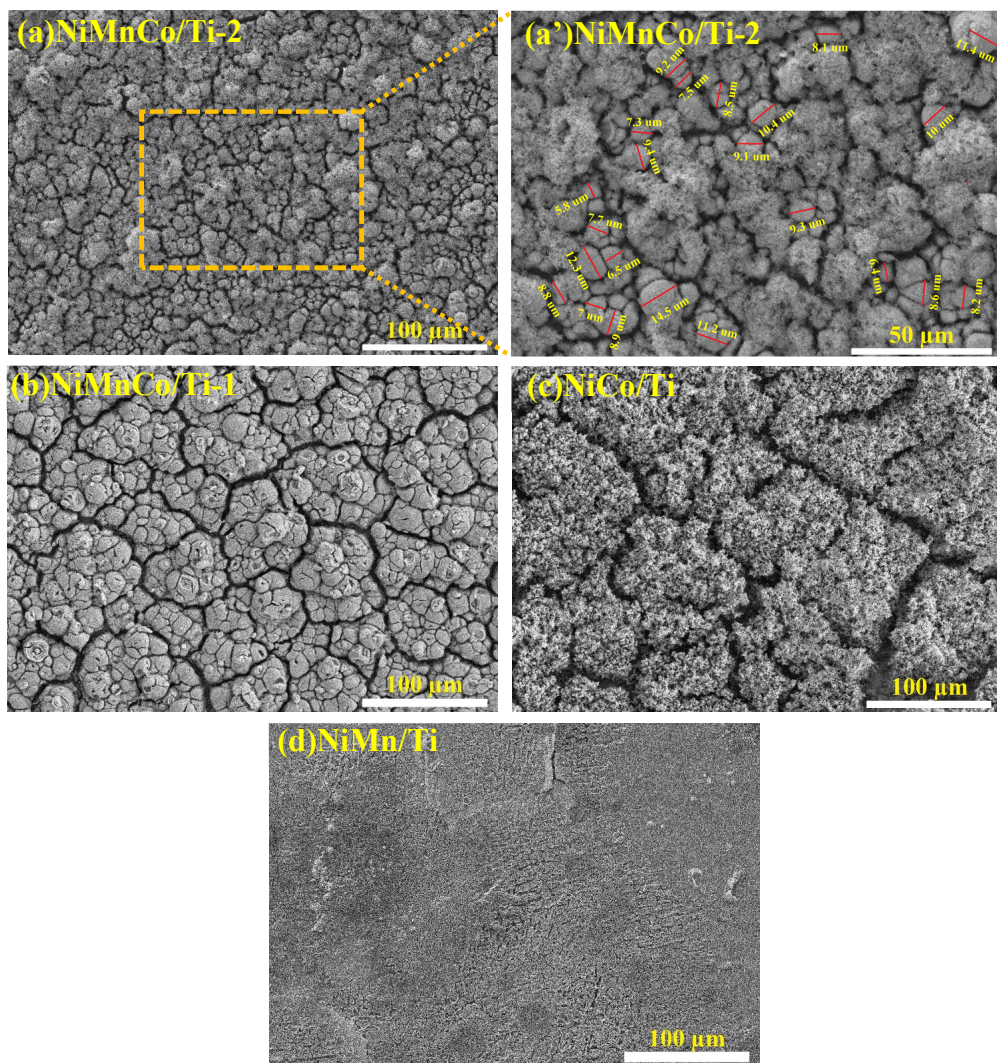


Figure 1. SEM views of synthesized 3D NiMnCo/Ti-2 (a, a'), NiMnCo/Ti-1 (b) electrocatalysts and bimetallic NiCo/Ti (c) and NiMn/Ti (d) catalyst-samples

Table 2. Summarized ICP-OES results of the studied electrocatalysts and catalyst-samples.

Catalyst	Ni loading ($\mu\text{g}_{\text{Ni}}\text{cm}^{-2}$)	Mn loading ($\mu\text{g}_{\text{Mn}}\text{cm}^{-2}$)	Co loading ($\mu\text{g}_{\text{Co}}\text{cm}^{-2}$)	Total metal loading ($\mu\text{g}_{\text{metal}}\text{cm}^{-2}$)	Wt. %		
					Ni	Mn	Co
NiCo/Ti	167.1	-	560.5	727.6	22.97	-	77.03
NiMn/Ti	106.18	128.58	-	234.76	45.23	54.77	-
NiMnCo/Ti-1	49.09	63.7	198.96	311.75	15.75	20.43	63.82
NiMnCo/Ti-2	68.75	97.55	184.35	350.65	19.6	27.82	52.58

4. Electrochemical Investigations for HER

4.1 In alkaline freshwater (1.0 M KOH)

The electrocatalytic HER performance of the fabricated catalysts was initially evaluated in an Ar-saturated alkaline media (1.0 M KOH) by recording LSVs using a three-electrode electrochemical cell. The LSV investigation of as-prepared electrocatalysts was carried out at a potential scan rate of 10 mV s^{-1} from open-circuit potential (OCP) to -0.43 V (vs. RHE) in a temperature range from 25°C up to 75°C , as shown in Fig. 2a. Both electrodes were prepared at least three times using each solution bath and the LSV analysis was conducted and obtained results were registered for each electrode to check the repetitiveness of performance.

The corresponding HER polarization curve of self-supported 3D NiMnCo/Ti-2 catalyst clearly demonstrated the enhanced catalytic activity over NiMnCo/Ti-1 electrode as different molar ratios of Co^{2+} ions (Table 1) in the solution baths and resultant variable Co-loading on both electrocatalysts (Table 2) strongly determine the electrocatalytic performance. The current density increased ca. 1.7 times with the increase of temperature from 25°C up to 75°C for both electrodes.

The polarization curves of the fabricated 3D NiMnCo/Ti-1, NiMnCo/Ti-2 electrocatalysts, along with two bimetallic catalyst-samples NiMn/Ti and NiCo/Ti (for comparison) were recorded at 25°C and exhibited in Fig. 2b.

The LSV plots demonstrated in Fig. 2b were used to extract the corresponding Tafel plots for those fabricated electrodes and samples. The Tafel slope is a pivotal parameter in determining the electrochemical kinetics and the rate-determining step of a reaction. As shown in Fig. 2c, the Tafel slope values were found to be 210, 231, 169 and 137 mV dec^{-1} for the synthesized 3D ternary NiMnCo/Ti-1, NiMnCo/Ti-2 electrocatalysts, and binary NiMn/Ti and NiCo/Ti sample electrodes, respectively. Moreover, the elevation of the column bars exhibited in Fig. 2d denoted the required overpotentials to achieve the benchmark current densities of 10, 20, and 50 mA cm^{-2} .

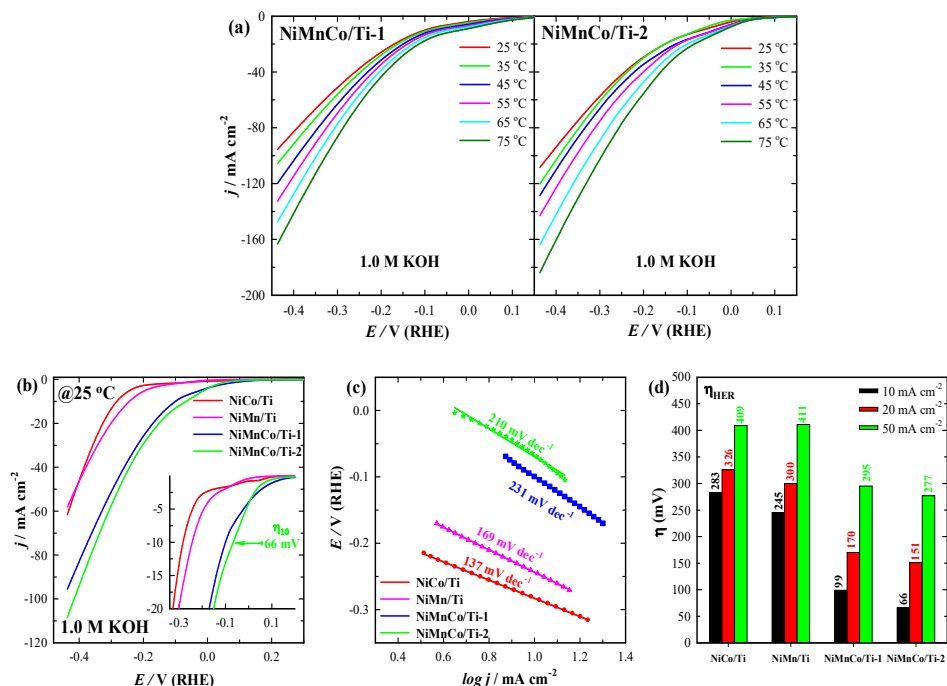


Figure 2. HER polarization curves of 3D NiMnCo/Ti catalysts in 1.0 M KOH at 10 mV s⁻¹ potential scan rate and 25 to 75°C temperature range (a). LSVs at only 25°C temperature along with sample-catalysts (b), the corresponding extracted Tafel plots (c) and the required overpotentials to reach the current densities of 10, 20 and 50 mA cm⁻² (d)

As demonstrated in Fig. 2d, the NiMnCo/Ti-2 electrocatalyst exhibits superior HER activity in alkaline electrolyte (1.0 M KOH) with the required lowest overpotential of 66 mV to attain the benchmark current density of 10 mA cm⁻² at 25°C. Nevertheless, the electrocatalytic activity of NiMnCo/Ti-2 electrocatalyst outperforms the respective NiMnCo/Ti-1 electrocatalyst ($\eta_{10} = 99$ mV) and fabricated both binary NiMn/Ti ($\eta_{10} = 245$ mV) and NiCo/Ti ($\eta_{10} = 283$ mV) sample electrodes (Table 3).

Table 3. Summarized electrochemical data of the investigated catalysts toward HER in alkaline media (1.0 M KOH)

Catalysts	j (mA cm ⁻²) in several temperatures at -0.43 V(vs. RHE)						η_{10} (mV) at 25°C	Tafel slope (mV dec ⁻¹)
	25°C	35°C	45°C	55°C	65°C	75°C		
NiCo/Ti	61.6	-	-	-	-	-	283	137
NiMn/Ti	58	-	-	-	-	-	245	169
NiMnCo/Ti-1	95.5	105.7	119.8	132.6	147.4	163.3	99	231
NiMnCo/Ti-2	108.3	120.2	128.6	142.9	163.8	183.8	66	210

Table 4. Comparison of electrocatalytic HER performance of as-synthesized electrocatalyst in alkaline electrolytes (1.0 M KOH) with other recently reported non-noble metal-based electrodes.

Electrocatalysts	Overpotential η_x (mV)	Tafel slope (mV dec ⁻¹)	Stability analysis	Ref.
NiMnCo/Ti-2	66 (η_{10})	210	50h@10 mA cm ⁻²	This work
NM@cNF/aNFO	57.3 (η_{10})	59.9	-	[76]
Co(OH) ₂ @NiFe/NF	87 (η_{10})	74	-	[77]
NF/Ni	71 (η_{10})	82.8	120h@50 mA cm ⁻²	[78]
CF/Ni-Ni(OH) ₂ -300	73 (η_{10})	33	100h@ η =150 mV	[79]
NiFeO/NiMoO/NF	46 (η_{10})	85	140h@100 mA cm ⁻²	[80]
NiP ₂ /NiSe ₂	89 (η_{10})	65.7	90h@10 mA cm ⁻²	[81]
Co ₇ Fe ₃ /Co-600	68 (η_{10})	55.8	100h@10 mA cm ⁻²	[82]
Ni ₂ P-CoCH/CFP	62 (η_{10})	76	90h	[83]
Ni-Se-Lu/NF	52 (η_{10})	63.8	70h@10 mA cm ⁻²	[84]
MoMn-NiCoS	70 (η_{10})	133.1	50h@10 mA cm ⁻²	[85]
MoCoNiS@NF	114 (η_{10})	88	24h@10 mA cm ⁻²	[86]
Mo-Ni ₃ S ₂ /CoFeOH/NF	109 (η_{10})	111	60h@100 mA cm ⁻²	[87]
CoP-NC/PET	63 (η_{10})	48.09	15h@10 mA cm ⁻²	[88]
MnCoPi-100	102 (η_{10})	102.24	48h@100 mA cm ⁻²	[89]
Co/CoP@NC	142 (η_{10})	67	15h@50 mA cm ⁻²	[90]
Ni-Fe-Sn	103 (η_{10})	97.4	50h@10 mA cm ⁻²	[91]
NiFeS/NF	75 (η_{10})	60.23	50h@-0.15 V	[92]
Cu-Co-P/NF	64 (η_{10})	40	50h@10 mA cm ⁻²	[93]
CoFeNiP/NF-0.1	75.6 (η_{10})	63	100h@100 mA cm ⁻²	[94]
a-Ni ₂ Fe/NF	183 (η_{100})	89.68	24h@-0.18 V (RHE)	[95]

4.2 In simulated and alkaline natural seawater

Though both binder-free, self-supported 3D NiMnCo/Ti-1 and NiMnCo/Ti-2 electrocatalysts have performed to be outstanding electrocatalysts towards HER in alkaline media using freshwater (DI water), thorough investigations have been carried out to explore the electrocatalytic performance towards more practical, feasible and natural resource-based seawater media. For investigation, an artificial or mimic seawater electrolyte has been formulated with a similar salinity (0.5~0.6 M) of natural seawater using 0.5 M NaCl with 1.0 M KOH (herein, simulated seawater, SSW) and alkaline seawater was prepared using natural seawater as mentioned above (*Section 2.3*).

The electrocatalytic HER performance was evaluated by recording linear sweep voltammograms in Ar-deaerated SSW and ASW individually at a potential scan rate of 10 mV s^{-1} from open-circuit potential (OCP) to -0.43 V (vs. RHE) in a temperature range from 25°C up to 75°C , as shown in Fig. 3a. The continuity of obtained results was examined via monitoring LSVs of multiple (at least three) electrodes fabricated from identical bath solutions. Fig. 3b shows the LSV curves of the obtained electrocatalysts and samples at 25°C , from which the overpotentials achieved at different current densities can be determined in SSW. An impressive HER performance of synthesized NiMnCo/Ti-2 electrocatalyst was recorded in formulated SSW as required an ultra-low overpotential of 29 mV to reach the benchmark current density of 10 mA cm^{-2} (Table 5), which outperforms fabricated 3D NiMnCo/Ti-1 ($\eta_{10} = 89 \text{ mV}$), NiMn/Ti ($\eta_{10} = 195 \text{ mV}$) and NiCo/Ti ($\eta_{10} = 267 \text{ mV}$). Besides, we also explored the Tafel slope of each fabricated electrocatalyst and catalyst-samples, as shown in Fig. 3c. The optimized NiMnCo/Ti-2 electrocatalyst presents a Tafel slope of 188 mV dec^{-1} , whereas NiMnCo/Ti-1, NiMn/Ti and NiCo/Ti have a Tafel slope of 148 , 192 and 141 mV dec^{-1} , respectively. From the LSV curves, the overpotentials of each electrode to reach current densities of 10 , 20 , and 50 mA cm^{-2} in SSW are calculated, as exhibited with column bars in Fig. 3d.

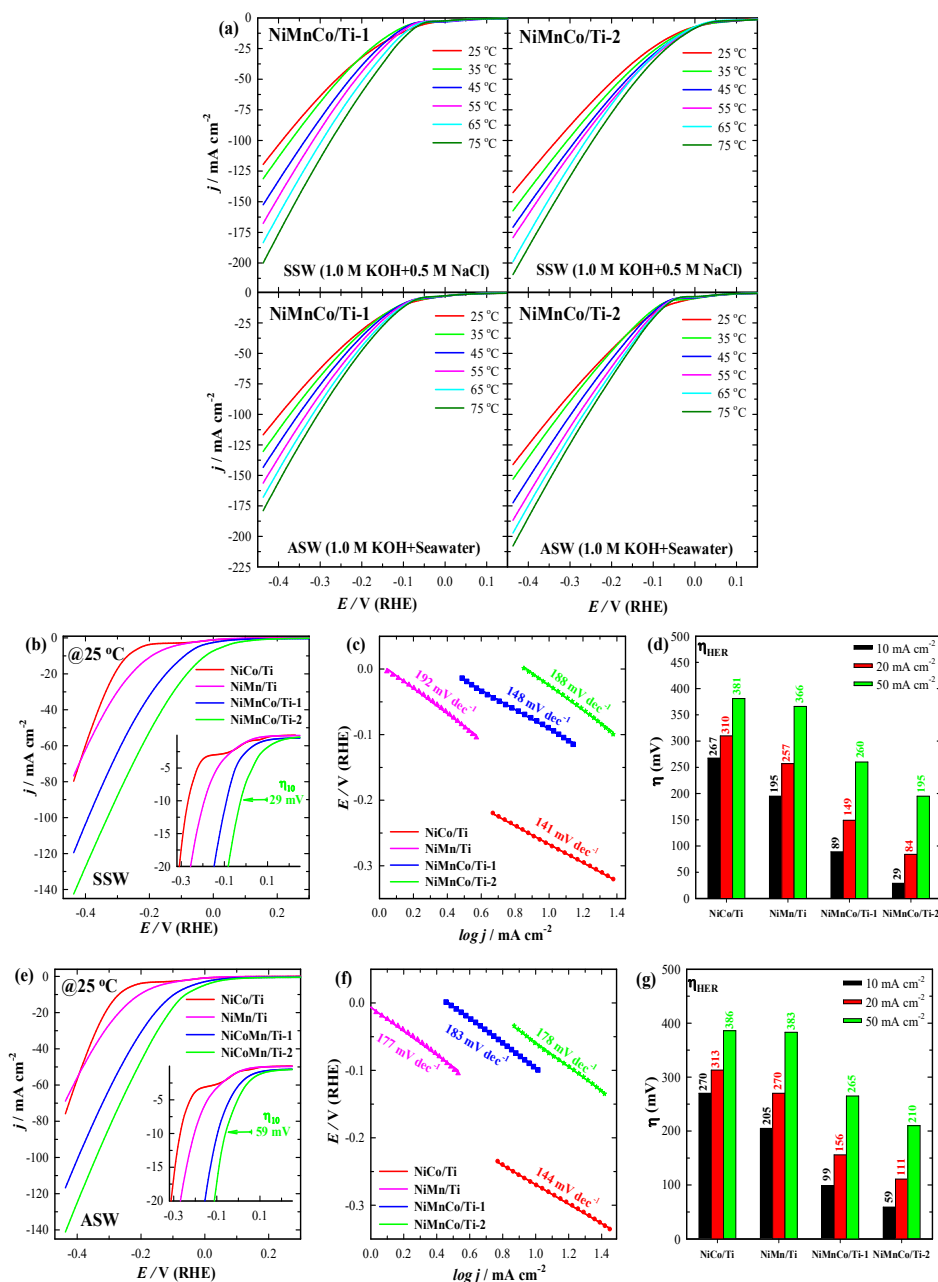


Figure 3. HER polarization curves of 3D NiMnCo/Ti electrocatalysts in SSW and ASW at a potential scan rate of 10 mV s⁻¹ in 25 to 75°C temperature range (a), LSVs at only 25°C temperature along with sample-catalysts (b, e), the corresponding extracted Tafel plots (c, f) and the required overpotentials to reaching the current densities of 10, 20 and 50 mA cm⁻² (d, g) in SSW and ASW, respectively

Table 5. Summarized electrochemical data of the investigated catalysts toward HER in simulated seawater, SSW (1.0 M KOH + 0.5 M NaCl)

Catalysts	j (mA cm ⁻²) in several temperatures at -0.43 V(vs. RHE)						η_{10} (mV) at 25°C	Tafel slope (mV dec ⁻¹)
	25°C	35°C	45°C	55°C	65°C	75°C		
NiCo/Ti	79.7	-	-	-	-	-	267	141
NiMn/Ti	76.7	-	-	-	-	-	195	192
NiMnCo/Ti-1	119.5	131.2	152.5	167.6	183.4	199.9	89	148
NiMnCo/Ti-2	142.5	157.4	170.8	179.3	198.9	209.4	29	188

Comparing the HER activity in SSW, the polarization curves in ASW were also summarized and depicted in Fig. 3e at 25°C temperature, where the recorded current densities were marginally declined. Corresponding Tafel slopes of each electrode were extracted using the LSV plots and demonstrated in Fig. 3f. Tafel slope values of 178, 183, 177, and 144 mV dec⁻¹ were derived for NiMnCo/Ti-2, NiMnCo/Ti-1, NiMn/Ti and NiCo/Ti, respectively (Table-6). The optimized NiMnCo/Ti-2 electrocatalyst demonstrated outstanding catalytic performance in adverse ASW, as the overpotential demand to attain the benchmark current densities of 10, 20, and 50 mA cm⁻² were only 59, 111 and 210 mV, respectively. The comparison bar chart, as presented in Fig. 3g comprehensively proves the astounding performance of NiMnCo/Ti-2 electrocatalyst outperforming respective synthesized electrodes.

Table 6. Summarized electrochemical data of the investigated catalysts toward HER in alkaline seawater, ASW (1.0 M KOH + natural seawater)

Catalysts	j (mA cm ⁻²) in several temperatures at -0.43 V(vs. RHE)						η_{10} (mV) at 25°C	Tafel slope (mV dec ⁻¹)
	25°C	35°C	45°C	55°C	65°C	75°C		
NiCo/Ti	75.8	-	-	-	-	-	270	144
NiMn/Ti	68.8	-	-	-	-	-	205	177
NiMnCo/Ti-1	116.7	130.4	143.4	156.3	167.9	178.9	99	183
NiMnCo/Ti-2	141.1	153.1	172.4	186.7	197.2	207.8	59	178

Table 7. Comparison of electrocatalytic HER performance of as-synthesized electrocatalyst in simulated/alkaline natural seawater with other recently reported non-noble metal-based electrodes.

Electrocatalysts	Electrolyte	Overpotential η_x (mV)	Tafel slope (mV dec ⁻¹)	Stability analysis	Ref.
NiMnCo/Ti-2	SSW*	29 (η_{10})	188	50h@10 mA cm ⁻²	This work
	ASW*	59 (η_{10})	178	50h@10 mA cm ⁻²	
MoMn-NiCoS	SSW	69 (η_{10})	130.3	-	[85]
	ASW	73 (η_{10})	134.4		
Co ₂ Mo ₃ O ₈ /MoO ₂ /NF	ASW	23 (η_{10})	20	100h@100 mA cm ⁻²	[96]
Mo-NiS@NiTe/NF	ASW	57 (η_{10})	57	100h@10 mA cm ⁻²	[97]
Ni@CNTs-Mo _x C/Ni ₂ P	SSW	65.4 (η_{10})	-	50h@50 mA cm ⁻²	[98]
	Seawater	65.9 (η_{10})	-	50h@50 mA cm ⁻²	
(NiFeCoV)S ₂	SSW	96 (η_{10})	-	50h@100 mA cm ⁻²	[99]
	ASW	110 (η_{10})	-	-	
Co-P@NN	SSW	55 (η_{10})	61.5	2880h@500 mA cm ⁻²	[100]
Mn _{0.25} Ni _{0.75} O	ASW	115 (η_{10})	70	125h@100 mA cm ⁻²	[101]
NC@CrN/Ni	ASW	28 (η_{10})	42	50h@1000 mA cm ⁻²	[102]
CNMRO	ASW	97 (η_{10})	-	24h@50 mA cm ⁻²	[103]
Ni-NiMoO ₄ /NF	ASW	27 (η_{10})	25.2	120h@100 mA cm ⁻²	[104]
Mo _x -Ni _{0.85} Se/MoSe ₂	SSW	110 (η_{10})	86.19	80h@20 mA cm ⁻²	[105]
NiFe@BNGC-700	SSW	297 (η_{50})	-	12h@50 mA cm ⁻²	[106]
	ASW	298 (η_{50})	-	12h@50 mA cm ⁻²	
Co-NiP@VP/NF	ASW	164 (η_{100})	65.41	-	[107]
(FeCoCu) ₃₀ (Al ₇₀ Mo ₃₀) ₇₀	SSW	137.14 (η_{100})	46.66	100h@100 mA cm ⁻²	[108]
	ASW	137.54 (η_{100})	49.08	250h@ η =296 mV	
S-NiMoO ₄ @NiFe-LDH	SSW	170 (η_{100})	69	20h	[109]

* SSW - Simulated Seawater; *ASW - Alkaline Seawater

Furthermore, the electrochemically active surface area (ECSA) of the synthesized 3D NiMnCo/Ti-2 electrocatalyst was determined from the measurements of double layer capacitance (C_{dl}) by recording CV curves in the 1 M KOH solution at various scan rates (5-50 mV s⁻¹) in the non-faradaic region (Figure 4).

The charging current, I_c , of the electrodes at each scan rate was determined from the CVs via Equation (2):

$$I_c [A] = (I_{anodic} - I_{cathodic})_{OCP} \quad (2)$$

C_{dl} values were evaluated by plotting a graph of charging current vs. scan rate and calculating the slope, as shown by Eq. (3):

$$\text{Slope} = C_{dl} [F] = \Delta I_c [A] / \Delta v [V s^{-1}] \quad (3)$$

Subsequently, the ECSA value for optimized NiMnCo/Ti-2 electrocatalyst was calculated using the specific capacitance (C_s) value of $40 \mu F cm^{-2}$ [75] and Eq. (4):

$$\text{ECSA} [cm^2] = C_{dl} [\mu F] / C_s [\mu F cm^{-2}] \quad (4)$$

C_{dl} was found to be 11.88 mF and the calculated ECSA value for NiMnCo/Ti-2 was $297 cm^2$, which is significantly larger than the geometric area of the catalyst. The NiMnCo/Ti-2 catalyst exhibited a high surface area, indicative of a high number of active sites and, consequently, significant electrocatalytic activity for HER.

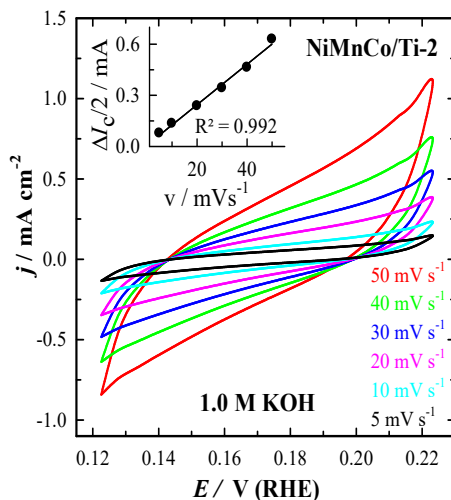


Figure 4. CVs of NiMnCo/Ti-2 in N_2 -saturated 1 M KOH in the non-faradaic potential region at different scan rates. The inset represents capacitive current as a function of scan rate.

4.3 Electrocatalytic stability studies for HER

The stability of electrocatalysts is crucial because it affects not only the efficiency but also the long-term economic viability, cost-effectiveness and scalability of industrial applications via electrochemical processes. As the direct electrolysis of seawater as a hydrogen source offers significant financial and environmental benefits compared to freshwater, seawater splitting faces major challenges due to the complex and harsh electrolyte conditions, including high salinity, the presence of chloride ions (Cl^-), and other impurities leading to catalyst deactivation. This can seriously contribute to compromise the long-term durability of the electrode materials due to surface passivation and leaching. A stable catalyst ensures the desired reactions to take place at a consistent rate for an extended period of time. Hence, the catalysts' activity and selectivity should be maintained under reaction conditions for a longer time span without substantial degradation or deactivation.

To address this critical factor and to evaluate the applicability of as-synthesized electrocatalysts for practical use with enhanced longevity, the stability of the optimized NiMnCo/Ti-2 catalyst was investigated by long-time operation assessments under all three reaction conditions. The durability of the optimized NiMnCo/Ti-2 electrocatalyst was evaluated by conducting long-time chronopotentiometry (CP) at a fixed current density of 10 mA cm^{-2} and chronoamperometry (CA) at a constant potential of -0.23 V (vs. RHE) for 50 hours at 25°C . Nevertheless, a multi-step CP analysis with current densities ranging from 20 mA cm^{-2} to 100 mA cm^{-2} was also carried out in 1.0 M KOH and simulated seawater for 18 hours to prove the robust nature, sustainable durability and suitability of the synthesized catalyst for practical seawater-splitting applications. The findings as demonstrated in Fig. 5a, the NiMnCo/Ti-2 electrocatalyst exhibits superior electrocatalytic stability by chronopotentiometric analysis at a constant current density of 10 mA cm^{-2} for 50 hours in an alkaline media, ASW and SSW. It is noteworthy that the CP investigation performed in SSW results in an insignificant potential decline of only 3.7 mV after 50 hours of continuous operation, whereas a modest 8.2 mV and 20.9 mV potential fluctuation were recorded in 1.0 M KOH and ASW electrolyte, respectively.

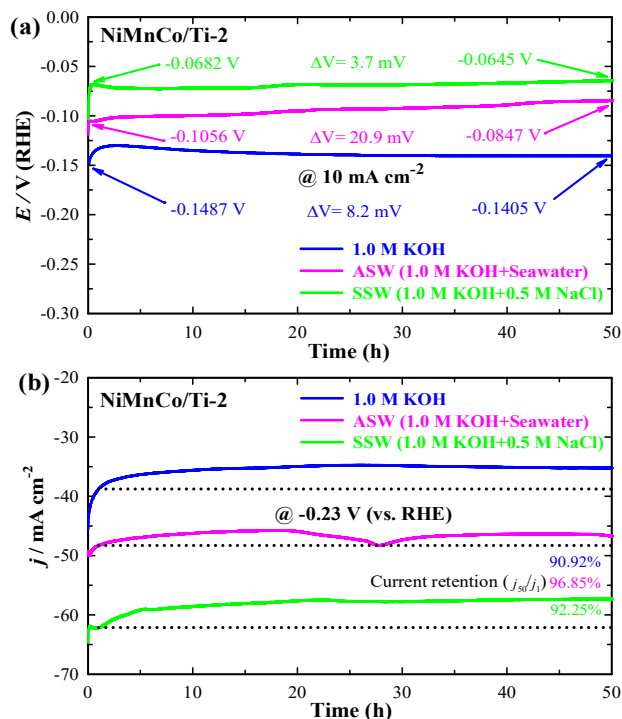


Figure 5. Chronopotentiometry (a) and chronoamperometry (b) plots of optimized NiMnCo/Ti-2 electrocatalyst at a constant current density of 10 mA cm^{-2} and at a fixed potential of -0.23 V (vs. RHE) for 50 h in 1.0 M KOH, alkaline seawater and simulated seawater, respectively

Fig. 5b illustrates the chronoamperometric investigations of the optimized NiMnCo/Ti-2 electrocatalyst at a static potential of -0.23 V (vs RHE) for 50 hours under all three investigating electrolytes where ca. 91-97% current densities retained throughout the investigations. Such negligible decline in current densities indicates that the electrocatalyst remained in good structural conditions without major corrosion and degradation even under aggressive seawater media.

Finally, the long-term durability of prepared optimized NiMnCo/Ti-2 electrocatalyst was investigated by multi-step chronopotentiometric investigations under alkaline media (Figure 6a) and SSW electrolyte (Figure 6b) to examine the longevity and scope of practical use for seawater electrolysis. These chronopotentiometric investigations were carried out by applying variable current densities from 20 mA cm^{-2} to 100 mA cm^{-2} for 18 hours in consecutive ascending-descending order. The recorded results also vividly highlight the exceptional long-term stability

and structural integrity of the optimized NiMnCo/Ti-2 electrocatalyst in these comparably adverse conditions.

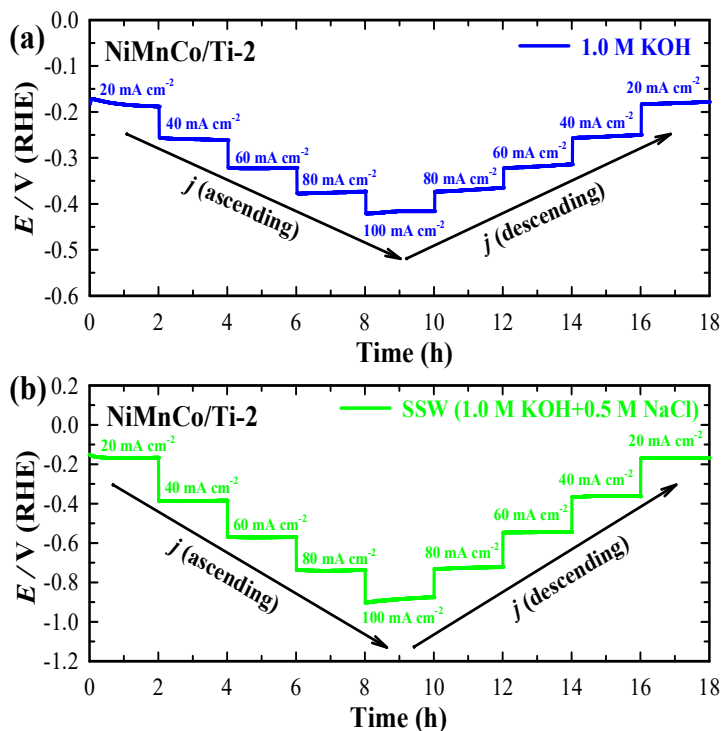


Figure 6. A multi-step chronopotentiometric analysis in 1.0 M KOH (a) and SSW (b) with variable current densities from 20 mA cm⁻² to 100 mA cm⁻² for 18 hours

5. Conclusion

In conclusion, we have successfully fabricated an affordable (Ni–Mn–Co) electrocatalyst via a simple one-step electrodeposition method on a 3D titanium substrate using the dynamic hydrogen bubble template (DHBT) technique. The synthesized NiMnCo/Ti electrodes demonstrated excellent electrocatalytic activity for HER in alkaline, simulated seawater (SSW), and alkaline natural seawater (ASW) environments, achieving low overpotentials and high current densities. SEM analysis revealed a unique cauliflower curd-shaped microspherical architecture with average grain diameters ranging from 7–14 μ m. Both NiMnCo/Ti-1 and NiMnCo/Ti-2 electrocatalysts outperformed their bimetallic counterparts, with the optimized NiMnCo/Ti-2 showing the best performance achieving a benchmark current density of 10 mA cm⁻² with ultra-low overpotentials

of 29, 59, and 66 mV in SSW, ASW, and 1.0 M KOH, respectively. Moreover, it required only 195, 210, and 277 mV to reach 50 mA cm^{-2} in the respective electrolytes.

This enhanced HER activity can be attributed to the significantly larger electrochemically active surface area (ECSA) of the 3D NiMnCo/Ti-2 electrode, which likely provides a high density of active sites. Additionally, the NiMnCo/Ti-1 electrocatalyst also exhibited promising HER activity with low overpotentials of 99 mV (1.0 M KOH and ASW) and 89 mV (SSW) to achieve 10 mA cm^{-2} .

Long-term stability was confirmed by chronoamperometric (CA) and chronopotentiometric (CP) tests over 50 hours in all three electrolytes. The NiMnCo/Ti-2 electrode retained over 90% of its initial current, with only minor potential fluctuations (ca. 4-21 mV). In alkaline seawater, the electrode exhibited slight instability and moderate fluctuations during CA and CP measurements, likely due to the formation of white precipitates on the electrode surface and the presence of contaminants in the electrolyte. Nevertheless, long-term durability was preserved throughout the study, despite these challenges. Notably, the electrocatalyst maintained excellent stability during multi-step chronopotentiometry under high and variable current densities over extended operation in both 1.0 M KOH and SSW media.

These findings demonstrate that the as-fabricated NiMnCo/Ti-2 electrode is a highly efficient, low-cost, and durable HER electrocatalyst, showing great potential for practical seawater and freshwater electrolysis. Its excellent catalytic activity and long-term operational stability make it a strong candidate for large-scale green hydrogen production from real seawater.

CRedit authorship contribution statement

Sukomol Barua: Writing – original draft, Methodology, Investigation, Formal analysis.
Aldona Balčiūnaitė: Writing – review & editing, Writing – original draft, Supervision, Conceptualization. **Daina Upskuvienė:** Methodology, Investigation. **Jūrate Vaičiūnienė:** Methodology, Investigation. **Loreta Tamašauskaitė-Tamašiūnaitė:** Visualization, Supervision, Data curation. **Eugenijus Norkus:** Writing – review & editing, Conceptualization.

Declaration of competing interest

The authors declare that they have no known competing financial interests or personal relationships that could have appeared to influence the work reported in this paper.

References

- [1] Q. Hassan, A.Z. Sameen, H.M. Salman, M. Jaszczur and A.K. Al-Jiboory, Hydrogen energy future: Advancements in storage technologies and implications for sustainability. *J Energy Storage*, 2023, **72**, 108404. [DOI:10.1016/j.est.2023.108404](https://doi.org/10.1016/j.est.2023.108404)
- [2] B.A. Yusuf, W. Yaseen, M.Xie, R.S. Zayyan, A.I. Muhammad, R. Nankya, J. Xie and Y. Xu, Recent advances in understanding and design of efficient hydrogen evolution electrocatalysts for water splitting: A comprehensive review. *Adv. Colloid Interface Sci.*, 2022, **311**, 102811. [DOI:10.1016/j.cis.2022.102811](https://doi.org/10.1016/j.cis.2022.102811)
- [3] H.M. Zhang and J Li, Strategies for overcoming seawater adverse effects on cathodic hydrogen evolution reaction electrocatalysts. *Fuel*, 2024, **367**, 131505., [DOI:10.1016/j.fuel.2024.131505](https://doi.org/10.1016/j.fuel.2024.131505)
- [4] J.Y. Loh, J.J. Foo, F.M. Yap, H. Liang and W.J. Ong. Unleashing the versatility of porous nanoarchitectures: A voyage for sustainable electrocatalytic water splitting. *Chin. J Catal.*, 2024, **58**, 37-85. [DOI:10.1016/S1872-2067\(23\)64581-4](https://doi.org/10.1016/S1872-2067(23)64581-4)
- [5] H. Sun, X. Xu, H. Kim, W Jung, W. Zhou and Z. Shao, Electrochemical water splitting: Bridging the gaps between fundamental research and industrial applications. *Energy Environ. Mater.*, 2022, e12441. [DOI:10.1002/eeem2.12441](https://doi.org/10.1002/eeem2.12441)
- [6] Y. Gong, J. Yao, P. Wang, Z. Li, H. Zhou and C. Xu, Perspective of hydrogen energy and recent progress in electrocatalytic water splitting. *Chin. J. Chem. Eng.*, 2022, **43**, 282-296. [DOI:10.1016/j.cjche.2022.02.010](https://doi.org/10.1016/j.cjche.2022.02.010)
- [7] X.W. Lv, W.W. Tian and Z.Y. Yuan, Recent advances in high-efficiency electrocatalytic water splitting systems. *Electrochem. Energy Rev.*, 2023, **6**, 23. [DOI:10.1007/s41918-022-00159-1](https://doi.org/10.1007/s41918-022-00159-1)
- [8] J.N. Bamba, A.T. Dumlao, R.M. Lazaro, D.D. Matienzo and J. Ocon, Green Hydrogen from Seawater Electrolysis: Recent Developments and Future Perspectives. *Curr. Opin. Electrochem.*, 2024, **48**, 101592. [DOI:10.1016/j.coelec.2024.101592](https://doi.org/10.1016/j.coelec.2024.101592)

- [9] F. Yang, Y. Luo, Q. Yu, Z. Zhang, S. Zhang, Z. Liu, W. Ren, H.M. Cheng, J. Li and B. Liu, A durable and efficient electrocatalyst for saline water splitting with current density exceeding 2000 mA cm⁻². *Adv. Funct. Mater.*, 2021, **31**, 2010367. DOI:10.1002/adfm.202010367
- [10] S. van Renssen, The hydrogen solution? *Nat. Clim. Chang.*, 2020 **10**, 799-801. DOI:10.1038/s41558-020-0891-0
- [11] IEA (2019), The Future of Hydrogen, IEA, Paris. Available at: <https://www.iea.org/reports/the-future-of-hydrogen>
- [12] British Petroleum (2021), Statistical review of world energy 2021. Available at: <https://www.bp.com/content/dam/bp/business-sites/en/global/corporate/pdfs/energy-economics/statistical-review/bp-stats-review-2021-full-report.pdf>
- [13] X.P. Li, C. Huang, W.K. Han, T. Ouyang, T. and Z.Q. Liu, Transition metal-based electrocatalysts for overall water splitting. *Chin Chem. Lett.*, 2021 **32**, 2597-2616. DOI:10.1016/j.cclet.2021.01.047
- [14] IEA (2021), Global Hydrogen Review 2021, IEA, Paris. Available at: <https://www.iea.org/reports/global-hydrogen-review-2021>
- [15] Y. Robiou du Pont, M.L. Jeffery, J. Gütschow, J. Rogelj, P. Christoff and M. Meinshausen, Equitable mitigation to achieve the Paris Agreement goals. *Nat. Clim. Chang.*, 2017, **7**, 38-43. DOI:10.1038/nclimate3186
- [16] P. Woods, H. Bustamante, K.F. Aguey-Zinsou, The hydrogen economy - Where is the water? *Energy Nexus*, 2022, **7**, 100123. DOI:10.1016/j.nexus.2022.100123
- [17] M. Chatenet, B.G. Pollet, D.R. Dekel, F. Dionigi, J. Deseure, P. Millet, R.D. Braatz, M.Z. Bazant, M. Eikerling, I. Staffell, P. Balcombe, Y. Shao-Horn and H. Schäfer, Water electrolysis: from textbook knowledge to the latest scientific strategies and industrial developments. *Chem. Soc. Rev.*, 2022, **51**, 4583-4762. DOI:10.1039/D0CS01079K
- [18] IEA (2021), Net Zero by 2050: a roadmap for the global energy sector, IEA, Paris. Available at: <https://www.iea.org/reports/net-zero-by-2050>
- [19] U.S. Department of Energy, US National Clean Hydrogen Strategy and Roadmap. Available at: https://www.hydrogen.energy.gov/docs/hydrogenprogramlibraries/pdfs/us-national-clean-hydrogen-strategy-roadmap.pdf?sfvrsn=c425b44f_5
- [20] U.S. Department of Energy (DOE). Available at: <https://www.energy.gov/topics/hydrogen-shot>
- [21] P. Kumar, A. Date, N. Mahmood, R.K. Das and B. Shabani, Freshwater supply for hydrogen production: An underestimated challenge. *Int J Hydrogen Energy*, 2024, **78**, 202-217. DOI:10.1016/j.ijhydene.2024.06.257
- [22] R.R. Beswick, A.M. Oliveira and Y. Yan, Does the green hydrogen economy have a water problem? *ACS Energy Lett.*, 2021, **6**, 3167-3169. DOI:10.1021/acsenenergylett.1c01375
- [23] A.M. Oliveira, R.R. Beswick and Y. Yan, A green hydrogen economy for a renewable energy society. *Curr. Opin. Chem. Eng.*, 2021, **33**, 100701. DOI:10.1016/j.coche.2021.100701

- [24] S. Jiao, X. Fu, S. Wang and Y. Zhao, Perfecting electrocatalysts via imperfections: towards the large-scale deployment of water electrolysis technology. *Energy Environ. Sci.*, 2021, **14**, 1722-1770. [DOI:10.1039/D0EE03635H](https://doi.org/10.1039/D0EE03635H)
- [25] Y. Xu, C. Wang, Y. Huang and J. Fu, Recent advances in electrocatalysts for neutral and large-current-density water electrolysis. *Nano Energy*, 2021, **80**, 105545. [DOI:10.1016/j.nanoen.2020.105545](https://doi.org/10.1016/j.nanoen.2020.105545)
- [26] Z. Li, X. Zhang, C. Ou, Y. Zhang, W. Wang, S. Dong and X. Dong, Transition metal-based self-supported anode for electrocatalytic water splitting at a large current density. *Coord. Chem. Rev.*, 2023, **495**, 215381. [DOI:10.1016/j.ccr.2023.215381](https://doi.org/10.1016/j.ccr.2023.215381)
- [27] Q. Wen, Y. Zhao, Y. Liu, H. Li and T. Zhai, Ultrahigh-current-density and long-term-durability electrocatalysts for water splitting. *Small*, 2022, **18**, 2104513. [DOI:10.1002/smll.202104513](https://doi.org/10.1002/smll.202104513)
- [28] S. Chen, Y. Zhuo, X. Wang, S. Li, J. Lu, D. Liu, H. Pan and Z. Wang, Advances of layered double hydroxide electrocatalysts for high-current-density alkaline water/seawater splitting. *Coord. Chem. Rev.*, 2024, **510**, 215832. [DOI:10.1016/j.ccr.2024.215832](https://doi.org/10.1016/j.ccr.2024.215832)
- [29] S. Wang, P. Yang, X. Sun, H. Xing, J. Hu, P. Chen, Z. Ciu, W. Zhu and Z. Ma, Synthesis of 3D heterostructure Co-doped Fe₂P electrocatalyst for overall seawater electrolysis. *Appl. Catal. B: Environ.*, 2021, **297**, 120386. [DOI:10.1016/j.apcatb.2021.120386](https://doi.org/10.1016/j.apcatb.2021.120386)
- [30] Y.S. Park, J. Lee, M.J. Jang, J. Yang, J. Jeong, J. Park, Y. Kim, M.H. Seo, Z. Chen and S.M. Choi, High-performance anion exchange membrane alkaline seawater electrolysis. *J Mater. Chem. A*, 2021, **9**, 9586-9592. [DOI:10.1039/D0TA12336F](https://doi.org/10.1039/D0TA12336F)
- [31] Z. Zhang, H. Yang, F. Zhang, M. Zou, J.C. Li, L. Zhang, P.X. Hou, C. Shi, L. Zhang, H.M. Cheng and C. Liu, Green and efficient electrolysis of seawater using carbon nanotube-based hybrid films. *Nano Energy*, 2024, **123**, 109356. [DOI:10.1016/j.nanoen.2024.109356](https://doi.org/10.1016/j.nanoen.2024.109356)
- [32] S. Dresp, F. Dionigi, M. Klingenhof and P. Strasser, Direct electrolytic splitting of seawater: opportunities and challenges. *ACS Energy Lett.*, 2019, **4**, 933-942. [DOI:10.1021/acsenergylett.9b00220](https://doi.org/10.1021/acsenergylett.9b00220)
- [33] W. Tong, M. Forster, F. Dionigi, S. Dresp, R. Sadeghi Erami, P. Strasser, A.J. Cowan and P. Farràs, Electrolysis of low-grade and saline surface water. *Nat. Energy*, 2020, **5**, 367-377. [DOI:10.1038/s41560-020-0550-8](https://doi.org/10.1038/s41560-020-0550-8)
- [34] F. Dionigi, T. Reier, Z. Pawolek, M. Gliech and P. Strasser, Design criteria, operating conditions, and nickel-iron hydroxide catalyst materials for selective seawater electrolysis. *ChemSusChem*, 2016, **9**, 962-972. [DOI:10.1002/cssc.201501581](https://doi.org/10.1002/cssc.201501581)
- [35] J. Liu, S. Duan, H. Shi, T. Wang, X. Yang, Y. Huang, G. Wu and Q. Li, Rationally designing efficient electrocatalysts for direct seawater splitting: challenges, achievements, and promises. *Angew. Chem.*, 2022, **134**, e202210753. [DOI:10.1002/ange.202210753](https://doi.org/10.1002/ange.202210753)
- [36] S. Song, Y. Wang, X. Tian, F. Sun, X. Liu, Y. Yuan, W. Li and J. Zang, S-modified NiFe-phosphate hierarchical hollow microspheres for efficient industrial-level seawater electrolysis. *J Colloid Interface Sci.*, 2023, **633**, 668-678. [DOI:10.1016/j.jcis.2022.11.113](https://doi.org/10.1016/j.jcis.2022.11.113)
- [37] R.F. Service, Seawater splitting could help green hydrogen grow. *Science*, 2023, **379**, 1075. [DOI:10.1126/science.adh7973](https://doi.org/10.1126/science.adh7973)

- [38] F. Sun, J. Qin, Z. Wang, M. Yu, X. Wu, X. Sun and J. Qiu, Energy-saving hydrogen production by chlorine-free hybrid seawater splitting coupling hydrazine degradation. *Nat. Commun.*, 2021, **12**, 4182. [DOI:10.1038/s41467-021-24529-3](https://doi.org/10.1038/s41467-021-24529-3)
- [39] H. Xu, Y. Zhao, G. He and H. Chen, Race on engineering noble metal single-atom electrocatalysts for water splitting. *Int. J. Hydrogen Energy*, 2022, **47**, 14257-14279. [DOI:10.1016/j.ijhydene.2022.02.152](https://doi.org/10.1016/j.ijhydene.2022.02.152)
- [40] N. Nie, D. Zhang, Z. Wang, S. Ge, Y. Gu, B. Yang, J. Lai and L. Wang, Stable p-block metals electronic perturbation in PtM@CNT (M= Ga, In, Pb and Bi) for acidic seawater hydrogen production at commercial current densities. *Appl. Catal. B: Environ.*, 2023, **322**, 122100. [DOI:10.1016/j.apcatb.2022.122100](https://doi.org/10.1016/j.apcatb.2022.122100)
- [41] J.N. Hansen, H. Prats, K.K. Toudahl, N.M. Secher, K. Chan, J. Kibsgaard and I. Chorkendorff, Is there anything better than Pt for HER? *ACS Energy Lett.*, 2021, **6**, 1175-1180. [DOI:10.1021/acsenergylett.1c00246](https://doi.org/10.1021/acsenergylett.1c00246)
- [42] S. Park, Y.L. Lee, Y. Yoon, S.Y. Park, S. Yim, W. Song, S. Myung, K.S. Lee, H. Chang, S.S. Lee and K.S. An, Reducing the high hydrogen binding strength of vanadium carbide MXene with atomic Pt confinement for high activity towards HER. *Appl. Catal. B: Environ.*, 2022, **304**, 120989. [DOI:10.1016/j.apcatb.2021.120989](https://doi.org/10.1016/j.apcatb.2021.120989)
- [43] X. Guo, H. Zhang, Z. Shen, X. Liu, W. Xia, M. Ma and D. Cao, Construction and prospect of noble metal-based catalysts for proton exchange membrane water electrolyzers. *Small Struct.*, 2023, **4**, 2300081. [DOI:10.1002/ssstr.202300081](https://doi.org/10.1002/ssstr.202300081)
- [44] S.C. Jesudass, S. Surendran, D.J. Moon, S. Shanmugapriya, J.Y. Kim, G. Janani, K. Veeramani, S. Mahadik, I.G. Kim, P. Jung, G. Kwon, K. Jin, J.K. Kim, K. Hong, Y.I. Park, T.H. Kim, J. Heo and U. Sim, Defect engineered ternary metal spinel-type Ni-Fe-Co oxide as bifunctional electrocatalyst for overall electrochemical water splitting. *J. Colloid Interface Sci.*, 2024, **663**, 566-576. [DOI:10.1016/j.jcis.2024.02.042](https://doi.org/10.1016/j.jcis.2024.02.042)
- [45] Z. Luo, Q. Peng, Z. Huang, L. Wang, Y. Yang, J. Dong, T.T. Isimjan and X. Yang, Fine-tune d-band center of cobalt vanadium oxide nanosheets by N-doping as a robust overall water splitting electrocatalyst. *J. Colloid Interface Sci.*, 2023, **629**, 111-120. [DOI:10.1016/j.jcis.2022.09.069](https://doi.org/10.1016/j.jcis.2022.09.069)
- [46] Z. Gao, T. Wang, Z. Zeng, Z. Guo, X. Xu, Y. Li, L. Lin, R. Jia and S. Han, Effect of oxygen vacancy on electrochemical performance of NiCo-layered double oxides as water splitting electrocatalyst. *J. Alloys Compd.*, 2023, **963**, 171273. [DOI:10.1016/j.jallcom.2023.171273](https://doi.org/10.1016/j.jallcom.2023.171273)
- [47] S. Ge, X. Shen, J. Gao, K. Ma, H. Zhao, R. Fu, C. Feng, Y. Zhao, Q. Jiao and H. Li, Synergy of Mo doping and heterostructures in FeCo₂S₄@Mo-NiCo LDH/NF as durable and corrosion-resistant bifunctional electrocatalyst towards seawater electrolysis at industrial current density. *Chem. Eng. J.*, 2024, **485**, 150161. [DOI:10.1016/j.cej.2024.150161](https://doi.org/10.1016/j.cej.2024.150161)
- [48] Y. Ma, L. Li, Y. Zhang, N. Jian, H. Pan, J. Deng and J. Li, Nickel foam supported Mn-doped NiFe-LDH nanosheet arrays as efficient bifunctional electrocatalysts for methanol oxidation and hydrogen evolution. *J. Colloid Interface Sci.*, 2024, **663**, 971-980. [DOI:10.1016/j.jcis.2024.02.191](https://doi.org/10.1016/j.jcis.2024.02.191)

- [49] A.R. Manchuri, K.C. Devarayapalli, B. Kim, Y. Lim and D.S. Lee, Ti_3C_2 MXene nanosheets integrated cobalt-doped nickel hydroxide heterostructured composite: An efficient electrocatalyst for overall water-splitting. *Green Energy Environ.*, 2024, DOI:10.1016/j.gee.2024.08.006
- [50] M. Khairy and K.G. Mahmoud, In-situ growth of nanostructured nickel sulphides on nickel foam platform for boosting the electrocatalytic activity of overall water splitting. *J. Alloys Compd.*, 2023, **935**, 168056. DOI:10.1016/j.jallcom.2022.168056
- [51] K. Premnath, J. Madhavan, S. Prasad, M.J. Aljaafreh, M.S. AlSalhi and S.P. Loke, Ultra-efficient, low-cost and carbon-supported transition metal sulphide as a platinum-free electrocatalyst towards hydrogen evolution reaction at alkaline medium. *Int. J. Hydrogen Energy*, 2022, **47**, 41974-41983. DOI:10.1016/j.ijhydene.2021.09.120
- [52] Y. Lu, Z. Li, Y. Xu, L. Tang, S. Xu, D. Li, J. Zhu and D. Jiang, Bimetallic Co-Mo nitride nanosheet arrays as high-performance bifunctional electrocatalysts for overall water splitting. *Chem. Eng. J.*, 2021, **411**, 128433. DOI:10.1016/j.cej.2021.128433
- [53] Q. Li, P. Yang, Y. Liu, W. Xiao, Z. Xiao, G. Xu, L. Wang, F. Liu and Z. Wu, In-situ construction of pomegranate-like nickel-vanadium nitride for hydrogen production through urea-assisted water-splitting. *J. Alloys Compd.*, 2023, **968**, 171861. DOI:10.1016/j.jallcom.2023.171861
- [54] Li, L. Zhang, F. Wang, L. Zhang, L. Li, H. Chen and Z. Wei, Rational design of porous Ni-Co-Fe ternary metal phosphides nanobricks as bifunctional electrocatalysts for efficient overall water splitting. *Appl. Catal. B: Environ.*, 2022, **310**, 121353. DOI:10.1016/j.apcatb.2022.121353
- [55] X. Wang, C. Wang, F. Lai, H. Sun, N. Yu and B. Geng, Self-supported CoFe-P nanosheets as a bifunctional catalyst for overall water splitting. *ACS Appl. Nano Mater.*, 2021, **4**, 12083-12090. DOI:10.1021/acsanm.1c02607
- [56] Y. Yang, Z. Lin, S. Gao, J. Su, Z. Lun, G. Xia, J. Chen, R. Zhang and Q. Chen, Tuning electronic structures of non-precious ternary alloys encapsulated in graphene layers for optimizing overall water splitting activity. *ACS Catal.*, 2017, **7**, 469-479. DOI:10.1021/acscatal.6b02573
- [57] C. Zhang, Z. Xu, Y. Yu, A. Long, X. Ge, Y. Song, Y. An and Y. Gu, Ternary NiMoCo alloys and fluffy carbon nanotubes grown on ZIF-67-derived polyhedral carbon frameworks as bifunctional electrocatalyst for efficient and stable overall water splitting. *Electrochim. Acta*, 2022, **424**, 140613. DOI:10.1016/j.electacta.2022.140613
- [58] F. Yang, Z. Li, F. Zhu, X. Chen, S. Ge, F. Yin, F.F. Yang, R. Yang, Y. Liu, L. Gao, Q. Wang, R. Feng, B. Jin and P. Hu, Three-dimensional multi-channel structure NiCo alloy used for boosting efficient overall water splitting. *Fuel*, 2024, **364**, 131119. DOI:10.1016/j.fuel.2024.131119
- [59] F. Arshad, T. ul Haq, A. Khan, Y. Haik, I. Hussain and F. Sher, Multifunctional porous NiCo bimetallic foams towards water splitting and methanol oxidation-assisted hydrogen production. *Energy Convers. Manag.*, 2022, **254**, 115262. DOI:10.1016/j.enconman.2022.115262
- [60] G.B. Darband, M. Maleki, A. Toghraci and S. Shanmugam, Electrodeposition of self-supported transition metal phosphides nanosheets as efficient hydrazine-assisted electrolytic hydrogen production catalyst. *Int. J. Hydrogen Energy*, 2023, **48**, 4253-4263. DOI:10.1016/j.ijhydene.2022.10.246

- [61] C.L. Huang, X.F. Chuah, C.T. Hsieh and S.Y. Lu, NiFe alloy nanotube arrays as highly efficient bifunctional electrocatalysts for overall water splitting at high current densities. *ACS Appl. Mater. Interfaces*, 2019, **11**, 24096-24106. [DOI:10.1021/acsami.9b05919](https://doi.org/10.1021/acsami.9b05919)
- [62] Z. Chen, C. Zhu, M. Cai, X. Yi and J. Li, Growth and morphology tuning of ordered nickel nanocones routed by one-step pulse electrodeposition. *Appl. Surf. Sci.*, 2020, **508**, 145291. [DOI:10.1016/j.apsusc.2020.145291](https://doi.org/10.1016/j.apsusc.2020.145291)
- [63] Z.M. Kazemi, A.S. Rouhaghdam, G.B. Darband, M. Maleki, D. Han and S. Shanmugam, Ultra-fast electrochemical preparation of Ni-Cu-Fe nano-micro dendrite as a highly active and stable electrocatalyst for overall water splitting. *Electrochim. Acta*, 2023, **456**, 142468. [DOI:10.1016/j.electacta.2023.142468](https://doi.org/10.1016/j.electacta.2023.142468)
- [64] Y. Zhang, W. Cui, L. Li, C. Zhan, F. Xiao and X. Quan, Effect of aligned porous electrode thickness and pore size on bubble removal capability and hydrogen evolution reaction performance. *J. Power Sources*, 2023, **580**, 233380. [DOI:10.1016/j.jpowsour.2023.233380](https://doi.org/10.1016/j.jpowsour.2023.233380)
- [65] C.C. Weber, J.A. Wrubel, L. Gubler, G. Bender, S. De Angelis and F.N. Büchi, How the porous transport layer interface affects catalyst utilization and performance in polymer electrolyte water electrolysis. *ACS Appl. Mater. Interfaces*, 2023, **15**, 34750-34763. [DOI:10.1021/acsami.3c04151](https://doi.org/10.1021/acsami.3c04151)
- [66] L. Yang, L. Wang, C. Xing, C. Wang, S. Chang and Z. Zhao, Bubble-template assisted fast electrochemical deposition of 3-D ternary Ni-Cu-Co alloy as promising catalyst for electrochemical overall water splitting. *Fuel*, 2024, **357**, 129890. [DOI:10.1016/j.fuel.2023.129890](https://doi.org/10.1016/j.fuel.2023.129890)
- [67] H. Jiang, N. Cong, H. Jiang, M. Tian, Z. Xie, H. Fang, J. Han, Z. Ren and Y. Zhu, Dynamic hydrogen bubble template electrodeposition of Ru on amorphous Co support for electrochemical hydrogen evolution. *Int. J. Hydrogen Energy*, 2023, **48**, 21599-21609. [DOI:10.1016/j.ijhydene.2023.03.077](https://doi.org/10.1016/j.ijhydene.2023.03.077)
- [68] E. Hassanizadeh, M. Mirjalili, M.H. Moayed and G.B. Darband, Ultra-fast electrodeposition of dynamic hydrogen bubble template nickel sulfide on a porous copper layer as an electrocatalyst toward hydrogen evolution reaction. *Int. J. Hydrogen Energy*, 2024, **55**, 729-739. [DOI:10.1016/j.ijhydene.2023.10.247](https://doi.org/10.1016/j.ijhydene.2023.10.247)
- [69] Y. Qian, M. Hu, L. Li, S. Cao, J. Xu, J. Hong, X. Liu, J. Xu and C. Guo, Dynamically assisted electrodeposition by hydrogen bubbles on carbonized wood: A NiFeCo nanoflower electrocatalyst for efficient hydrogen evolution. *Fuel*, 2024, **361**, 130653. [DOI:10.1016/j.fuel.2023.130653](https://doi.org/10.1016/j.fuel.2023.130653)
- [70] H. Qu, Y. Ma, X. Li, Y. Duan, Y. Li, F. Liu, B. Yu, M. Tian, Z. Li, Y. Yu, B. Li, Z. Lv and L. Wang, Ternary alloy (FeCoNi) nanoparticles supported on hollow porous carbon with defects for enhanced oxygen evolution reaction. *J. Colloid Interface Sci.*, 2023, **645**, 107-114. [DOI:10.1016/j.jcis.2023.04.122](https://doi.org/10.1016/j.jcis.2023.04.122)
- [71] R. Ge, J. Huo, Y. Li, T. Liao, J. Zhang, M. Zhu, T. Ahamad, S. Li, H. Liu, L. Feng and W. Li, Electrocatalyst nanoarchitectonics with molybdenum-cobalt bimetallic alloy encapsulated in nitrogen-doped carbon for water splitting reaction. *J. Alloys Compd.*, 2022, **904**, 164084. [DOI:10.1016/j.jallcom.2022.164084](https://doi.org/10.1016/j.jallcom.2022.164084)

- [72] Q. Liu, Z. Yan, J. Gao and E. Wang, Surface-oxidized iron-cobalt-nickel alloy with continuous variable composition for hydrogen and oxygen evolution reaction. *ACS Sustain. Chem. Eng.*, 2022, **10**, 14926-14934. [DOI:10.1021/acssuschemeng.2c04892](https://doi.org/10.1021/acssuschemeng.2c04892)
- [73] S. Barua, A. Balčiūnaitė, J. Vaičiūnienė, L. Tamašauskaitė-Tamašiūnaitė and E. Norkus, Bimetallic 3D Nickel-Manganese/Titanium Bifunctional Electrocatalysts for Efficient Hydrogen and Oxygen Evolution Reaction in Alkaline and Acidic Media. *Coatings*, 2023, **13**, 1102. [DOI:10.3390/coatings13061102](https://doi.org/10.3390/coatings13061102)
- [74] S. Barua, A. Balčiūnaitė, D. Upskuvienė, J. Vaičiūnienė, L. Tamašauskaitė-Tamašiūnaitė and E. Norkus, 3D Nickel-Manganese bimetallic electrocatalysts for an enhanced hydrogen evolution reaction performance in simulated seawater/alkaline natural seawater. *Int. J. Hydrogen Energy*, 2024, **79**, 1490-1500. [DOI:10.1016/j.ijhydene.2024.07.131](https://doi.org/10.1016/j.ijhydene.2024.07.131)
- [75] A. Zabelaitė, A. Balčiūnaitė, D. Upskuvienė, D. Šimkūnaitė, R. Levinas, G. Niaura, J. Vaičiūnienė, V. Jasulaitienė, L. Tamašauskaitė-Tamašiūnaitė, E. Norkus. Investigation of hydrogen and oxygen evolution on cobalt-nanoparticles-supported graphitic carbon nitride. *Materials*, 2023, **16**, 5923. [DOI:10.3390/ma16175923](https://doi.org/10.3390/ma16175923)
- [76] B. Yao, W. Zhang, L. She, W. Ren, L. Hou, Y. Fautrelle, X. Lu, X. Yu and X. Li, Controlled direct electrodeposition of crystalline NiFe/amorphous NiFe-(oxy) hydroxide on NiMo alloy as a highly efficient bifunctional electrocatalyst for overall water splitting. *Chem. Eng. J.*, 2022, **446**, 137420. [DOI:10.1016/j.cej.2022.137420](https://doi.org/10.1016/j.cej.2022.137420)
- [77] H. Wang, Y. Yan, W. Zhang, S. Sun and S. Yao, Preparation of Co(OH)₂@NiFe/NF bifunctional electrocatalyst by electrodeposition for efficient water splitting. *J. Solid State Chem.*, 2023, **323**, 124048. [DOI:10.1016/j.jssc.2023.124048](https://doi.org/10.1016/j.jssc.2023.124048)
- [78] X. Wang, J. Wang, J. Zhang, J. Wei, X. Tong, R. Xu and L. Yang, Ultrafast fabrication of porous NF/Ni for water splitting in alkaline media. *J. Power Sources*, 2024, **621**, 235321. [DOI:10.1016/j.jpowsour.2024.235321](https://doi.org/10.1016/j.jpowsour.2024.235321)
- [79] W. Zhang, Q. Yin, Y. Zhang, S. Peng and Y. Li, Electrodeposited crystalline-amorphous Ni-Ni(OH)₂ electrocatalysts for efficient hydrogen evolution via alkaline water splitting. *J. Alloys Compd.*, 2023, **948**, 169727. [DOI:10.1016/j.jallcom.2023.169727](https://doi.org/10.1016/j.jallcom.2023.169727)
- [80] Y. Shen, P. Wu, C. Wang, W. Yuan, W. Yang and X. Shang, Electrodeposition of amorphous Ni-Fe-Mo composite as a binder-free and high-performance electrocatalyst for hydrogen generation from alkaline water electrolysis. *Int. J. Hydrogen Energy*, 2023, **48**, 33130-33138. [DOI:10.1016/j.ijhydene.2023.03.327](https://doi.org/10.1016/j.ijhydene.2023.03.327)
- [81] L. Yang, L. Huang, Y. Yao and L. Jiao, In-situ construction of lattice-matching NiP₂/NiSe₂ heterointerfaces with electron redistribution for boosting overall water splitting. *Appl. Catal. B: Environ.*, 2021, **282**, 119584. [DOI:10.1016/j.apcatb.2020.119584](https://doi.org/10.1016/j.apcatb.2020.119584)
- [82] X. Wang, X. Xu, Y. Nie, R. Wang and J. Zou, Electronic-state modulation of metallic Co-assisted Co₇Fe₃ alloy heterostructure for highly efficient and stable overall water splitting. *Adv. Sci.*, 2023, **10**, 2301961. [DOI:10.1002/adv.202301961](https://doi.org/10.1002/adv.202301961)
- [83] S. Zhang, C. Tan, R. Yan, X. Zou, FL. Hu, Y. Mi, C. Yan and S. Zhao, Constructing built-in electric field in heterogeneous nanowire arrays for efficient overall water electrolysis. *Angew. Chem. Int. Ed.*, 2023, **62**, e202302795. [DOI:10.1002/anie.202302795](https://doi.org/10.1002/anie.202302795)

- [84] W. Tan, X. Liu, W. Liu, H. He and Y. Yang, Galvanostatic electrodeposition of a self-supported Ni-Se-Lu/NF electrocatalyst for efficient alkaline hydrogen evolution reaction. *Int. J. Hydrogen Energy*, 2024, **80**, 270-279. DOI:10.1016/j.ijhydene.2024.07.151
- [85] HM. Zhang, J. Li, Y. Gao, J. Sun, S. Geng and Y. Meng, High-valence Mo, Mn co-doped amorphous bimetallic sulfide for efficient overall alkaline water/seawater electrolysis. *Fuel*, 2024, **371**, 132111. DOI:10.1016/j.fuel.2024.132111
- [86] R. He, P. Thangasamy, J. Wu, K. Yu, X. Yu, W. Tang, D. Quiroz, D. Alyones, Z. Chen, H. Luo and M. Zhou, Synergistically coupling of trimetallic sulfides on Ni foam as porous self-supported electrodes for alkaline water splitting. *Electrochim. Acta*, 2023, **470**, 143342. DOI:10.1016/j.electacta.2023.143342
- [87] J. Hou, Y. Sheng, D. Bi, N. Chen, Q. Lai and Y. Liang, Interface engineering of crystalline-amorphous heterostructures with strong electronic interactions for efficient alkaline overall water splitting. *J. Alloys Compd.*, 2024, **977**, 173447. DOI:10.1016/j.jallcom.2024.173447
- [88] WH. Sun, YQ. Hua and X. Zhang, Assembly of amorphous CoP electrocatalysts on flexible polyester textile for alkaline hydrogen evolution reaction. *Int. J. Hydrogen Energy*, 2024, **63**, 28-35. DOI:10.1016/j.ijhydene.2024.03.171
- [89] F. Yang, G. Dong, L. Meng, L. Liu, X. Liu, Z. Zhang, M. Zhao and W. Zhang, One-step electrodeposition of bifunctional MnCoPi electrocatalysts with wrinkled globular-flowers-like structure for highly efficient electrocatalytic water splitting. *Int. J. Hydrogen Energy*, 2024, **77**, 589-597. DOI:10.1016/j.ijhydene.2024.06.235
- [90] S. Liao, Z. Zhang, Y. Li, Y. Zheng and D. Dang, Co/CoP@NC heterostructures as bifunctional catalysts to enhance the alkaline water splitting. *Int. J. Hydrogen Energy*, 2024, **81**, 624-631. DOI:10.1016/j.ijhydene.2024.07.274
- [91] J. Lian, Y. Wu, Z. Lu and Q. Zang, Cyclic voltammetry electrodeposition of self-standing Ni-Fe-Sn ternary alloys for accelerating alkaline hydrogen evolution. *Int. J. Hydrogen Energy*, 2023, **48**, 24295-24305. DOI:10.1016/j.ijhydene.2023.03.221
- [92] L. Meng, H. Xuan, J. Wang, X. Liang, Y. Li, J. Yang, and P. Han, One-step electrodeposition synthesis of bimetallic sulfides for highly efficient electrocatalytic water splitting. *Int. J. Hydrogen Energy*, 2024, **51**, 271-280. DOI:10.1016/j.ijhydene.2023.08.143
- [93] D. Duan, J. Gao, Y. Wang, X. Zhou, S. Liu and Y. Wang, Electrodeposition of copper-cobalt bimetallic phosphide on nickel foam as an efficient catalyst for overall water splitting. *J. Electroanal. Chem.*, 2023, **939**, 117478. DOI:10.1016/j.jelechem.2023.117478
- [94] R. Ye, Z. Sheng, P. Yang, L. Xu, Y. Tao, X. Wu and X. Cui, Ni-doped CoFeP as high-efficient electrocatalysts for water-splitting. *Electrochim. Acta*, 2024, **507**, 145152. DOI:10.1016/j.electacta.2024.145152
- [95] X. Tian, Y. Wang, F. Sun, R. Zhu, M. Han and J. Zang, In-situ activation of three-dimensional porous NiFe alloy: Synergistic NiFe hydroxide/alloy as composite active sites for efficiently catalyzing alkaline water splitting. *J. Alloys Compd.*, 2024, **997**, 174942. DOI:10.1016/j.jallcom.2024.174942
- [96] J. Sun, S. Qin, Z. Zhang, C. Li, X. Xu, Z. Li and X. Meng, Joule heating synthesis of well lattice-matched Co₂Mo₃O₈/MoO₂ heterointerfaces with greatly improved hydrogen evolution

- reaction in alkaline seawater electrolysis with 12.4% STH efficiency. *Appl. Catal. B: Environ.*, 2023, **338**, 123015. [DOI:10.1016/j.apcatb.2023.123015](https://doi.org/10.1016/j.apcatb.2023.123015)
- [97] K. Zhang, E. Yang, Y. Zheng, D. Yu, J. Chen and Y. Lou, Robust and hydrophilic Mo-NiS@NiTe core-shell heterostructure nanorod arrays for efficient hydrogen evolution reaction in alkaline freshwater and seawater. *Appl. Surf. Sci.*, 2023, **637**, 157977. [DOI:10.1016/j.apsusc.2023.157977](https://doi.org/10.1016/j.apsusc.2023.157977)
- [98] J. Wang, D.T Tran, K. Chang, S. Prabhakaran, J. Zhao, D.H. Kim, N.H. Kim and J.H. Lee, Hierarchical Ni@CNTs-bridged Mo_xC/Ni₂P heterostructure micro-pillars for enhanced seawater splitting and Mg/seawater battery. *Nano Energy*, 2023, **111**, 108440. [DOI:10.1016/j.nanoen.2023.108440](https://doi.org/10.1016/j.nanoen.2023.108440)
- [99] C. Feng, M. Chen, Y. Zhou, Z. Xie, X. Li, P. Xiaokaiti, Y. Kansha, A. Abudula and G. Guan, High-entropy NiFeCoV disulfides for enhanced alkaline water/seawater electrolysis. *J. Colloid Interface Sci.*, 2023, **645**, 724-734. [DOI:10.1016/j.jcis.2023.04.172](https://doi.org/10.1016/j.jcis.2023.04.172)
- [100] R. Liang, J. Fan, F. Lei, P. Li, C. Fu, Z. Lu and W. Hao, Fabrication of ultra-stable and high-efficient CoP-based electrode towards seawater splitting at industrial-grade current density. *J. Colloid Interface Sci.*, 2023, **645**, 227-240. [DOI:10.1016/j.jcis.2023.04.143](https://doi.org/10.1016/j.jcis.2023.04.143)
- [101] N. Logeshwaran, S. Vijayapradeep, A.R. Kim, P. Sampath, S. Ramakrishnan, M.B. Poudel, D.H. Kim and D.J. Yoo, Study of engineering electronic structure modulated non-noble metal oxides for scaled-up alkaline blend seawater splitting. *J. Energy Chem.*, 2023, **86**, 167-179. [DOI:10.1016/j.jechem.2023.06.039](https://doi.org/10.1016/j.jechem.2023.06.039)
- [102] Z. Sun, B. Chu, S. Wang, L. Dong, Q. Pang, M. Fan, X. Zhang, H. He, B. Li. and Z. Chen, Hydrogen-bond induced and hetero coupling dual effects in N-doped carbon coated CrN/Ni nanosheets for efficient alkaline freshwater/seawater hydrogen evolution. *J. Colloid Interface Sci.*, 2023, **646**, 361-369. [DOI:10.1016/j.jcis.2023.05.006](https://doi.org/10.1016/j.jcis.2023.05.006)
- [103] X. Hao, J. Yu, W. Wang, H. Zhang, T. Cai, L. Mu, W. Shi and G. She, Highly efficient electrocatalytic seawater splitting to produce hydrogen with an amorphous medium-entropy oxide electrocatalyst (Co_{0.40}Ni_{0.30}Mo_{0.17}Re_{0.13})O. *Int. J. Hydrogen Energy*, 2024, **76**, 152-159. [DOI:10.1016/j.ijhydene.2024.02.215](https://doi.org/10.1016/j.ijhydene.2024.02.215)
- [104] C. Fang, R. Li, X. Wang, F. Duan, J. Lin, Y. Hu and Z. Cui, Defect-promoted nanoparticles-nanorod Ni-NiMoO₄ heterogeneous nanostructures as efficient electrocatalysts to overall water/urea splitting in fresh/sea water. *Chem. Eng. J.*, 2024, **484**, 149498. [DOI:10.1016/j.cej.2024.149498](https://doi.org/10.1016/j.cej.2024.149498)
- [105] ZM. He, CX. Zhang, SQ. Guo, P. Xu, Y. Ji, SW. Luo, X. Qi, YD. Liu, NY. Cheng, SX. Dou, YX. Wang and BW. Zhang, Mo-doping heterojunction: interfacial engineering in an efficient electrocatalyst for superior simulated seawater hydrogen evolution. *Chem. Sci.*, 2024, **15**, 1123-1131. [DOI:10.1039/D3SC05220F](https://doi.org/10.1039/D3SC05220F)
- [106] R. Kalusulingam, K. Ravi, S. Mathi, N. Yadhav, A.S. Mikheykin, A.V. Biradar, K. Srinivasan and T.N. Myasoedova, Bimetallic Ni-Fe nanoparticles encapsulated with biomass-derived N-doped graphitic carbon core-shell nanostructures an efficient bifunctional electrocatalyst for enhanced overall seawater splitting and human urine electrolysis. *Mater. Today Sustain.*, 2024, **27**, 100864. [DOI:10.1016/j.mtsust.2024.100864](https://doi.org/10.1016/j.mtsust.2024.100864)

- [107] M. Liu, H. Zhao, X. Du and X. Zhang, Efficient hydrogen evolution reaction in alkaline seawater and urea using flower-like Co-NiP@VP/NF electrocatalyst. *Fuel*, 2025, **381**, 133717. DOI:[10.1016/j.fuel.2024.133717](https://doi.org/10.1016/j.fuel.2024.133717)
- [108] X. Ji, H. Wang, S. Cao, P. Chen, Y. Tong, Y. Ren, K. Wang, J. Zhang, X. Zhang and X. Pang, Advanced multi-component FeCoCuAlMo intermetallic electrocatalysts for efficient and sustainable hydrogen evolution in alkaline freshwater and seawater. *Int. J. Hydrogen Energy*, 2024, **89**, 836-846. DOI:[10.1016/j.ijhydene.2024.09.436](https://doi.org/10.1016/j.ijhydene.2024.09.436)
- [109] H. Wang, L. Chen, L. Tan, X. Liu, Y. Wen, W. Hou and T. Zhan, Electrodeposition of NiFe-layered double hydroxide layer on sulfur-modified nickel molybdate nanorods for highly efficient seawater splitting. *J. Colloid Interface Sci.*, 2022, **613**, 349-358. DOI:[10.1016/j.jcis.2022.01.044](https://doi.org/10.1016/j.jcis.2022.01.044)

OTHER PUBLICATION

O1. **S. Barua**, A. Balčiūnaitė, J. Vaičiūnienė, L. Tamašauskaitė-Tamašiūnaitė and E. Norkus, High-efficiency borohydride oxidation and oxygen reduction on titanium-supported Au(NiMo) catalysts for Alkaline fuel cells. *Chem. Phys. Impact*, 2025, **10**, 100827. DOI:10.1016/j.chphi.2025.100827

LIST OF CONFERENCE PRESENTATIONS

The main results of the doctoral thesis were presented in 13 conference reports (C: 1–13).

C1. **S. Barua**, A. Balčiūnaitė, J. Vaičiūnienė, L. Tamašauskaitė-Tamašiūnaitė and E. Norkus, Three-dimensional Au(NiMo)/Ti catalysts for efficient oxygen evolution. *65th International Conference for Students of Physics and Natural Sciences “Open Readings 2022”* 15th-18th March, 2022, Vilnius, LITHUANIA. **(Oral Presentation-Virtual)**.

C2. **S. Barua**, A. Balčiūnaitė, J. Vaičiūnienė, L. Tamašauskaitė-Tamašiūnaitė and E. Norkus, Three-dimensional Au(NiMo)/Ti catalysts for efficient hydrogen evolution reaction. *12th Conference of Doctoral Students and Young Researchers “FizTeCh 2022”*, 19th-20th October, 2022, Vilnius, LITHUANIA. **(Poster Presentation-P5)**. Awarded for the best poster presentation.

C3. **S. Barua**, A. Balčiūnaitė, J. Vaičiūnienė, L. Tamašauskaitė-Tamašiūnaitė and E. Norkus, Bimetallic Nickel-Manganese/Titanium Electrocatalyst for Efficient Hydrogen Evolution Reaction. *Chemistry and Chemical Technology “CCT 2023”*, 10th March, 2023, Vilnius, LITHUANIA. **(Poster Presentation-P074)**.

C4. **S. Barua**, A. Balčiūnaitė, J. Vaičiūnienė, L. Tamašauskaitė-Tamašiūnaitė and E. Norkus, Bimetallic Nickel-Manganese Bifunctional Electrocatalyst for Efficient Alkaline Water Splitting. **74th International Society of Electrochemistry (ISE) Annual Meeting**, 3rd-8th September, 2023, Lyon, FRANCE. **(Poster Presentation-S06-P006)**.

C5. **S. Barua**, A. Balčiūnaitė, J. Vaičiūnienė, L. Tamašauskaitė-Tamašiūnaitė and E. Norkus, 3D Nickel-Manganese/Titanium Bifunctional Electrocatalysts for Efficient Hydrogen and Oxygen Evolution Reaction in Alkaline and Acidic Media. *International Summit on Catalysis, Chemical Engineering and Technology “ISCCET 2023”*, 12th-13th October, 2023, Barcelona, SPAIN. **(Oral Presentation)**.

C6. **S. Barua**, A. Balčiūnaitė, J. Vaičiūnienė, L. Tamašauskaitė-Tamašiūnaitė and E. Norkus, A Comparative Study of Bimetallic Nickel-Manganese/Titanium Bifunctional Electrocatalysts for Alkaline Freshwater and Simulated Seawater Splitting. *13th Conference of Doctoral Students and Young Researchers “FizTeCh 2023”*, 18th-19th October, 2023, Vilnius, LITHUANIA. (**Oral Presentation-O11**).

C7. **S. Barua**, A. Balčiūnaitė, J. Vaičiūnienė, L. Tamašauskaitė-Tamašiūnaitė and E. Norkus, An Enhanced Hydrogen Evolution Reaction Performance by Nickel-Manganese Bimetallic Electrocatalysts towards Alkaline Natural Seawater and Simulated Seawater Splitting. *67th International Conference for Students of Physics and Natural Sciences “Open Readings 2024”*, 23rd-26th April, 2024, Vilnius, LITHUANIA. (**Poster Presentation-P1-71**).

C8. **S. Barua**, A. Balčiūnaitė, J. Vaičiūnienė, L. Tamašauskaitė-Tamašiūnaitė and E. Norkus, Facile one-step fabrication of 3D nickel-manganese/titanium electrocatalysts for hydrogen evolution reaction in simulated seawater and alkaline natural seawater. *1st International Symposium on Materials, Energy and Environment “ISMEE 2023”*, 2nd-3rd May, 2024, University of Chittagong, Chattogram, BANGLADESH. (**Online Oral Presentation, ONOR_0037**).

C9. **S. Barua**, A. Balčiūnaitė, J. Vaičiūnienė, L. Tamašauskaitė-Tamašiūnaitė and E. Norkus, Comparison of the Activity of 3D Nickel-Manganese/Titanium Bifunctional Electrocatalysts for Alkaline Natural Seawater and Simulated Seawater Splitting. **Electrocatalysis 2024-Electrocatalysis in Complex Structures**, 22nd-24th May, 2024, Friedrich-Alexander-Universität Erlangen-Nürnberg (FAU), GERMANY. (**Poster Presentation-001**).

C10. **S. Barua**, A. Balčiūnaitė, J. Vaičiūnienė, L. Tamašauskaitė-Tamašiūnaitė and E. Norkus, Bimetallic 3D Nickel-Manganese Coatings: High-performance HER and Stable OER Electrocatalysts for Alkaline Water Splitting and Overall Seawater Splitting. *14th Conference of Doctoral Students and Young Researchers “FizTeCh 2024”*, 15th-17th October, 2024, Vilnius, LITHUANIA. (**Oral Presentation-O3**).

C11. **S. Barua**, A. Balčiūnaitė, J. Vaičiūnienė, L. Tamašauskaitė-Tamašiūnaitė and E. Norkus, A comparative study of hydrogen evolution reaction performance by non-noble transition metal-based 3D electrocatalysts towards alkaline water splitting. *68th International Conference for Students of Physics and Natural Sciences “Open Readings 2025”*, 13th-16th May, 2025, Vilnius, LITHUANIA. (**Poster Presentation-P4-22**).

C12. S. Barua, A. Balčiūnaitė, J. Vaičiūnienė, L. Tamašauskaitė-Tamašiūnaitė and E. Norkus, 3D NiMnCo trimetallic electrocatalysts with cauliflower curd-shaped micro-sized nodular morphology for an efficient and sustainable hydrogen evolution reaction in alkaline media and simulated seawater. *13th International Conference on Environmental Catalysis “ICEC 2025”*, 2nd-5th June, 2025, Palermo, ITALY. (**Poster Presentation-P2-3**).

C13. A. Balčiūnaitė, S. Barua, J. Vaičiūnienė, L. Tamašauskaitė-Tamašiūnaitė and E. Norkus, Activity of Non-Noble Transition Metal-Based 3D Electrocatalysts for Alkaline Natural and Simulated Seawater Splitting. *“Grotthuss Conference 2025”*, 4th-6th June, 2025, Vilnius, LITHUANIA. (**Poster Presentation-P-058**).

LIST OF OTHER CONFERENCE PRESENTATIONS

OC1. S. Barua, A. Balčiūnaitė, F. Višnevskaja, J. Vaičiūnienė, L. Tamašauskaitė-Tamašiūnaitė and E. Norkus, Investigation of 3D NiMo coatings decorated with Au particles for borohydride oxidation, *11th Conference of Doctoral Students and Young Researchers “FizTeCh 2021”*, 20th-21st October, 2021, Vilnius, LITHUANIA. (**Poster Presentation-P6**).

OC2. S. Barua, A. Balčiūnaitė, J. Vaičiūnienė, L. Tamašauskaitė-Tamašiūnaitė and E. Norkus, Facile Fabrication of Au(NiMo)/Ti Catalysts and Investigation of their Electrocatalytic Activities for Borohydride Oxidation and Oxygen Reduction Reaction. *International Summit on Catalysis, Chemical Engineering and Technology “ISCCET 2023”*, 12th-13th October, 2023, Barcelona, SPAIN. (**Poster Presentation-PO-2**).

OC3. S. Barua, A. Balčiūnaitė, J. Vaičiūnienė, L. Tamašauskaitė-Tamašiūnaitė and E. Norkus, Au-decorated NiMo/Ti Electrocatalysts for Efficient Borohydride Electro-oxidation and Oxygen Reduction Reaction in Alkaline Media. *18th ICC - International Congress on Catalysis “Roots and Wings for a Better World”*, 14th-19th July, 2024, Lyon, FRANCE. (**Oral Presentation-FRI-T14-05**).

LIST OF AWARDS

- A1. Best Poster Award in **FizTeCh 2022**.
- A2. Mobility Fund from the Research Council of Lithuania to participate in an international conference in Barcelona, Spain. **(P-DAK-23-78)**.
- A3. Financial Grant for study results from the Research Council of Lithuania. **(P-DAP-23-201)**.
- A4. Mobility Fund from the Research Council of Lithuania to participate in an international conference in Nürnberg, Germany. **(P-DAK-24-37)**.
- A5. Mobility Fund from the Research Council of Lithuania to participate in an international conference in Palermo, Italy. **(P-DAK-25-28)**.
- A6. Financial Grant for study results from the Research Council of Lithuania. **(P-DAP-25-146)**.

CURRICULUM VITAE

PERSONAL INFORMATION

Name	Sukomol Barua.
Nationality	BANGLADESHI.
Address	Saulėtekio 25, LT-10257, Vilnius, Lithuania.
Phone no.	+370 6070 4836.
E-mail	sukomol.barua@ftmc.lt

ACADEMIC BACKGROUND

Mar 2007 – Feb 2011	B.Sc. in Chemistry at University of Chittagong, Bangladesh.
Jun 2011 – Jul 2012	M.Sc. in Chemistry at University of Chittagong, Bangladesh.
Oct 2018 – Sep 2020	M.Sc. in Chemistry at Uniwersytet im. Adama Mickiewicza w Poznaniu, Poland.
Oct 2021 – Sep 2025	Doctoral studies at the State Research Institute Center for Physical Sciences and Technology (FTMC).

PROFESSIONAL EXPERIENCE

Oct 2021 – Oct 2022	PhD Student at FTMC.
Nov 2022 – Jan 2024	Senior Engineer at FTMC.
Jan 2024 – Present	Junior Researcher at FTMC.

Vilniaus universiteto leidykla
Saulėtekio al. 9, III rūmai, LT-10222 Vilnius
El. p. info@leidykla.vu.lt, www.leidykla.vu.lt
bookshop.vu.lt, journals.vu.lt
Tiražas 20 egz.